



UNIVERSITY OF  
BIRMINGHAM

**MICROSTRUCTURAL DEVELOPMENT OF HIGH  
SOLID FOOD SYSTEMS DURING FREEZE-DRYING**

by

**Nur Hafizah Malik**

A thesis submitted to  
The University of Birmingham  
for the degree of  
DOCTOR OF PHILOSOPHY

School of Chemical Engineering  
The University of Birmingham  
July 2018

UNIVERSITY OF  
BIRMINGHAM

**University of Birmingham Research Archive**  
**e-theses repository**

This unpublished thesis/dissertation is copyright of the author and/or third parties. The intellectual property rights of the author or third parties in respect of this work are as defined by The Copyright Designs and Patents Act 1988 or as modified by any successor legislation.

Any use made of information contained in this thesis/dissertation must be in accordance with that legislation and must be properly acknowledged. Further distribution or reproduction in any format is prohibited without the permission of the copyright holder.

# ABSTRACT

Freeze-drying as an energy demanding operation involves the phase transition of water from liquid to solid and eventually gas under low temperature and pressure. It has important application in the food industry for production of dried materials with high sensorial, nutritional and reconstitution properties such as instant coffee and ready to eat meals. Understanding the relation between operating conditions and product quality is essential to design processes that are energy efficient whilst producing dried product of desired characteristics.

In the present work, freeze-dried microstructure development and evaluation for formulations with high solid content (20-60% w/w) have been considered. Gum arabic and coffee were used as a model and real food system, respectively. Freeze-drying processes were operated by varying the material's concentration and properties as well as freezing and primary drying conditions. Imaging techniques such as high resolution camera, scanning electron microscopy (SEM) and X-ray computed tomography (XRCT) were used for microstructural evaluation and performance of freeze-dried solids was assessed on reconstitution behaviour.

Initially, crystallization of water in concentrated solutions was studied under the influence of temperature oscillation, slow, fast and unidirectional freezing. It has been demonstrated that large crystal dendrites developed on fluctuating temperature and different freezing rates applied produced comparable crystal networks. Also, crystal size becomes smaller as water content reduced and distinct orientation of crystal growth was visible at lower concentration. Microstructure formation was then evaluated on the effect of initial solid content and primary drying temperatures. At increasing initial concentration and drying temperature, the final dried systems showed extensive structure expansion. Finally, the potential of aeration to assist freeze-drying of high solid solutions has been indicated by improved structure uniformity and porosity.

Reconstitution of the freeze-dried solids appeared to be influenced by the microstructure generated and physical mechanisms involved during dissolution. High porosity and presence of large pores allowed dried products to be easily dissolved. Different dissolution mechanisms between gum arabic and coffee had a strong impact on the kinetics of dissolution. The concept of process-microstructure-property relationship is thus very clear in this study.

## **ACKNOWLEDGEMENTS**

Alhamdulillah, firstly I would like to express my gratitude to Allah for the opportunity to embark on this PhD journey in the University of Birmingham.

I would like to thank both of my supervisors, Prof. Serafim Bakalis and Prof. Peter Jonathan Fryer for their guidance, encouragement and trust while giving me the opportunity to grow intellectually. Special thanks goes to Ourania Gouseti for her invaluable guidance, moral support and being attentive with my work throughout my research especially during the writing stage.

For the members of my research group and lab mates, thank you for being readily available to share knowledge and really helpful in any ways that you can. I am also grateful for the support from the administrative team of the department and to Lynn Draper I truly appreciate your help and kindness all along.

I am also very thankful to Faiqa, Hajar, Gina, Anisa, Suaida and Hazwan for the unconditional moral support, helping me with analysis and public presentation and I am forever grateful with the friendship we build along this journey.

My final gratitude is to my beloved parents, siblings, relatives and friends in Malaysia for their never ending encouragement, strength and trust in me without which I would not be here.

CHAPTER 1 .....	1
INTRODUCTION .....	1
1. 1 Research background .....	1
1. 2 Objectives of research .....	5
1. 3 Layout of thesis .....	6
1.4 Public presentations.....	7
CHAPTER 2.....	9
LITERATURE REVIEW .....	9
2.1 Introduction .....	9
2.2 Principles of freeze-drying technology .....	9
2.2.1 Freezing step.....	13
2.3.1.1 Ice crystals formation .....	13
2.3.1.2 Influential role of ice crystals in freeze-drying .....	17
2.2.2 Primary drying .....	21
2.2.2.1 Heat and mass transfer mechanism.....	22
2.2.2.2 Significance of shelf temperature ( $T_s$ ) and chamber pressure ( $P_c$ ).....	24
2.2.3 Differential scanning calorimetry (DSC) .....	30
2.2.4 Secondary drying .....	32
2.3 Characterization of food microstructure .....	34
2.3.1 Electron microscopy .....	35
2.3.1.1 Scanning electron microscopy (SEM).....	36
2.3.1.2 Cryo-SEM .....	38
2.3.1.3 Environmental SEM (ESEM).....	38
2.3.1.4 Transmission electron microscopy (TEM).....	39
2.3.1.5 X-ray computed tomography (XRCT) .....	39
2.4 Significance of water transport properties during rehydration.....	41
2.5 Materials.....	44
2.5.1 Gum Arabic .....	44
2.5.2 Coffee .....	45
2.6 Conclusion.....	47
CHAPTER 3.....	49
MATERIALS AND METHODS .....	49
3.1 Materials.....	49
3.2 Methods.....	49
3.2.1 Preparation of samples.....	49
3.2.2 Aeration .....	50
3.2.3 Freeze-drying cycles.....	50
3.2.3.1 Different freezing step.....	51

3.2.3.2	Different primary drying conditions .....	54
3.2.4	Differential scanning calorimetry (DSC) .....	55
3.2.5	Structure analysis.....	57
3.2.5.1	Scanning electron microscopy (SEM).....	57
3.2.5.2	X-ray computed tomography (XRCT).....	58
3.2.5.3	Image analysis.....	59
3.2.5.4	Porosity analysis .....	60
3.2.6	Reconstitution process .....	60
CHAPTER 4	.....	63
INFLUENCE OF FREEZING CONDITIONS ON ICE CRYSTALS FORMATION AND RECONSTITUTION BEHAVIOUR OF CONCENTRATED FREEZE-DRIED SYSTEMS. ....		63
4.1	Introduction .....	63
4.2	Thermal characterization.....	65
4.2.1	Crystallization.....	65
4.2.2	Heating endotherm of gum arabic and coffee solutions.....	68
4.3	Influence of temperature oscillation.....	72
4.3.1	Cooling profiles of gum arabic and coffee solutions.....	73
4.3.2	Appearance and microstructure of freeze-dried solids .....	75
4.3.2.1	Appearance of freeze-dried cake.....	75
4.3.2.2	Microstructure .....	79
4.3.3	Reconstitution behaviour .....	84
4.4	Influence of different cooling rates .....	89
4.4.1	Cooling profile.....	89
4.4.2	Microstructure properties of freeze-dried systems .....	93
4.4.3	Reconstitution behavior .....	97
4.5	Unidirectional freezing.....	99
4.5.1	Cooling profile.....	99
4.5.2	Microstructure .....	102
4.5.3	Reconstitution.....	108
4.6	Summary .....	110
CHAPTER 5	.....	116
EFFECT OF SOLID CONTENT AND PRIMARY DRYING TEMPERATURE ON MICROSTRUCTURAL DEVELOPMENT AND RECONSTITUTION OF FREEZE-DRIED SYSTEMS .....		116
5.1	Introduction .....	116
5.2	Product temperature evolution during freeze-drying .....	117
5.3	Microstructure .....	119
5.3.1	Pore structure of the freeze-dried cake .....	119
5.3.2	Pore size distribution .....	126
5.3.3	Porosity.....	130
5.4	Reconstitution behavior.....	132

5.5	Summary .....	137
CHAPTER 6 .....		140
FREEZE-DRYING OF AERATED SYSTEMS .....		140
6.1	Introduction .....	140
6.2	Effect of freezing conditions on microstructure and dissolution of aerated freeze-dried systems. ....	141
6.2.1	Freezing with temperature oscillation .....	143
6.2.1.1	Microstructural properties .....	143
6.2.1.2	Reconstitution.....	149
6.2.2	Freezing with different cooling rates .....	151
6.2.2.1	Microstructure .....	155
6.2.2.2	Reconstitution.....	159
6.3	Effect of different primary drying temperatures .....	161
6.3.1	Microstructure .....	161
6.3.2	Reconstitution.....	166
6.4	Summary .....	169
CHAPTER 7 .....		173
CONCLUSION AND FUTURE WORK .....		173
7.1	Introduction .....	173
7.1.1	Freeze-drying with different freezing conditions .....	173
7.1.2	Freeze-drying at different primary drying temperatures .....	178
7.1.3	Freeze-drying of aerated systems. ....	180
7.2	Conclusion.....	182
7.3	Suggestion for future work.....	183

## LIST OF TABLES

Table 4-1 Phase change enthalpy associated with cooling and melting as well as glass transition point of gum arabic and coffee solutions.....	71
Table 4-2 Effect of concentration on freezing properties of gum arabic and coffee solutions	74
Table 4-3 Data from image analysis on overall porosity of the freeze-dried systems .....	82
Table 4-4 Data from pycnometer on overall porosity of the freeze-dried systems .....	83
Table 4-5 Nucleation temperature ( $T_n$ ) extracted from the cooling curves of the concentrated solutions.....	91
Table 4-6 Freezing properties derived from cooling curves.....	101
Table 5-1 Weibull's function parameters derived from dissolution data of gum arabic using equation (7).....	136
Table 5-2 Weibull's function parameters derived from dissolution data of coffee using equation (7) .....	136
Table 6-1 Effect of concentration on freezing properties of aerated coffee and gum arabic solutions.....	142
Table 6-2 Noticeable nucleation point ( $T_n$ ) of aerated solutions from different freezing conditions. ....	154
Table 6-3 Parameters estimated from Weibull function.....	169

## LIST OF FIGURES

Figure 2.1 The relationship between temperature and pressure on physical states of water. Adapted from Yu et al. (2011).....	10
Figure 2.2 Schematic diagram of cooling curve showing phenomena involve in the freezing process. Adapted from Sánchez et al. (2011) .....	13
Figure 2.3 Phase diagram of sucrose-water solution. Adapted from (Abdelwahed et al. 2006). .....	16
Figure 2.4 Example of different microstructure between a) freeze-dried and b) air-dried food. (SEM micrographs were adapted from Marabi & Saguy, (2004)). .....	21
Figure 2.5 The dynamic relation between product ( $T_p$ )and shelf ( $T_s$ ) temperature as well as chamber pressure ( $P_c$ ) on sublimation rate. Adapted from Chang & Patro (2004). .....	27
Figure 2.6 Typical DSC thermogram showing transition points that can be identified during cooling and heating cycle. Adapted from Rahman (2006).....	30
Figure 2.7 Diagram on signals produced after interaction of specimen with electron beam. Adapted from Stokes (2013).....	37
Figure 2.8 Schematic on interactions of X-ray with a substance. Adapted from Barigou & Douaire (2013).....	41
Figure 3.1 Picture of ultrasonic cleaner used for de-gassing.....	50
Figure 3.2 Picture of: (a-b) carbon steel baking tin used to fill sample and c) samples loaded on stainless steel tray .....	51
Figure 3.3 Freeze-drying cycle with temperature oscillation in the freezing step. ....	52
Figure 3.4 Picture of: a) rapid freezer used for freezing; b: Samples inside the rapid freezer .	53
Figure 3.5 Freeze-drying cycles with different cooling rates; 0.6°C/min and 2°C/min.....	53
Figure 3.6 Illustration on insulated sample holder used in unidirectional freezing .....	54
Figure 3.7 Freeze-drying cycles with different primary drying temperatures: -20°C, -30°C and -40°C.....	54
Figure 3.8 Freeze-drying cycle for control condition.....	55
Figure 3.9 Illustration on determination of onset crystallization, melting and glass transition points on DSC thermogram. ....	56
Figure 3.10 Picture of sample prepared for SEM observation. ....	57
Figure 3.11 Illustration on set up for X-ray micro CT observation.....	58
Figure 3.12 Example of binary image obtained after thresholding and cleaning.....	59
Figure 3.13 Illustration on set up used for recording reconstitution process. ....	61
Figure 3.14 Illustration on set up used in conductivity measurement .....	61
Figure 4.1 DSC thermograms of 20-60% w/w: a) gum arabic and b) coffee solutions obtained during cooling at 1°C/min .....	66
Figure 4.2 Effect of solid content on the onset crystallization temperature. ....	67
Figure 4.3 DSC thermogram of 20-60% w/w a) gum arabic and b) coffee during heating at 1°C/min.....	69
Figure 4.4 Effect of solid content on the onset melting temperature of gum arabic and coffee solutions.....	69
Figure 4.5 Devitrification exotherm observed during heating cycle of 50% gum arabic solution. .....	72
Figure 4.6 Comparison of freezing behaviour between concentrated gum arabic and coffee solutions during freezing to -40°C at 1°C /min.....	73
Figure 4.7 Freeze-dried cake of 50 and 60% w/w (a) gum arabic and (b) coffee obtained at different freezing conditions.....	76

Figure 4.8 Scanning electron microscopy (SEM) images of freeze-dried gum arabic and coffee at 100x magnification affected by different freezing conditions.....	79
Figure 4.9 Effect of formulations and freezing conditions on the mean size of ice crystals...	82
Figure 4.10 Area reduction of freeze-dried particles during reconstitution in 10ml distilled water: a) gum arabic b) coffee. ....	84
Figure 4.11 Snapshots images during reconstitution of freeze-dried coffee samples: .....	86
Figure 4.12 Snapshots from dissolution of oscillated 50% coffee oscillated in hot distilled water (90°C) .....	86
Figure 4.13 Snapshot images during reconstitution of freeze-dried gum arabic:.....	88
Figure 4.14 Schematic on freezing profile. ....	90
Figure 4.15 Representative freezing curves of concentrated gum arabic and coffee solutions during freezing with shelf ramping (SR) and shelf pre-cooling (PC) methods.....	90
Figure 4.16 Effect of cooling rates and concentrations on freezing temperature of gum arabic and coffee solutions. ....	92
Figure 4.17 SEM images (200x, 1000x) of the freeze-dried 50% gum arabic and coffee after freezing with different method .....	93
Figure 4.18 SEM images (200x, 1000x) of freeze-dried 60% gum arabic and coffee after freezing with different methods.....	93
Figure 4.19 Effect of shelf ramping (SR) and pre-cooling (PC) on ice crystal size distribution of the freeze-dried gum arabic and coffee solutions.....	95
Figure 4.20 Overall porosity of freeze-dried systems affected by formulation and freezing methods.....	96
Figure 4.21 Reconstitution of freeze-dried particles frozen at different cooling rates.....	97
Figure 4.22 Representative real time temperature profile during unidirectional freezing of concentrated systems. ....	100
Figure 4.23 Determination of $T_n$ and $T_f$ for fast cooled 50% coffee .....	100
Figure 4.24 Collapsed/puffed freeze-dried cake obtained after freeze-drying of: a) 60% coffee and b)60% gum arabic systems. ....	102
Figure 4.25 Scanning electron micrographs of surface structure (a-b) and inner structure (c-d) of freeze-dried 50% gum arabic. Images at 200x and 1000x magnification.....	104
Figure 4.26 Scanning electron micrographs of surface structure (a-b) and inner structure (c-d) of freeze-dried 50% coffee. Images at 200x and 1000x magnification.....	104
Figure 4.27 Scanning electron micrographs of surface structure (a-b) and inner structure (c-d) of freeze-dried 60% gum arabic. Images at 200x and 1000x magnification. ....	106
Figure 4.28 Scanning electron micrographs of surface structure (a-b) and inner structure (c-d) of freeze-dried 60% coffee. Images at 200x and 1000x magnification.....	107
Figure 4.29 Average pore size and porosity of unidirectional frozen freeze-dried samples .	108
Figure 4.30 Change in amount of solid dissolved during reconstitution of concentrated freeze-dried gum arabic and coffee. ....	108
Figure 5.1 Freeze-drying temperature profile of gum arabic solutions under various shelf temperatures (-20, -30 and -40C) .....	117
Figure 5.2 Vertical cross-section of freeze-dried gum arabic solutions dried at -20, -30 and -40°C.....	121
Figure 5.3 Horizontal cross-section of freeze-dried gum arabic solutions dried at -20, -30 and -40°C.....	123
Figure 5.4 Vertical cross-sections of freeze-dried coffee solutions dried at -20, -30 and -40°C. ....	125

Figure 5.5 Horizontal cross-sections of freeze-dried coffee solutions dried at -20, -30 and -40°C. ....	126
Figure 5.6 Pore size distribution of freeze-dried gum arabic processed at different primary drying temperatures. ....	127
Figure 5.7 Pore size distribution of freeze-dried coffee processed at different primary drying temperatures. ....	129
Figure 5.8 Overall porosity of freeze-dried a) gum arabic and b) coffee at different concentrations and primary drying temperatures determined from SEM images. ....	130
Figure 5.9 Effect of freeze-drying cycles and concentrations on dissolution profiles of freeze-dried gum arabic and coffee. Data is fitted with Weibull's function. ....	134
Figure 6.1 Time and temperature profiles of aerated solutions during cooling in freeze-drier at 1°C/min. ....	141
Figure 6.2 Freeze-dried cake of aerated systems after constant freezing at -40°C and freezing with temperature oscillation. ....	143
Figure 6.3 Picture of 60% solutions after being aerated and freeze-dried. ....	144
Figure 6.4 SEM images at 500x magnification of aerated freeze-dried samples affected by temperature oscillation during freezing. ....	146
Figure 6.5 Effect of freezing cycles on mean size of ice crystals and porosity of the freeze-dried systems. ....	148
Figure 6.6 Average size of 50 air bubbles in freeze-dried structures from different freezing cycles. ....	149
Figure 6.7 Area reduction of freeze-dried particles during reconstitution in distilled water. ....	150
Figure 6.8 Cooling profiles of aerated solutions during shelf ramp and shelf pre-cooled freezing in rapid freezer. ....	152
Figure 6.9 Determination of freezing temperature ( $T_f$ ) for rapidly cooled coffee solutions. ....	153
Figure 6.10 Effect of freezing conditions and concentrations on freezing temperature ( $T_f$ ) of the aerated solutions. ....	154
Figure 6.11 SEM images (200x, 1000x) of the aerated freeze-dried 50% gum arabic and coffee after freezing with different methods. Green and red arrows each point to pores from air and ice crystal. ....	155
Figure 6.12 SEM images (200x, 1000x) of the aerated freeze-dried 60% coffee and gum arabic after freezing with different methods. Green and red arrows each point to pores from air and ice crystal. ....	155
Figure 6.13 Effect of freezing conditions and concentrations on average size of ice crystals and porosity of the aerated freeze-dried systems. ....	157
Figure 6.14 Size distribution of air bubbles in the freeze-dried matrices of aerated solutions. ....	158
Figure 6.15 Reconstitution of the aerated freeze-dried (a) gum arabic (b) coffee ....	159
Figure 6.16 Micro CT images of aerated freeze-dried gum arabic (50 and 60% w/w) dried at -20, -30 and -40°C. Blue arrows and yellow circles represent the incorporated air. ....	161
Figure 6.17 Micro CT images of aerated freeze-dried coffee (50 and 60% w/w) dried at -20, -30 and -40°C. Blue arrows represent the incorporated air. ....	162
Figure 6.18 Representative of close up image of the aerated freeze-dried 50% gum arabic. ....	163
Figure 6.19 Effect of primary drying temperature and concentration on pore area equivalent diameter. ....	165
Figure 6.20 Porosity of the aerated freeze-dried solids at different drying temperatures. ....	166
Figure 6.21 Reconstitution expressed as amount of solid dissolved against time affected by concentrations and primary drying temperatures. ....	167

## ABBREVIATIONS

3D	Three Dimensional
DSC	Differential Scanning Calorimetry
ESEM	Environmental Scanning Electron Microscopy
PC	Pre-Cooling
SEM	Scanning Electron Microscopy
SR	Shelf Ramp
TEM	Transmission Electron Microscopy
XRCT	X-Ray Computed Tomography

## NOMENCLATURES

<i>atm</i>	Atmosphere (unit pressure)
$C_g$	Concentration of maximally freeze-concentrated solution
$C_o$	Maximum conductivity
$C_t$	Conductivity at time $t$
<i>cm</i>	Centimetre
<i>exp</i>	Exponential
$^{\circ}\text{C}$	Degree celcius
$\Delta G$	Change in Gibb's free energy
$\Delta H$	Change in enthalpy
$\Delta T$	Change in temperature
$\frac{dm}{dt}$	Rate of sublimation
$H_f$	Heat of fusion of water-ice
<i>hr</i>	Hour
$K$	Heat transfer coefficient
$k$	Weilbull's equation rate constant ( $\text{min}^{-1}$ )
$\mu\text{m}$	Micrometre

<i>min</i>	Minute
<i>ml</i>	Millilitre
<i>mm</i>	Milimeter
$M_t$	Mass dissolved at time $t$
$M_\infty$	Mass dissolved at equilibrium
$m$	Mass of sample
$n$	Weibull's shape parameter
$P_o$	Vapour pressure of ice
$P_c$	Chamber pressure
<i>rpm</i>	Round per minute (mixing speed)
$R_p$	Product resistance
$R_s$	Stopper resistance
<i>sec</i>	Second
$t$	Time
$T_c$	Collapse temperature
$T_d$	Devitrification temperature
$T_{eu}$	Eutectic temperature
$T_f$	Freezing temperature
$T_{f\ onset}$	Onset freezing temperature
$T_g$	Glass transition temperature
$T'_g$	Glass transition temperature of maximally freeze-concentrated
$T_p$	Product temperature
$T_s$	Shelf temperature
$T_m$	Melting temperature
$T_n$	Nucleation temperature
<i>w/w</i>	Mass ratio between solute and solvent (%)
$y$	Solid dissolved at time $t$
$y_{max}$	100% dissolved solid

# CHAPTER 1

## Introduction

### 1. 1 Research background

Food microstructure refers to the organization of either solid, liquid or gaseous elements within a food and their interrelationship (Herremans et al. 2013; Aguilera et al. 2000). Structural elements are rather diverse ranging from plant cell walls, protein strands, starch granules, fat and ice crystals, oil and water droplets to air bubbles (Aguilera 2005). The arrangement and interaction between these elements play significant roles in describing food functionality as well as the physicochemical, nutritional and physical characteristics. For example, the eating quality and melting rate of ice-cream depend on the interaction, size and distribution of ice crystals, air bubbles and fat globules (Muse & Hartel 2004; Flores & Goff 1999) while the distribution and ratio of air to solid elements in milk powders determine its instant properties (Sharma et al. 2012).

Advancement of processing technology has enabled the transformation, preservation, creation and even destruction of food structure affecting the final attributes. The mass and heat transfer phenomena during processing (e.g. baking, fermenting, freezing) induce changes in the physical, chemical and biochemical characteristics of the raw materials producing food of diverse forms. Often physical changes are related to structural properties which also have implications on the bioavailability of nutrients, sensorial properties and storage stability. Drying is among the unit operations being implemented at large scale to produce safe, convenient and good quality food products. Dehydrated food has been commercially produced using the sun, hot air, osmotic and freeze-drying techniques. In addition, novel drying technologies such as microwave, ultrasound, super critical, superheated steam, infrared, high electric field drying

have been proposed to promote sustainability in the food industry (Kumar et al. 2014; Moses et al. 2014; Huang et al. 2009; Reyes et al. 2008).

Among the different drying processes, freeze-drying remains significant for dehydration of delicate biological materials including antibiotics, microorganisms (Nireesha et al. 2013; Chang & Patro, 2004; Tsinontides et al. 2004), encapsulated aroma or flavour, coffee, fruits and vegetables (Cieurzyńska et al. 2011; Ratti, 2001; Sagara & Ichiba, 1994) which are sensitive to thermal treatment. With the continuous demand for wholesome food, this technique stands out in the aspect of maximum, nutrients, flavour, aroma and structure retention. In terms of microstructure, freeze-dried products are recognized for being highly porous that offers light weight and easy reconstitution attributes (Meda & Ratti 2005; Marabi & Saguy 2004). In freeze-drying, water in solid state (ice) is removed by means of sublimation. Food is basically dehydrated in three consecutive steps starting with freezing, followed by sublimation termed as primary drying and ends with evaporation or secondary drying. The phase transition of water from liquid to solid and finally to vapour is contributed by the combination of low temperature (less than 0°C) and pressure (less than 0.006 atm) involved. This processing condition has given rise to some well-known advantages mentioned before.

One of the concerns in operating at such low temperature and pressure is the heavy usage of refrigeration and vacuum systems leading to 4-8 times higher operational costs than spray and air drying (Ratti 2001). The issue pertaining to energy utilization efficiency has been recognized in the literature. Luo & Zhou (2008), Liapis & Bruttini (2008) and Liu et al. (2008) have proposed operational models based on the different heat and mass transfer principles as well as materials formulations as a simple and convenient tool to optimize and minimize energy consumption. Meanwhile, determining the end point of the primary drying stage has been suggested by Patel et al. (2010) to be useful for optimization of the sublimation process.

Continual research over the past decades have also focused on reducing vacuum consumption and drying time by suggesting freeze-drying under atmospheric condition (Claussen et al. 2007), combination of drying methods including osmotic, microwave and air drying (Prosapio & Norton 2017; Wang et al. 2010; Huang et al. 2009; Xu et al. 2006) and using foaming or aeration as pre-treatment before freeze-drying (Raharitsifa & Ratti 2010). In addition, extensive process designs based on controlling the processing parameters particularly shelf temperature ( $T_s$ ) and chamber pressure ( $P_c$ ) involved in each processing step has been made to produce high quality dried products in a reasonable amount of time (Parker et al. 2010; Lewis et al. 2010; Krokida et al. 1998; Pikal et al. 1990).

Microstructure of freeze-dried foods is technically controlled by ice crystal formation which creates pores as drying proceeds. In the drying stage, voids left by the sublimated ice crystal can have an impact on the quality of the dehydration process as well as properties of the end product. Small ice crystals from rapid freezing have been associated with high resistance to vapour flow across the dry layer consequently prolongs the sublimation time (Patel & Pikal 2011; Hottot et al. 2004a; Searles et al. 2001a; Kochs et al. 1993). Besides, the importance of ice crystallization phenomenon on product quality such as freeze-dried cake texture and appearance, porosity, colour, rehydration properties and retention of bioactive ingredients is well established in the literature (Esfandiary et al. 2016; Harnkarnsujarit et al. 2012; Ceballos et al. 2012; Harnkarnsujarit & Charoenrein 2011). However, understanding the link between freezing conditions and properties of the dried materials is still a matter of on-going research. For example, small needle-like ice crystals formed after rapid freezing of protein-based food (Harnkarnsujarit, et al. 2016) and carrot (Voda et al. 2012) associated with narrow voids in the freeze-dried structure led to increased rehydration capacity. At the same time, high water uptake has been linked with slowly frozen freeze-dried rice which has voids of large ice crystals (Koh

et al. 2011). On the other hand, Harnkansujarit et al. (2012) obtained an enhanced mechanical strength for freeze-dried sugar solutions frozen at high cooling rate (low freezing temperature;  $< -40^{\circ}\text{C}$ ) due to the large number of small pores in the freeze-dried solids that affected crust formation in the freeze-dried solids. The resulting structural difference and product properties from previous studies showed that freezing conditions such as cooling rate, degree of supercooling and ice nucleation temperature are fundamental to be addressed in modulating the efficiency of subsequent drying process and the quality of freeze-dried solids.

Nevertheless, heat and mass transfer in the drying step needs proper control to avoid internal ice melting and collapse of pores due to product temperature reaching higher than its glass transition ( $T_g$ ) or collapse temperature ( $T_c$ ). A collapsed freeze-dried cake has often been described as having dense structure (Krokida et al. 1998) and poor rehydration capacity (Barresi, et al. 2009). Combination of different heat input and vacuum level are continuously being researched to allow appropriate rate of water vapour removal whilst maintaining the desirable porous structure (Sablani et al. 2007; Gan et al. 2005; Sablani & Rahman 2002). Knowledge of glass transition ( $T_g$ ), collapse ( $T_c$ ) and melting temperatures ( $T_m$ ) of food materials is important for the choice of the most appropriate processing parameters (Roos 1997).

Indeed, freeze-drying is a complex and energy intensive operation. Therefore, towards a low energy impact operation, processing high solid systems is considered in this work. Gum arabic and coffee were used as a model and real food systems, respectively. Both materials are characterized as hydrocolloids rich in arabinogalactan, arabinogalactan-protein complex and glycoprotein (Gashua et al. 2016; Capek et al. 2010). Most food contains 40-80% water and large latent heat is involved in the water crystallization process. The low water content in concentrated materials means less water to be solidified and sublimated which can help to

minimize the energy requirement during operation. However, at reduced water availability it is increasingly difficult for water phase transitions since molecular mobility is restricted. A good understanding about the relation between operating conditions and product quality provide basis to design energy efficient processes that lead to products with desired attributes.

## **1. 2 Objectives of research**

This research has focused on understanding the factors affecting microstructural development during freeze-drying of gum arabic and coffee solutions as well as its reconstitution behaviour thereafter especially at high initial concentration. The specific objectives involved in this work are listed below:

- i) To understand the effect of freezing conditions which includes temperature oscillation, shelf ramp freezing (slow cooling), shelf pre-cooled freezing (fast cooling) and unidirectional freezing on ice crystals development hence the microstructure and reconstitution behaviour of high solid freeze-dried systems.
- ii) To analyse and compare microstructural characteristics as well as reconstitution kinetics of freeze-dried solids generated at different initial solid content and primary drying shelf temperatures.
- iii) To study the effect of aeration prior to freeze-drying of high solid solutions at different freezing and primary drying cycles on the microstructural and reconstitution quality of the final dried product.

- iv) To observe macrostructure and microstructure of freeze-dried systems using different imaging techniques: high resolution camera, scanning electron microscopy (SEM) and X-ray micro-computed tomography (XRCT).
  
- v) To study the influence of materials and the freeze-dried microstructure on its reconstitution properties.

### **1.3 Layout of thesis**

The work conducted in this research is divided into 7 chapters in this thesis. The content of each chapter is summarized below:

Chapter 1 Details background and objectives of the research study as well as outline of the thesis

Chapter 2 Introduces relevant literature which comprises of four sections:

- Section 2.2 reviews the principles of freeze-drying technology. This section also includes explanation on water phase diagram and the significance of material's thermal characteristics on process design.
- Section 2.3 is about microstructural characterization discussing parameters used to describe microstructure and the existence of various microscopic techniques.
- Section 2.4 includes discussion on the importance of water transport properties during rehydration of porous microstructure,
- Section 2.5 reviews the properties of gum arabic and coffee to represent hydrocolloid system.

- Chapter 3 Describes the materials, equipments and methodologies used in this research.
- Chapter 4 Presents an experimental study on different freezing conditions during freeze-drying of 50 and 60% w/w gum arabic and coffee solutions. The effect of the investigated conditions on product quality is discussed based on freeze-dried cake appearance, microstructural features and reconstitution behaviour.
- Chapter 5 Focuses on the influence of initial solid content and primary drying temperatures on microstructural as well as the reconstitution kinetics of the freeze-dried materials.
- Chapter 6 Further extends the effect of investigated freezing and primary drying conditions on aerated concentrated gum arabic and coffee solutions.
- Chapter 7 Summarise the conclusions from each experimental section and some suggestions for future work that are expected to further extend the knowledge gained from the present work.

#### **1.4 Public presentations**

- Part of the findings of this project has been presented (as poster) at the 29<sup>th</sup> European Federation of Food Science and Technology (EFFoST) International Conference held in Athens, Greece from 10-12 November 2015.
- Part of the findings of this project has been presented (as poster) at the 18<sup>th</sup> World Congress of Food Science and Technology (IUFoST) took place in Dublin, Ireland from 21-25 August 2016.

- Part of this project has been presented at the 1<sup>st</sup> International Conference on Sustainable Energy and Resource Use in Food Chains held in London, United Kingdom from 19-21 February 2017.
- Part of the findings in this study has been presented (as poster) at the 3<sup>rd</sup> UK Hydrocolloids Symposium took place at the University of Nottingham on 13 September 2017.
- Part of the findings has been presented at the 31<sup>st</sup> EFFoST International Conference held in Sitges, Spain from 13-16 November 2017.
- A manuscript about the effect of freezing on microstructure and reconstitution of freeze-dried high solid systems has been accepted for publication in *Journal of Food Hydrocolloids* on 6<sup>th</sup> May 2018. (Malik et al. 2018)

## **CHAPTER 2**

### **Literature review**

#### **2.1 Introduction**

The main interest in this current work has centred in the food microstructural development during freeze-drying especially for the high solid system. Processing concentrated materials was considered to address the energy intensive aspect of this dehydration technology. Freeze-drying such materials has some operational challenges that need to be addressed. For instance, formation of ice crystals in highly concentrated system is restricted due to the low water availability and mobility. Therefore, the principles of freeze-drying and the concept of process-microstructure-property relationship are reviewed in this literature study.

The freeze-drying process is discussed in section 2.2 with relation to the fundamentals of each processing stage and the influential effect of operating parameters on the whole process as well as end product properties. Discussion also includes description of water state diagram to describe the phase transitions involved during freezing and freeze-drying. Techniques available for microstructure observation and food microstructural properties is then discussed in section 2.3. Also, water transport properties during rehydration and the influence on process kinetics is presented in section 2.4. Finally, characterization of the materials studied which are gum arabic and coffee are presented in section 2.5.

#### **2.2 Principles of freeze-drying technology**

Freeze drying or lyophilization as a method of preservation begun in the era of World War II when it was employed for medicinal purposes. Significant developments took place around the 1950s and 1960s with the advancements of vacuum and refrigeration technology

(Franks 1998). Until today, this dehydration technique has been fully integrated in biopharmaceutical production for stabilization of bioactive compounds. Following the increasing concern on food quality and safety, it has been considered as an important method to process and preserve food. The growing interest in freeze-drying is driven by the advantages of dehydrating heat sensitive products containing bioactive compounds and producing final dried product with preserved structure, nutritional value, aroma and flavour. Among the commercially available freeze-dried food products are instant coffee, fruits, ready to eat meals, powdered milk and eggs.

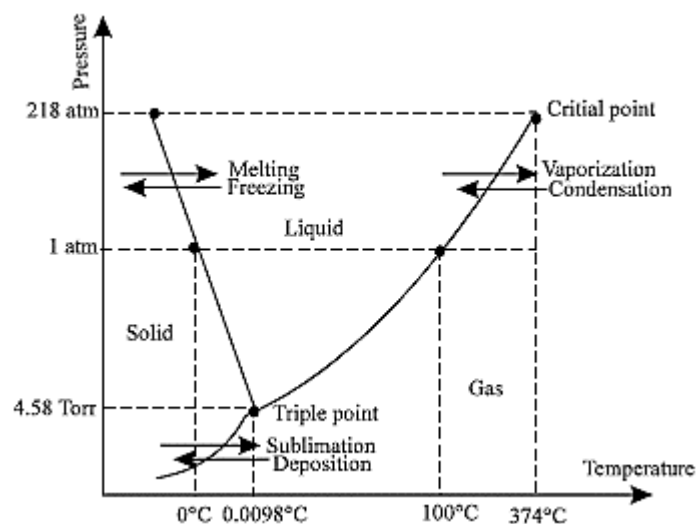


Figure 2.1 The relationship between temperature and pressure on physical states of water. Adapted from Yu et al. (2011).

The water phase diagram in figure 2.1 adapted from Yu et al. (2011) illustrates that water as a single component system can exist in liquid (water) and/or solid (ice) and/or gas (vapour) phases depending on the pressure and temperature conditions. The steep line between liquid and solid states is indicative of where water and ice are in equilibrium. Namely, freezing and melting are the transitions involved between these two phases. Meanwhile, the boundary line between liquid and gas shows the equilibrium states of water and vapour which is

associated with vapourization and condensation process. Solid and gas phases are divided by the sublimation/deposition curve at very low pressure and temperature. These three lines intersect with each other at a temperature around  $0.01^{\circ}\text{C}$  and below atmospheric pressure which corresponds to the thermodynamic equilibrium between all phases or better known as the triple point.

As the name implies, this dehydration technology requires material to be initially frozen to induce water crystallization before being dried through sublimation of the ice and evaporation of unfrozen liquid. From figure 2.1, it is shown that phase transitions in freeze-drying take place under the region of below atmospheric pressure and low temperature conditions. These processing conditions make freeze-drying an effective technique to dehydrate food products containing thermal sensitive materials such as volatile compounds, vitamins and minerals. Retention of these substances is important for they often contribute to the taste, aroma, flavor and nutritional value of food products (Ceballos et al. 2012; Wang et al. 2007; Asami et al. 2003). Freeze-drying is also valued for the production of highly porous microstructures and easily rehydrated dried products as opposed to hot air drying (Ratti 2001). This structural feature is due to the removal of water in solid phase that preserves the structural rigidity (Harnkarnsujarit et al. 2016; Voda et al. 2012; Ceballos et al. 2012; Sablani & Rahman 2002). The porous microstructure plays an important role in heat and mass transfer during processing or utilisation of the food material. The pores left by the sublimated ice crystals should allow sufficient heat and mass transfer to prevent structural changes phenomenon known as collapse due to overheating of the food materials during dehydration. Significant changes in volume can occur if the temperature of the material exceeds the critical points like collapse, glass transition and melting temperatures. More detail explanation about structural transformation in freeze-drying is discussed in section 2.2.1.1 and 2.2.2.2. Another important feature of freeze-drying is

that it is time and energy demanding drying operation (Kasper & Friess 2011). For this reason, many literatures have focused on energy efficient process designs particularly on reducing drying time as it accounts for almost half of the total energy consumption (Patel et al. 2010; Huang et al. 2009; Velardi & Barresi 2008; Sadikoglu et al. 1998)

Freeze-drying is a three stage drying process typically carried out in a chamber equipped with:

- Temperature controlled shelf
- Refrigeration unit
- Vacuum pump
- Condenser

The refrigeration unit helps to remove heat from the thermal fluid (silicone oil) as well as the condenser to allow cooling of the shelf during freeze-drying. While the vacuum pump keeps the drying chamber under very low pressures, the condenser maintains the vapour pressure of water at low level to enable sublimation at very low temperatures, typically between -50 to -80°C. The sublimed water is removed from the system and it is then converted back to ice by the condenser.

During freeze-drying, simultaneous heat and mass transfer occur. Understanding the thermodynamic behaviour of product formulations during freeze-drying and principles of each step is necessary to achieve high process efficiency and final product quality (Rambhatla et al. 2006; Rambhatla et al. 2004; Pikal et al. 1984). Freezing is controlled by the heat transfer process where energy is required to be removed from the product consequently, phase transition of liquid water to solid ice occurs. In the primary and secondary drying stage, a dynamic balance between heat and mass transfer process is crucial to obtain sufficiently a dried product.

### 2.2.1 Freezing step

Water crystallization is the first step in freeze-drying in which the liquid phase is immobilized through ice crystal formation. The ice crystal lattice plays an important role in determining the rate of subsequent drying process and structural characteristics as well as quality of the freeze-dried materials (Petzold & Aguilera 2009; Ratti 2001). The freezing process can be divided into three consecutive steps namely supercooling, ice nucleation and crystal growth. Interaction between these steps affects the ice crystal structure and size.

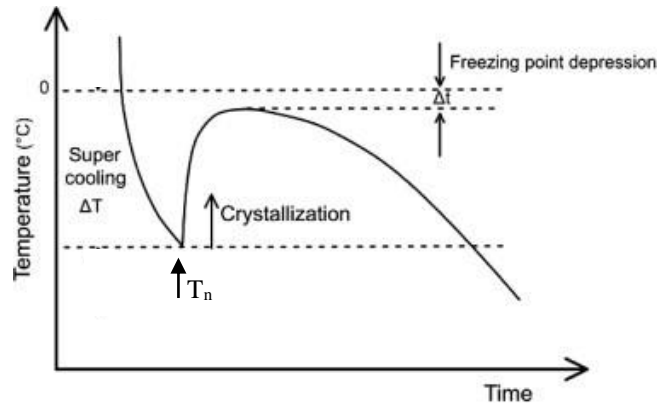


Figure 2.2 Schematic diagram of cooling curve showing phenomena involve in the freezing process. Adapted from Sánchez et al. (2011)

#### 2.3.1.1 Ice crystals formation

Development of ice crystals begins with the continuous withdrawal of sensible heat from materials until sufficient supercooling is achieved for ice nucleation. The decreasing temperature forces water molecules to come together and ice nucleation takes place once clusters of water molecules has reach maximum dimension to form stable ice nuclei in the super-cooled solution. As illustrated in figure 2.2 (adapted from Sánchez et al. (2011)), degree supercooling represents the difference between initial freezing temperature and the nucleation

temperature ( $T_n$ ) reflecting the random nucleation. It acts as the main driving force for the nucleation process and is a function of temperature and concentration of the food solution (Kasper & Friess 2011; Kiani & Sun 2011; Charoenrein & Preechathamwong 2010). In pure water system, the equilibrium freezing temperature corresponds to  $0^\circ\text{C}$  and essentially reduced to  $<0^\circ\text{C}$  in the case of water-solute system. Nucleation of ice can either occur homogeneously in a crystal free environment or heterogeneously due to the presence of foreign nucleation sites. Homogeneous nucleation is often related with larger supercooling than heterogeneous nucleation since walls of a container, dust particles or surface film can act as catalyst to promote ice nucleation at higher temperatures reducing the extent of required supercooling (Leiter 2015). In addition, ice can also nucleate from formerly created crystals which is then called secondary nucleation. For this type of nucleation, small fragments from previously created crystals (crystal seeds) are usually added and stable nuclei form on those seeds. Numerical simulations based on heat and mass transfer phenomenon have been developed by Lopez-Quiroga et al. (2016) to better describe the dynamics of these nucleation mechanisms. This numerical study estimated the crystal growth rate in non-seeded and seed induced freezing of concentrated solutions.

Ice nuclei formation has great influence on the crystal size, size distribution and shape which depends on the thermodynamic conditions. This includes supercooling, mass transfer and surface properties of the materials. Based on the classical nucleation theory, this process can be described with the change in Gibbs free energy ( $\Delta G$ ) which equal to the sum of change of volume free energy ( $\Delta G_v$ ) and change in the surface free energy ( $\Delta G_s$ ) where the critical nucleus radii is reached when  $\Delta G$  is at maximum. Nucleation rate which reflects the number of ice crystal formed can be expressed with Arrhenius type relationship (Kiani & Sun 2011), equation (1):

$$J = A \exp\left(-\frac{\Delta G_c}{kt}\right) \quad (1)$$

Where  $k$  is the Boltzmann constant and  $\Delta G_c$  is the critical free energy for nucleation. The pre-exponential term  $A$  was interpreted as the collision kinetics of the molecules which depends on the diffusion coefficient (Leiter 2015). This equation implies that high nucleation rate is promoted with increased collision between molecules corresponding to high supercooling.

As temperature is further reduced, crystal growth proceeds from the stable crystal lattice formed (Kasper & Friess 2011). At this stage, water molecules from the bulk solution diffuse to the crystal surface and arranged themselves into the crystal matrix until phase equilibrium is reached. Crystal growth is controlled by the rate of latent heat released during the phase transformation and diffusion of water molecules from the solution to the crystal matrix (Kaale & Eikevik 2014). The rate of crystal growth principally increases with decreasing temperature but at a certain temperature, the growth reaches maximum rate and eventually ceases due to restricted mobility with further temperature reduction.

In general, the ice nucleation and crystal growth are dependent on the initial supercooling exerted. At high super-cooling, large crystallization heat can be absorbed to create many small nuclei for development of small ice crystals (Geidobler & Winter 2013). On the contrary, the lower degree of supercooling means ice is nucleated at higher temperature, reducing the rate of ice nucleation. This condition often results in growth of large crystals as crystal growth proceeds faster than ice nucleation under slow cooling rate (Rambhatla et al. 2004).

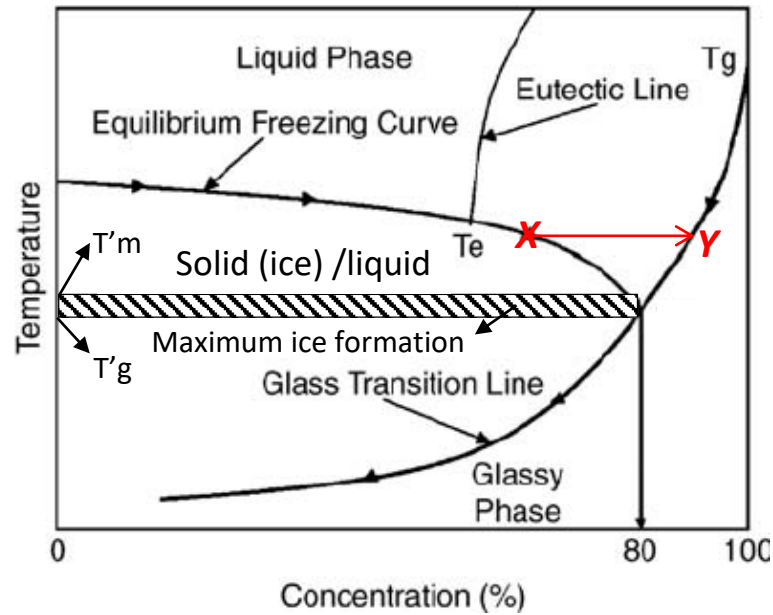


Figure 2.3 Phase diagram of sucrose-water solution. Adapted from (Abdelwahed et al. 2006).

Ice crystals development is also influenced by the solute concentration within a solution. Figure 2.3 illustrates the change in concentration and state of material during freezing where the remaining unfrozen solution progressively becomes more concentrated as water is being crystallized. Following the temperature reduction along the equilibrium freezing curve, the eutectic temperature ( $T_e$ ) is reached before glass transition line. In theory, all constituents will crystallize simultaneously at  $T_e$  producing a crystalline structure. However, this is a less common freezing behaviour for biological products in which freezing often continues beyond this point until the glass transition line resulting in maximally freeze-concentrated material. At this point, the solution develops into a highly viscous material with viscosity in the order of  $10^{14}$ Pa and crystallization stops as mobility of water molecules has decreased (Rahman et al. 2002a). Maximum ice formation has been noted to occur when the product is maintained between the end point of freezing curve refers to onset of melting ( $T'_m$ ) and glass transition of the maximally freeze-concentrated solute phase ( $T'_g$ ) (Roos 1997). Glass transition is related to reversible phase transition in amorphous materials between the supercooled liquid and solid

glassy system (Kasper & Friess 2011). In an ideal drying process, it is necessary to ensure product temperature ( $T_p$ ) does not exceed the corresponding  $T'_g$ . Under this condition, structural deformation or collapse can be avoided as material fluidity is very weak when it is in solid-glassy state. Meanwhile, insufficient cooling of the material can render structural stability during drying. For example, if the solution is cooled to point  $X$  (which is higher than  $T'_g$  at that concentration), drying proceeds to point  $Y$  and with continuous heating collapse may take place due to high molecular mobility when solution is above  $T'_g$ . Detailed explanation on collapse of frozen material during dehydration is made available in section 2.2.2.

The size, distribution and shape of ice crystal formed are the key in shaping the microstructure of the freeze-dried materials and kinetics of the freeze-drying process. Studies on ice crystal formation can provide insights on the factors involved such as temperature, cooling rate and concentration during crystallization. Controlling these parameters is essential to obtain ice crystals of desired morphology thereby producing quality final dried products.

#### **2.3.1.2 Influential role of ice crystals in freeze-drying**

In freeze-drying, freezing is either carried out by shelf ramp method in which sample temperature is reduced gradually with the freeze-drier's shelf or by placing samples on a pre-cooled shelf or through immersion in liquid nitrogen. While freezing conditions affect the freeze-drying efficiency and product quality various freezing techniques have been introduced to induce ice nucleation producing ice crystals of desired sizes and shapes. A comprehensive discussion on the different freezing methods available has been reviewed by Kasper & Friess (2011) and Kiani & Sun (2011). Much of the methods presented focus on modifying the cooling rate and ice nucleation temperatures as these aspects define the crystal structure, size and size

distribution. Techniques such as quench freezing and high pressure shift freezing were shown to modify the degree of supercooling and freezing rate by promoting nucleation at low temperature for small crystals development. Meanwhile, addition of nucleating agents, ultrasonic-freezing, electro-freezing and ice-fog techniques were introduced for definite influence on the nucleation process where nucleation is triggered at the required temperature. As an example, in ice fog method the material's temperature is reduced to the desired nucleation temperature before nitrogen gas is released to the chamber initiating the nucleation process (Patel et al. 2009; Rambhatla et al. 2004). The adequacy of ultrasonic ice nucleation has been reported to control the freezing of ice-cream, potatoes, bacteria and pharmaceutical products (Mortazavi & Tabatabaie 2008; Li & Sun 2002; Kiani et al. 2013). Ultrasound provides acoustic cavitation that initiates nucleation as well as increase the heat and mass transfer rate (Zheng & Sun 2006). On the other hand, freezing with controlled temperature profiles, such as annealing may allow more complete crystallization resulting in growth of large ice crystals due to recrystallization phenomenon known as Ostwald ripening effect (Searles et al. 2001a; Hottot et al. 2007). Overall, these methods demonstrated that using a well-controlled freezing condition enables production of ice crystals with required sizes and shapes to improve the subsequent drying process and structural quality of the final dried product.

A significant number of literatures have demonstrated the correlation between characteristics of ice crystals and product quality. Formation of small ice crystals is preferred in production of most frozen goods for preservation of cellular structure (Sanz et al. 1999a; Alizadeh et al. 2007; Degner et al. 2013). The success of rapid freezing in producing high quality frozen products as a result of fine ice crystals formation has been documented for foods ranging from fruits and vegetables, (Otero et al. 2000; Sandy Van Buggenhout et al. 2005), salmon fillets (Alizadeh et al. 2007) and food emulsions (Degner et al. 2013). Also, a study on

application of microwave radiation during freezing of meat tissue showed that on increasing microwave power due to a series of brief temperature oscillations, ice crystal size was significantly reduced improving the tissue resistance towards freeze related damage (Xanthakis et al. 2014). Small crystals grow in intracellular as well as intercellular locations and are uniformly distributed causing less physical injury to the cell tissues (Kiani et al. 2011). Besides preserving the cell tissues, fine ice crystals are important in ice cream production for the sensorial quality (Caillet et al. 2003). Meanwhile, growth of large crystals can be detrimental to the cellular food matrix where deteriorative reactions such as enzymatic browning, lipid oxidation and protein degradation can be accelerated (Alizadeh et al. 2007; Gormley et al. 2002). On the other end, development of large ice crystals can be desirable in freeze-related processes such as freeze-concentration and freeze-drying (Petzold & Aguilera 2009) related to the improved transport properties in the time of processing. In these processes ice crystals determine the heat and mass transfer properties during processing in addition to the microstructure of end product. For instance, it has been shown recently during freeze-concentration of coffee extract, high solute recovery was achieved after annealing due to increased size and circularity of the ice crystals (Robles et al. 2016). Furthermore, growth of large crystals has been linked with reduced vapour flow resistance during sublimation thereby, resulted in shorter freeze-drying time (Searles et al. 2001b; Hottot et al. 2004a; Searles 2010).

Besides process efficiency, ice crystals have influential roles in determining attributes of the final dried products. One of the important features of freeze-dried products is their reconstitution property that often defines the end product quality. It is well-known that freeze-dried foods in general show a better rehydration ratio (4-6 times higher) than air-dried foods (Voda et al. 2012; Souza et al. 2011; Meda & Ratti 2005; Marabi & Saguy 2004) due to its highly porous microstructure (example in figure 2.4). Following that kinetics of freezing

determine the microstructure of freeze-dried solid and consequently the final properties, different studies have attempted to relate freezing conditions with pore structure and rate of water uptake during rehydration. Wettability of freeze-dried tropical fruit pulp has been analysed by Ceballos et al. (2012) as a function of freezing rate. A direct relationship was found between freezing rate and the duration for water to penetrate into the porous microstructure. Wettability process was recorded 3 times faster with decreasing freezing rate from 3 °C/min to 0.5 °C/min. Similarly, slow freezing was demonstrated to result in highest rehydration capacity for freeze-dried apple and rice porridge (Antal et al. 2013; Koh et al. 2011). The large ice crystals as a template for big pores increased the water uptake during rehydration as a result of reduced capillary tortuosity (Ceballos et al. 2012). Although these findings suggest that slow freezing prior to freeze-drying is preferable for high reconstitution quality, Harnkarnsujarit et al. (2016) and Voda et al. (2012) reported an instantaneous rehydration of freeze-dried bean curd and carrot subjected to very rapid freezing which forms fine ice crystals. The result was explained by the fact that capillary suction increased within the narrow entities in freeze-dried matrix. Earlier investigation by Farkas & Singh (1991) also examined the effect of freezing methods namely slow freezing to -15 °C, blast freezing and liquid nitrogen immersion on rehydration of freeze-dried chicken meat. Poor rehydration was found on sample frozen to -15 °C caused by aggregation of muscle protein which strongly suggest that properties of material being dried especially chemical composition influence the rehydration time.

It therefore appears that while ice crystallization shows determinant effect on the rehydration properties of freeze-dried products, different conclusions were made for the influence of freezing conditions on rehydration quality. This discrepancy indicates that there may be different factors involved that determine the link between porosity and reconstitution kinetics. Rehydration of dried particles is discussed further in section 2.4.

Previous studies corroborate the idea that manipulation of the freezing conditions is dependent on the end use of the solid crystal matrix and several works have shown condition in favour of large crystal growth for freeze-drying purposes (Searles et al. 2001a; Hottot et al. 2007; Ceballos et al. 2012; Antal et al. 2013). Moreover, the direct correlation between ice crystal growth on drying time found by Searles et al. (2001b) and rehydration characteristics indicates the importance of controlling ice crystals formation on process efficiency and economics as well as product quality. It is towards these aspects that the present work wishes to contribute by studying ice crystal development in high solid solutions under different freezing conditions.

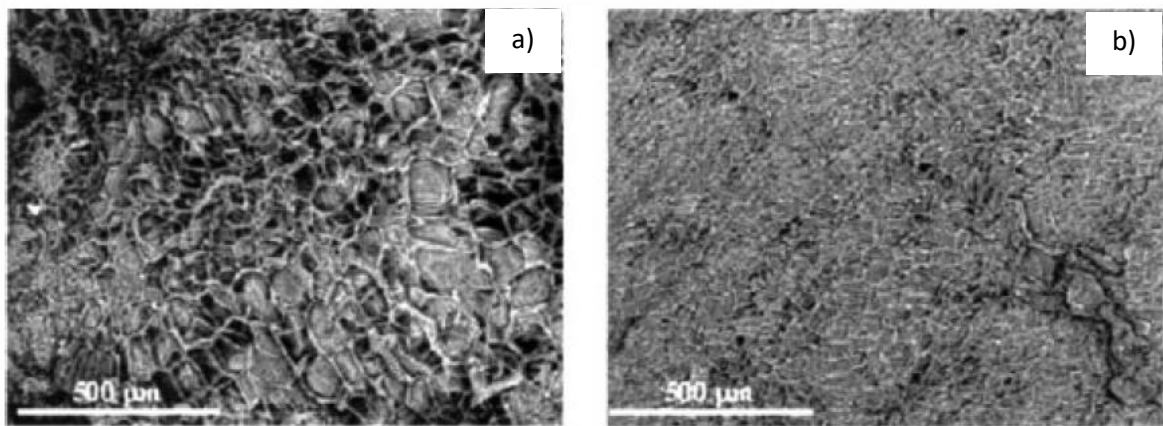


Figure 2.4 Example of different microstructure between a) freeze-dried and b) air-dried food. (SEM micrographs were adapted from Marabi & Saguy, (2004)).

### 2.2.2 Primary drying

Primary drying is an essential part of the freeze drying process involving sublimation of the ice from the frozen mass. It is known for long processing time in which majority of liquid in form of ice is removed at this stage and therefore, demand the most energy consumption for maintenance of the compressor and refrigeration units for the ice condensers (Patel et al. 2010; Jin et al. 2018). At the end of freezing, a vacuum condition is introduced to the freeze-drying

chamber by reducing the chamber pressure ( $P_c$ ) to a level lower than vapour pressure of the ice. This low pressure condition will allow direct migration of ice in form of vapour from the product (see figure 2.1). Simultaneously, heat is introduced to the system either through conduction, radiation and convection modes compensating the latent heat loss during sublimation at the freezing front. The principle driving force in primary drying is the vapour pressure difference between vapour pressure of ice in the product and ice on the condenser. This difference is a function of the temperature variation between the product at the sublimation front and temperature of the condenser.

#### **2.2.2.1 Heat and mass transfer mechanism.**

While heat travels from the heated shelf to the bottom of the freeze-drying pan or vial in the conductive manner, heat can also be supplied from the surrounding through radiation and convection. From the literatures on heat transfer mechanisms in primary drying (Ganguly et al. 2013; Pikal et al. 1984; Scutellà et al. 2017), radiation heat was pointed out to originate from hot surfaces such as door and wall of the drying chamber, shelf as well as the wall of the tray or vial. Convection on the other hand is associated with gas collision within the vapour phase. In addition, direct heat conduction from the shelf to the sample holder depends on conductivity of each medium involved. Conductivity of the materials changes continuously as sublimation proceeds affecting the drying rate. Corresponding to these heat transfer operations, the overall heat transfer coefficient ( $K_v$ ) can be expressed as the sum of three terms:

$$K_v = K_c + K_r + K_g \tag{2}$$

Where  $K_c$ ,  $K_r$  and  $K_g$  each refers to conductive, radiative and convective heating (Pisano et al. 2011).

Analysis on heat transport properties in primary drying has been conducted experimentally and numerically for process design purposes. A theoretical model was developed by Pikal et al. (1984) to estimate the involvement of conductive, radiative and convective heating during sublimation which contribute to the vial heat transfer coefficient. The relative contributions of all three mechanisms were reported to depend on the chamber pressure and type of container used for the sample. Meanwhile, the contribution of key heat transfer modes was determined experimentally by Ganguly et al. (2013) based on measurement of heat transfer rate under varied heat input, chamber pressure and vial distance from the shelf. Significant influence of heat from radiation and comparable contribution of conductive and convective heating at high pressure ( $> 0.1$  bar) during vial lyophilisation were concluded in this previous work. Also, Sadikoglu et al. (1998) employed rigorous unsteady state mathematical model to describe the dynamic behaviour of drying stages in freeze-drying of bulk solution in tray. The model presented considered the heat supply from the bottom and top surface of the materials being dried. Despite the various heat transfer modes involved, the overall heat transfer coefficient essentially was found to depend on the operating conditions applied.

As described above, the transfer of heat to the product is also followed with migration of water vapour from the top of the product to the condenser. During sublimation, vapour is required to be removed quickly in order to prevent pressure build up inside the drying chamber. This condition can increase freezing front temperature and consequently caused melting. The mass transfer process has been identified to be hindered by a series of resistance from the semi-dried materials, product container and the pathway from chamber to condenser (Rambhatla et al. 2006; Tang & Pikal 2004; Pikal et al. 1984). Resistance against water vapour flow has

considerable influence on product temperature while drying and consequently the primary drying time. Among these barriers, resistance at the sublimation interface is the parameter that can be controlled through process design while the other two are affected by equipment design. One of the most crucial aspects which determine the product resistance and eventually sublimation rate is the structural nature of the partially dried material and this has been highlighted in many literatures (Nakagawa et al. 2006; Hottot et al. 2004b; Searles et al. 2001b; Sagara & Ichiba 1994). In these studies, the pore structures were controlled to achieve minimum drying time due to reduced product resistance. Accordingly, the structural properties were related to the freezing conditions that favour formation of big ice crystals leading to increase mass transfer rate at the sublimation interface. Previous works revealed the correlation between pore structures which are the template of ice crystals formed during freezing with primary drying duration.

The success of this heat and mass controlled processing stage depends on the operating conditions applied. In practice, maintaining the balance between heat input from heated shelf and mass transport across the materials throughout the process can lead to sufficiently dried product obtained in reasonable time (Franks 1998). Different variables originating from freeze-drying conditions (shelf temperature ( $T_s$ ), pressure chamber ( $P_c$ ), condenser temperature, fill volume and sample thickness) and microstructure of the frozen mass influence the heat and mass transfer processes. Therefore, it is essential to manipulate these factors accordingly in order to attain the most suitable freeze-drying cycle.

#### **2.2.2.2 Significance of shelf temperature ( $T_s$ ) and chamber pressure ( $P_c$ ).**

Process control in the primary drying stage is related to the control of product temperature without going above the collapse ( $T_c$ ) or glass transition temperature ( $T'_g$ ) for

amorphous glass system and eutectic temperature ( $T_{eu}$ ) for crystalline matrix. Many parameters such as condenser capacity and temperature, product container and fill depth are involved in obtaining efficient process design and high quality freeze-dried products but in this review only  $T_s$  and  $P_c$  are explored. The heat and pressure applied during freeze-drying are known to influence the heat and mass transport in the sample, which determine the evolution of product temperature ( $T_p$ ) and microstructure throughout the process.

Heat input from the shelf, determined by the set  $T_s$ , indirectly controls product temperature throughout the process by providing energy for sublimation. Changes in  $T_p$  during drying can give an indication on the physical state of the product as heat transfer affects the sublimation rate. Although high  $T_s$  gives high sublimation rate thus reducing the costs associated with energy consumption, being cautious is important to avoid overheating of the materials being dried. Intensive heating can cause the product to reach above its  $T_c$  or  $T'_g$  and  $T_m$  resulting in loss of structural rigidity and poorly dried end products (Roos 1997; Franks 1998).

With respect to pressure, the sublimation rate practically corresponds to the pressure difference between pressure at subliming interface and  $P_c$  which is represented in equation 3 for vial freeze-drying (Chang & Patro 2004; Tang & Pikal 2004). In principle, lower  $P_c$  and condenser temperature would accelerate the dehydration process as this can maximize the pressure difference between chamber and ice at the product temperature ( $P_0 - P_c$ ). However large variation in heat transfer have been associated with the condition of very low  $P_c$  (Tang & Pikal 2004). Some authors have pointed out that manipulation of  $P_c$  has more significant impact than  $T_s$  on the primary drying step as the applied pressure determines the pressure difference between  $P_c$  and the sublimating front, which as mentioned earlier can play a key role on modifying the temperature of sublimation. The change in pressure affects the heat transfer coefficient ( $K_v$ )

mainly related to the thermal conductivity and permeability of the material (Araki & Sagara 2006; Sagara 2001). In addition, pressure difference is also associated with the temperature applied where optimal energy is required to maximize the vapour pressure of the product (Nireesha et al. 2013). Due to the dynamic relationship between  $T_s$ , heat input on the sample,  $T_p$  and  $P_c$ , manipulating these processing factors is important to carry out sublimation in a manner that optimize the removal of water vapour from material whilst preserving the structural integrity.

$$\frac{dm}{dt} = \frac{P_0 - P_c}{R_s - R_p}$$

(3)

Where,

$\frac{dm}{dt}$  = rate of sublimation

$P_0$  = vapour pressure of ice at sublimation front

$P_c$  = chamber pressure

$R_p$  = product resistance

$R_s$  = stopper resistance

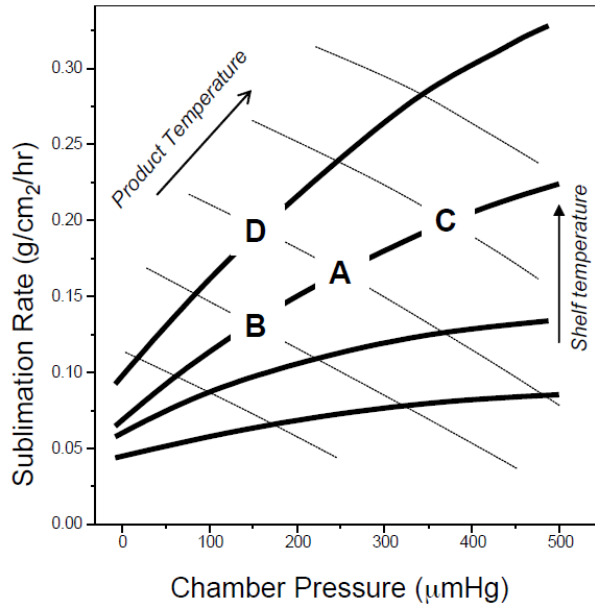


Figure 2.5 The dynamic relation between product ( $T_p$ ) and shelf ( $T_s$ ) temperature as well as chamber pressure ( $P_c$ ) on sublimation rate. Adapted from Chang & Patro (2004).

Illustration on the interdependence of  $T_s$ ,  $P_c$ ,  $T_p$  and sublimation rate in figure 2.5 showed that high drying rate without overheating the materials can be achieved through a combination of high heat input and low pressure condition. For example, consider a sample has point C as the maximum allowable temperature, a greater sublimation rate will be obtained if drying condition shifted from point B to D (increasing  $T_s$ ). While changing from B to C which increases the  $P_c$  will also improve the sublimation rate, but brings  $T_p$  close to the maximum tolerable temperature (Chang & Patro 2004). Thus, it is demonstrated that operating with temperature as high as possible while maintaining product below the critical temperatures ( $T_{eu}$  and  $T_c$ ) by lowering the pressure can lead to efficient freeze-drying cycle producing high quality freeze-dried product.

In addition, Tang & Pikal (2004) proposed the empirical equation 4 to have an initial estimation of optimal  $P_c$  with target  $T_p$  is known. Pressure derived from this equation was suggested to result in high drying rate and homogenous heat transfer.

$$P_c = 0.29 \times 10^{(0.019 \times T_p)} \quad (4)$$

Recently, predictive modelling on dry layer resistance under different range of  $T_s$  and  $P_c$  has been developed by Kodama et al. (2013). The predictive modelling was suggested to be a practical tool to have estimation on  $T_p$  during sublimation hence allowing appropriate process control. A review article by Franks (1998) highlighted two probabilities that can occur in a poorly designed process. A very slow drying and drop of product temperature can be expected when heat supplied is not enough to compensate the latent heat loss during sublimation due to low driving force. On the other hand, excessive heat supply is associated with significant viscosity reduction of the maximally freeze-concentrated solution due to product being exposed to condition above its  $T_c$  or glass transition point ( $T'_g$ ) (as mentioned in section 2.2.2.1). Under this condition, mobility of the amorphous glassy phase increase to the extent that collapse of pores can occur. Viscosity in the range of  $10^4$  to  $10^7$  Pa S proposed by Bellows & King (1972) to be responsible for the loss of structure in freeze-dried systems has been noted in different literatures (Krokida et al. 1998; Karathanos et al. 1996b; Tsourouflis et al. 1976). It is important to differentiate that the point for glass transition to occur in dried solid is denoted by  $T_g$  whereas  $T'_g$  refers to the glass transition of maximally freeze-concentrated solution. Meanwhile, crystalline materials may melt when warmed to their  $T_{cu}$  also imparting loss of structure.

Collapse during dehydration has been discussed extensively in many literatures (Trelea et al. 2007; Overcashier et al. 1999; Karathanos et al. 1996a) for it results in loss of desired product characteristics such as reduced porosity, high residual moisture content, less rehydration capacity and loss of volatile compounds (Liliana et al. 2015; Pikal & Shah 1990). In a work on collapse of fruit products, Karathanos et al. (1996) reported that volumetric shrinkage was not evident under low drying temperature, but all materials collapsed when dried above  $T_g$ . Also, quality analysis on freeze-dried fruits by Khalloufi & Ratti (2003) showed collapsed materials having discontinued microstructure with poor connectivity. Collapse as a dynamic process has been discussed by Levi & Karel (1995) who suggested that the rate of collapse increased with increasing difference between  $T_p$  and  $T_g$ ,  $(T-T_g)$  and the duration of sample under this condition. To & Flink (1978) quantitatively relate collapse of carbohydrates with moisture content, molecular weight and solids composition. A linear relationship between  $\log T_c$  and moisture content was reported. However, a linear plot was only obtained by Tsourouflis et al. (1976) when  $T_c$  was plotted against  $\log$  moisture content. The theory of distorted hydrogen bonding with additional water molecules to the system was applied in the later work to explain the effect of moisture on collapse. Accordingly, all studies showed the correlation between collapse and glass transition phenomena. These transition scenarios were pointed out to be identical in a way that  $T_c$  and  $T_g$  are similarly affected by moisture content and molecular weight (To & Flink 1978; Levi & Karel 1995). Lower  $T_c$  and  $T_g$  was related with low molecular weight substances and increasing water content. Glass transition is generally regarded as reversible while collapse is a non-reversible process and  $T_c$  has been identified to be slightly higher (by  $2^\circ\text{C}$ ) than  $T_g$  (Tang & Pikal 2004; Pikal & Shah 1990). Thus, it is relevant for thermal properties of materials to be used as the reference point in determining appropriate drying conditions which can be estimated either through thermal or microscopic analysis.

### 2.2.3 Differential scanning calorimetry (DSC)

Physical changes are known to be associated with changes in properties from crystalline to liquid state or glass to a rubber and vice versa. Differential scanning calorimetry (DSC) has been one of the approaches used in determining the temperature at which these phase transitions occur in materials to be used for designing freeze-drying cycles (Greco et al. 2013; Pikal & Shah 1990). This is a technique that examines variation in heat flow between the material under investigation and a reference material throughout cooling, heating or isothermal cycles (Liu 2006). It allows quantitative determination of enthalpy associated with crystallization, melting, glass transition and devitrification which are mainly the physical changes involved during freeze-drying. A typical DSC thermogram is presented as changes in heat flow as a function of temperature or time. Figure 2.6 shows the crystallization, glass transition and melting curves during cooling and heating for samples containing freezable water. From the curves, onset temperatures ( $T_c$ ,  $T'_g$ ,  $T'_m$ ) of different thermal events can be identified indicating point of the physical changes begin. Such information is useful for formulation development and process design as it provides insights on the physical stability of materials in maximally freeze concentrated solution.

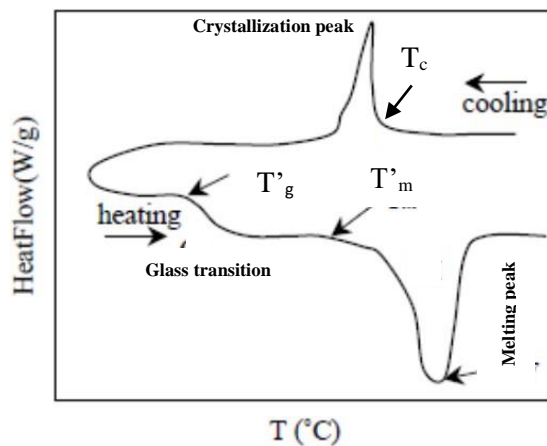


Figure 2.6 Typical DSC thermogram showing transition points that can be identified during cooling and heating cycle. Adapted from Rahman (2006)

Much of the early calorimetric studies focused on amorphous systems of, in most cases organic materials such as carbohydrate, protein and fat that form amorphous structures under low moisture and temperature conditions (Le Meste et al. 2002). A series of thermal characterization on amorphous carbohydrate solutions has been conducted by Roos & Karel (1993;1991;1990). In these studies, phase transitions mainly crystallization, glass transition and melting were studied with varied moisture content to determine the plasticizing effect of water on stability of amorphous solution. Overall, it was concluded that the point for physical changes decreases with increasing moisture content. In addition, influence of molecular weight on glass transition has been highlighted in which higher  $T_g$  values were associated with high molecular weight carbohydrates.  $T_g$  values were shown to increase in the order of disaccharides > hexoses > pentoses. The results gave an early indication on drying behaviour, water sorption and storage stability of dehydrated products. Glass transition of maximally freeze-concentrated sugar solutions ( $T'_g$ ) of less than  $-40^\circ\text{C}$  and the relative concentrations ( $C'_g$ ) at 80% on average were also reported in the later study. This knowledge on stability of the freeze-concentrated solutions is particularly importance in designing optimal drying conditions.

Other works have also proven the efficacy of DSC technique to provide information on the maximum allowable drying temperatures particularly the glass transition and melting. Recently, data from DSC analysis were used for construction of state diagram that details the different physical states of sugar solutions as a function of temperature (Ruiz-Cabrera et al. 2016). Initially, amount of water in the ternary sugar mixture was identified to influence the transition temperatures in which reducing water content from 0.8 to 0.35 (g solid/g sample) reduced the freezing point by  $14^\circ\text{C}$ . Decreasing  $T_g$  due to the plasticizing effect of water was also observed on increasing amount of water which is known as the main plasticizer for amorphous carbohydrates. Also, development of the state diagram demonstrated small variation

in the onset melting ( $T'_m$ ) and glass transition ( $T'_g$ ) of maximally freeze-concentrated solutions between the concentrations but were significantly affected by types of sugar. The investigated sugar solutions; glucose, fructose and sucrose showed  $T'_m$  in the range of  $-43$  to  $32^\circ\text{C}$  and  $T'_g$  from  $-56$  to  $-43^\circ\text{C}$  with the maximum and minimum values corresponded to sucrose and fructose solutions respectively. These variations were affected by the different in molecular weight of sugar studied. Meanwhile, quite similar  $T'_g$  between  $-42$  to  $-34^\circ\text{C}$  has been determined by Sacha & Nail (2009) for sugar solutions with 2-58% sucrose. In case of solution with different solute mixtures, Seo et al.(2006) proposed that size and shape of sugar molecules can affects  $T_g$  of the sugar mixtures. In the study, modified Gordon-Taylor equation was applied to analyse  $T_g$  of monosaccharide–disaccharide and monosaccharide–trisaccharide mixtures.

The observed trends from earlier investigations show that physical changes are dependent on the solution characteristics; concentration, molecular weight and mixture of solutes. In light of these factors having influence on the phase transitions during freezing and freeze-drying, the present work conducted thermal characterization on a series of concentration of gum arabic and coffee solutions. This experiment was aimed to understand the principle behind the effect of amount and types of solutes investigated on crystallization, melting and glass transition temperatures.

#### **2.2.4 Secondary drying**

At the end of sublimation, the amorphous solid still contains 5-20% unfrozen water (Pikal et al. 1990). In order to have dried solid with less than 1% residual moisture, shelf temperature ( $T_s$ ) is elevated above ambient temperature,  $>25^\circ\text{C}$  (Tang & Pikal 2004; Lopez-Quiroga et al. 2012). High temperature condition enable diffusion, desorption and evaporation

of water molecules from the amorphous structure. Although operating at temperature well above primary drying, the principle of maintaining product below its glass or collapse temperatures is as much important as in the primary drying stage. The early stage of secondary drying, where the material still contain high residual moisture, constitutes high risk of collapse. For this reason, gradual temperature transition has been proposed during heating from primary to secondary drying in preventing loss of porous structure (Tang & Pikal 2004; Patel et al. 2010). Raising the  $T_s$  too early can also lead to structural collapse due to risk of ice melting as the secondary drying proceeds without all of the ice being removed. Therefore, several approaches based on monitoring temperature and pressure changes were introduced to determine the end point of sublimation (Patel et al. 2010). Knowledge on when primary drying ends is important to prevent desorption and evaporation from sample containing residual ice.

In secondary drying, diffusion of water within the solid structure and evaporation at the solid-vapour interface were considered as the rate limiting mass transfer process. Analysis on kinetics of secondary drying by Pikal et al. (1990) showed that high  $T_s$  and specific surface area of material as well as low initial concentration increase the rate of water removed. Also, no apparent effect of chamber pressure ( $P_c$ ) on drying kinetics was found, suggesting that low pressure does not necessarily speed up secondary drying. Recently, ice nucleation temperature ( $T_n$ ), which determine the size of crystal, was reported to be one of the factors that control the rate of water desorption from dried solid. In the study, Oddone et al. (2017) found that large ice crystals from high  $T_n$  freezing slows down the desorption process due to low specific surface area of the product. However, faster overall drying time (primary and secondary drying) was also obtained with increasing  $T_s$  that decreased the increment of secondary drying time. Excel based modelling developed by Sahni & Pikal (2017) further confirmed the direct relationship

between operating temperature and material properties on kinetics of the water removal. These previous findings indicate the importance of controlling microstructure on efficiency of drying.

Ideally, the final dried product will have very low residual moisture content and porous solid structure. These characteristics are important to develop a dehydrated product with long shelf stability and high rehydration quality.

### **2.3 Characterization of food microstructure**

The concept of process-structure-property relationship has gained considerable attention in modern food processing. This development is driven by the fact that most food structural elements control product acceptability and quality. For instance, dispersion of ice crystals, air and fat globules in ice-cream determine its creaminess and cooling sensation (Petzold & Aguilera 2009). Also, spreadability of margarine and butter is influenced by the interaction between fat globules and water molecules as emulsion systems (Heertje 1993). Although air bubbles or other gasses are very light, they are important in regulating the texture properties of bread, whipped cream, mousses and carbonated drinks (Kaufmann & Palzer 2011). Meanwhile, transport phenomenon including reconstitution properties of dried foods such as ready to eat meals, instant coffee and soups as well as oil uptake during frying are too affected by the air fraction present.

In principle, food microstructure is the result of processing techniques or conditions applied. Processing steps such as freezing, overrun and hardening in ice-cream making affect the distribution and size of air bubbles as well as ice crystals (Caillet et al. 2003). As mentioned previously, freezing conditions during freeze-drying also showed determinant effects on morphology of freeze-dried cake consequently its rehydration properties (Harnkarnsujarit et al.

2016; Ceballos et al. 2012). Correlation between drying temperature and porosity of freeze-dried foods has been investigated in a series of studies by (Sablani et al. 2007; Sablani & Rahman 2002; Rahman 2001). High drying temperature was found to reduce percentage of open pores in freeze-dried garlic whereas opposite trend on porosity development was identified for apple and yellow dates. In the literature, the significance of understanding food microstructure characteristics for process design has been highlighted to create products with preferable quality traits and functional properties (Petzold & Aguilera 2009; Aguilera 2008; Aguilera 2005).

There are several parameters commonly used to characterize food microstructure. Porosity in terms of pore size distribution, connectivity, fraction of open and closed pores are being quantified to define porous structure of dried food (Rahman 2001). Information about the size, distribution and shape of ice crystals were used to describe the properties of frozen meat (Sanz et al. 1999b), food emulsion (Degner et al. 2013) and salmon (Alizadeh et al. 2007). Also, distance between particles and tortuosity have been included to characterize microstructure of dairy products (Silva et al. 2015). Several high magnification imaging techniques have evolved in the past decades to derive the aforementioned quantitative information. Electron microscopy and tomography approach are extensively applied in visualizing food microstructure.

### **2.3.1 Electron microscopy**

The discovery of electron optics has led to development of electron microscopy which is a useful tool in studying food structure under wide range of magnification from macroscopic down to less than a nanometer. This imaging technique differ with light microscope mainly by the use of electron beam instead of light to focus on the sample. Scanning electron microscopy (SEM), cryo-SEM, environment SEM (ESEM) and transmission electron microscopy (TEM)

are among the instruments usually used in conjunction with studying food microstructure. Several main components of these microscopes are electron gun for emission of high energy electrons, vacuum system allowing electrons to be accelerated and focused towards sample and detectors to collect signals from interaction between sample and electrons.

### **2.3.1.1 Scanning electron microscopy (SEM)**

In the present study, scanning electron microscopy (SEM) has been employed for visualisation of freeze-dried structures. The principle behind this electron microscopy involves scanning a focused beam of high energy electrons pixel by pixel across material surface where electrons lose energy once encountered with material's surface. This interaction produces secondary signals listed as heat, X-rays, secondary and backscattered electrons as illustrated in figure 2.7. These signals are then collected by detector to reveal topographical, morphological and compositional information of the surface. Secondary electrons are the results of energy absorbing scattering of primary electrons and emitted close to the surface providing topographic characteristics of material. Meanwhile, backward scattering produced backscattered electrons with energy about 50eV up to the energy of primary electrons. This slight higher energy than secondary electrons give rise to image that reflect compositional information. X-ray energies enable microanalysis that reflect chemical elements of the samples through energy dispersive spectroscopy (EDS) detection (Stokes 2013). While SEM works with moderate electron energies around 10keV, it is able to produce 3 dimensional (3D) images with nanometer resolution (Klang et al. 2013).

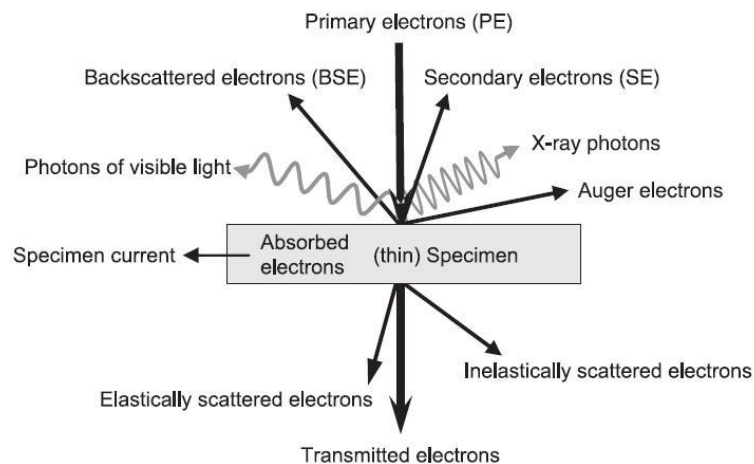


Figure 2.7 Diagram on signals produced after interaction of specimen with electron beam.  
Adapted from Stokes (2013)

The high resolution SEM micrographs has allowed characterization of goat cheese curd showing differences in protein matrix at different processing steps (Rovira et al. 2011). In the same study, processing of SEM images led to quantification of pore number, area and perimeter, strand thickness, and porosity. The reduced stickiness of powder particles imparted by addition of carriers during spray drying of mango juice was made visible using SEM observation showing differences between crystalline and amorphous surface (Cano-Chauca et al. 2005).

This microscopic evaluation has also been successfully applied in previous studies for characterization of freeze-dried solids. Correlation between freezing conditions with pore morphologies was obtained through SEM observation. SEM images from investigations by (Harnkarnsujarit et al. 2016; Harnkarnsujarit et al. 2012) provide evidence of the reduced pore sizes with increasing freezing rate. Meanwhile, SEM micrographs of fresh and freeze-dried garlic clearly revealed the influence of drying temperature on pore formation. It was shown that high shelf temperature ( $-5^{\circ}\text{C}$ ) resulted in freeze-dried garlic with less open pores than samples dried at  $-15$  and  $-25^{\circ}\text{C}$ . Also, Voda et al. (2012) carried out microstructural observation on freeze-dried carrot to analyse the influence of thermal pre-treatments on stability of cellular

tissue. The cellular structure of freeze-dried hydrocolloids observed under SEM illustrate the variation of cell wall thickness, cells area, elongation and roundness between gel systems studied.

### **2.3.1.2 Cryo-SEM**

Cryo-SEM is an important imaging technique for frozen product in order to characterize ice crystals. Contrary to SEM, the low temperature operation enabling direct observation of ice crystals without thawing. Although it only requires simple physical fixation, formation of ice during transfer of samples may interfere with observation of main ice crystals on samples surface. Thus, additional step of sublimation is carried out in the cryo-chamber before coating to remove unwanted surface ice (Klang et al. 2013). Nevertheless, artefacts from chemical fixation, structural collapse or shrinkage can be avoided.

Fernández et al. (2006) employed cryo-SEM in observation of frozen gelatin gel to study the effect of high pressure freezing on microstructure. The efficacy of this method to monitor ice recrystallization in sugar solutions at temperature range closed to glass transition temperatures (-21 to -50°C) was shown by (Hagiwara et al. 2005). Changes in microstructure of potato tissues affected by ultrasound assisted freezing has been monitored with cryo-SEM in which the detrimental effect of extracellular ice crystals on cell wall integrity was displayed (Sun & Li, 2003).

### **2.3.1.3 Environmental SEM (ESEM)**

In order to ease sample preparation and increase range of application of SEM, ESEM was developed. Operating under non-vacuum condition offers advantages for scanning

hydrated and liquid samples. Development on the use of this instrument in conjunction with food structure has been reviewed in James (2009) discussing various applications in static and dynamic environment. Donald et al. (2000) has demonstrated the suitability of ESEM in characterizing colloidal dispersion whereas Noronha et al. (2008) showed that ESEM allows detailed and truer visualisation of protein matrix and fat globules in cheese.

#### **2.3.1.4 Transmission electron microscopy (TEM)**

As the name implies, an image from TEM is generated based on electrons that passed through the sample rather than the collection of scattered electrons used for SEM. This imaging principle produces 2D image detailing the structure beyond materials surface and can be seen on fluorescent screen or digital camera (Eddleston et al. 2010). Observation with TEM offers high spatial resolution down to 0.07nm (Datye 2003) as electron is transmitted to very thin sample usually less than 100nm. The high resolution advantage has made it a valuable tool to study interfacial structure and states of protein in various types of dairy products for example, yoghurt (Kabláb 1993), whey protein gels (Langton & Hermansson 1996) and processed milk (Hillbrick et al. 1999).

#### **2.3.1.5 X-ray computed tomography (XRCT)**

Internal structure of freeze-dried systems in the current work has also been visualised using X-ray Computed Tomography (XRCT) which is a non-invasive 3D imaging method significant in the medical field, material and food sciences. Image projection in this technique is based on the difference in X-ray attenuation generated by density difference within material. A series of radiographs is recorded as X-ray beam is focused on the sample. Rotation of the

sample provides a sets of 2D projected images that are later stacked using suitable computed reconstruction algorithm to reconstruct 3D image.

In XRCT, spatial resolution of the image projected is controlled by the X-ray source, position of the sample between source and detector as well as size of the sample being scanned. Resolution in the range of 100-200 $\mu\text{m}$  is common in most instruments and with further development of microtomographic imaging, resolution down to nano meter scale has been made possible (Landis & Keane 2010). As a rule of thumb, finer microstructural details (high resolution) can be visible in the image with micro focus X-ray, closer distance between sample and source as well as small sample size (Landis & Keane 2010). However, the choice of these factors is usually a trade-off between the required resolution, area of field of view and scanning time ( Barigou & Douaire 2013; Paulus et al. 2000;). Different maximum achievable resolution power has been reported including resolution of 4 $\mu\text{m}$  for resolving porosity of pharmaceutical granules (Farber et al. 2003) and freeze-dried carrot (Dalen et al. 2013) whilst higher resolution at about 8 $\mu\text{m}$  was used for quantifying bread crumb's microstructure (Falcone et al. 2005). Meanwhile, Babin et al. (2007a) selected 10 and 40 $\mu\text{m}$  as resolution for extruded starch cut into small and large dimension respectively to have representative volume of the sample.

The adsorption mode of tomography made it useful to characterize cellular food products where porosity and pore size distribution determine to a large extent the physical, textural, sensory and functional properties. Microstructural investigations with XRCT has been applied in detailing the spatial cell size and cell wall thickness distribution, connectivity and porosity of various types of foods. Recently, Cafarelli et al. (2014) were able to correlate the size and geometrical aspects of bubbles in bread using this technique. Fast XRCT experiments has been carried out to follow growth of bubbles during bread making providing real time information on microstructural evolution (Babin et al. 2006). Other applications include the

study of relationship between cellular structure and mechanical strength of extruded starch foam (Babin et al. 2007b), internal structure of carrot in freeze-dried, rehydrating and rehydrated form (Dalen et al. 2013) as well as microstructure differences in coffee beans before and after roasting (Frisullo et al. 2012). In addition, Mousavi et al. (2007) have demonstrated the ability of XRCT to describe ice crystals structure of frozen mycoprotein products. In the analysis, freeze-drying was carried out prior to scanning to remove moisture from the frozen sample. In order to extract 3D quantitative information from XRCT images of various aerated confectionaries and bread crumb, Lim & Barigou (2004) and Falcone et al. (2005) proposed image analysis with stereological technique and calculations.

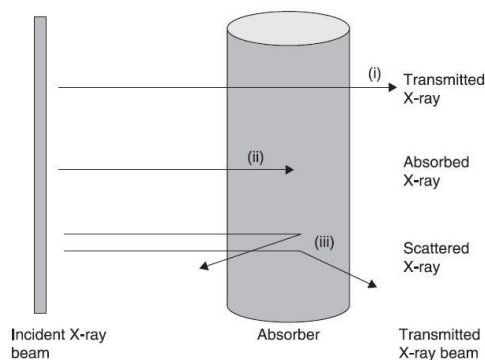


Figure 2.8 Schematic on interactions of X-ray with a substance. Adapted from Barigou & Douaire (2013)

#### 2.4 Significance of water transport properties during rehydration

The growing demand for convenient food has made reconstitution an important quality trait for dried foods. It is important to consumer that dehydrated products can easily and quickly dissolve. Rehydration can be described as the process of wetting, disintegration and dissolution of solid particles in solvent (Forny et al. 2011). Wetting as an initial step is of particular importance where it involves movement of water across and within the dried solid and can cause swelling. In addition to the significant role of microstructure on kinetics of rehydration

(Voda et al. 2012; Souza et al. 2011; Krokida & Philippopoulos 2005), different mechanisms during water uptake also exert influential effect on the reconstitution phenomena. Molecular diffusion, capillary imbibition and molecular relaxation related to swelling are among the additional factors recognized to govern the reconstitution process (Marabi et al. 2003). These physical mechanisms can be affected by properties of the materials being dissolved which include molecular structure, composition and molecular weight. For example, due to different porosity and chemical composition between conventionally dried apple and potato, imbibition of water in these dried fruits were followed by different changes in mass and volume (Witrowa-Rajchert & Lewicki 2006). The porous structure of apple led to more rapid mass gain than the volume increment whereas starch in potato considerably absorbed water and swelling was observed to cause faster increase in volume compared to the relative increase in mass. Based on this observation, this report highlighted that the process of water absorption during rehydration can either related to filling of voids formed upon drying (the case for apple) or to the penetration into the solid matrix (as demonstrated by potato), depending on the type of material used, especially its chemical composition.

With increasing recognition on the water transport mechanisms, numerical analysis based on Weibull's distribution function (see equation 5) has been proposed in several studies.

$$\frac{M_t}{M_\infty} = 1 - \exp(-kt^n)$$

(5)

Where;

$M_t$  = mass dissolved at time  $t$

$M_\infty$  = mass dissolved at equilibrium

$t$  = time

$k$  = rate constant

$n$  = shape parameter

This generic empirical equation is typically used in drug dissolution/release studies (Kosmidis & Macheras 2007; Skrdla 2007; Papadopoulou et al. 2006) but has also been shown to be applicable in describing the physical mechanisms associated with rehydration of dried food (Souza et al. 2011; Garcia-Pascual et al. 2006; Machado et al. 1998). It is typically described with process rate constant (k) and shape parameter (n) which indicates the possible transport properties and shape of dissolution curve (Cascone 2017; K.H et al. 2014). Although has been criticized for lack of kinetic fundamental, the Weibull equation is of particular interest due to the physical meaning associated with the parameters (Martínez et al. 2009). The estimates of exponent n were used to differentiate the principle movement of water that govern the rehydration process. The classification was based on Fickian diffusion and non-Fickian diffusion (e.g. capillary imbibition, relaxation mechanisms or combination thereof) generally used for polymeric substances (Marabi et al. 2003; Peppas & Brannon-Peppas 1994). It has been interpreted by Cunha et al. (1998) that a small value of the shape parameter ( $n \leq 0.75$ ) indicates diffusion controlled process whereas external resistance and molecular relaxation become the rate limiting factor when n value is close to 1 or higher. Similarly, Machado et al. (1998) has suggested internal diffusion play an important role during rehydration of breakfast cereals reporting lower shape factor around 0.50. Evaluation of rehydration kinetics between air-dried and freeze-dried carrots with normalized Weibull's equation has also revealed the different water movement between samples during rehydration (Marabi & Saguy 2004). In this study, Fickian diffusion was associated with rehydration of air-dried carrot while more porous structure of freeze-dried carrot has been suggested to follow capillary imbibition based on the derived shape parameter.

These studies highlight that understanding the different water transport mechanisms is an important factor to consider in describing reconstitution properties of dried foods.

## 2.5 Materials

### 2.5.1 Gum Arabic

Gum arabic is recognized as a gummy exudate from *Acacia tress* grown abundantly in the African region. It is an important hydrocolloid found in food and non-food industries such as in pharmaceutical, textile and cosmetic production (Sanchez et al. 2017). As a food additive, gum arabic is used to influence the viscosity, body and texture of food thereby, inducing desirable characteristics.

This highly branched polysaccharide was identified to have a core structure of  $\beta$  1,3-galactopyranose with  $\beta$  1,6-galactopyranose linked side chains consisting of galactose, arabinose, rhamnose and glucuronic acids (Osman et al. 1993). Significant number of studies have been done on the molecular characterization in order to relate to its unique functional properties (Randall et al. 1989; Osman et al. 1993; Al-Assaf et al. 2007; Sanchez et al. 2008; Gashua et al. 2016). Fractionation through chromatography techniques performed in these investigations consistently show that gum arabic constitutes of three main fractions which differ in molecular weight and protein content. The molecules identified are arabinogalactan with molecular weight of  $2.9 \times 10^5$  g mol<sup>-1</sup> and accounts for about 90% w/w of total gum followed by arabinogalactan-protein and galactoprotein each around 10 and 1 % w/w of the whole gum with molecular weight of  $1.9 \times 10^6$  g mol<sup>-1</sup> and  $2.5 \times 10^5$  g mol<sup>-1</sup> respectively.

The complex mixture of hydrophilic carbohydrate and hydrophobic protein have great influence on its physicochemical quality which determine the functional properties. Gum arabic is known to dissolve well in aqueous solutions in comparison to other gums where it is soluble up to 50% w/v concentration. However, dispersion becomes difficult at higher concentration due to self-aggregation of molecules with increasing solute fraction (Sanchez et al. 2017). The

contradiction between having good solubility and tendency for molecular aggregation can be associated with the high protein content in glycoprotein fraction and its hydrophobic nature (Renard et al. 2006). Emulsifying properties is considered the most important physicochemical features of gum arabic. Research on emulsification properties of this natural gum showed that fraction of arabinogalactan-protein is mainly responsible for the emulsion stability (M. et al. 2011). For instance, emulsifying ability was improved by increasing the proportion of arabinogalactan-protein through Maillard reaction demonstrating that this fraction is responsible for the emulsification properties (Al-Assaf et al. 2007).

These physicochemical properties of gum arabic made it possible to be used either as thickener, stabilizer, encapsulating agent or emulsifier in food products such as confectionery, beer brewing and soft drinks (Sanchez et al. 2017). As an example, for the good oil binding property of the protein region, gum arabic is commonly used to emulsify flavour oil in soft drinks to maintain uniform dispersion of oil in the product. In addition, gum arabic is added to alcoholic beverages for stabilization of foam and colour pigment. Gum arabic is also an important ingredient in confectionery to prevent or retard sugar crystallization. The nutritional aspect of gum arabic has also been highlighted where it has been recognized as natural source of dietary fiber improving the gut health (Glover et al. 2009; Phillips & Phillips 2011; Khalid et al. 2014).

## **2.5.2 Coffee**

Coffee known for its stimulating aroma and taste is among the most preferred drinks worldwide making it one of the largest traded commodity (Mussatto et al. 2011). Out of the 70 species of coffee beans derived from *Coffea* L. plant, arabica and robusta are the only species

widely exploited for commercial production. Coffee beverage is typically made directly from roasted beans or dried extract.

In principle, several processing steps are applied in making coffee beans suitable for consumption as drinks. The coffee production begins with de-husking or pulping of green cherries to reveal the green bean. After green bean cleaning, roasting is carried out for development of its distinctive flavour, aroma and colour where chemical reactions and chemical-physical changes such as dehydration, non-enzymatic browning and pyrolysis take place (Frisullo et al. 2012). This step is followed by cooling and grinding before being prepared for shipment. In case of instant coffee production an invention of the 20<sup>th</sup> century, volatile compounds and soluble solids are extracted from the ground coffee prior to drying. The extract is more often dried using spray or freeze-drying techniques to yield shelf stable soluble coffee powder and granules. These dehydration technologies mainly differ in terms of the range of temperature and pressure involved as well as operating costs. The high temperature used in spray drying provide high production capacities at low energy costs yet there is concern about the thermal impact on volatile compounds. In contrast, freeze-drying is an expensive technology but yield instant coffee with high volatiles retention and porous microstructure (Burmester et al. 2011).

Carbohydrates are the main constituent in coffee and are responsible for the sensorial appeal of the coffee beverage. It can be grouped into low and high molecular weight substances. Sucrose is an important low molecular mass carbohydrate involved in Maillard reaction during roasting for colour and flavour development. High molecular weight polysaccharides help to provide creamy sensation to the drink by increasing its viscosity (Nunes & Coimbra 2002). The principle polysaccharides present in coffee are arabinogalactan-proteins, galactomannans and cellulose where high roasting temperature significantly alter the structure and number of these

compounds. Among other chemical compositions traced in coffee are protein, lipids, caffeine and chlorogenic acids which also experience many changes during roasting except for the thermal stable caffeine. Thus, the final chemical compounds in coffee beverages depends on the extend of roasting affecting the sensorial properties perceived by consumers.

Coffee drinks can be prepared either from ground roasted beans or dried coffee extract usually in powder or granule form. Instant coffee powder/granule offers convenience to coffee drinkers. Aroma, flavour and solubility are the key characteristics that define quality of this product. Factors ranging from the species of coffee bean used, roasting of the beans and dehydration of the coffee extract have significant influence on the quality instant coffee.

## **2.6 Conclusion**

Freeze-drying is known to produce highest quality dehydrated products mainly related to preservation of primary structure, good rehydration properties and minimal loss of heat sensitive ingredients. These advantages are however, achieved at high operating and maintenance costs coming from the long duration of drying under continuous vacuum and sub-zero temperature. Literature studies have shown the interrelated relationship between processing conditions and process efficiency as well as the attributes of final product. In process design, freezing and primary drying conditions are often manipulated due to the significant impact on microstructural development which controls the process cycle and product quality. Many researches have included microstructural evaluation in their studies to understand the effect of process variables on drying kinetics and characteristics of end product.

Food products typically contain 40-80% of water in which large energy input is associated with the solidification and sublimation process. In the era of sustainable

development, manufacturers are motivated towards development of energy efficient processes. Thus, freeze-drying of high solid formulations are investigated in this study for its potential to reduce the energy intensity associated with freeze-drying. As small fraction of water is involved, understanding the thermal properties and structural changes of concentrated system during freeze-drying would be useful towards the economical process design. The influential role of glass transition ( $T_g$ ), collapse ( $T_c$ ) and melting temperatures ( $T_m$ ) in determining process variables has also been presented in this chapter to highlight the importance of formulation properties such as solid content and composition in process design. Gum arabic and coffee solutions of various concentrations (20-60% w/w) are used as model and real food examples in this investigations to compare the freeze-drying behaviour and microstructure as well as reconstitution properties of the freeze-dried solids.

## **CHAPTER 3**

### **Materials and methods**

#### **3.1 Materials**

Gum arabic and coffee were used in this work to represent model and real food systems respectively. These materials were selected as both share identical polysaccharide known as arabinogalactans. Gum arabic powder from acacia tree was supplied by Sigma-Aldrich Co. (Gillingham, UK) and freeze-dried coffee granules (Douwe Egberts/Kenco) were purchased from local supermarket (Sainsbury) in Birmingham, United Kingdom. Preparation of solutions with re-dissolved instant coffee enable concentration to be easily adjusted (Burmester et al. 2011). Also, the selected instant coffee was free from other ingredients besides roasted coffee bean (ingredient list). Materials were kept in air-tight container to prevent moisture absorption and stored in a cool and dry place until usage.

Distilled water was used as solvent in solutions preparation and dissolution experiments.

#### **3.2 Methods**

##### **3.2.1 Preparation of samples**

Materials were weighed accordingly and mixed with distilled water to prepare solutions of 20, 30, 40 50 and 60% w/w solute. Laboratory hot plate was used to control heating between 45-50°C and mixing at 250 rpm during sample dissolution.

Degassing was applied to each solution to remove excess air bubbles incorporated during sample preparation. Ultrasonic cleaning bath with degas function (USC 300-THD, 45Hz, VWR International Ltd, Leighton Buzzard, UK) shown in figure 3.1 was used to degas the coffee

solutions while air bubbles in the gum arabic solutions were removed manually after overnight gravimetric separation at room temperature (20°C).



Figure 3.1 Picture of ultrasonic cleaner used for de-gassing.

### 3.2.2 Aeration

In studying the effect of air on microstructural development of high solid solution, aeration was applied for samples with 50 and 60% solute (w/w). Aerated systems were prepared by incorporating 30-40% of air into the degassed system using domestic food processor (Kenwood Mini Chopper - CH180A 300 Watt, Kenwood Limited, Havant, UK). The amount of air added were controlled by initially determining the duration of aeration required to achieve density of  $0.8\text{gcm}^{-3}$  and  $1.2\text{gcm}^{-3}$  each for coffee and gum arabic solutions.

### 3.2.3 Freeze-drying cycles

Virtis Advantage Plus Benchtop shelf based Freeze-Dryer (SP Industries, Warminster, PA) was used to carry out the freeze-drying experiments. Carbon steel baking tins with internal diameter of 9.5cm and 2.5cm height (figure 3.2) were used to fill the sample until 0.5cm height equivalent to 28ml is reached. These trays were carefully placed on a stainless steel tray and loaded on to the freeze-drier shelf.

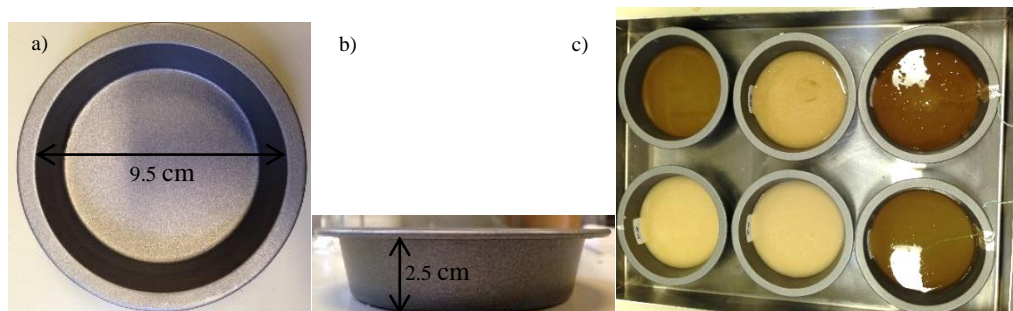


Figure 3.2 Picture of: (a-b) carbon steel baking tin used to fill sample and c) samples loaded on stainless steel tray

Several freeze-drying cycles involving different freezing and primary drying conditions were investigated in this work. The condenser temperature and chamber pressure was kept at  $-80^{\circ}\text{C}$  and 0.1mbar respectively for all cycles.

### 3.2.3.1 Different freezing step

In experiments for varied freezing steps, two freezing units namely freeze drier and rapid freezer both operating at  $1^{\circ}\text{C}/\text{min}$  were utilized. The freezing unit in freeze-drier was used for temperature oscillation experiment. In this set of investigation, shelf-ramped freezing method was applied where sample's temperature was reduced gradually with shelf temperature to the freezing set point,  $-40^{\circ}\text{C}$  (Kasper & Friess 2011). After freezing temperature is reached, samples were either subjected to temperature fluctuation between  $-20$  and  $-40^{\circ}\text{C}$  for 4hr with 30min holding at each temperature followed by 2hr tempering at  $-40^{\circ}\text{C}$  (shown in figure 3.3) or kept at  $-40^{\circ}\text{C}$  for 6hr prior to sublimation. Product temperature during freezing were recorded onto a computer equipped with Mentor and Wizard software from The Virtis Company, NY.

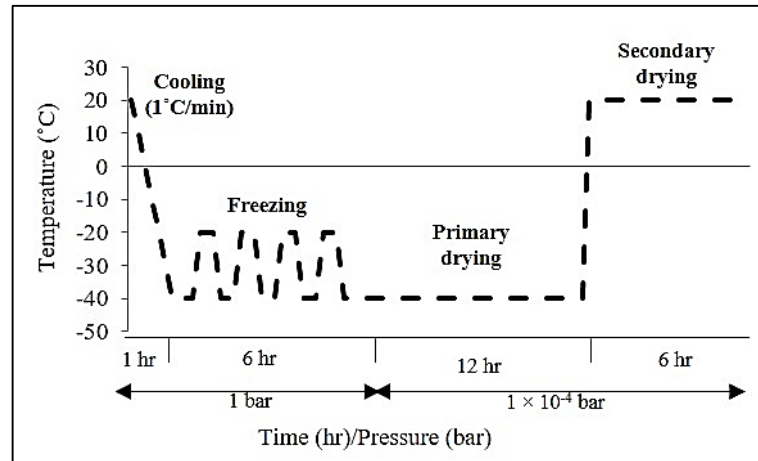


Figure 3.3 Freeze-drying cycle with temperature oscillation in the freezing step.

Meanwhile, rapid freezer shown in figure 3.4 (Bright Clini-RF, Bright Instruments Ltd, Luton, UK) was used for the set of study on the effect of different cooling rates. For freezing in rapid freezer, samples were either placed on shelf that has been pre-cooled to  $-40^{\circ}\text{C}$  (PC) or cooled with shelf ramping (SR) technique to generate slow ( $1 \pm 0.13^{\circ}\text{C}/\text{min}$ ) and fast ( $5 \pm 2^{\circ}\text{C}/\text{min}$ ) cooling conditions respectively (see figure 3.5). K-type temperature probes were carefully positioned at the middle of the aluminium tray using strong adhesive tape to avoid dislocation of the thermocouples. The cooling profile of samples to reach the desired freezing temperature was recorded with a data logger (Pico-log TC-08, Cambridgeshire, UK). Frozen samples were then transferred to the freeze-drier chamber that has been pre-cooled to  $-40^{\circ}\text{C}$  to prevent samples from melting.

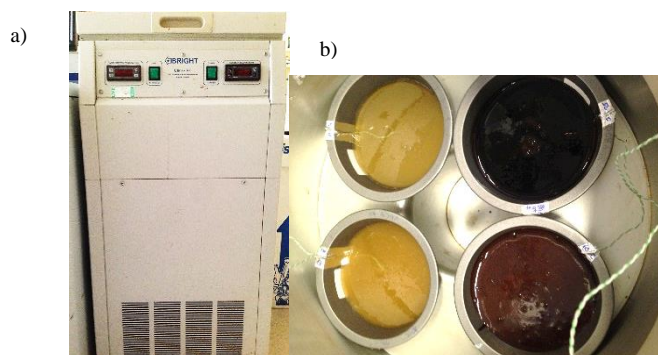


Figure 3.4 Picture of: a) Rapid freezer used for freezing; b: Samples inside the rapid freezer

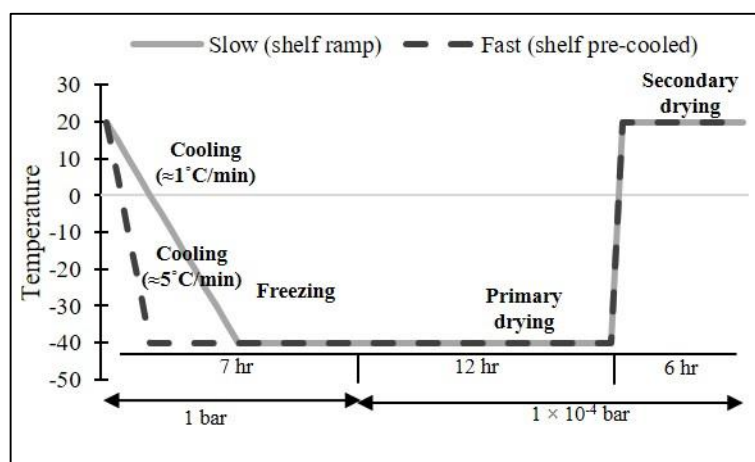


Figure 3.5 Freeze-drying cycles with different cooling profiles; slow (shelf ramp, SR) and fast (pre-cooled shelf, PC)

A rapid freezer was also used for unidirectional freezing and the apparatus used for this experiment is shown in figure 3.6. A plastic syringe (1.5 cm height and 2.6 cm diameter) covered at the bottom with paraffin film was used as the sample holder. The solution was filled until 0.5cm height is reached to give 2.65 cm<sup>3</sup> of volume. The freezing cylinder was then insulated with polystyrene foam to ensure heat travel specifically from the bottom. A temperature probe was carefully placed at the middle section with approximately 0.3cm distance from the bottom. The sample was then placed on a stainless steel plate before being frozen in the rapid freezer with shelf-ramp technique. A Pico-log data logger was used to record the freezing profile of each sample.

Total freezing time for all investigated conditions was kept constant at 6hr with 1hr of cooling from room temperature to the set freezing temperature. Triplicate samples were used and nucleation as well as freezing temperatures were derived from the cooling curves.

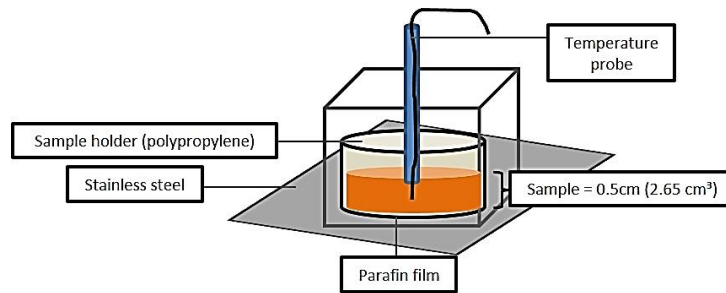


Figure 3.6 Illustration on insulated sample holder used in unidirectional freezing

### 3.2.3.2 Different primary drying conditions

The effect of heat input during sublimation phase on structural development was studied by controlling the shelf at three different temperatures namely -20, -30 and -40°C (figure 3.7). The freeze-drying protocols were studied on solutions with 20, 30, 40, 50 and 60% solid content.

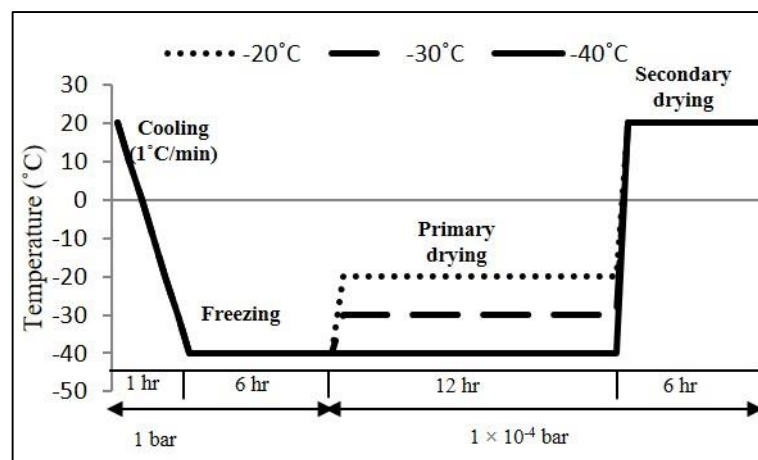


Figure 3.7 Freeze-drying cycles with different primary drying temperatures: -20°C, -30°C and -40°C.

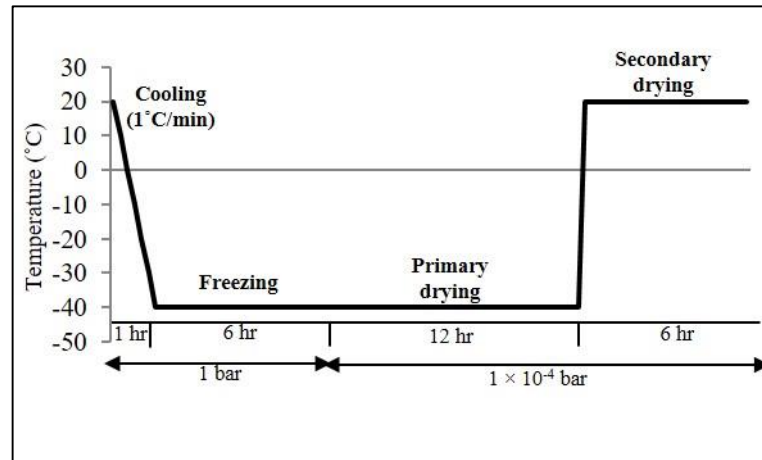


Figure 3.8 Freeze-drying cycle for control condition

A control freeze-drying process illustrated in figure 3.8 was conducted for comparison with the different cycles investigated. In this condition, solutions were cooled to  $-40^{\circ}\text{C}$  and maintained at this temperature for 6 hr to freeze the samples. The vacuum pump was switched on to continue drying at  $1 \times 10^{-4}$  bar from  $-40^{\circ}\text{C}$  to  $20^{\circ}\text{C}$  for another 18hr.

### 3.2.4 Differential scanning calorimetry (DSC)

State and phase transitions of the (degassed) gum arabic and coffee solutions were analysed with a differential scanning calorimeter (DSC, Mettler Toledo 822e with liquid  $\text{N}_2$  cooling) from Mettler Scientific Instruments, Göttingen, Germany. Approximately 7-18mg of sample was placed on a pre-weighed  $40\mu\text{l}$  DSC aluminium pan before being hermetically sealed. An empty aluminium pan was used as reference and both pans were scanned from  $20$  to  $-80^{\circ}\text{C}$  at  $1^{\circ}\text{C}/\text{min}$ , then held at  $-80^{\circ}\text{C}$  for 5min and finally heated to  $20^{\circ}\text{C}$  using the same rate. Meanwhile, thermal profile of 60% gum arabic was obtained by scanning from  $50^{\circ}\text{C}$  to  $-80^{\circ}\text{C}$ .

The higher temperature was applied because crystallisation peak for this system could not be observed when scanned from 20°C. This exemption was due to the tendency for this particular sample to solidify at room temperature during sample preparation affected by the high gum concentration and the small amount used for DSC analysis.

The freezing ( $T_f$ ), melting ( $T_m$ ) and glass transition temperatures ( $T_g$ ) were reported as the onset temperature while the phase change enthalpy,  $\Delta H$  ( $Jg^{-1}$ ) was measured from the peak area of the corresponding thermogram with Origin 9.0 software. The onset temperatures were determined based on the intersection point between tangent line and point of maximum slope as shown in figure 3.9. All values were reported from an average of two readings.

The percentage of freezable water (FW%) for each formulation was estimated from the calculated enthalpy of cooling  $\Delta H_c$  ( $Jg^{-1}$ ) using equation adapted from Xanthakis et al. (2014):

$$FW\% = \frac{Q \times 100}{H_f \times m} \quad (6)$$

Where,

$Q$  = Enthalpy of cooling ( $Jg^{-1}$ )

$H_f$  = heat of fusion of ice – water ( $333.50 Jg^{-1}$ )

$m$  = mass of the sample (g)

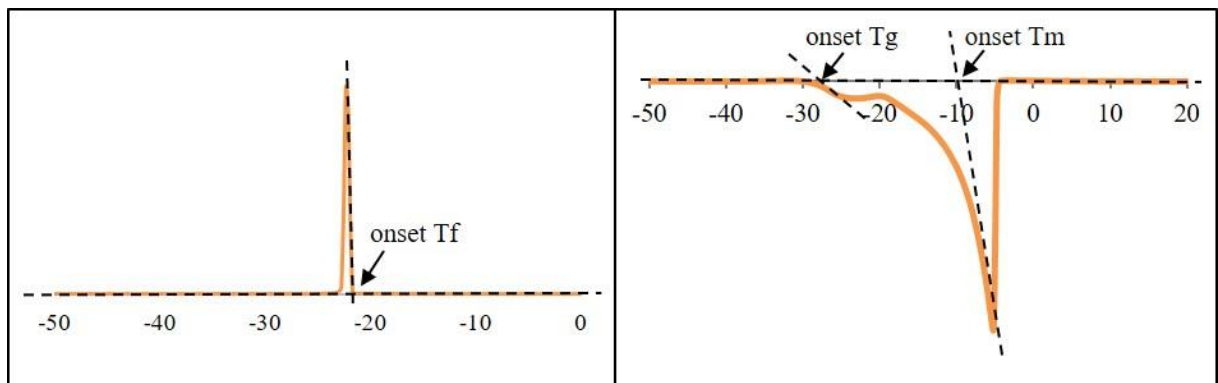


Figure 3.9 Illustration on determination of onset crystallization, melting and glass transition points on DSC thermogram.

### 3.2.5 Structure analysis

Structural attributes of the freeze-dried systems were analyzed at macro and microscopic level with different techniques to understand structural development affected by the different process designs.

Obtained freeze-dried cakes were first fractured carefully lengthwise by hand and cross-sections were photographed using a digital single-lens reflex camera (Canon DSLR EOS 5D Mark II).

#### 3.2.5.1 Scanning electron microscopy (SEM)

Microscopic evaluation with scanning electron microscopy (SEM) was carried out in this study to understand and quantify the internal microstructure of the freeze-dried systems.

A section from the middle of the cake representative of the cake's morphology alongside its height was observed with Hitachi TM3030 Desktop SEM (Krefeld, Germany). Samples (5 mm × 10 mm) were fixed to an aluminium stub using double sided carbon tape before being transferred to the SEM chamber. Images were collected using energy dispersive X-ray (EDX) mode while the microscope was set under low vacuum (100 Pa) at magnifications ranging from 100X to 1000X. The SEM micrographs were then analysed using ImageJ analysis system (described in section 3.2.4.4) to quantify the pore structures of the freeze-dried solids.

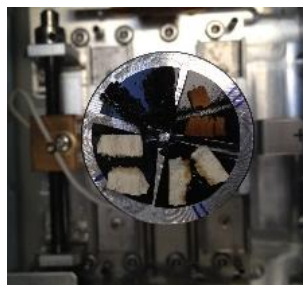


Figure 3.10 Picture of sample prepared for SEM observation.

### 3.2.5.2 X-ray computed tomography (XRCT)

X-ray computed tomography (XRCT) technique was also used for microstructural observation. While freeze-dried products have porous microstructure and X-rays are strongly absorbed by solid structure than voids, images with good contrast between these structural elements are obtained (Babin et al. 2007a).

Shadow images of the freeze-dried samples were acquired with Skyscan 1172 (Bruker MicroCT, Kontich, Belgium) using a medium camera setting (2000 × 1048 pixels) with X-ray source set to 50 -70 kV (100  $\mu$ A). Before scanning, the samples were carefully mounted on a sample holder equipped with blue tac to prevent the sample from moving while rotating. The distance between X-ray source, object and camera was adjusted to produce images with a pixel size of 8 $\mu$ m. Schematic view of the experimental set up is shown in figure 3.11. Three frame averaging, rotation step of 0.40° and exposure time between 200 -300 ms were chosen to minimise the noise, covering a view of 180°. A typical scan took around 25-30 min. NRecon software package (Bruker MicroCT) was used for reconstruction of the 2D cross-section images. Approximately 600 slices were obtained for each sample, from the top to the bottom of the sample (height = 0.5cm).

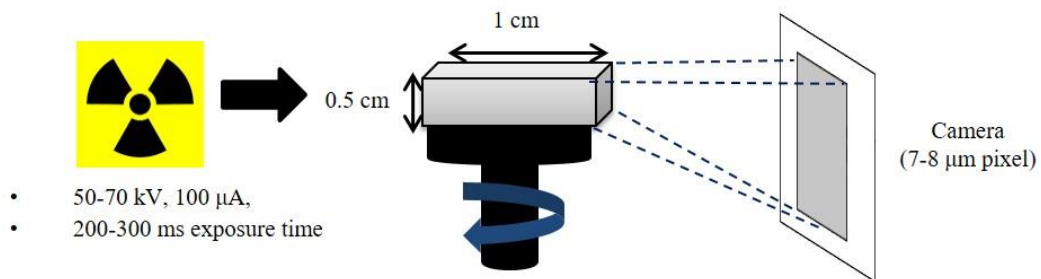


Figure 3.11 Illustration on set up for X-ray micro CT observation.

### 3.2.5.3 Image analysis

Binary images were then obtained from the reconstructed images using CTAn software package (Bruker MicroCT). Analytic performance described in (Parker et al. 2010; Peters et al. 2014) was adopted with some modifications. The creation of binary images was based on thresholding to a 255 point of grey scale where pores were used as reference. Selection of appropriate threshold indices to separate void space from the solid matrix was confirmed by comparing the binary image with reconstructed grey-scale image.

Both SEM and X-ray images were analysed using imageJ, a Java image processing program. Through this software, image cleaning processes mainly thresholding (only for SEM images) and despeckle filter function were adopted to enable size and number of pores as well as overall porosity to be quantified. An example of binarized image is shown in figure 3.10. Pore sizes in microns ( $\mu\text{m}$ ) were determined as the diameter of a circle with area equivalent to the of the selected pore area which is represented by white pixel (see figure 3.12). Meanwhile, porosity (%) was calculated as the fraction between the sums of pore area to the total area of the image (Silva et al. 2015).

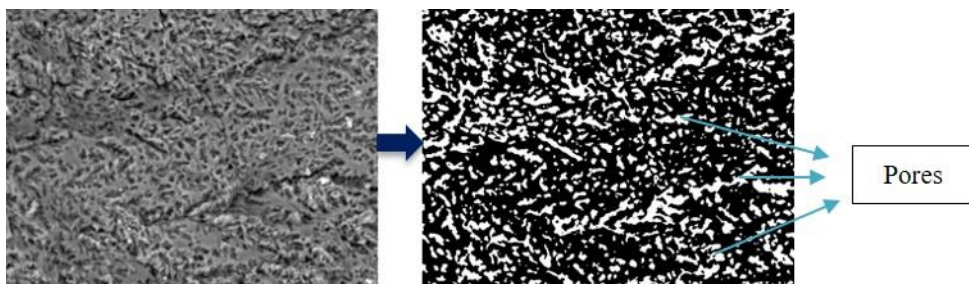


Figure 3.12 Example of binary image obtained after thresholding and cleaning.

#### **3.2.5.4 Porosity analysis**

An instrumental technique was also adopted to determine porosity of the freeze-dried solids from temperature oscillation experiment. Results were obtained using a gas displacement technique with a helium pycnometer (AccuPyc-II-1340). Each sample was cut into cubes ( $150\text{mm}^2$ ) to fit the sample chamber with a 75% filling ratio. Percentage of the pore volume was presented based on 5 repetitions of gas purges and measurements.

#### **3.2.6 Reconstitution process**

Performance of the freeze-dried coffee and gum arabic were then evaluated based on the reconstitution behaviour. An inverted light microscope and conductivity meter were used to record and monitor the reconstitution process.

Reconstitution of dehydrated samples from temperature oscillation experiment were recorded with the inverted light microscope (Zeiss Axio vert. A1, Jena, Germany). Individual particles of each sample (freeze-dried coffee and gum arabic) was prepared by cutting into approximately  $5 \times 10^{-3} \text{ cm}^2$ . Each particle was placed in a  $0.3 \text{ cm}^3$  glass petri dish which contains 10ml distilled water at room temperature. Image resolution was set as  $1376 \times 1038$  pixels and images were recorded at 5 frames per second by the open source software  $\mu$ Manager. To enhance the contrast of the image a black and a white hardboard was put underneath the glass petri dish during the reconstitution of gum arabic and freeze dried coffee respectively.

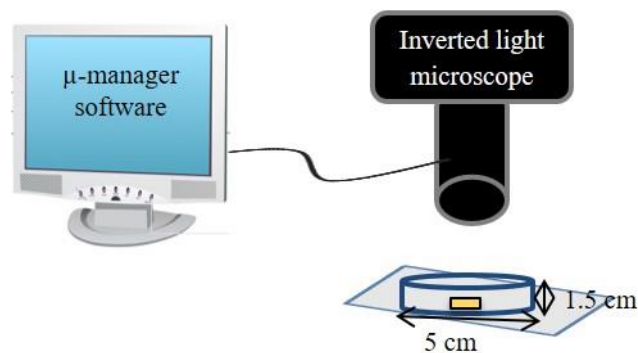


Figure 3.13 Illustration on set up used for recording reconstitution process.

Thermo Scientific™ Orion™ Star A212 conductivity benchtop meter was also used to evaluate reconstitution property of the freeze-dried solids by measuring changes in conductivity values over time. A conductivity probe was inserted in a 250ml beaker filled with 100ml distilled water. The freeze-dried samples in  $1\text{cm}^3$  were dissolved in the distilled water using magnetic stirrer operating at 1000rpm. Reading of conductivity values were taken until sample is completely dissolved and was analyzed to determine the amount of solid dissolved as a function of time. Dissolution of all freeze-dried samples were run in three replications.

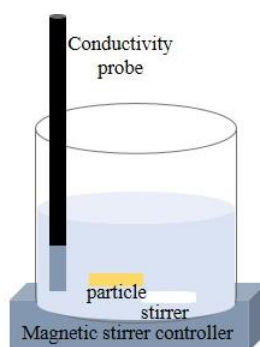


Figure 3.14 Illustration on set up used in conductivity measurement

The total amount of solute released at each time interval (5 sec) was expressed as the percentage ratio of conductivity measured at corresponding time to the maximum conductivity value measured, as follows:

$$\text{Solute released (\%)} = \frac{C_t}{C_o}$$

(6)

$C_t$  = conductivity at time t;  $C_o$  = conductivity measured at the end of reconstitution.

## CHAPTER 4

### **Influence of freezing conditions on ice crystals formation and reconstitution behaviour of concentrated freeze-dried systems.**

#### **4.1 Introduction**

Freeze-drying as discussed in the literature has important application in the food industry to produce dried materials with porous structure, long shelf life, high rehydration capacity and preserved nutrients. The removal of water in the form of ice in this drying technology indicates that the freezing step has determinant effect on the morphology of the freeze-dried cake and hence properties of the dehydrated product. Freezing involves ice nucleation and crystal growth phase that control morphology of the ice crystals formed and consequently the voids left after drying. In high solid systems, freezing of water is challenged by the limited water availability and molecular mobility due to the low water content and high viscosity associated with concentrated solutions.

Several approaches on modification of freezing process in order to control ice crystal's size and shape have been previously discussed (Kiani & Sun 2011). Among the techniques highlighted are addition of nucleating agents such as *Pseudomonas Syringae* and silver iodide (AgI) (Searles et al. 2001b), nitrogen gas (Rambhatla et al. 2004), high pressure shift freezing (Li & Sun 2002) and the emerging technique ultrasonic vibration (Nakagawa et al. 2006). These methods were introduced to have control on the onset of ice nucleation and eventually growth of the desired ice crystal morphology. Annealing is another practice shown to be able to control water crystallization. It is carried out at the end of the freezing process by holding the sample above the glass transition temperature, and below melting, for a certain period of time. This

holding step has been shown to promote growth of large crystals, assisted by the recrystallisation phenomenon known as Ostwald ripening (Hottot et al. 2007).

The size, distribution and shape of ice crystals formed also play an important role to allow sufficient heat and mass transfer during drying and porosity of the end product. For instance, small ice crystals from a high degree of supercooling has been associated with high vapour flow resistance and a prolonged sublimation process but shorter secondary drying because of high specific surface area (Ceballos et al. 2012; Rambhatla et al. 2006). As discussed in the literature, there is a risk of structural collapse with slow drying where product can reach temperature above its melting ( $T_m$ ) and glass transition point ( $T_g$ ) after prolonged exposure in the drying stage (Franks 1998; Roos 1997). A collapsed freeze-dried cake is often associated with dense structure (Krokida et al. 1998) and poor rehydration capacity (Barresi et al. 2009). Knowledge on glass transition ( $T_g$ ), collapse ( $T_c$ ) and melting temperatures ( $T_m$ ) of food materials is important for the choice of the most appropriate processing parameters (Roos 1997).

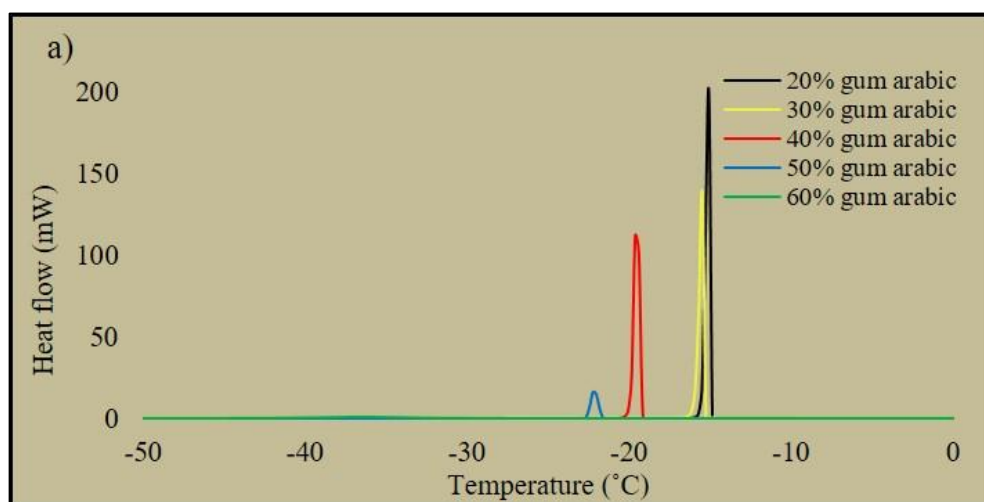
In the meantime, rehydration being one of the important attributes of a freeze-dried product has been demonstrated to be affected by freezing conditions applied. For example, rapid freezing to temperatures  $<-80^\circ\text{C}$  associated with formation of needle-like ice crystals and eventually narrow voids was reported to have caused instantaneous rehydration of the freeze-dried soy bean and carrot (Harnkarnsujarit et al. 2016; Voda et al. 2012). On the contrary, slowly frozen (to  $-5$  and  $-20^\circ\text{C}$ ) freeze-dried starchy foods where large ice crystals formed has been linked with high water uptake during rehydration of the freeze-dried solid (Koh et al. 2011). These studies highlighted the importance of controlling ice crystal formation to ensure desired quality characteristics of the final dried product.

On that account, different freezing conditions; temperature oscillation (section 4.2), shelf ramping (slow rate) and shelf pre-cooling (fast rate) (section 4.3) and unidirectional freezing (section 4.4) were applied on the 50 and 60% w/w solutions in this chapter focusing the influence on ice crystal development, freeze-dried structure and reconstitution behaviour of the final dried product. Thermal characterization of the materials used in this study is initially investigated at different concentration.

## 4.2 Thermal characterization

To characterize the phase transition temperatures at different concentrations, 20–60% w/w gum arabic and coffee solutions were scanned with differential scanning calorimetry (DSC) as detailed in section 3.2.4. This thermal analysis shows the comparison on the onset of freezing ( $T_{f \text{ onset}}$ ) and melting ( $T_{m \text{ onset}}$ ) as well as glass transition ( $T_g$ ) temperatures between materials and concentrations.

### 4.2.1 Crystallization



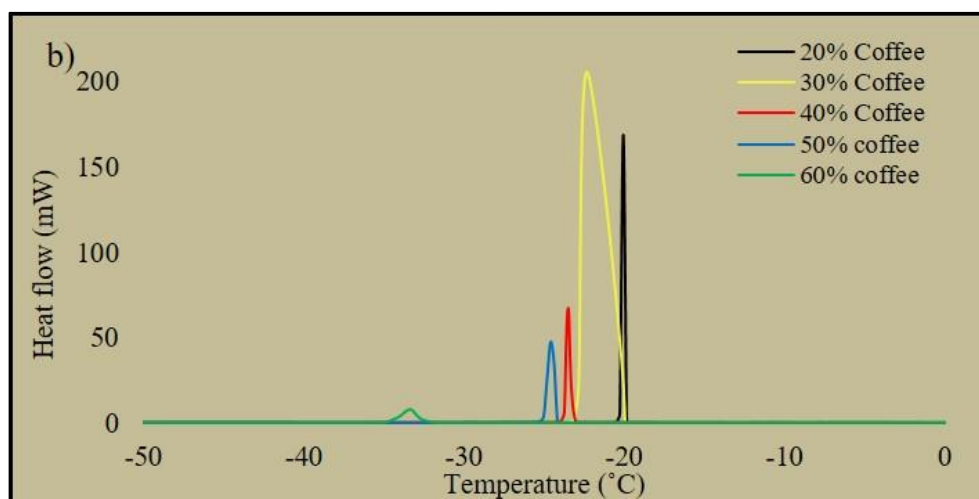


Figure 4.1 DSC thermograms of 20-60% w/w: a) gum arabic and b) coffee solutions obtained during cooling at 1°C/min

Cooling trace of gum arabic and coffee solutions at various solute fractions with a rate of 1°C/min is shown in figure 4.1. The crystallization peaks of both systems were observed to shift to lower temperatures with increasing solid content which shows the practical challenge in freezing concentrated systems. In this analysis, crystallization temperature is reported as the temperature where the first crystallite forms known as the onset temperature. It is defined as the intersection point between the tangent and point of maximum slope as shown in figure 3.9. Crystallization of gum arabic decreased from -16 to -31°C with 40% solid increment and coffee showed an almost similar reduction but at a lower temperature range (from -21 to -33°C) shown in figure 4.2. The decreasing pattern of  $T_{f\ onset}$  with increasing concentration has been described to be related with the lower water availability and reduced mobility of the water molecules at higher solid contents due to increased viscosity (Roos & Karel 1991). Also, Lopez-Quiroga et al. (2016) recently reported that almost half of free water content in sugar solutions reduced upon increasing sugar content from 20 to 60% w/w. In principle, solutions with high solute fraction usually has more bound water trapped within the membrane of food matrix thus, limiting its availability for crystallization. Contrary, free water is readily available for phase

transition because it is loosely bound within the intercellular section of food matrix (Khan et al. 2017; Vaclavik & Christian 2014). The reduced availability of water molecules and its mobility with increasing solute fraction therefore, resulted in  $T_{f \text{ onset}}$  depression of the investigated solutions.

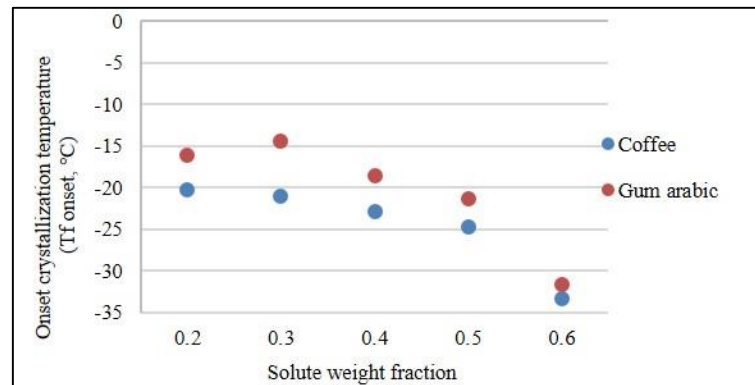
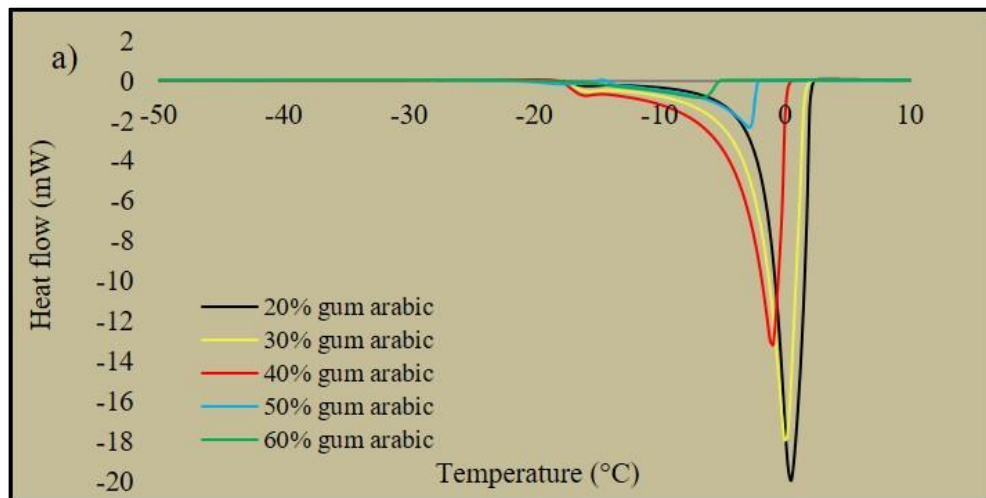


Figure 4.2 Effect of solid content on the onset crystallization temperature.

As in figure 4.2, gum arabic crystallized around 3 to 5°C higher than coffee where smaller gap observed at higher concentration. The difference in molecular weight and molecular interactions of these systems may have caused such variation (Rahman 2006). Although gum arabic and coffee share similar main polysaccharides, (arabinogalactan, galactomannan, etc.) coffee generally exhibits lower molecular weight due to breakdown of these polysaccharides during roasting (Gashua et al. 2016; Passos et al. 2014; Arya & Rao 2007; Randall et al. 1989). A model that predicts the freezing point of concentrated fruit juices has shown the effect of molecular weight on freezing point depression (Auleda et al. 2011). In the previous study, apple juice with significant proportion of low molecular weight fructose was found to froze at lower temperatures than pear and peach juices. Harnkarnsujarit et al. (2012) also reported that maltodextrin-sugar mixtures with smallest average molecular weight gave the lowest freezing temperature.

Significant reduction of the onset  $T_{f\ onset}$  in the range of 8 to 10°C was observed when solid content increased from 50 to 60% w/w while differences in  $T_{f\ onset}$  values between other concentrations were only around 1.2 to 2.5 °C. This big gap in temperature reduction could be influenced by characteristic of the formulation. A study on thermophysical properties of coffee revealed the non-Newtonian behaviour of 60% coffee at room temperature as opposed to the Newtonian behaviour showed by coffee solutions with 35-50% dry matter content (Burmester et al. 2011). This difference in flow behaviour indicates that solution of more than 50% solids tend to have significant physical characteristics affecting the phase transition process.

#### 4.2.2 Heating endotherm of gum arabic and coffee solutions.



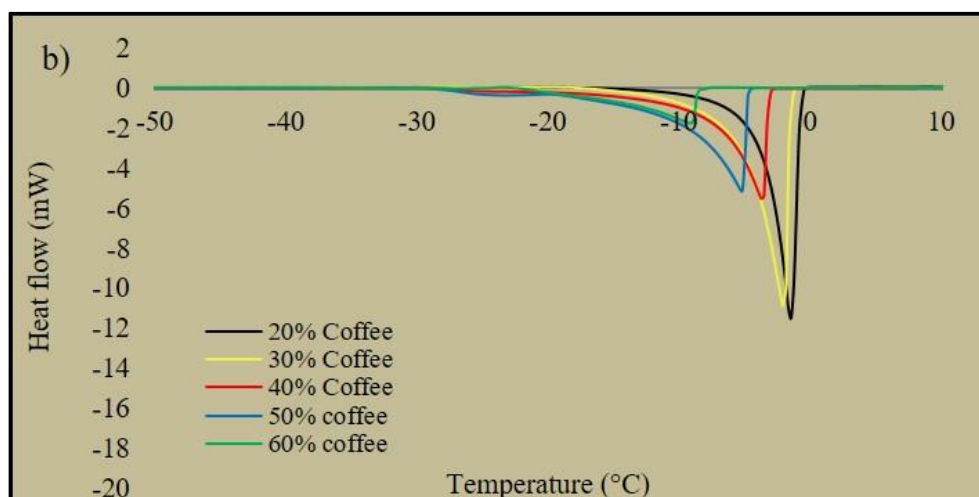


Figure 4.3 DSC thermogram of 20-60% w/w a) gum arabic and b) coffee during heating at 1°C/min.

The melting endotherm to 20°C of the investigated materials after cooling cycle to -80°C are shown in figure 4.3. Similar to  $T_{f\text{onset}}$ , high amount of solute also reduced the  $T_{m\text{onset}}$  attributed by the lowering effect of soluble solids in solution. This pattern is in accordance with previous research on sugar solutions and starch which showed lower  $T_m$  at higher solute concentration (Homer et al. 2014; Arvanitoyannis et al. 1993). Also, the values found for gum arabic are within the range of data reported for mixtures of fructose, glucose and sucrose (Ruiz-Cabrera et al. 2016).  $T_{m\text{onset}}$  of the low molecular weight sugar mixtures reduced from -1.6 to -15.8°C with solid content varied from 0.2 to 0.65 g solid/g sample.

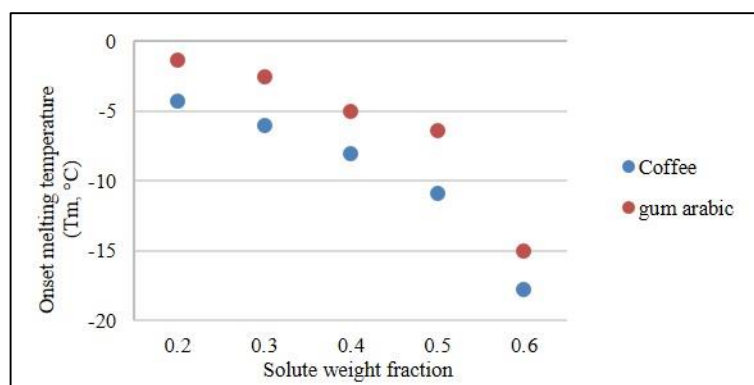


Figure 4.4 Effect of solid content on the onset melting temperature of gum arabic and coffee solutions.

The phase change enthalpy ( $\Delta H$ ) during cooling and melting determined from total area of the corresponding phase change peaks are summarized in table 4-1 with values representing mean of two readings. It is apparent from this table that energy required for the phase transitions is smaller in concentrated systems than those of less solute fraction. This decreasing value suggests the potential of processing high solid systems in reducing energy consumption during freeze-drying (Lopez-Quiroga et al. 2016). Besides, linear correlation between change in enthalpy of ice melting with total sugar content in mango has been shown by Zhao et al. (2015). On average, slightly lower enthalpy of cooling but higher enthalpy of melting was determined for gum arabic solutions in comparison with values obtained for coffee. Estimation of the freezable water content (FW%) from the enthalpy values using equation 7 show that 40% increase in solid content (20 to 60%) reduced FW% of the solutions on average by 75% for gum arabic and 43% for coffee. The reduced percentage is indicative on the challenge for water to crystallize in higher solid solutions. Notably, higher FW% was measured for 30% coffee than 20% coffee with difference of 8%. This result is in accordance with the narrower crystallization peak in figure 4.1 (smaller enthalpy) observed for the least concentrated coffee system. Gum arabic overall showed lower percentage of freezable water content (average of 11% difference) than coffee and may be attributed to the different molecular organisations and interactions occurring between the two materials due to non-identical composition (Rahman 2006). For example, in the food industry, gum arabic as the gummy exudate from Acacia trees is known as additives that can influence the viscosity, body and texture of food product (Gómez-Díaz et al. 2008) suggesting it tend to form more viscous solution than coffee affecting the water availability and mobility.

Table 4-1 Values of phase change enthalpy associated with cooling and melting, glass transition point and freezable water content of gum arabic and coffee solutions.

Gum arabic solutions	20% (w/w)	30% (w/w)	40% (w/w)	50% (w/w)	60% (w/w)
$\Delta H_c$ (J/g)	2.46	1.52	1.47	1.27	0.35
$\Delta H_m$ (J/g)	3.21	2.56	1.73	1.30	0.95
$T_g$ (°C)	-17.31	-16.89	-15.92	-21.24	n/o
FW (%)	43.22	26.67	17.07	14.96	10.57
Coffee solutions	20% (w/w)	30% (w/w)	40% (w/w)	50% (w/w)	60% (w/w)
$\Delta H_c$ (J/g)	2.61	3.26	1.77	1.64	0.73
$\Delta H_m$ (J/g)	3.11	2.28	1.83	1.35	0.79
$T_g$ (°C)	-26.95	-26.30	-27.17	-27.84	n/o
FW (%)	30.51	39.38	33.22	20.75	17.80

The glass transition appeared as small endothermal peak before melting were observed in most solutions but difficult to be estimated in the most concentrated coffee and gum arabic solutions with the current experimental design. Glass transition temperature ( $T_g$ ) determined for coffee solutions were between -26 to -28°C whereas values of -16 to -21°C were obtained for gum arabic solutions. However, figure 4.5 shows that the low  $T_g$  (-21°C) obtained for 50% gum arabic was followed by devitrification with onset at -16.5°C and subsequent melting. The occurrence of devitrification exotherm indicates the delayed ice formation in this solution. In this case, nucleation of ice represented by  $T_{f\text{ onset}}$  occurred during the initial cooling to -80°C and the crystallization appear during the rewarming cycle. Development of ice above  $T_g$  is known to increase the concentration of solute but as latent heat of crystallization is released, viscosity is reduced which makes devitrification continues until  $T_m$  is reached. This result agrees with the thermal behaviour of non-annealed 65% sucrose showing  $T_d$  at much lower temperature, -57°C and  $T_g$  at -77°C (Roos & Karel 1991). However, maximum ice formation of the concentrated sucrose solution after annealing resulted in disappearance of the devitrification region increasing  $T_g$  as much as 31°C. Thus, it is expected that annealing would have increase the  $T_g$  of 50% gum arabic. In addition, Roos & Karel (1991) have also shown the trend of  $T_g$  increases with concentration particularly for solutions with more than 60% solute.

Every 5% increment of sucrose content (from 64 to 80% w/w),  $T_g$  was found to increase within the range of 9 to 14°C. It is therefore possible to assume that the highly concentrated gum arabic and coffee solutions have higher  $T_g$  than the 50% systems. Support to this assumption is that in the highly concentrated solution, water availability and mobility is restricted and higher temperature would be required to induce state transition since at low temperature physical changes are kinetically inhibited.

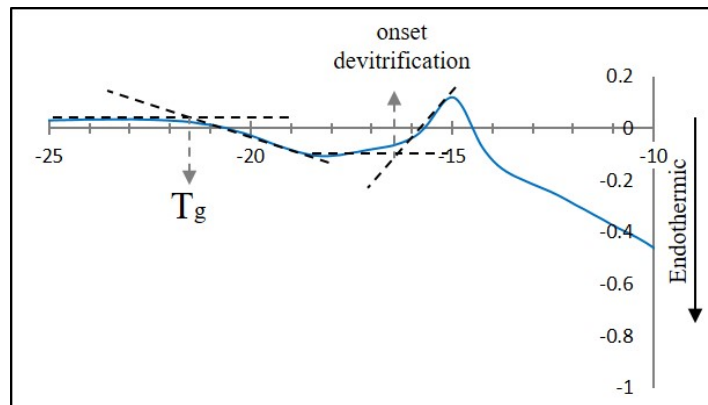


Figure 4.5 Devitrification exotherm observed during heating cycle of 50% gum arabic solution.

### 4.3 Influence of temperature oscillation

Results from freezing with temperature oscillation are presented in terms of freezing properties derived from the time and temperature profile recorded when 50 and 60% w/w solutions were cooled from 20 to -40°C in freeze-dryer (section 4.3.1), description about the appearance and comparison on microstructural properties (section 4.3.2) as well as reconstitution of the freeze-dried solids (section 4.3.3). Solutions with >40% solid were of particular interest in this section as part of the difficulty in ice formation associated with high solid/viscous solutions (Arvanitoyannis et al. 1993; Homer et al. 2014) in which freezable water

content found previous section was only between 10-20% for 50-60% w/w solutions. Also, freeze-drying concentrated systems is currently not a common practice but has the potential in lowering total energy expenditure during manufacturing (Lopez-Quiroga et al. 2016; Sagara & Ichiba, 1994).

#### 4.3.1 Cooling profiles of gum arabic and coffee solutions.

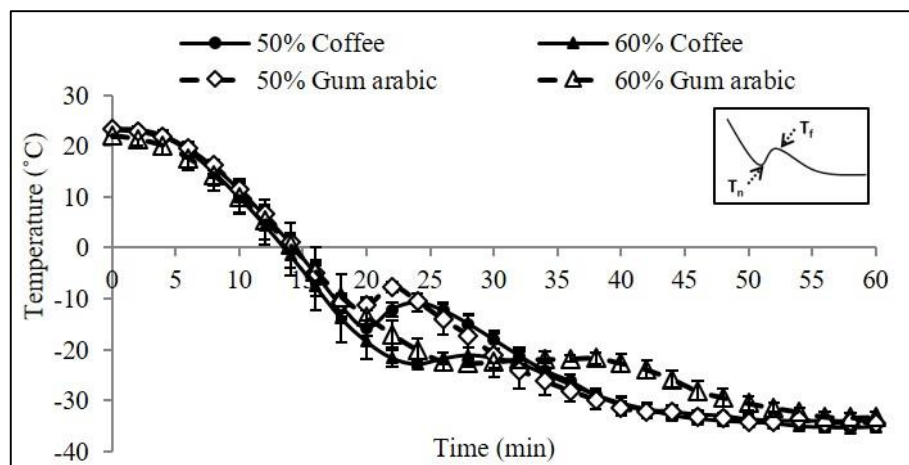


Figure 4.6 Comparison of freezing behaviour between concentrated gum arabic and coffee solutions during freezing to -40°C in freeze-drier operated at 1°C/min

Cooling profiles of the investigated coffee and gum arabic solutions are shown in figure 4.6. The curves are representative of a typical freezing curve, showing supercooling and freezing regimes (Rahman et al. 2002). Based on the freezing curves, nucleation ( $T_n$ ) identified as the lowest point of the curve represents the beginning of water crystallization where ice nuclei initially developed. Meanwhile,  $T_f$  related to the phase transition stage (liquid to solid) is determined as the highest peak reached before sample's temperature decreases towards the freezer's temperature (-40°C) as shown in the inset of figure 4.6, and their values are presented in table 4-2.

Table 4-2 Effect of concentration on freezing properties of gum arabic and coffee solutions

<i>System</i>	<i>50% Coffee</i>	<i>60% Coffee</i>	<i>50% Gum Arabic</i>	<i>60% Gum arabic</i>
<i>Nucleation temperature, <math>T_n</math> (°C)</i>	$-16.2 \pm 2.10$	$-22.9 \pm 1.04$	$-11.2 \pm 1.88$	n/o
<i>Freezing temperature, <math>T_f</math> (°C)</i>	$-10.8 \pm 2.10$	$-22.0 \pm 4.00$	$-7.6 \pm 1.77$	$-21.6 \pm 1.99$

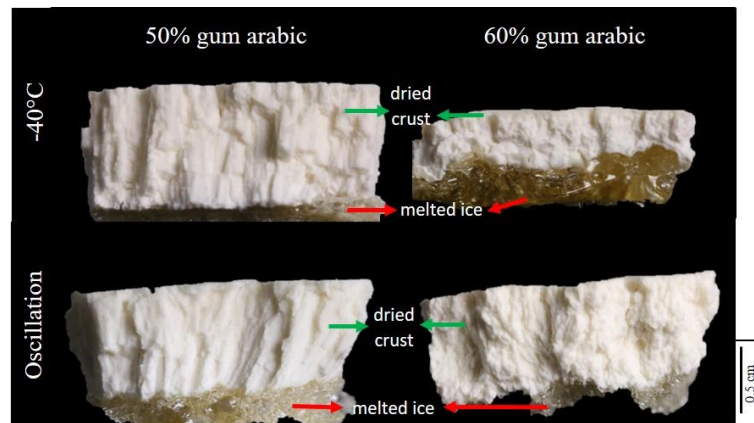
In order to relate the recorded freezing properties with the one obtained in DSC analysis, it is noted that  $T_n$  and  $T_{f\text{ onset}}$  both signify the first appearance of ice nuclei, while  $T_f$  and  $T_m$  are indicative of the thermodynamic transitions. It can be seen that nucleation of ice from the recorded freezing profiles (table 4-2) were higher by approximately 10°C than that of  $T_{f\text{ onset}}$  measured in calorimetric experiment (figure 4.2). The difference between the two techniques might be linked with the different cooling rates exerted on the sample. Although both methods operated at 1°C/min, it was noted that experimental settings in the freeze-drier resulted in initial lag phase and subsequent faster cooling rate at 2.5°C/min as determined from the freezing curve (figure 4.6). Also, the fact that samples in DSC pan were hermetically sealed suggesting the absence of impurities from the air in contrast to the exposed surface of samples in the freeze-drying pan where air-borne impurities could have triggered nucleation at higher temperature (Roos et al. 2013; Kasper & Friess 2011). Meanwhile, both freezing curves and DSC endotherms showed comparable thermodynamic transition temperatures ( $T_f$  and  $T_m$ ) for the 50% solutions. 60% samples however, had lower temperature (by 5-7°C) than  $T_m$  determined from the melting endotherm. Despite these differences, similar trend of decreasing freezing temperature on increasing concentration is observed in both analyses. This finding showed the importance of water molecules availability and mobility in order for the phase transition to occur in which an average of 22% reduction in percentage of freezable water was found when solid content increased from 50 to 60% (table 4-1).

In the recorded time and temperature profiles,  $T_f$  for coffee solutions were lower than values reported by Burmester et al. (2011) where  $T_f$  was measured at  $-6 \pm 6^\circ\text{C}$  and  $-12 \pm 6^\circ\text{C}$  each for 50% and 60% coffee. However, Moreno et al. (2015) identified  $T_f$  at  $-9.8 \pm 0.24^\circ\text{C}$  for coffee solution with 50% solid close to the value presented in table 4-2. It can also be noted that, the supercooling peak was not visible during freezing of 60% gum arabic in which  $T_n$  was difficult to be identified. Product temperature appeared to fall directly to the crystal growth stage indicated by the freezing plateau. Similar freezing behaviour was found during fast freezing ( $0.11^\circ\text{C}/\text{min}$ ) of starch gel system in Rahman et al. (2002), possible to be linked with the reduced supercooling occurring at higher viscosities, which in this work might be caused by the increasing solid concentration (Leloux 1999). In the next section, these freezing properties are used to relate with the ice crystals and consequently pore structure of the final freeze-dried products.

### 4.3.2 Appearance and microstructure of freeze-dried solids

#### 4.3.2.1 Appearance of freeze-dried cake

a)



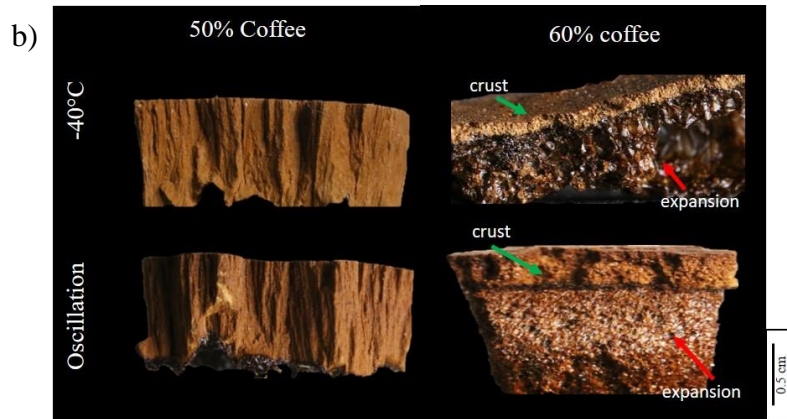


Figure 4.7 Freeze-dried cake of 50 and 60% w/w (a) gum arabic and (b) coffee obtained at different freezing conditions

Visual aspects of the freeze-dried cakes obtained from all investigated conditions is shown in figure 4.7. Samples were cut in the middle section for this evaluation to reveal internal macrostructure of the freeze-dried systems.

Images from the high resolution camera revealed the influence of formulation and freezing conditions on appearance of the dried solids. Non-uniform appearance of the freeze-dried cakes was evident with formation of dried layer on the top and bottom part displaying a darker and glass-like structure, suggesting that the material melted and re-solidified during drying. This non-uniformity appeared to develop in a great extent for the 60% systems. In example, the bottom part of the freeze-dried 60% coffee had higher thickness than the dried layer on top indicating structural expansion. In the literature, significant structural changes during freeze-drying have been usually characterized with structure collapse and shrinkage (Esfandiary et al. 2016; Ullrich et al. 2015; Abdelwahed et al. 2006; Karanthanos et al. 1996). However, in the current observation, the freeze-dried systems puffed rather than collapsed in response to the material not being dried properly. The glassy structure underneath the dried top layer is likely to be the results of product going above its  $T_m$  despite primary drying temperature

was set at below  $T_m$  (see figure 4.4). In terms of puffing, it is possible to relate it with the increased internal pressure due to high resistance to vapour flow. When water vapour from sublimated ice crystals could not escape rapidly, more vapour will be trapped inside as drying proceeds elevating the sample's pressure and temperature which could melt the remaining ice crystals. As the drying chamber was in high vacuum condition ( $1 \times 10^{-4}$  bar), the high internal pressure, temperature and possible melting may have caused stress to the sample that it puffed.

Meanwhile, freeze-drying the 50% systems resulted in better cake appearance but minor collapse still present at the very bottom of the dried solid. The different degree of structural changes between the two concentrations strongly suggest the influence of dried surface porosity. The low water availability in 60% solutions is expected to have less ice formation compared to the 50% samples resulting in fewer number of ice crystals to be sublimated. Thus, porosity of the dried surface of the highly concentrated systems is lower than the dried solids of 50% solutions affecting the movement of water vapour in the drying stage. In addition, as reported in DSC analysis (figure 4.4), both 60% gum arabic and coffee have lower  $T_m$  than the 50% concentrations. This low  $T_m$  would make the 60% solutions be more susceptible for significant changes in volume than the less concentrated systems as it is easier to be exceeded during processing.

It is worth noting that more uniform dried solids developed upon freezing with temperature oscillation indicated by the increase in dried layer thickness and less obvious melting appearance. As temperature is not constant during the oscillation period, ice crystals would have gained some degree of mobility that affects the crystal growth pattern and eventually the porosity of final dried materials. This will be discussed later in the next section in relation to the microstructure observed with scanning electron microscopy (SEM). This

observation showed the possibility of temperature fluctuation on improving the macroscopic attributes of the freeze-dried solids.

### 4.3.2.2 Microstructure

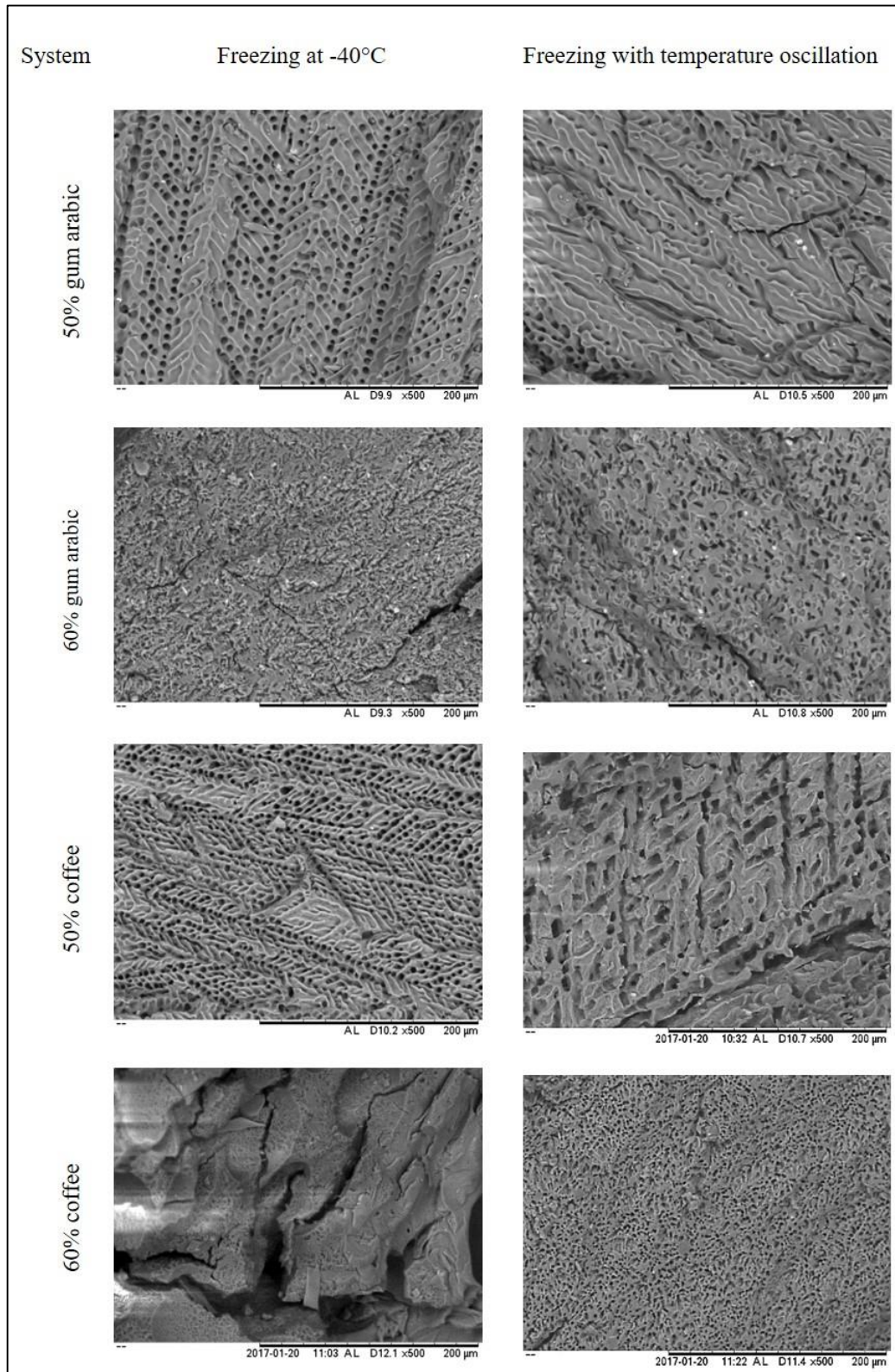


Figure 4.8 Scanning electron microscopy (SEM) images of freeze-dried gum arabic and coffee at 100x magnification affected by different freezing conditions.

Additionally, figure 4.8 shows the representative microstructures of the freeze-dried samples obtained through scanning electron microscopy (SEM). The SEM micrographs revealed the interconnected solid network and pores vacated after sublimation of the ice crystals created during freezing. Average diameters of equivalent circular diameter as the obtained pores are shown in figure 4.9.

In terms of microstructure features, the freeze-dried solids overall have pore channels identical to the formation of dendritic ice crystals, a typical ice structures found in most foods (Petzold & Aguilera 2009). Bigger pores were displayed by samples freeze-dried with temperature oscillations, indicating larger ice crystal formation. The bar graph in figure 4.9 clearly revealed that the pores vacated by the sublimated ice crystals doubled in size after being subjected to temperature oscillations. This observation could be the result of sample being held at a temperature above  $T_g$  and below  $T_m$  during the freezing cycle. This temperature range has been discussed to result in higher crystallization (Roos 1997). Above  $T_g$ , viscosity of the system is known to decrease substantially which increases the molecular movement and mass transfer thus, allowing rearrangements of small crystals towards formation of larger crystals. Temperature fluctuations during freezing have similar effects as annealing which promotes growth of large ice crystals due to Ostwald ripening effect (Kasper & Friess 2011; Gormley et al. 2002). Ice crystals enlargement has also been linked with reduced freeze-drying duration attributed by the decrease in vapour flow resistance during drying (Hottot et al. 2004a; Searles et al. 2001a). Also, hexagonal plates ice crystals were seen in the oscillated system especially in 60% gum arabic representing stable crystal structure. The fact that dendrites morphology originates from hexagonal plate, suggests that the liquid phase does not have sufficient time to arrange regularly into several hexagonal units or branched into dendritic crystal morphology

during the temperature fluctuation (Kasper & Friess 2011; Kiani & Sun 2011; Petzold & Aguilera 2009).

Comparing between solute fractions, the 50% samples showed formation of wider dendrites (60-135 $\mu\text{m}$ ) with distinct directionality and circular pores. The directionality may have been affected by the cooling direction in which samples were cooled from the bottom that is in contact with the frozen shelf to the top that was exposed to the freeze-drying chamber. Meanwhile, freeze-drying the 60% solutions formed freeze-dried solids with much narrower dendrites within the range of 20-30 $\mu\text{m}$  and formation of circular pores were not observed. Reduction in crystal size on increasing concentration has also previously been reported by Pardo et al. (2002) indicating the significant influence of solutes on water crystallization. Data is also in accordance with the freezing properties reported in table 4-2 where mean pore size decreases with decreasing nucleation temperature ( $T_n$ ) driven by the relatively low water accessibility and mobility on increasing solid content. In principle, ice nucleation is more pronounced at low temperature creating numerous nuclei to act as template for development of small ice crystals in the crystallization stage (Geidobler & Winter 2013; Rambhatla et al. 2004). Besides, study on crystal growth in supercooled solutions has reported growth of thinner dendrites with increasing solute concentration (Teraoka et al. 2002).

Meanwhile, some cracks were observed, especially for the 60% coffee freeze-dried without temperature oscillation (see figure 4.8). This is the system that has an appearance with notable puffing in figure 4.7 which may be partially responsible for cracking. In addition, cracking and shrinkage in freeze-drying have been identified in a recent studies as a response to increase in pressure during evaporation of unfrozen liquid (Patel et al. 2017; Ullrich et al. 2015). Loss of unfrozen water from the porous solid developed drying tension within the surface region which can be released through contraction or cracking. In the later study, both

mechanisms were found to be inversely correlated in which greater cracks were correlated with high disaccharide content, sample depth and cooling rate. Therefore, the observed cracks in concentrated coffee could also be attributed by this phenomenon.

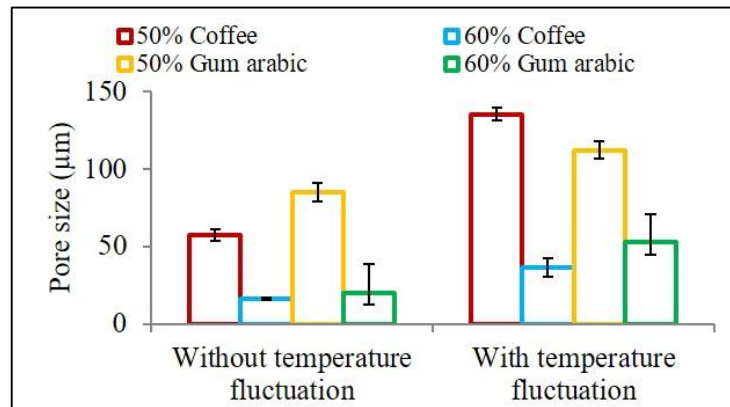


Figure 4.9 Effect of formulations and freezing conditions on the mean size of ice crystals.

Table 4-3 Data from image analysis on overall porosity of the freeze-dried systems

Sample	-40°C	Oscillation
50% Coffee	49.15 ± 2.81	57.95 ± 3.55
60% Coffee	28.41 ± 5.93	27.58 ± 1.67
50% Gum arabic	67.23 ± 2.89	78.29 ± 2.01
60% Gum arabic	35.09 ± 2.67	39.23 ± 1.23

Table 4-3 contain the porosity values quantified from image analysis on binary SEM micrographs of freeze-dried coffee and gum arabic solutions. As mentioned in chapter 3, porosity in this study is defined as the ratio between pore area and total area of the image (Silva et al. 2015) representing overall porosity of the freeze-dried cake. Results showed that dried matrices with 50% initial solid content have approximately 20% more pore area than higher concentration systems (qualitatively indicated in figure 4.8). The higher porosity could be due to the fact that 50% solutions has higher volume of water than concentrated systems and can create more ice crystals. The crystals were eventually left as pores after dehydration. The

presence of circular pores, wider dendritic voids and thinner walls than freeze-dried 60% solids might have also led to higher porosity.

Considering the effect of freezing conditions, slightly higher total porosities by about 4 to 9% were observed on fluctuating temperature during freezing excluding the 60% coffee, in which freezing cycle showed no apparent effect on the total porosity. As analysis involved the top layer of the freeze-dried cake, the exception on 60% coffee reinforced the low permeability of the crust layer that lead to the observed inner structural expansion (as seen in figure 4.7 and 4.8).

Table 4-4 Data from pycnometer on overall porosity of the freeze-dried systems

Sample	-40°C	Oscillation
50% Coffee	34.3 ± 0.05	33.9 ± 0.02
60% Coffee	30.2 ± 0.36	35.0 ± 0.17
50% Gum arabic	34.8 ± 0.06	34.9 ± 0.08
60% Gum arabic	34.1 ± 0.07	25.5 ± 0.04

However, porosity values measured with gas displacement method showed insignificant difference between the investigated conditions (see table 4-4). The porosity for all freeze-dried matrices was in the range of 25-35% with the smallest reading obtained for gum arabic solution. The measured values were also generally lower by approximately 35-55% than one obtained through image analysis. From this experimental data, it can be inferred that the dried solids consist of closed pores that are not measurable with helium pycnometer. Previously, C.S.Chang, (1988) applied fine grinding for true density measurement of a substance with pycnometer in order to exclude the significant effect of closed pore volume. Therefore, measurement with pycnometer in this work gave estimation on the open porosity. There was no significant difference in the open porosity between investigated samples. It appears that both

imaging and instrumental technique gave the least porosity for 60% gum arabic with pores resembling the hexagonal and column crystals. This low porosity is affected by the bigger solid area surrounding these pores and the less interconnectivity observed between pores in figure 4.8. Porosity as an important indicator of food structure is controlled by various factors from pore size, shape, interconnectivity, distribution and thickness of the pore membrane to method used for its estimation.

### 4.3.3 Reconstitution behaviour

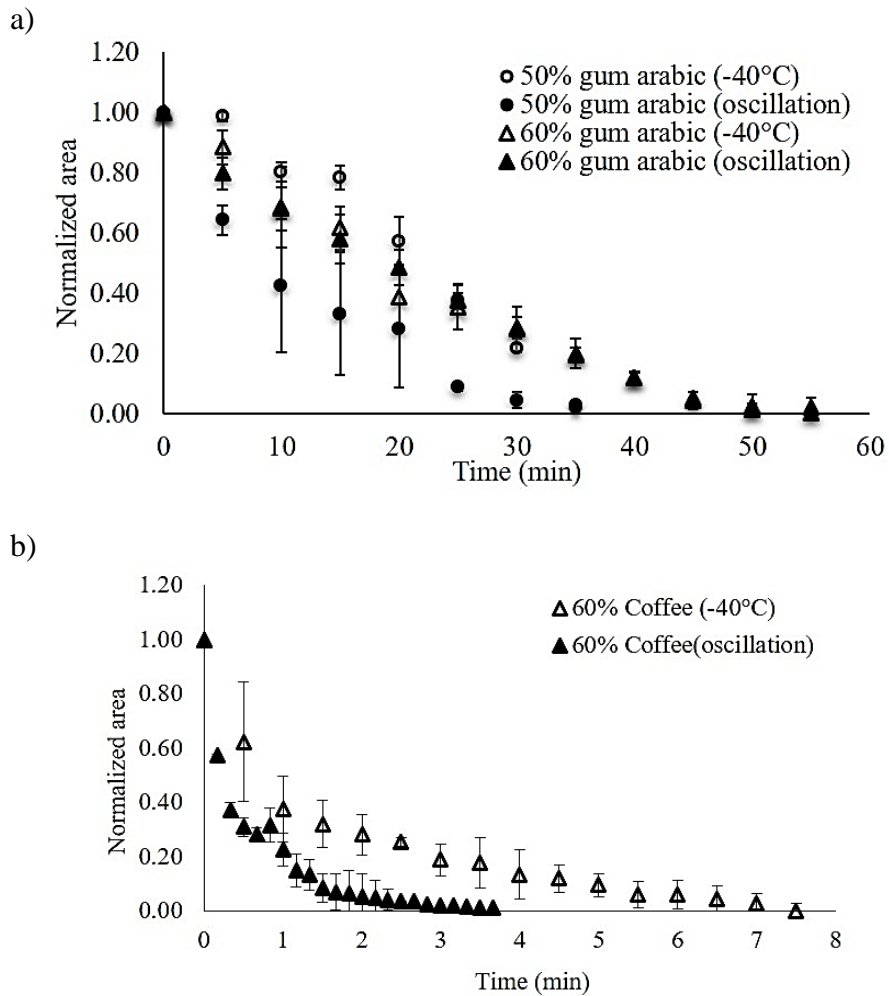
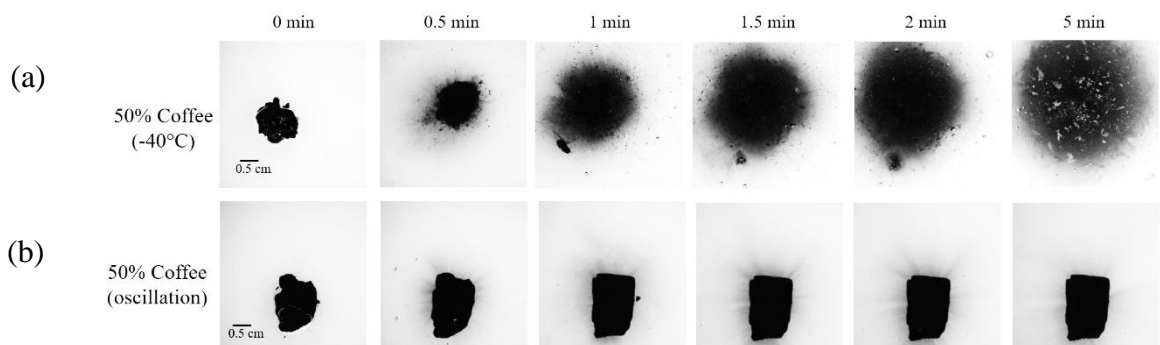


Figure 4.10 Area reduction of freeze-dried particles during reconstitution in 10ml distilled water: a) gum arabic b) coffee.

The freeze dried coffee and gum arabic processed under different freezing conditions were analysed for interaction with water. Dissolution of samples in distilled water were observed under inverted light microscope and recorded using micro manager software. Dissolution kinetics are presented as normalized area reduction of solid particles over time in figure 4.10.

Graphs clearly show the notable difference in dissolution duration between the materials studied. In general, coffee dissolved 8 times faster than gum arabic with area reduced rapidly at the initial stage followed by smaller decrement as dissolution continues. This observation indicated different mechanisms involved during reconstitution of both systems. Snapshot images in figure 4.11 (a-d) revealed that in most cases, coffee particles disintegrated into small fragments instantly once in contact with water. Disintegration helps to increase surface area of the particles and resulted in fast reconstitution rate. Unlike coffee, gum arabic dissolved by first absorbing water prior to disintegration showing slower initial area reduction than coffee. The very slow water uptake at the early stage of dissolution is also evidence in figure 4.13 (a-d) where significant changes was only evident after 10<sup>th</sup> min. This could be attributed by the formation of gel-like layer surrounding the particle which can slows down transport of water to the sample and leaching of solute into the water (Miller-Chou & Koenig 2003; Kravtchenko et al. 1999).



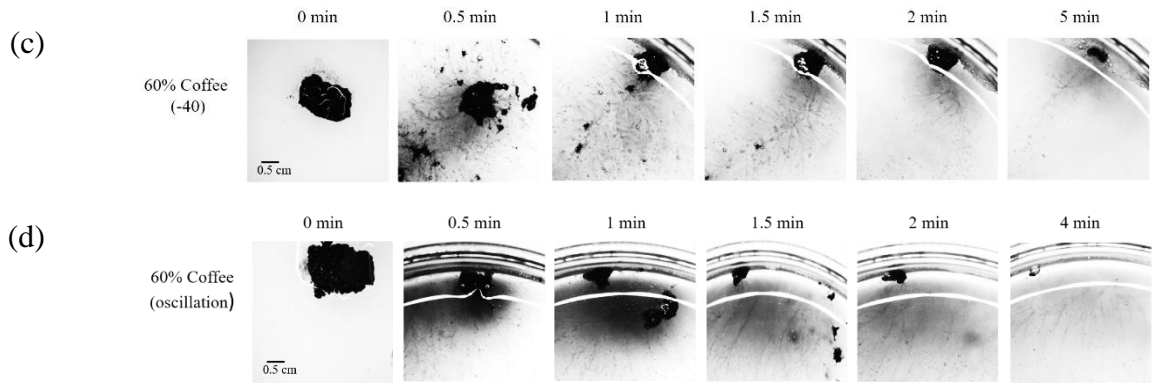


Figure 4.11 Snapshots images during reconstitution of freeze-dried coffee samples: a) 50% (-40°C), b) 50% (oscillation), c) 60% (-40°C), d) 60% (oscillation).

Notably, reconstitution kinetics of 50% coffee is not shown in figure 4.10. Dissolution of 50% coffee frozen at -40°C was followed with cloud formation as evidence in figure 4.11(a) and made it difficult to identify the dissolving particle. Hence, data on area reduction is not shown in the graph. Nevertheless, it was shown that sample dispersed rapidly suggesting that particle quickly dissolved. For the system frozen with temperature oscillation (figure 4.11 (b)), it was surprising to observe the particle only rehydrates without dissolving. However, figure 4.12 shows that when dissolution for this particular sample was carried out at higher water temperature (90°C) it dissolved in under 5 min, forming a cloud similar to that formed during reconstitution of the 50% coffee frozen at -40°C. This sample might have been contaminated with moisture during sample preparation for dissolution analysis. Freeze-dried products are known for being hygroscopic a property related to tendency to absorb moisture from surrounding (Patel & Pikal 2011).

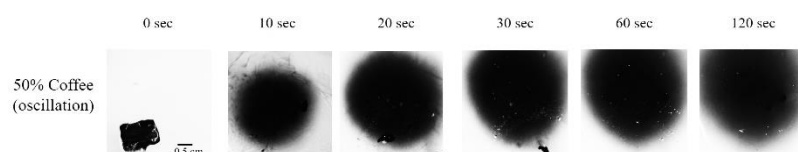
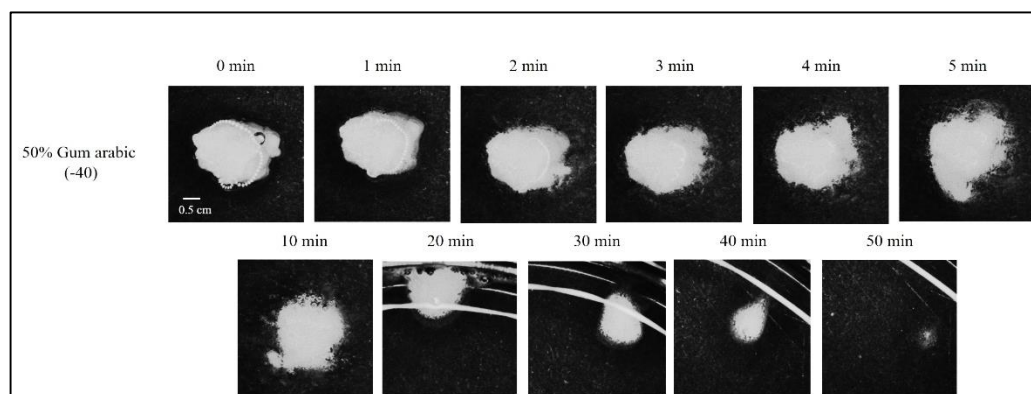


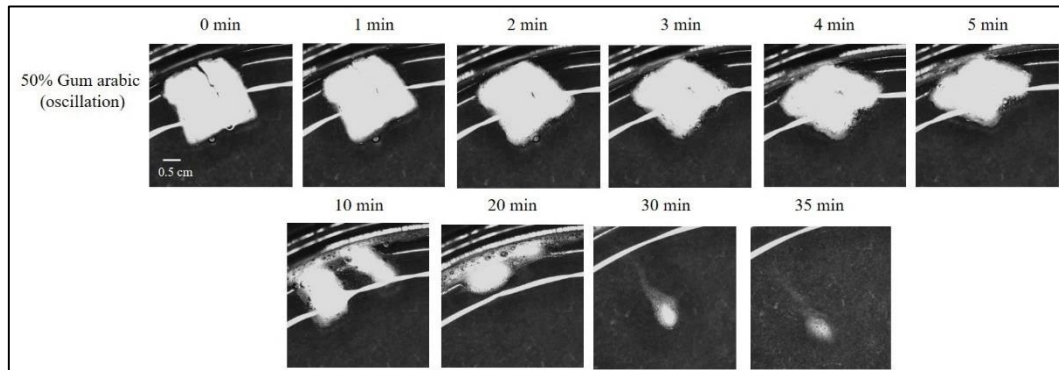
Figure 4.12 Snapshots from dissolution of oscillated 50% coffee oscillated in hot distilled water (90°C)

Nevertheless, reconstitution kinetics appeared to be dependent on the microstructure obtained. It was observed that fast reconstitution occurred in freeze-dried solids with wide dendritic voids and high porosity. Essentially, faster dissolution was recorded for the freeze-dried 50% formulations than the 60% systems. For gum arabic, the less concentrated dried solid dissolved 10 min earlier than particles of 60% concentration. High reconstitution rate was also displayed by oscillated samples associated with the formation of wider dendrite network and increased porosities. Although gum arabic shows overlapping dissolution curves, a trend of gradual area reduction especially at the early stage can be seen for non-oscillated samples. Also, it appears that dissolution of the puffed 60% coffee frozen at  $-40^{\circ}\text{C}$  (figure 4.11 (c)), was followed by slower reconstitution of the top layer because of its less porous structure. Zea et al. (2013) and Saifullah et al. (2016) reported similar findings on the effect of porosity with fruit tablets prepared from freeze-dried powder. Earlier investigations on the relationship between pore size and rehydration kinetics have demonstrated that small pores caused slower rehydration in freeze-dried rice (Koh et al. 2011) but faster rehydration in freeze-dried soy bean curd (Harnkarnsujarit et al. 2016). This contradictory conclusion pointed out the mechanism of hydration, such as the relative importance of capillary imbibition and molecular diffusion involved during water transport across porous food materials, largely determines the link between porosity and reconstitution kinetics (Saguy et al. 2005; Meda & Ratti 2005).

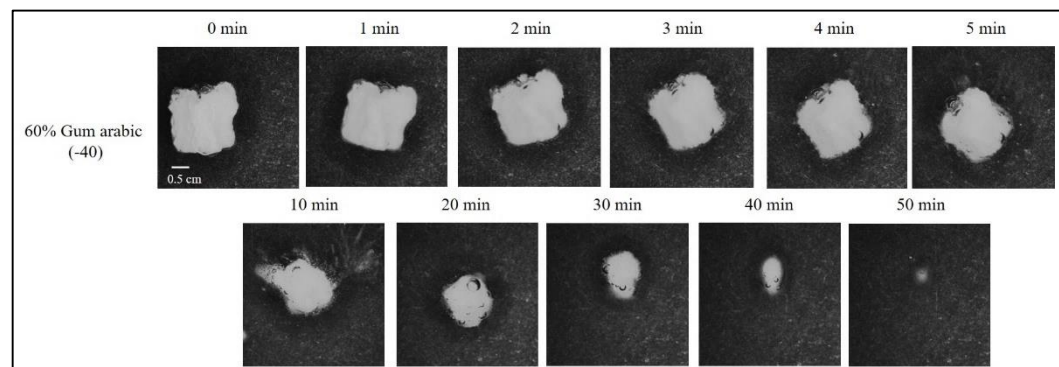
a)



b)



c)



d)

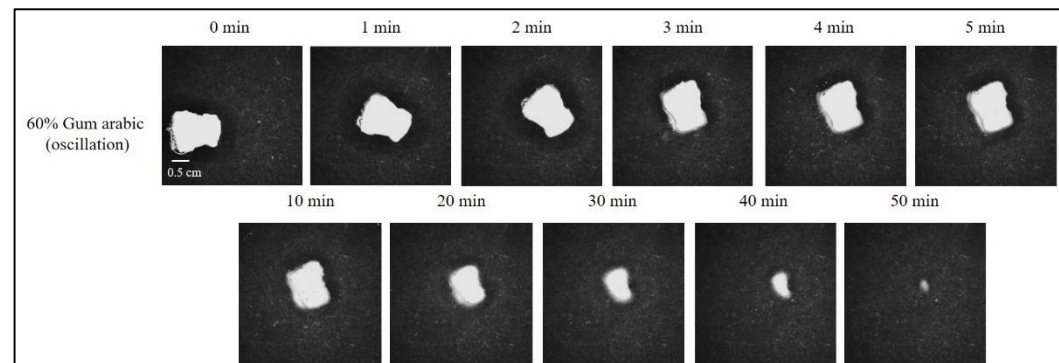


Figure 4.13 Snapshot images during reconstitution of freeze-dried gum arabic: a) 50% (-40°C), b) 50% (oscillation), c) 60% (-40°C), d) 60% (oscillation)

Overall, dissolution data showed the determinant effect of microstructure and hydration mechanism on dissolution behaviour of freeze-dried products. It was found that large pores and high overall porosity are the preferred structural features for rapid dissolution of the freeze-

dried systems investigated. Therefore, it is important to control microstructure formation during processing in order to obtain end product of desired quality.

#### **4.4 Influence of different cooling rates**

Freezing of the concentrated gum arabic and coffee solutions were further investigated under the influence of varied cooling profiles. Samples were frozen in the rapid freezer. Shelf ramping (i.e. placing the sample on the shelf at room temperature and subsequently cooling the shelf at 1°C/min to -40°C) and shelf pre-cooling (i.e. pre-cooling of the shelf at -40°C and then placing the sample on the cold shelf) were conducted to establish difference in initial cooling rates of the freezing process. Microstructure and reconstitution of the freeze-dried systems were analyzed to evaluate the effect of freezing conditions applied.

##### **4.4.1 Cooling profile**

Shelf ramp (SR) and shelf pre-cooled (PC) freezing were conducted to investigate the effect of cooling rates on ice crystals formation of the concentrated gum arabic and coffee solutions. As described earlier,  $T_n$  and  $T_f$  each is determined as the lowest temperature reached before crystallization and the peak temperature reached during crystallization (illustrated in figures 4.14 and 4.15). In this study, supercooling region where appropriate is shown between the equilibrium freezing point of sample ( $T_f < 0^\circ\text{C}$ ) and  $T_n$  indicating the driving force for nucleation to start.

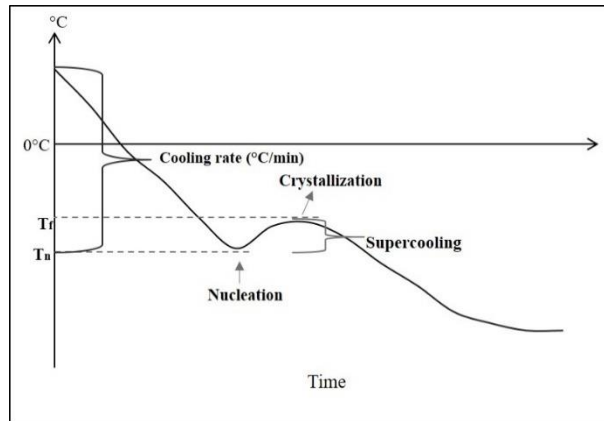


Figure 4.14 Schematic on freezing profile.

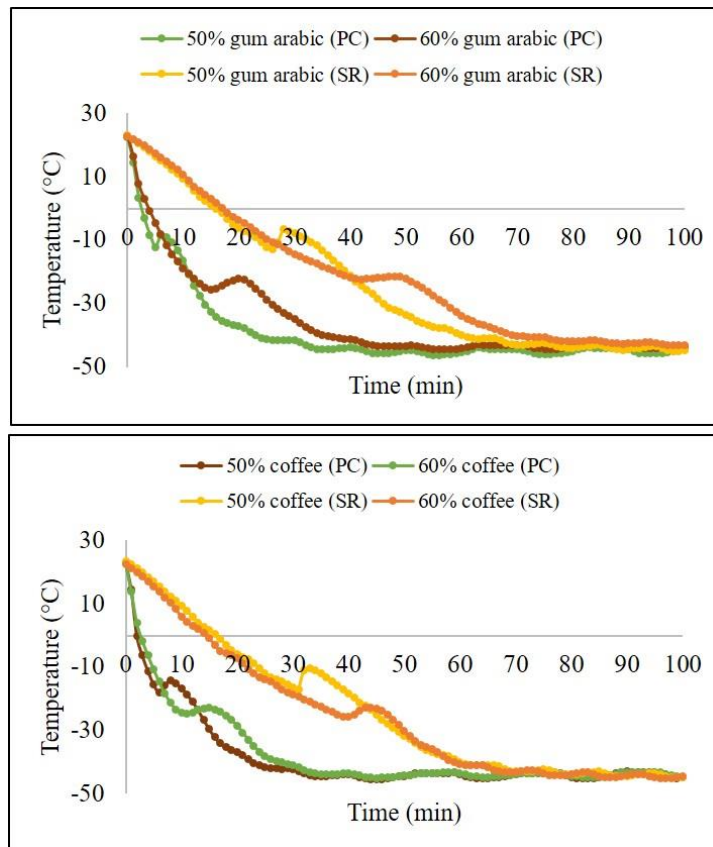


Figure 4.15 Representative freezing curves of concentrated gum arabic and coffee solutions during freezing with shelf ramping (SR) and shelf pre-cooling (PC) methods.

The average cooling rate of SR and PC methods determined from the initial slope were  $1 \pm 0.1^\circ\text{C}/\text{min}$  and  $5 \pm 2^\circ\text{C}/\text{min}$  accordingly. It is clear that cooling method had influence on

the overall freezing time. The freezing time required to reach  $-40^{\circ}\text{C}$  was half an hour longer using SR technique than freezing on a pre-cooled shelf.

$T_n$  identified from the cooling curves are given in table 4-5. As expected, 60% solutions nucleated at lower temperature than 50% concentration with an overall difference of  $10^{\circ}\text{C}$  in agreement with the values recorded during freezing in freeze-drier (table 4-2). This result further highlighted that limited number and mobility of water molecules in high solid solutions increase the driving force required for crystallization to begin (Kasper & Friess 2011). However,  $T_n$  was not easy to be identified during freezing of 60% gum arabic with SR method. Supercooling was not visible in the time and temperature profile as these samples appeared to reach the crystallization stage directly (see figure 4.15) similar to the freezing profile of 60% gum arabic shown in figure 4.6. The highly concentrated gum arabic exhibited freezing plateau for 6 min corresponding to the crystal growth stage. Small variation ( $< 1.5^{\circ}\text{C}$ ) in  $T_n$  was obtained between the freezing rates applied suggesting that ice nucleation was more sensitive towards the concentration of sample.

Table 4-5 Nucleation temperature ( $T_n$ ) extracted from the cooling curves of the concentrated solutions.

<i>System</i>	<i>50% gum arabic</i>	<i>60% gum arabic</i>	<i>50% coffee</i>	<i>60% coffee</i>
<i>Shelf-ramping (0.6°C/min)</i>	$-12.20 \pm 0.89$	n/o	$-16.06 \pm 2.11$	$-25.01 \pm 0.69$
<i>Shelf pre-cooling (2°C/min)</i>	$-11.03 \pm 1.53$	$-26.36 \pm 1.77$	$-14.57 \pm 3.65$	$-25.38 \pm 1.07$

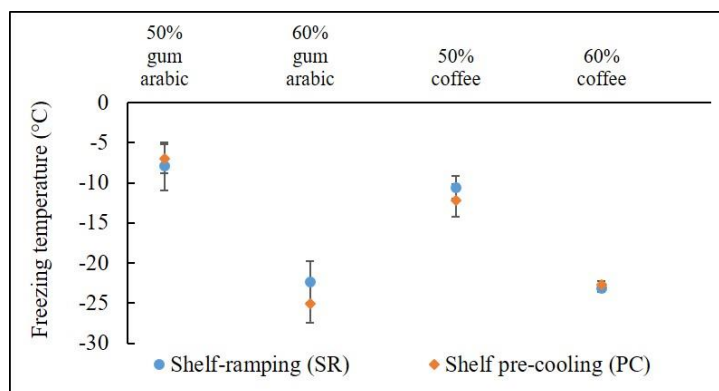


Figure 4.16 Effect of cooling rates and concentrations on freezing temperature of gum arabic and coffee solutions.

Figure 4.16 shows  $T_f$  of the concentrated solutions at different cooling rates. Similar to nucleation,  $T_f$  was not greatly influenced by the freezing methods investigated compared to the effect of concentration. Nevertheless, during fast cooling of the 60% gum arabic, which exhibited supercooling,  $T_f$  decreased slightly by 2.6 °C than the normal shelf ramp freezing where supercooling was not observed. This small reduction might be associated with the freezing point depression effect as the solution becomes more concentrated upon supercooling. Meanwhile, due to the reduced water content and molecular movement, freezing of the 60% formulations was measured at 16°C and 11°C lower than values identified for the less concentrated gum arabic and coffee solutions accordingly. It is noted that for 50% coffee and 60% gum arabic, crystallization temperature close to those in figure 4.16 have been reported for 50 and 60% sucrose cooled at 2 to 2.6°C /min (Rahman et al. 2002).

Comparing the phase transition time between 50 and 60% solution, longer crystallization took place during freezing of the most concentrated solution. This is indicated by the isothermal region observed before temperature fell towards the freezing set point, -40°C. The constant temperature due to latent heat of crystallization remained for about 2 and 6 min each for 60% coffee and gum arabic solution.

The variation in freezing behavior especially observed in gum arabic solutions showed that material's properties as an additional factor besides operating condition that can influence the heat and mass transfer process during freezing.

#### 4.4.2 Microstructure properties of freeze-dried systems

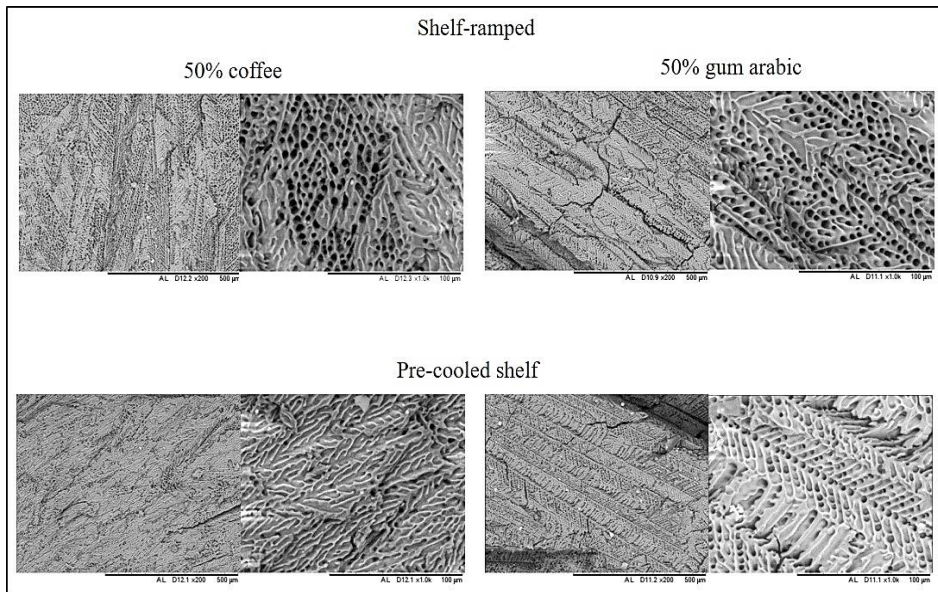


Figure 4.17 SEM images (200x, 1000x) of the freeze-dried 50% gum arabic (right side) and 50% coffee (left side) after freezing with different methods

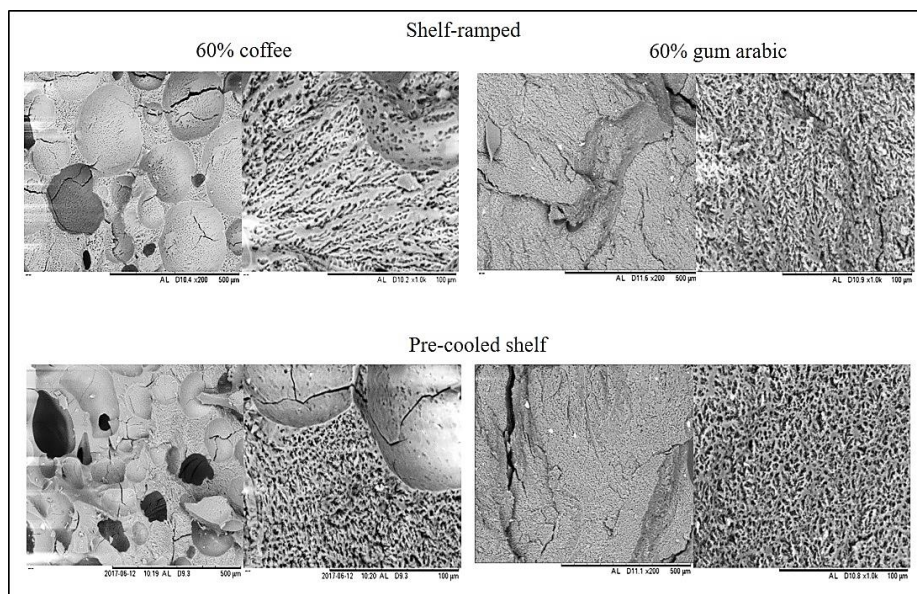


Figure 4.18 SEM images (200x, 1000x) of freeze-dried 60% gum arabic (right side) and 60% coffee (left side) after freezing with different methods.

The SEM images in figure 4.17 and 4.18 show the freeze-dried solids obtained after coffee and gum arabic solutions were subjected to slow (SR) and fast cooling (PC). It appears that the internal structure of freeze-dried systems is similar in nature with the microstructure observed in the temperature oscillation experiment (see figure 4.8). Channel-like entities representing crystal dendrites and circular pores were observed in 50% formulation whereas in the highly concentrated systems, significantly smaller crystal dendrites developed. Also, appreciable air bubbles were seen in the 60% coffee which strongly suggest that the material experienced structural expansion during drying. As discussed earlier, the puffed structure is related with the high dry layer resistance to vapour flow due to crust formation at the top part of the dried cake (see figure 4.7 (b)). The high product resistance slows down the transport of water vapour across the dried layer where at constant  $T_s$  and  $P_c$ , can eventually increase the pressure of the sample to the extent that it puffed.

Differences in pore structure can be seen between the two concentrations studied and can be correlated with the water molecules accessibility and mobility of each system. The higher water content in 50% systems led to development of wider crystal dendrites compared to ice crystals in the 60% systems. As has previously been discussed, crystallization in high solid solution is expected to be limited as viscosity tend to increase with concentration that reduces the water molecules mobility (Arvanitoyannis et al. 1993). Hence, under restricted water availability and movement, the possibility for ice nucleation is higher at low temperature where small nuclei and consequently small ice crystals tend to develop (Geidobler & Winter 2013). Moreover, the pore size distribution in figure 4.19 showed that at 50% solute, pore sizes centred around 80-120 $\mu$ m which is on average 40 $\mu$ m bigger than the pores in systems with 60% initial solid content. This result demonstrated the determinant effect of solid content on size of ice crystals developed during freezing.

Cracks seen in the freeze-dried solids from temperature oscillation experiment, were also visible in this study but being more obvious in 50% gum arabic and the 60% systems. It is also noted that cracking in 60% coffee were only visible on the air bubbles. While cracks can be developed due to stress released during drying (as discussed in section 4.3.2.2) there is also possibility of cracking during sample preparation for SEM observation. This is attributed to the delicate structure of porous freeze-dried systems especially for the cracked air bubbles in 60% coffee.

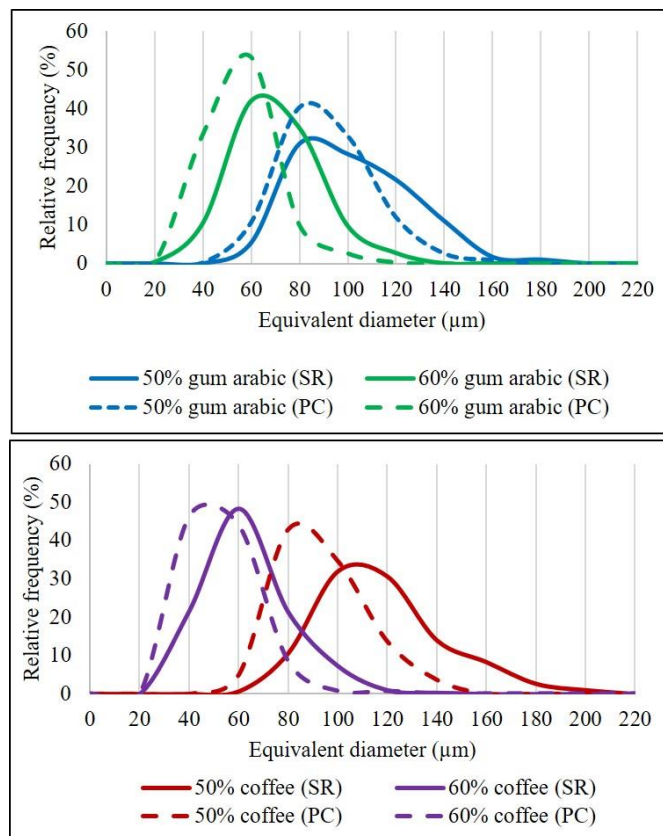


Figure 4.19 Effect of shelf ramping (SR) and pre-cooling (PC) on ice crystal size distribution of the freeze-dried gum arabic and coffee solutions.

Microstructural features of the freeze-dried solids appear not to vary significantly with the cooling rates applied. Although, according to data on pore size distribution in figure 4.19, slightly smaller ice crystals developed at high cooling rate. Graphs revealed that the fast cooling

(PC) on average reduced pore sizes by 20µm for gum arabic and coffee samples. It was also noted that freeze-dried 50% gum arabic and 60% coffee from both cooling methods shared quite similar size distributions as very close freezing temperatures were determined between the methods studied. The minimum variation in mean crystals size between these freezing methods has also been reported in freeze-drying of protein based products resulted in similar sublimation rate (Hottot et al. 2007).

In terms of porosity (see figure 4.20), smaller ice crystals led to decreased ratios of the pore to solid area. Freezing on a pre-cooled shelf reduced the overall porosity by approximately 9 and 13% each for the freeze-dried 50% gum arabic and coffee. However, freeze-drying of the 60% samples exhibited minimum variation (<1%) between the investigated freezing conditions. Despite having ice crystals size centred between 40-60µm, 60% coffee have comparable porosity with the less concentrated systems. This high porosity is mostly influenced by the large air bubbles formed after the system puffed in the drying step.

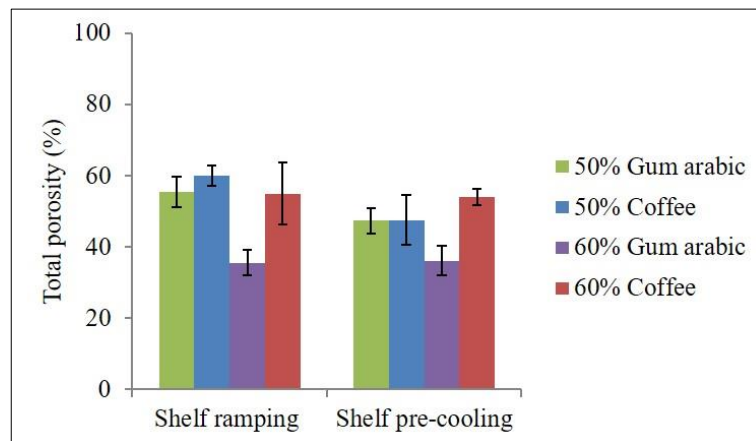


Figure 4.20 Overall porosity of freeze-dried systems affected by formulation and freezing methods.

#### 4.4.3 Reconstitution behavior

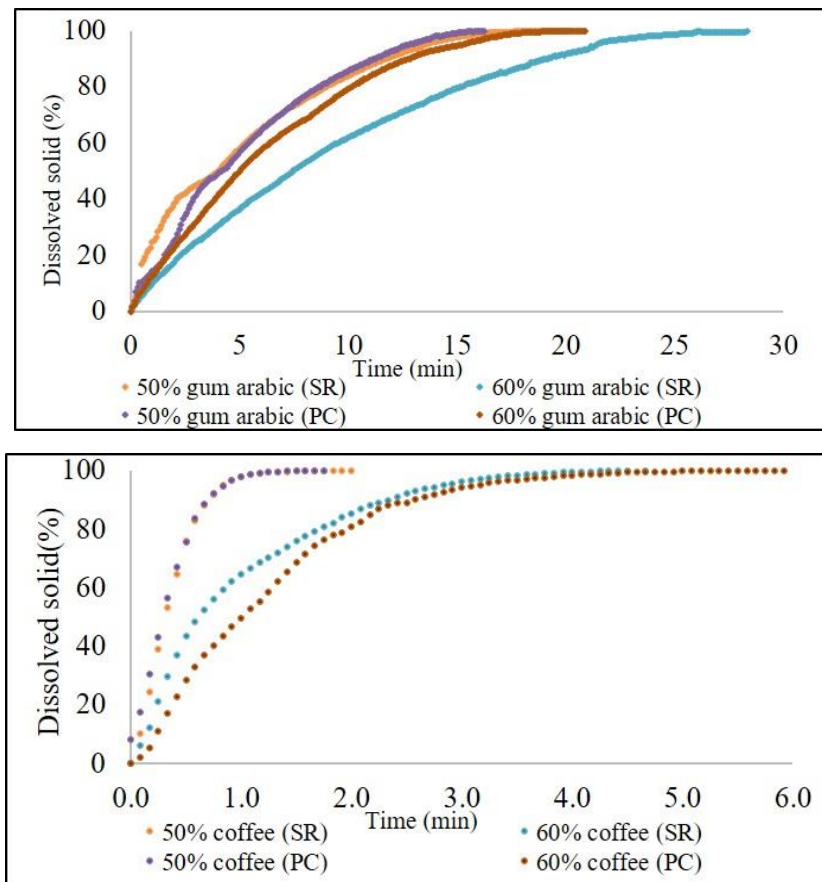


Figure 4.21 Reconstitution of freeze-dried particles frozen at different cooling rates.

In this section, conductivity values were measured to characterize reconstitution of the freeze-dried samples. Amount of solid dissolved derived from these values is presented as a function of time in figure 4.21.

Overlapping of the curves suggest that little or no effect were found on dissolution behaviour between the cooling rates studied. It seems that in this case, reconstitution was more of a function of sample's formulation rather than the freezing methods applied. This finding can be related to the lack of observable differences in ice crystals formation hence microstructure of the freeze-dried solids between both freezing conditions.

Significant influence of concentration on reconstitution time of freeze-dried coffee is indicated by the sharp initial increment of solid dissolved recorded for 50% systems compared to the 60% systems. For this sample, the rate of solid dissolved is  $0.5\% \text{ min}^{-1}$  while the rate for 60% coffee is slower, at  $0.2\% \text{ min}^{-1}$ . The difference in pore size between the two concentrations played an influential role on the reconstitution process. The higher concentrated systems with small pores dissolved slowly affected by the high capillary tortuosity in small cavities which has previously been reported to result in long wetting time and reduced rehydration ratio freeze-dried rice porridge and fruit pulp (Koh et al. 2011; Ceballos et al. 2012).

The instantaneous dissolution of coffee reported in previous section was also evident in this figure showing complete rehydration almost 5-7 times faster than gum arabic. This notable difference has previously been associated with the variation in dissolution mechanisms displayed by both systems (see figure 4.11 and 4.13) despite having comparable inner structure in terms of pore shape and porosity. This behaviour shows that wetting, disintegration and dissolution steps involved during rehydration are not only driven by microstructure but also properties of the material. Several internal factors such as molecular weight, polymer composition and conformation have been discussed by Miller-Chou & Koenig (2003) to have control on polymer dissolution. It was pointed out that high molecular weight polymers dissolved at slower rate due to tendency for significant swelling during wetting which slows down the movement of water to the dried particle. Food ingredients like starch and protein are among examples of food polymers with this dissolution characteristic (Hogekamp & Schubert 2003). The use of gum arabic as an excellent food thickener and stabilizer shows that it forms viscous dispersion in aqueous environment. Therefore, reconstitution of gum arabic was much slower compared to the freeze-dried coffee. In addition, swelling might have taken effect considerably during dissolution of the slowly frozen 60% gum arabic that it exhibited more

gradual reconstitution than the other gum arabic solutions although significant microstructural difference was not observed.

## **4.5 Unidirectional freezing**

In this section, the aspect of heat transfer direction on ice crystallization is explored where concentrated gum arabic and coffee solutions were frozen in a manner that heat is travelled from one direction. Solution in an insulated container was frozen in rapid freezer ensuring that heat advances exclusively from the bottom (see figure 3.5). This freezing set up was investigated as preliminary approach to control orientation of ice crystal structure throughout the frozen solution which can affects efficiency of freeze-drying process and reconstitution behavior of final dried product. The homogenous orientation and structure along the heat/mass transfer direction during sublimation is likely to provide opportunity for improvement of drying efficiency (Jin et al. 2018) and product quality. Similar properties analyzed in previous sections were also examined in this study.

### **4.5.1 Cooling profile**

The time and temperature plot during unidirectional freezing is shown in figure 4.22 where all samples able to reach the freezing shelf temperature ( $-40^{\circ}\text{C}$ ) within half an hour under this experimental set up. Parameters related to the freezing profiles are summarized in table 4-6. It is clear from this table that cooling rate decreases with increasing solute content affected by the low availability of free water in highly concentrated solution (Lopez-Quiroga et al. 2016). It is noted that the cooling rates were quite close to the average rate measured during freezing with shelf pre-cooled method in section 4.4 ( $5 \pm 2^{\circ}\text{C}/\text{min}$ ). The effect of concentration

on nucleation and freezing point depression can also be seen in the freezing curves. Both gum arabic and coffee had temperature difference of about 12 to 17°C between the two concentrations studied during ice nucleation and crystallization. This rather large temperature difference is consistent with the observation made in previous sections, further linked the high driving force for crystallization (low  $T_f$ ) with high solid solutions.

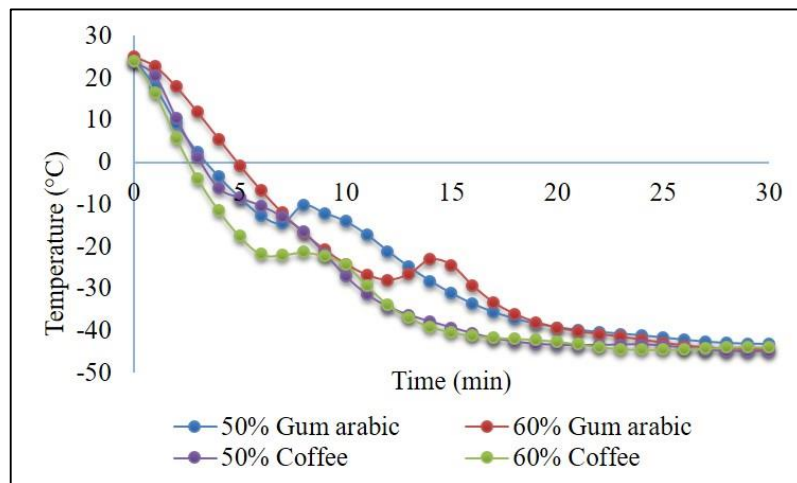


Figure 4.22 Representative real time temperature profile during unidirectional freezing of concentrated systems in rapid freezer.

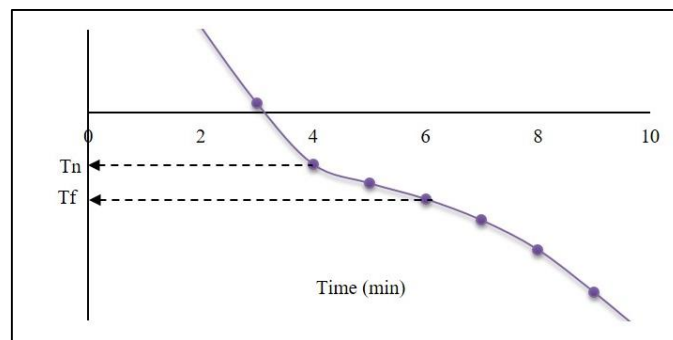


Figure 4.23 Determination of  $T_n$  and  $T_f$  for 50% coffee.

As for the type of materials investigated, nucleation of ice in gum arabic solutions was 4-6°C lower than coffee solutions whereas for  $T_f$ , only 60% gum arabic showed lower temperature than coffee. However, this trend differs from the values presented in oscillation

(see table 4-2) and different cooling rates (see table 4-5) experiments which coffee solutions consistently showed lower  $T_n$  and  $T_f$  than gum arabic. This variability could be influenced by the random nature of the nucleation process which has been noted that product within the same batch can exhibit variation in  $T_n$  from -2 to -18°C (Esfandiary et al. 2016).

Notably, freezing curve of coffee solutions showed no visible supercooling region as seen in earlier sections (see figure 4.6 and 4.15(a)). Freezing plateau for about 2 min at around -22°C was observed during freezing of 60% coffee but the phase transition phase was not easy to be identified in the freezing curve of 50% coffee. The slightly higher cooling rate of coffee could have triggered crystallization to occur faster than gum arabic that solution begin to crystallized near the nucleation point. Thus, increase in temperature due to release of latent heat of crystallization after nucleation was not visible. As growth of ice crystals generally followed with an isothermal region, crystal growth phase of this particular sample was assumed to occur between the 4<sup>th</sup> to 7<sup>th</sup> min as small temperature differences ( $\Delta T \approx 2^\circ\text{C}$ ) were noticed within this time frame compared to other region suggesting the phase transition stage. For this reason,  $T_n$  as well as  $T_f$  were determined as in figure 4.23.

Table 4-6 Freezing properties derived from cooling curves.

<i>Parameters</i>	<i>50% Gum arabic</i>	<i>50% Coffee</i>	<i>60% Gum arabic</i>	<i>60% Coffee</i>
<i>Cooling rate (°C/min)</i>	8.80 ± 3.05	8.90 ± 2.39	5.50 ± 0.51	6.20 ± 0.77
<i>Nucleation temperature (°C)</i>	-11.1 ± 3.06	-6.74 ± 2.19	-28.05 ± 0.30	-22.01 ± 1.97
<i>Freezing temperature (°C)</i>	-9.82 ± 0.59	-10.98 ± 3.54	-26.84 ± 3.07	-22.59 ± 4.67

## 4.5.2 Microstructure

The effect of unidirectional freezing on ice crystals development was evaluated based on the freeze-dried microstructure observed under SEM presented in figure 4.25 until 4.28. However, freeze-drying of the highly concentrated systems resulted in freeze-dried solids (shown in figure 4.24) with extensive puffing and melted bottom which are signs of structural instability during freeze-drying. This rather distinct appearance of a freeze-dried solid is similar with the observation made earlier in this chapter (figure 4.6 and 4.18). In the present work, structural expansion has been linked with collapse phenomenon which normally associated with shrunken pore structure (Patel et al. 2017).

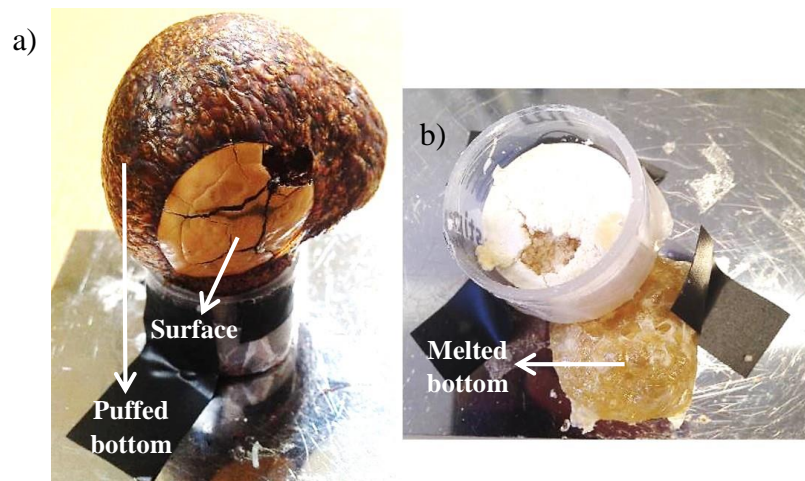


Figure 4.24 Collapsed/puffed freeze-dried cake obtained after freeze-drying of: a) 60% coffee and b) 60% gum arabic systems.

Albeit, for the purpose of microstructure evaluation, the puffed freeze-dried 60% coffee and the dried top part of the 60% gum arabic were still used for SEM observation as presented in figure 4.27 and 4.28. The surface of freeze-dried solids with 50% initial concentration exhibited significant cracks and appear to be more porous than the surface of 60% gum arabic.

It is also noted that the pores on the surface seems slightly bigger in 50% coffee compared to 50% gum arabic. Although cracks have been linked with the stress during drying and mechanical deformation of the freeze-dried cake (Esfandiary et al. 2016), Zhai et al. (2003) however, discussed the probability of cracking to enhance drying rate as it provides pathway for water vapour to be removed. The porous surface suggests that in the less concentrated system, water vapour is easily removed due to low product resistance at the subliming interface thus, preventing significant structural changes. Considering that resistance have direct influence on material's pressure and temperature in the time of drying (Chang & Patro 2004), the impermeable surface of the 60% freeze-dried solids provides explanation for the observed puffing and melting. It is known that high product resistance can increase pressure and temperature within the drying matrix as water vapour is trapped inside. This condition has been discussed earlier in section 4.3 and 4.4 able to promote melting of the frozen structure if the product's temperature exceeds its  $T_m$  and significant stress within the sample that it puffed. The high resistance to vapour flow is likely to be associated with the less ice crystals to sublimate in 60% systems resulting in lower porosity of the dried layer than 50% freeze-dried solids. Although, studies have also shown that freeze-drying of high solid content solutions exhibited high product resistance due to the tendency of solute to accumulate at the freezing front (Lewis et al. 2010; Sagara & Ichiba 1994).

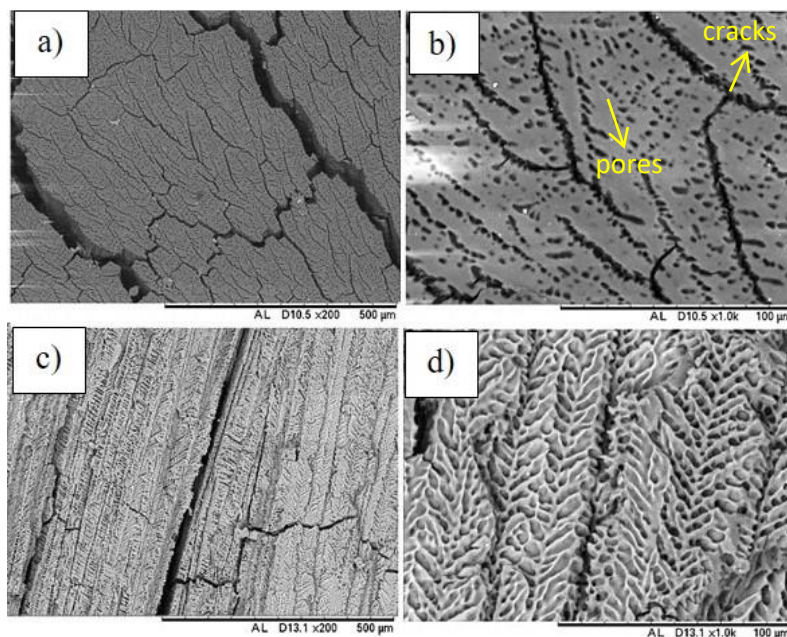


Figure 4.25 Scanning electron micrographs of surface structure (a-b) and inner structure (c-d) of freeze-dried 50% gum arabic. Images at 200x and 1000x magnification

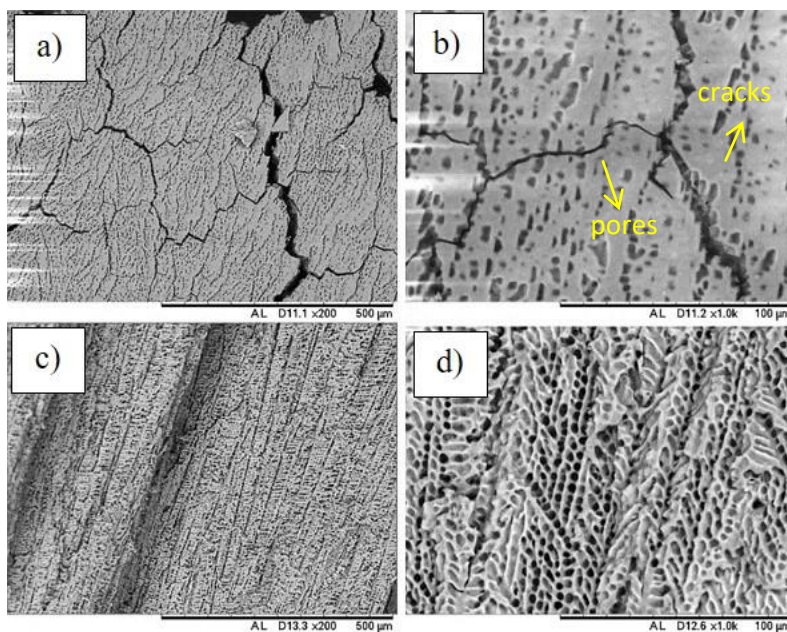


Figure 4.26 Scanning electron micrographs of surface structure (a-b) and inner structure (c-d) of freeze-dried 50% coffee. Images at 200x and 1000x magnification.

In the SEM images, orientation of crystal growth parallel to the direction of heat flow from bottom to top can be clearly seen in the 50% freeze-dried cakes. Although, similar

orientation was also found when heat flow was not controlled only from one direction as presented in figure 4.8 and 4.17. This similarity indicates that in both conditions (with and without insulated container), heat travelled exclusively from the coldest part of the sample which in this work happen to be from the bottom that is closest to the frozen shelf. The parallel orientation of ice crystals with heat/mass transfer direction (lamellar structure) has been suggested for easier heat and mass transfer in sublimation and thus reduce the drying time (Jin et al. 2018). Meanwhile, the dried layer of 60% gum arabic showed no specific orientation of the ice crystals. The high solid content and its influence on splitting of the crystal dendrites might be the reason for this observation. In principle, when ice nucleus begins to grow in a solution especially with high solid fraction, solute is pushed towards the ice crystal finger tips. This behaviour results in accumulation of solute at the freezing front decreasing the equilibrium  $T_f$  of the system which promotes local supercooling. The crystal tip starts to split due to unstable condition for crystal growth and protrusion advances in forward direction as well as to the side depending on where solute was rejected (Petzold & Aguilera 2009). Investigation on growth pattern of crystal dendrites in solutions of different concentrations and supercooling by Teraoka et al. (2002) revealed the sequential change in structure of growing ice from disk to highly branched morphology. In previous study, dislocation phenomenon which change the direction of crystal structure was also identified showing higher occurrence when concentration increased. Hence, it seems possible that splitting of the dendrites at different directions caused crystal growth in 60% gum arabic to be advancing in no particular orientation.

Examination of the puffed freeze-dried 60% coffee showed a dense solid network without evidence of pores from sublimated ice crystals. This structure is clearly different than the normal porous features expected for freeze-dried solids. Cracks were also visible on the surface which is related to the increase pressure of the system in the drying stage. As a result

of puffing, several air pockets surrounded by thick solid matrix can be seen within the cake structure. At high magnification (figure 4.28 (d)) the exterior of the solid part exhibited a structure that looks like it has been stretched. This feature points out that the freeze-concentrated 60% coffee may have gained structural mobility due to melting of the ice in addition to the increased inner pressure and therefore unable to maintain its shape. The same scenario could have also caused the partially dried matrix of 60% gum arabic to lose its porous structure.

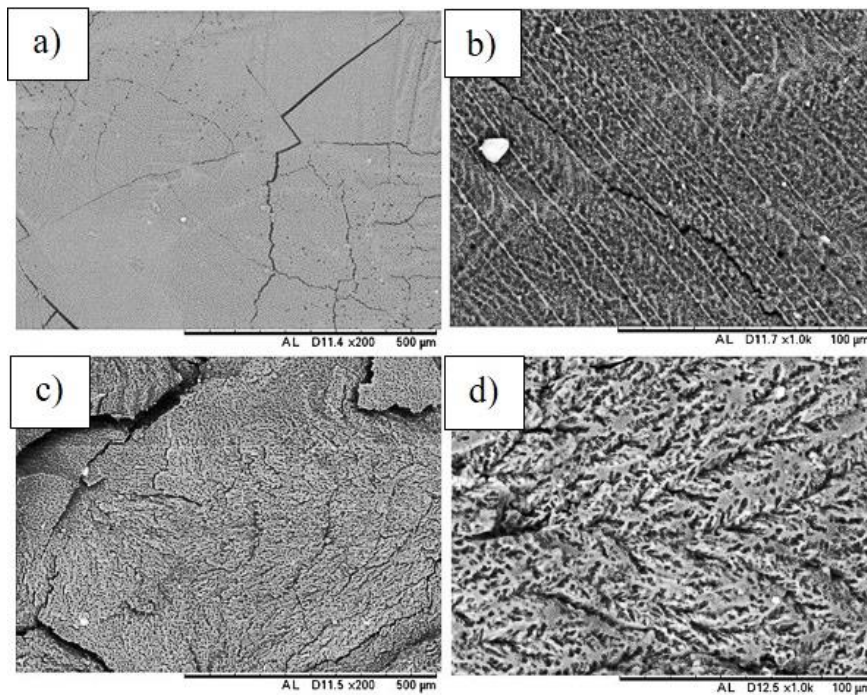


Figure 4.27 Scanning electron micrographs of surface structure (a-b) and inner structure (c-d) of freeze-dried 60% gum arabic. Images at 200x and 1000x magnification.

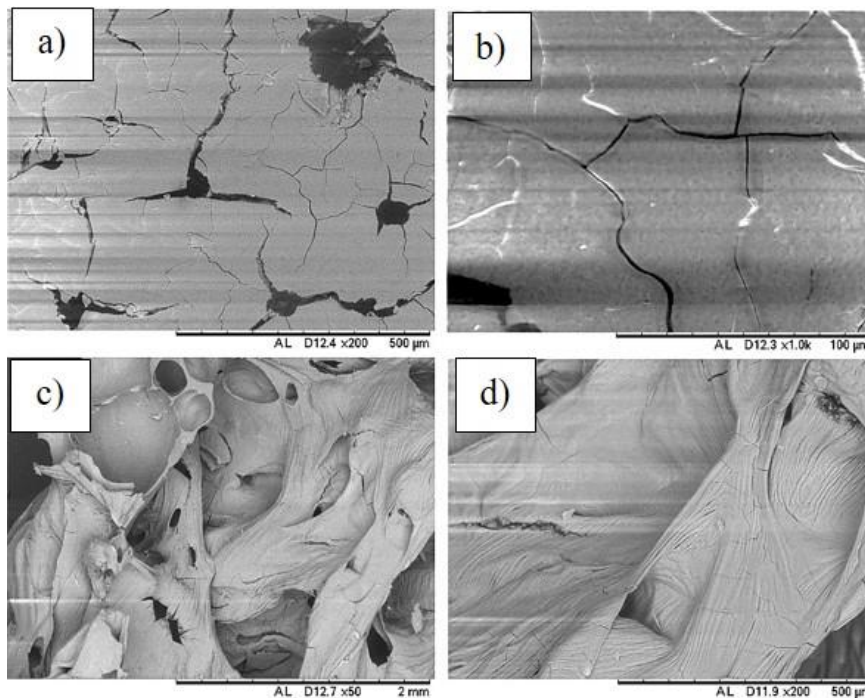


Figure 4.28 Scanning electron micrographs of surface structure (a-b) and inner structure (c-d) of freeze-dried 60% coffee. Images at 200x and 1000x magnification.

In the aspect of mean pore size which reflects the size of ice crystals (figure 4.29), both 50% gum arabic and coffee shared almost similar size at approximately  $50\mu\text{m}$ . The observed crystal dendrites in 60% gum arabic were on average  $18\mu\text{m}$  smaller than ice crystals formed in the less concentrated freeze-dried solids. This reduction in pore sizes with increasing concentration is again in accordance with the effect of solid content on  $T_n$  and  $T_f$ . It has been shown in this work that the low water content and its restricted mobility in highly concentrated solutions resulted in appearance of ice nuclei and occurrence of crystal growth at considerably lower temperature than 50% solutions. Hence, under this condition, small nuclei formed to develop into smaller crystal dendrites than system with higher water availability (50% w/w solutions). Figure 4.29 also shows that the freeze-dried structures of 50% initial solid content have higher overall porosity than 60% gum arabic in accordance with the measured pore sizes.

It is important to note that image analysis for determination of the pore sizes was not carried out on the SEM images of 60% coffee (see figure 4.27) due to the absence of crystal pores.

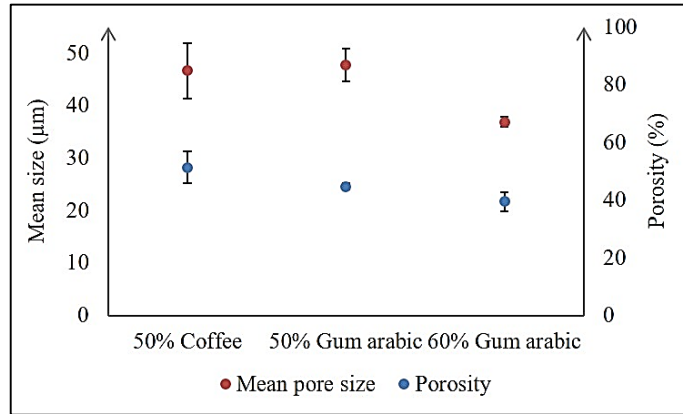


Figure 4.29 Average pore size and porosity of unidirectional frozen freeze-dried samples

### 4.5.3 Reconstitution

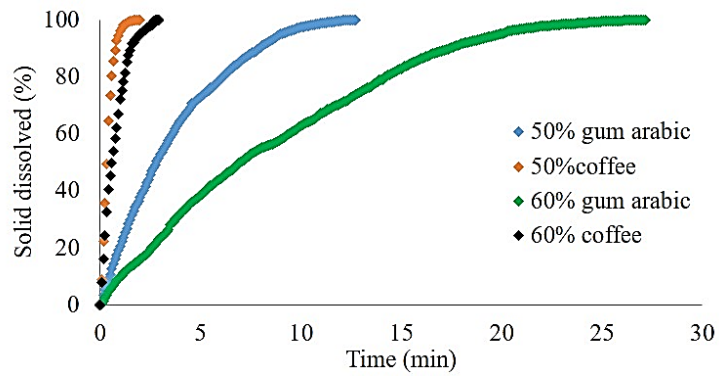


Figure 4.30 Change in amount of solid dissolved during reconstitution of concentrated freeze-dried gum arabic and coffee.

Reconstitution data in figure 4.30 shows the faster dissolution of freeze-dried coffee and samples from lower initial solid content. It reinforces the results from previous sections where freeze-dried solids with bigger pores and high porosity dissolved in the shortest time interval. This behaviour is likely to be affected by the increasing molecular diffusivity with porosity. The relationship between porosity and effective moisture diffusivity has been shown earlier in rehydration of dried carrots in which high bulk and open porosity resulted in increased moisture diffusion and faster rehydration (Marabi & Saguy 2004). In addition to the wide dendrites and porous surface of 50% dried systems, pores of parallel to the heat flow direction may have allowed water to diffuse through the solid particle with minimum resistance. Further, it was observed that despite the close cooling rates established between the uni-directionally frozen 60% gum arabic and the fast frozen 60% gum arabic, the slightly smaller pores (by 20 $\mu$ m) measured for the uni-directionally frozen system could have led to slower reconstitution (by 6 min) than the dried solid obtained with shelf pre-cooled freezing technique.

The apparent difference in dissolution kinetics between gum arabic and coffee has been recognized in previous analyses (section 4.3.3 and 4.4.3) attributed by the dissimilar response in water uptake mechanism. In this section, 50% gum arabic had longer dissolution time than 50% coffee by a factor of 6 while at higher concentration, gum arabic dissolved 9 times slower than coffee. With respect to each category that is gum arabic and coffee, slower reconstitution was exhibited by the 60% systems which experienced significant structural change in the drying process. However, the extensive puffing observed in 60% coffee demonstrated quite comparable dissolution with the 50% coffee compared to the difference observed for gum arabic. This relatively fast reconstitution is linked with the highly porous structure of the puffed bottom layer of the material.

## 4.6 Summary

This chapter has discussed microstructural development of concentrated freeze-dried systems (50 and 60% w/w) in relation to different freezing conditions namely (i) temperature oscillation; (ii) slow and fast cooling rates; (iii) unidirectional freezing. Thermal characterization of the materials used (gum arabic and coffee) with DSC was first presented for concentrations from 20 to 60% w/w. Ice nucleation ( $T_n$ ) and crystallization ( $T_f$ ) points derived from the freezing curves of each experimental set up were used to characterize the freezing behavior of the concentrated gum arabic and coffee solutions. The freeze-dried solids were then evaluated in terms of microstructure and reconstitution properties.

DSC analysis revealed the reduction of onset crystallization ( $T_{f-onset}$ ) and thermodynamic transition temperatures ( $T_m$ ) with increasing solid content.  $T_{f-onset}$  decreased as much as 16°C and 12°C each for gum arabic and coffee solutions when concentration increased from 20 to 60% w/w.  $T_m$  for gum arabic were measured in general at higher temperatures by 3°C compared to coffee. Increasing concentration also resulted in decreasing phase change enthalpy suggesting the possibility of reducing energy consumption in freeze-drying. As for glass transition,  $T_g$  for gum arabic were relatively constant between -16 to -17°C for concentrations of 20-40% w/w. Analysis on the melting endotherm of 50% gum arabic identified delayed ice formation due to the appearance of devitrification peak resulted in reduced  $T_g$  (-21°C). Lower  $T_g$  values between -26 to -28°C were measured for coffee solutions with 20-50% solutes. Meanwhile,  $T_g$  was difficult to be determined for the highly concentrated system (60% w/w) and was assumed to have the highest  $T_g$  among all concentrations. Assumption was made based on the restricted water molecules mobility at increasing solid content and where possibility of molecular movement could only increase with temperature.

In this set of experimental work, four freezing curves have been presented based on the different freezing conditions applied. Overall, a rather consistent nucleation ( $T_n$ ) and freezing temperatures ( $T_f$ ) were determined from each freezing profiles depending on the concentration and types of material. It has been demonstrated that  $T_n$  and  $T_f$  reduced on increasing solid content and gum arabic had lower transition temperatures than coffee on most occasions. Nucleation of ice in the 50% solutions occurred on average at  $-11^\circ\text{C}$  and  $-16^\circ\text{C}$  each for gum arabic and coffee solutions. Crystallization in these systems was followed at higher temperature which was identified at  $-8^\circ\text{C}$  for gum arabic and  $-11^\circ\text{C}$  for coffee. In the meantime, at 60% solid content,  $T_n$  and  $T_f$  between both materials varied by only  $1^\circ\text{C}$  on most circumstances showing values between  $-22$  to  $-28^\circ\text{C}$ . Greater temperature difference (by 4 to  $6^\circ\text{C}$ ) between 60% gum arabic and coffee was noted during unidirectional freezing in which the values were lower for gum arabic. Different freezing properties displayed by 50 and 60% formulations was associated with the different water molecule availability and mobility between the two concentrations. Comparing  $T_n$  with the onset of freezing derived from DSC thermograms which also signify the beginning of crystallisation, DSC produced lower values by  $10^\circ\text{C}$ . The large temperature variation was linked with the volume of sample used and presence of impurities which could have influenced the probability of nucleation.

Examination of the freeze-dried structures from all investigated freezing processes at macro and microscopic scale detailed the influence of formulation and freezing conditions on appearance as well as microstructural attributes of the final dried products. At all experimental set ups, freeze-drying the 60% w/w formulation especially coffee, produced freeze-dried solids with extensive structural expansion. This study has identified the non-typical structural changes during freeze-drying of the concentrated solutions where puffing was observed instead of the collapsed structure and volume reduction often referred to in the literature. Formation of

distinctive layers with dried top crust and porous bottom structure was recognized in such system. This observation was further confirmed with SEM evaluation showing the less porous crust surface and air bubbles within the dried matrices. It was suggested that internal pressure build up during sublimation affected by the high resistance to vapour flow contributed to the observed structural expansion. This obstruction of vapour flow was linked with the low porosity at the top crust due to less ice to sublimate in concentrated solutions and the possible solute accumulation at the freezing front in the time of freezing. At lower initial concentration and application of temperature oscillation during freezing, lesser extent of puffing was obtained indicated by the increased dry layer thickness and absence of entrapped air inside the freeze-dried solids.

Microstructural features were analysed and compared between the freeze-dried samples in terms of pore structure, size, size distribution and overall porosity. Overall, SEM images exhibited the porous structure of freeze-dried solids with the pore shape resembled formation of ice crystal dendrites. It was found that at 50% initial concentration, the pores were of circular and dendritic shapes displaying directionality parallel to the heat flow during freezing (bottom to top). The less concentrated systems were also characterized with pore sizes in the range of 60-135 $\mu\text{m}$  depending on the freezing treatments applied and types of material. As for the 60% solid content, much narrower dendritic pores developed mostly between 30-80  $\mu\text{m}$ . Difference in  $T_n$  and  $T_f$  that is driven by the accessibility of water molecules between these two concentrations led to the variation in pore size distribution.

In the aspect of freezing conditions studied, fluctuating temperature between -20 and -40 $^{\circ}\text{C}$  promoted growth of large ice crystals increasing the mean pore sizes, porosity and modified morphology of ice crystals in 60% gum arabic. Bigger ice crystals formation was affected by the increased molecular motion and mass transfer with temperature enabling

rearrangement of the small crystals to larger crystals. In addition, instrumental porosity measurement was conducted using pycnometer. Data from this technique indicated that open porosity was not markedly affected by the freezing process with porosity measured between 25-35% for all investigated systems. The lower porosity values measured with instrumental technique than results obtained through image analysis provide evidence that samples consisted of closed pores that were not measurable with helium pycnometer.

Microstructure obtained at different cooling rates (0.65°C/min and 2.22°C/min) however, displayed no pronounced effect on the size of ice crystals. Pores were measured to be slightly smaller upon shelf pre-cooled technique (fast cooling) than pores of freeze-dried solids frozen with shelf ramping method (slow cooling). While this was not expected, time and temperature profiles recorded at both freezing conditions confirmed the small differences observed.  $T_n$  and  $T_f$  which have determinant effect on ice crystals development were found to be more sensitive towards sample's formulation rather than the freezing methods investigated. Also, the effect of reduced porosity at high freezing rate was only observed in dried matrices with 50% initial concentration as 60% samples exhibited minimum variation (<1%) in porosity between the investigated freezing conditions. In the meantime, although smaller ice crystals (40-60µm) than 50% systems developed in 60% coffee, comparable porosity was obtained as a consequence of air bubbles formed after the system puffed.

Experiment with unidirectional freezing has shown that concentration exerted influence on the orientation of crystal growth. Growth pattern parallel to the direction of heat flow which is from bottom to top was visible in the freeze-dried cake with 50% initial solid content. The fact that crystal growth involved sequential transition from disk to branched morphologies, splitting of crystal dendrites at different directions led to ice crystals in 60% gum arabic advancing in no particular orientation. The high probability of solute accumulation at the ice

finger tips in higher concentrated solution which gave rise to constitutional supercooling was linked with the difference observed between 50 and 60% freeze-dried systems. Reduction in pore size and porosity at increasing solid content was also evident in this experimental work.

Freeze-dried solids from all investigated freezing processes were also subjected to reconstitution test either through real time video recording or conductivity measurement. This analysis was aimed to understand the effect of microstructure on performance of the dried materials. Based on the experimental design involved in this work, reconstitution results can be classified into three categories:

- 1) Effect of material: In this aspect, coffee dissolved 5 to 8 times faster than gum arabic. The greater extent of swelling observed in gum arabic and instantaneous disintegration of coffee particles were identified as the factor that led to variation in dissolution kinetics between both materials.
- 2) Effect of concentrations: Generally, less concentrated dried matrices reconstituted in the shortest time interval attributed by the large pores and high overall porosity measured. Difference in reconstitution time between 50 and 60% concentrations varied from as high as 20 min to as small as 2 min. Reduced variation between the two concentrations was observed during reconstitution of coffee where the puffed microstructure of 60% coffee influenced its fast reconstitution.
- 3) Effect of freezing condition: Temperature oscillation which produced freeze-dried structure with increased pore size and porosity effectively reduced the reconstitution time. On the other end, the lack of observable difference in microstructure after slow and fast freezing contributed to the overlapping dissolution curves indicated the minimal effect on dissolution

behavior. Reconstitution of dried particles from unidirectional freezing also showed the preference of dehydrated materials with big pores for fast reconstitution. 60% gum arabic with the smallest crystal size and melted bottom dissolved the slowest.

Overall, reconstitution data has shown the influential effect of microstructure developed after freeze-drying on dissolution process. In particular, it was found that increase in pore size and porosity allowed the freeze-dried particles to easily dissolved. However, different dissolution behavior exhibited by gum arabic and coffee systems revealed the determinant effect of hydration mechanism on the relation between porosity with reconstitution kinetics.

Concluding this chapter, the potential to control the freeze-dried microstructure of high solid system using different freezing methods has been demonstrated. Improved structure uniformity and development of big pores upon temperature oscillations contributes to the existing literature on manipulating ice crystals morphology during water crystallization.

## **CHAPTER 5**

### **Effect of solid content and primary drying temperature on microstructural development and reconstitution of freeze-dried systems**

#### **5.1 Introduction**

In the previous chapter, microstructure development during freeze-drying of high solid systems and their reconstitution thereafter were investigated in the aspect of varied freezing cycles. To further investigate the importance of processing parameters, this chapter presents microstructure and reconstitution properties of freeze-dried systems developed under the influence of different solid content and primary drying temperatures.

The final microstructure and properties of freeze-dried materials are in part dependent on the product initial formulation and shelf temperature during drying. These variables significantly influence the simultaneous mass and heat transport properties throughout the operation. For instance, collapse and glass transition points are widely recognized as indicators of the highest drying temperature allowed, and they are a function of product formulation that can be of different solid fraction or composition (Cieurzyńska & Lenart 2016; Harnkarnsujarit et al. 2012; Tsourouflis et al. 1976). This relationship has also been presented in chapter 4 (section 4.1) suggesting that selection of suitable operating temperatures is indirectly controlled by the composition of materials being processed.

Sublimation of the ice is a major part of the freeze-drying process, with most of the water in a product being eliminated at this stage. It requires the longest duration and highest energy consumption compared to freezing and secondary drying (Cieurzyńska & Lenart, 2011; Ratti, 2001). For this reason, primary drying has long been the focus area in process design

usually through manipulation of shelf temperature and chamber pressure (Patel et al. 2010; Barresi et al. 2009; Hammami et al. 1999; Sadikoglu et al. 1998). Thus, the objective of this chapter is to analyse and compare microstructural development between freeze-dried systems with different initial solid contents and primary drying temperatures, as well as its influence on their reconstitution behaviour.

## 5.2 Product temperature evolution during freeze-drying

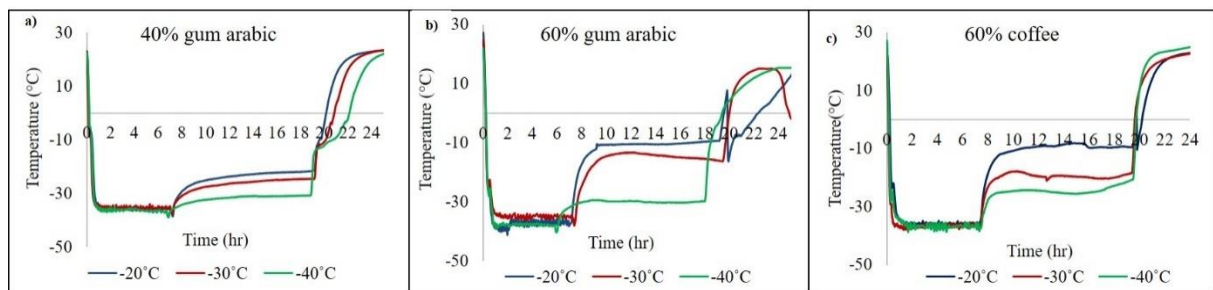


Figure 5.1 Examples of temperature profile during freeze-drying of gum arabic and coffee solutions under various shelf temperatures (-20, -30 and -40°C)  
 (a) 40% gum arabic; (b) 60% gum arabic; (c) 60% coffee

Figure 5.1 shows representative of temperature profiles for 40 and 60% w/w solutions during freeze-drying at three primary drying temperatures, as recorded using a K-type thermocouple (see section 3.2.3.1 for experimental details). In this set of experiment, samples were frozen to  $-40^{\circ}\text{C}$  and kept at this condition for 6hr, followed by 12hr of sublimation at the investigated temperatures ranging between  $-20^{\circ}\text{C}$  and  $-40^{\circ}\text{C}$  and further dehydrated at  $20^{\circ}\text{C}$  for 6hr.

The recorded product temperature revealed that concentrated systems underwent sublimation at higher temperatures compared to the less concentrated systems when shelf ( $T_s$ ) was set at high temperatures ( $-20$  and  $-30^{\circ}\text{C}$ ). For the 60% initial solid content of both systems,

temperature difference of 10 and 15 °C was found between the shelf and the recorded product temperature each for primary drying set at -20 and -30 °C. Notably, 60% coffee showed big temperature difference ( $\approx 15$  °C) during primary drying at -40 °C. The significant temperature difference observed between  $T_p$  (for both materials) from  $T_s$  show the possibility of physical changes in the frozen mass developed during freezing. On the other hand, during 12hr of drying, the 40% concentration did not deviate significantly from the set shelf temperatures. This variation in drying behaviour between the two concentrations is likely to be linked with the difference in thermodynamic stability. In this study, thermodynamic stability refers to the ability of the materials in maximally freeze-concentrated state to withstand the pre-set drying temperatures ( $T_s$ ) without exhibiting phase transitions like melting or glass transition (Figure 2.3). Thermal analysis in chapter 4 revealed the decreasing values of melting temperature ( $T_m$ ) with increasing solid content (see figure 4.4) where  $T_m$  for 40% gum arabic was measured at -5 °C, which is 10 °C higher than the value determined for 60% gum arabic. Coffee solutions on average have lower  $T_m$  (by 3 to 5 °C) than gum arabic indicating its less thermodynamic stability during processing. In the literature study (section 2.2.1.1), it has been discussed that at the end of freezing, solution become maximally freeze-concentrated as water has crystallized and further reduced the melting point (Roos, 1997). Thus, the lower transition point ( $T_m$ ) for highly concentrated systems strongly suggest the greater possibility for the materials to experience overheating during freeze-drying particularly when exposed to high primary drying temperature as it is easier to be exceeded (Roos 1997; Franks 1998).

Furthermore, in Figure 5.1(b), there is a notable temperature change in the 60% system dehydrated at -20 °C during the early stages of secondary drying. This observation is indicative that matrix of the freeze-dried solids such as viscosity may have been altered which caused temperature probe to move. At this processing condition, product temperature in the primary

drying stage was recorded to be very close to its  $T_m$ ,  $-15^\circ\text{C}$  (figure 4.4). Melting of the ice crystals developed during freezing could have occurred while drying resulting in increased mobility of the previously frozen matrix. It is possible that as drying proceeds to secondary drying, the increase  $T_s$  to  $20^\circ\text{C}$  may further change the physical state of the material which is assumed to be mobile causing the observed temperature change. Details on the possible physical changes is discussed further in the next section. Besides, it has been pointed out that there is a risk of collapse during early secondary drying when product temperature exceeds  $T_g$  (Patel et al. 2017; Pikal et al. 1990). Following the product temperature evolution during freeze-drying showed strong correlation between shelf temperature and concentration on the drying behaviour of the materials. The observed temperature difference between  $T_s$  and  $T_p$  for concentrated systems especially at high drying temperatures demonstrated the possibility of overheating which can affect freeze-drying efficiency. This section points out the importance of regulating primary drying shelf temperature in accordance with the properties of materials used in order to have efficient freeze-drying for high solid solutions. Useful information on thermal history of materials during processing can be used to relate with features of the end product.

## **5.3 Microstructure**

### **5.3.1 Pore structure of the freeze-dried cake**

Figures 5.2 and 5.3 each show the vertical and horizontal cross-sections of XRCT images of the freeze-dried gum arabic after binarisation with C-Tan image analysis software as affected by the different initial solid content and primary drying temperatures. Morphology of ice crystals was visible in previous chapter with SEM visualisation due to the interaction with high energy electron that revealed the characteristics of material's surface (Stokes 2013).

Images acquired with XRCT technique however, provide microstructural features based on differences in X-ray absorption capacity between voids and solid affected by the different density. Thus, the cross-sections reflect the pores (black entities) and solid (white entities) network formed after freeze-drying. The freeze-dried systems were found not to vary significantly between drying temperatures but increasing the solid concentration notably changed the microstructure of the freeze-dried cakes.

Overall, the freeze-dried systems with low gum arabic content (20-40% w/w) show needle-like pores whereas large circular pores were observed at higher concentrations. Development of large circular pores in the freeze-dried solids of 40 and 50% initial solid content was especially observed at the bottom of the samples while 60% system displayed circular pores throughout the sample height. This structural feature observed for the most concentrated formulation could be linked with the high sublimation temperature displayed in figure 5.1 (b) which indicated the possible significant structural changes during drying. Also, it is worth to consider the microscopic visualisation under SEM in previous chapter which revealed the development of dendritic and circular shaped pores in the freeze-dried solids of 50 and 60% concentrated systems. Thus, it would be relevant to relate the needle-like entities with the dendritic crystals formed.

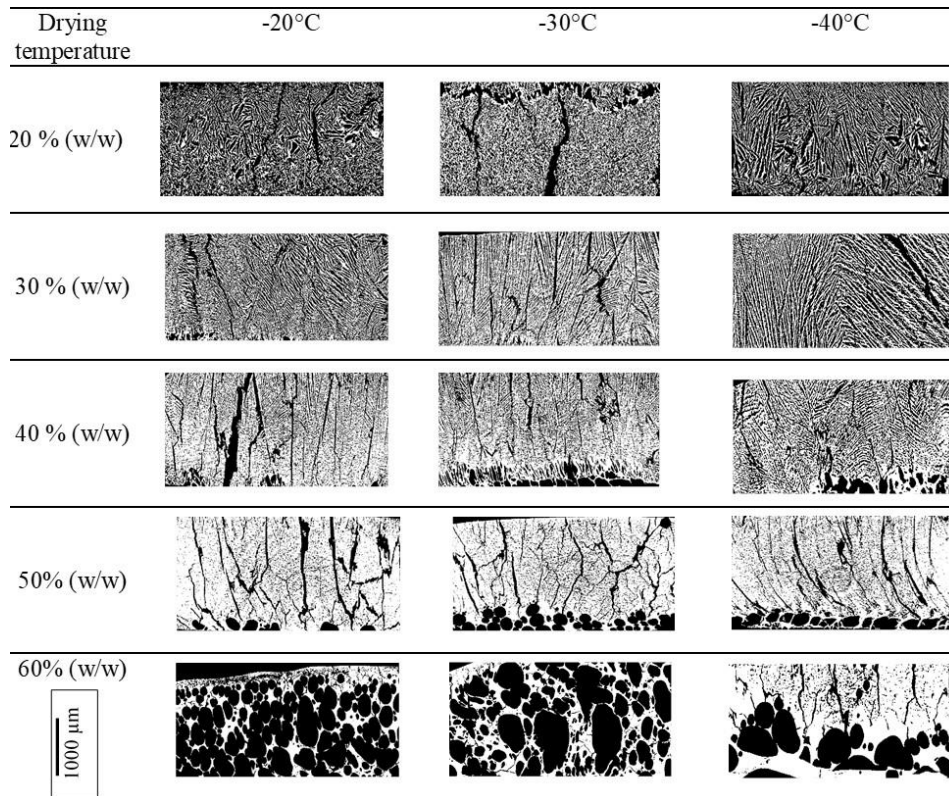


Figure 5.2 Vertical cross-section of freeze-dried gum arabic solutions dried at -20, -30 and -40°C.

The term puffing has been used in chapter 4 to describe the phenomenon of structural instability during freeze-drying of the studied solutions. In fact, Tsourouflis et al. (1976) has regarded puffing as part of the structural collapse due to collapse of capillaries in the dry layer. The microstructures obtained particularly for the 40-60% concentrated systems appeared to be consistent with the earlier description. Therefore, it seems possible to relate the observed microstructure with the internal stress caused by entrapment of water vapour from the sublimated ice crystals corresponding to the high resistance at drying interface. This observation further highlights that the less ice crystals to be sublimated in concentrated solution due to low freezable water content (see Table 4-1) can increase resistance at the sublimation front affected by reduced porosity. Additionally, increased in pressure also increase the inner temperature (through the produced latent heat) which can influence product to surpass its  $T_m$ .

It has been shown previously by Sagara & Ichiba (1994) during freeze-drying of coffee that high resistance at the sublimation interface due to solute accumulation during freezing contributed to the high internal pressure, increased the product's temperature beyond its  $T_m$  and eventually led to puffing. In this current investigation, it appeared that 60% gum arabic displayed the most affected morphologies when dried at -20 and -30°C. As evident during temperature recoding, the  $T_p$  was raised near its  $T_m$  (-15°C) under these high operating shelf temperatures. In this condition, viscosity hence mobility of the freeze-concentrated solution could have been gained, contributing to the loss of previously frozen structure. In the literature review, viscosity in the range of  $10^4$  to  $10^7$  Pas was proposed as the critical range that contributes to the loss of structure (Karanthanos et al. 1996). Therefore, the combination of increased internal pressure, melted surroundings and the freeze-drier operating at vacuum condition may further caused the significant expansion at high operating temperatures. Previously, Khalloufi & Ratti (2003) showed the higher risk of structural instability with increasing drying temperature during freeze-drying of apple and pear. It was found that dried fruits obtained with high drying temperature displayed discolouration and poorly interconnected pores.

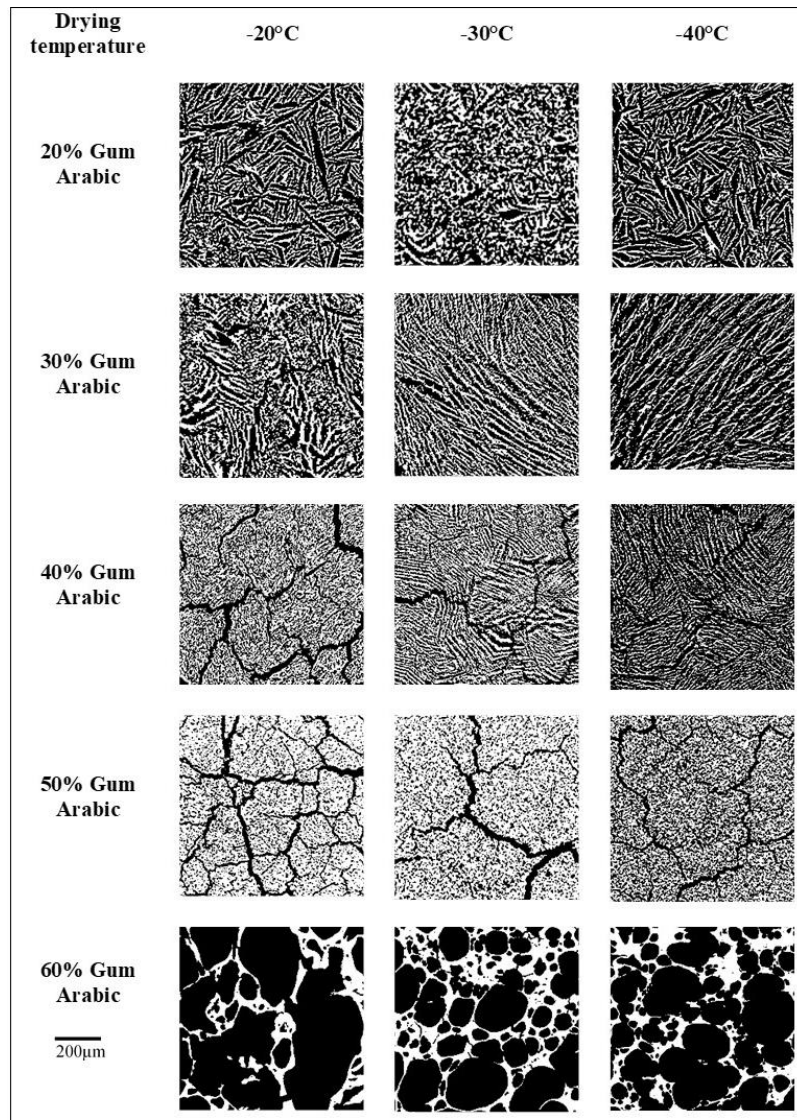


Figure 5.3 Horizontal cross-section of freeze-dried gum arabic solutions dried at -20, -30 and -40°C

The lower degree of puffing in the dried cake of 40 and 50% initial concentration as discussed in section 4.3.2, is driven by the fact that both systems have higher water content to be crystallized and sublimated compared to the solution with 60% gum arabic. Hence, more pores created in the less concentrated solutions influencing the rate of heat and mass transfer in the time of drying. Moreover, DSC analysis in section 4.2 showed the link of high  $T_m$  values with less concentrated solutions. The higher  $T_m$  of 40% (-5°C) and 50% (-6°C) gum arabic

solutions indicate that both samples have greater thermodynamic stability than the 60% system causing variation in structural response during freeze-drying between these concentrations. Differences in thermal properties between concentrations points out the importance of regulating the primary drying shelf temperature in order to control structural evolution in the freeze-dried system.

From the binary images, cracks were seen in some parts of the freeze-dried cake being more obvious in 50% w/w sample. The cracked appearance was also visible under SEM visualization in chapter 4 which suggest it may in part be due to the inner structural expansion. Meanwhile, cracks observed in the freeze-dried solid of 20 and 30% initial concentration could be due to stress developed during evaporation of unfrozen water in the secondary drying stage as suggested in recent studies by Ullrich et al. (2015) and Patel et al.(2017). As unfrozen water is evaporated at high temperature (20 °C), pressure within the solid matrix could have increased which is then released when tensile stress exceeds the tensile strength allowing unfrozen liquid to be removed.

Microstructure of the freeze-dried coffee solutions processed at different drying temperatures is presented in Figure 5.4 and 5.5. Microstructural development seems to be consistent with the trend observed in freeze-dried gum arabic. For instance, needle-like pores were also displayed by the freeze-dried matrix of 20 to 40% w/w initial concentration. Coffee solutions with higher solid fraction were similarly identified to experience structural expansion with development of large circular pores. However, a greater expansion was noticed for 60% coffee than 60% gum arabic dried at -40°C. This difference could be explained by the lower melting ( $T_m$ ) of coffee compared to gum arabic. Hence, the lower transition points make the 60% coffee more susceptible to significant structural changes compared to gum arabic.

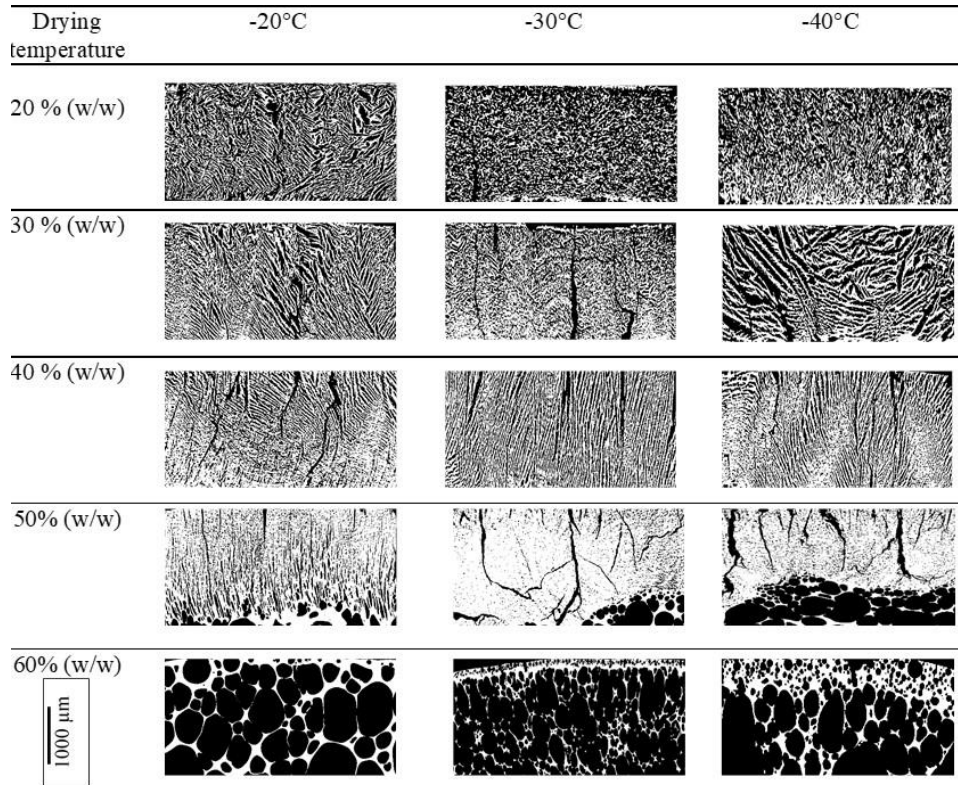


Figure 5.4 Vertical cross-sections of freeze-dried coffee solutions dried at -20, -30 and -40°C.

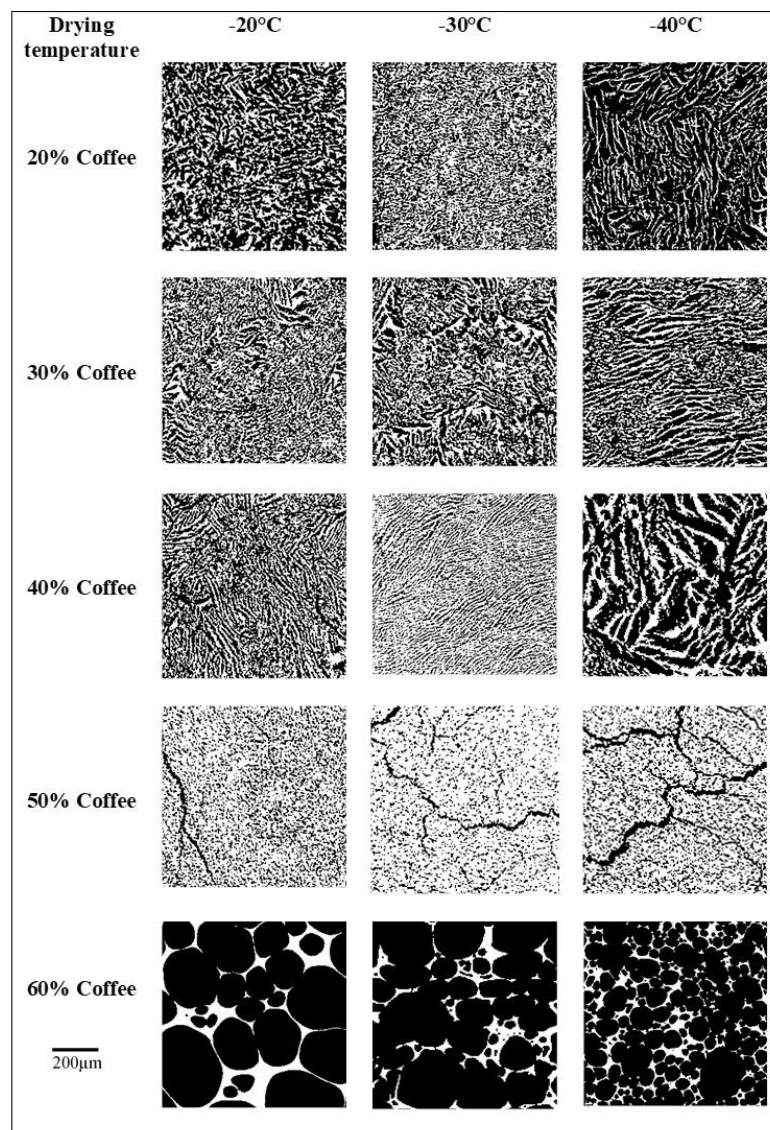


Figure 5.5 Horizontal cross-sections of freeze-dried coffee solutions dried at -20, -30 and -40°C.

### 5.3.2 Pore size distribution

The pore size distribution of freeze-dried gum arabic is given in figure 5.6 for all concentrations and drying temperatures investigated. As detailed in chapter 3, pores in this study were determined as diameter of a circle with area equivalent to the pore area. It can be clearly seen from the graphs that at highest concentration, significantly larger pores in the range of 200-1800µm developed. Meanwhile, pores of 6 to 8 times smaller were found in samples

with lower solid content. Distribution of large pores in the 60% systems is in accordance with the puffed freeze-dried cake generated.

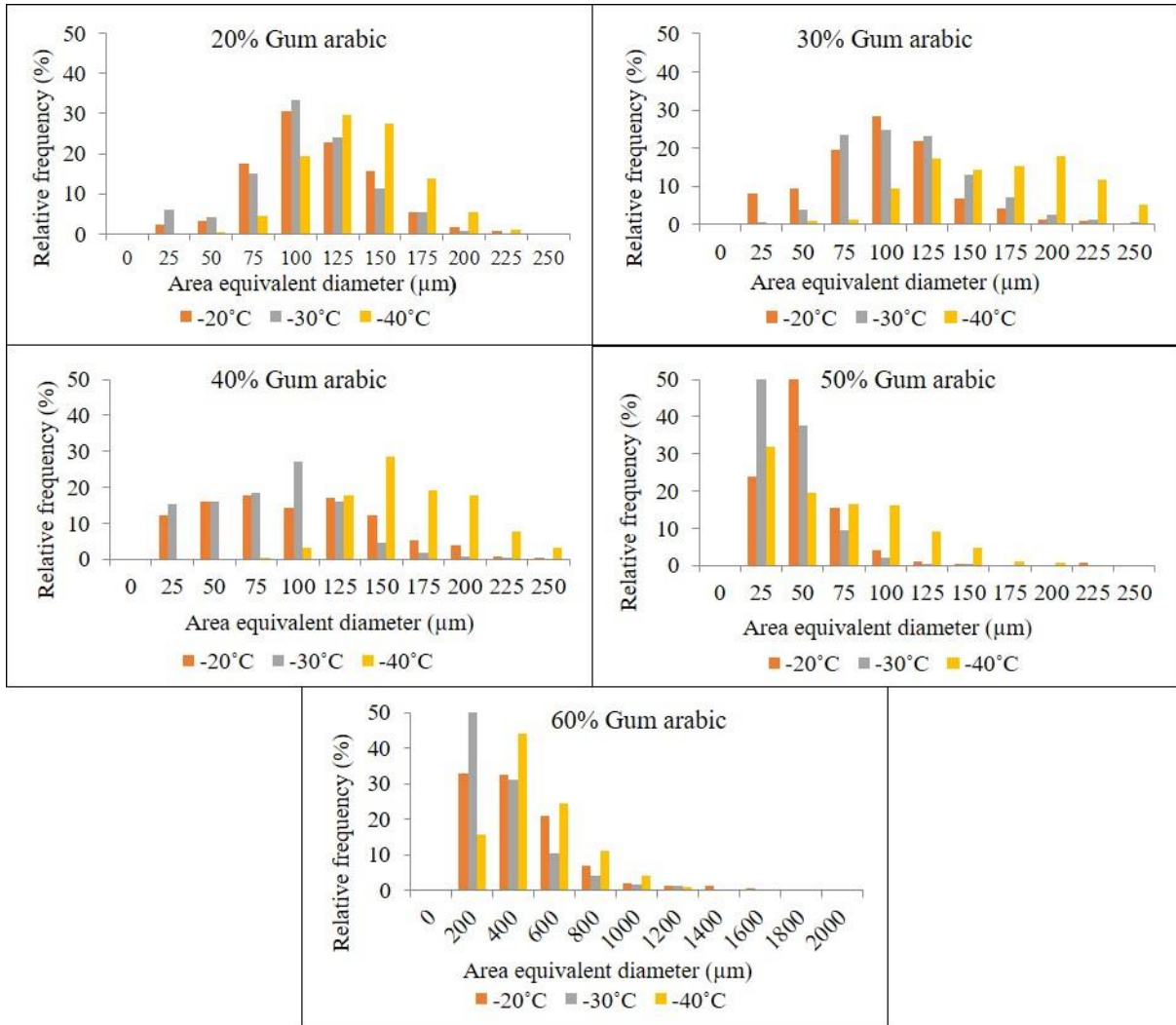


Figure 5.6 Pore size distribution of freeze-dried gum arabic processed at different primary drying temperatures.

Freeze-dried solids of 20-40% systems displayed broader pore size distributions than the higher concentrated systems with slightly bigger pores identified when dried at -40°C. This data seems to be consistent with research on the effect of drying temperature on pore formation of freeze-dried garlic (Sablani et al. 2007). The previous analysis showed greater distribution

of smaller pores in sample freeze-dried at  $-5^{\circ}\text{C}$  as opposed to primary drying set at  $-25^{\circ}\text{C}$  due to the tendency of large and open pores to collapse at high drying rate. Overall, high drying temperatures,  $-20$  and  $-30^{\circ}\text{C}$  resulted in more or less similar pore size distributions for all concentrations. This result agrees qualitatively with the binary images in figure 5.2-5.5. The very fine entities observed at the upper layer of 50% gum arabic were measured to be less than  $100\mu\text{m}$ . Meanwhile, despite the notable expansion observed in the vertical cross-section of 60% gum arabic dried at  $-20^{\circ}\text{C}$ , high distribution (20-30%) of pores in the range of  $200\text{-}600\mu\text{m}$  were measured in the freeze-dried cake. This data could be linked with more pore interconnectivity shown in the horizontal cross-section that formed few large pores ( $800\text{-}1400\mu\text{m}$ ) compared to the one dried at lower temperatures.

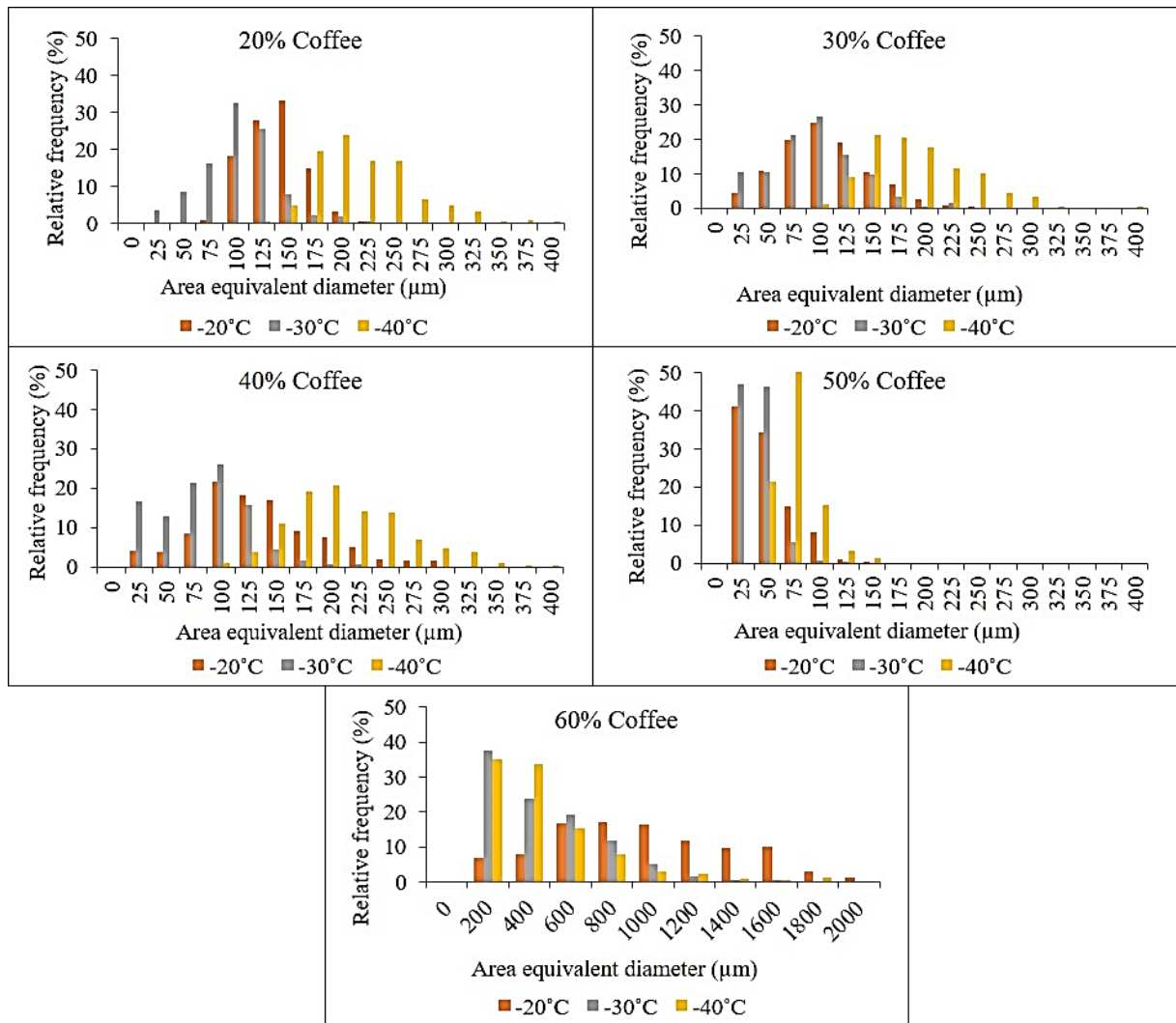


Figure 5.7 Pore size distribution of freeze-dried coffee processed at different primary drying temperatures.

In figure 5.7, the broader pore size distribution in freeze-dried coffee compared to gum arabic is presented. Pores of bigger than 250 $\mu\text{m}$  and up to 400 $\mu\text{m}$  have been measured for the dried systems of 20-50% w/w initial solid content. Similar notable variation between 60% concentration and the rest of the samples was also evidenced in the freeze-dried coffee having pores distributed from 200-2000 $\mu\text{m}$ . In general, trend of pore sizes in freeze-dried gum arabic can also be found in freeze-dried coffee (e.g. larger pores at primary drying temperature of -40 $^{\circ}\text{C}$  compared to -20 and -30 $^{\circ}\text{C}$  for systems with 20-40% solids, large pore sizes for the 60%

initial concentration system, and small pores for the top layer of the 50% initial concentration system) confirming the pore structures revealed in the binary images. Bar graphs of 60% coffee also indicate the greater structure expansion and heterogeneity of pore sizes when drying conducted at  $-20^{\circ}\text{C}$ . This sample has wider pore size distribution (up to  $2000\mu\text{m}$ ) than the pore sizes developed at  $-30$  and  $-40^{\circ}\text{C}$  (up to  $1200\mu\text{m}$ ). At lower temperatures, the pore sizes distribution skewed to the left with highest frequency shown at 200 and  $400\mu\text{m}$ . This result might be due to the fact that higher drying rate at  $-20^{\circ}\text{C}$  could have caused more internal pressure build up due to surface hardening during rapid drying resulting in significant puffing (Rahman 2001).

### 5.3.3 Porosity

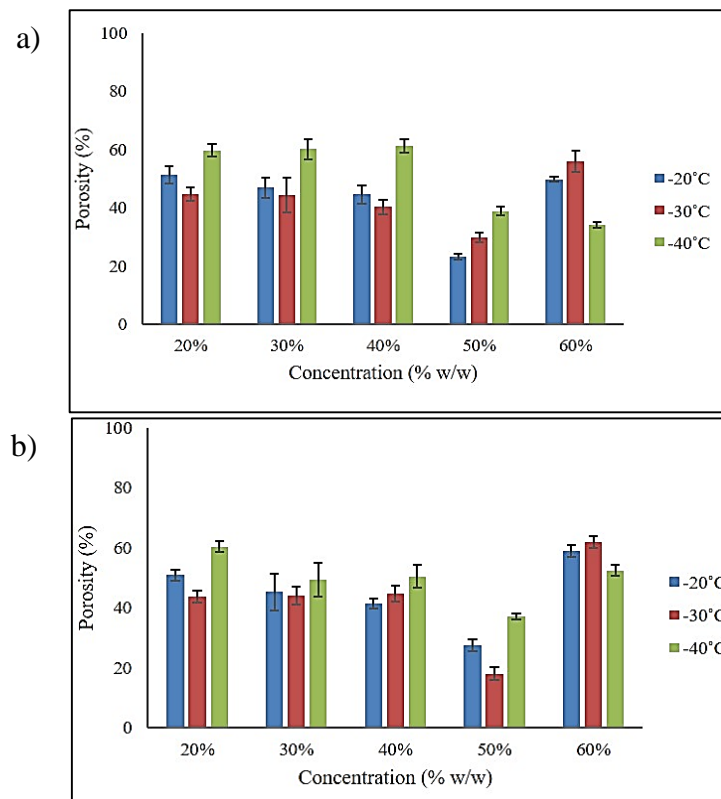


Figure 5.8 Overall porosity of freeze-dried a) gum arabic and b) coffee at different concentrations and primary drying temperatures determined from SEM images.

Image analysis was used for determination of the total porosity, defined as the ratio between the pore area and the total area of the cross-section (Silva et al. 2015). Figure 5.8 shows that freeze-drying conditions had little effect on the porosity values. Nevertheless, for concentration from 20 to 50% w/w, highest fraction of pore area was quantified for samples dried at -40°C. This could be related to the presence of bigger pores in these samples compared to pore sizes from higher drying temperature. Besides, drying at such low temperature may help preserve the materials in solid amorphous state during drying especially for the lower concentration formulations due to the systems being below the melting temperature,  $T_m$  (reported in chapter 4). Hence, collapse of pores could have been avoided that produced final dried product with higher porosity (Rahman 2001).

At 50% concentration, both materials showed lowest overall porosity with less than two fifths of the freeze-dried structure were voids. The low porosity value may be a factor of less tendency for ice crystal formation in high solid solution that led to lower number of ice crystals compared to the 20, 30 and 40% solutions. While pores developed from ice sublimation, smaller amount of ice crystals can produce final dried product with less pores. This is indicated by the very small voids in the upper part of the freeze-dried 50% systems displayed in figure 5.2 and 5.4. The effect of concentration on porosity was also reported in (Cassanelli et al. 2017) where 1% increment of gellan gum resulted in freeze-dried structure with total porosity about 12% less than lower polymer concentration. This previous finding further reinforce that water content and mobility can considerably affect the amount of ice crystal form influencing the pore development during freeze-drying. In the case of 60% samples, structural expansion resulted in high overall porosity of the freeze-dried solids. Unlike the less concentrated samples, lowest drying temperatures produced end product with smallest porosity values in the freeze-dried 60% gum arabic and coffee. In general, data on porosity of the freeze-

dried solids is in accordance with the trend observed in the microstructure evaluation. These structural parameters play an important role in determining the reconstitution properties of freeze-dried product.

#### 5.4 Reconstitution behavior

Reconstitution of freeze-dried coffee and gum arabic processed at three drying temperatures was analysed based on changes in conductivity values. The values were used to derive the amount of solid dissolved as a function of time using equation 6. Dissolution curves of the freeze-dried samples at various concentrations are presented in figure 5.8 displaying the increasing amount of mass dissolved with time. Experimental data fitted with Weibull's equation as detailed in equation 7 (Skrdla 2007) is also shown in the dissolution curves.

$$\frac{y}{y_{max}} = 1 - \exp(-kt^n) \quad (7)$$

Where;

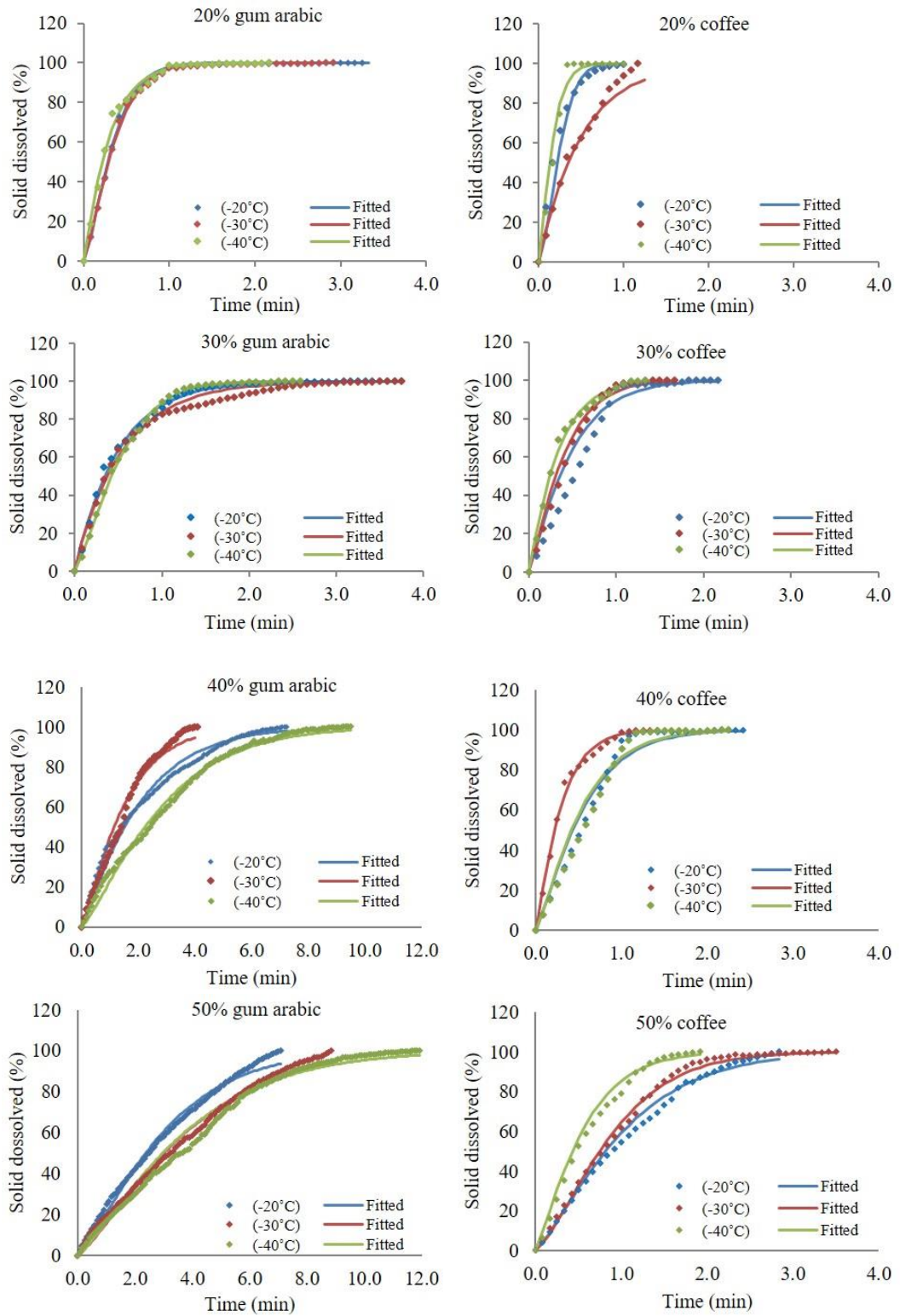
$y$  = solid dissolved at time  $t$

$y_{max}$  = 100% dissolved solid

$t$  = time (min)

$k$  = rate constant (% min<sup>-1</sup>)

$n$  = shape parameter



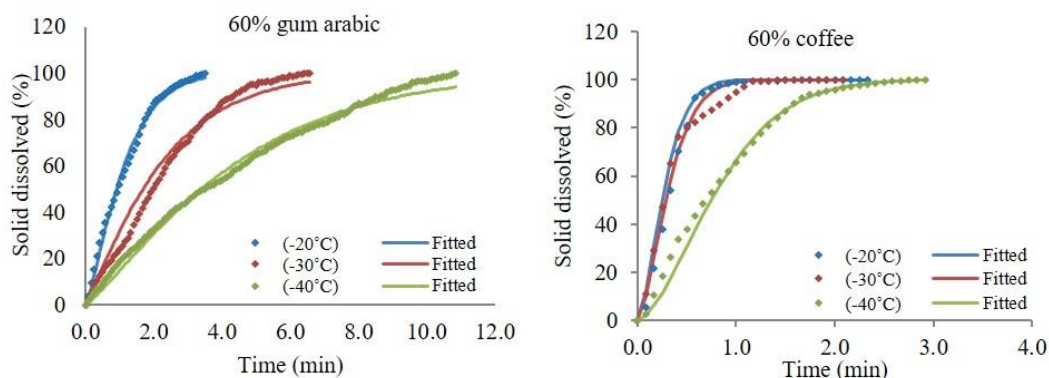


Figure 5.9 Effect of freeze-drying cycles and concentrations on dissolution profiles of freeze-dried gum arabic and coffee. Data is fitted with Weibull's function.

Comparing between materials, coffee as expected, dissolved overall quicker than gum arabic, in particular at high initial solid content. Dissolution duration for freeze-dried coffee was on average 2-5 times faster compared to dehydrated gum arabic. This difference which has been highlighted in previous chapter was attributed by the variation in physical mechanisms involved during dissolution of both systems (see figure 4.11 and 4.13). The rapid disintegration of coffee particles and apparent initial step of water adsorption by dried gum arabic particles contributed to the variation in dissolution kinetics between these materials.

Graphs of dissolution also provide evidence on the variable effect of drying temperature on the dissolution kinetics of the freeze-dried samples. In the case of gum arabic, only the 60% concentration was markedly affected by processing temperature showing the decreasing slope at lower temperature. This indicates that 60% gum arabic dried at the coolest temperature (-40°C) dissolved the slowest which contradicts the faster rehydration recorded by Barresi et al. (2009) for carbohydrate components freeze-dried at -50°C than at -32°C. Although structure expansion was observed for concentrated gum arabic at all drying temperatures, a rather thicker cell wall surrounding the voids can be seen in X-ray cross-section of sample dried at -40°C possibly causing its long dissolution time. Meanwhile, dissolution of freeze-dried gum arabic from lower concentrations (20 to 50% w/w) showed no apparent variation between drying

temperatures studied. Similar dissolution patterns can also be observed for dried coffee from 20-40% w/w concentrations which reached complete dissolution within 1min for all drying temperatures. This small difference in dissolution behaviour of less concentrated formulations could be related to the comparable microstructure observed (figure 5.2 and 5.3) and porosity measured between the temperatures applied. However, dissolution of 50% coffee has revealed a pattern not observed in any other samples in which fastest dissolution has been recorded for sample dried at -40°C. Referring to the microstructure obtained, the system displayed bigger circular voids and cracks compared to the one dried at higher temperatures contributing to its faster dissolution. This result shows that dissolution of the freeze-dried materials is strongly controlled by the microstructural features.

On the other end, concentration showed considerable effect on the dissolution behaviour that is likely to be driven by differences in microstructure. Rapid dissolution is consistently displayed by freeze-dried systems with 20, 30 and 40% initial solid content. These systems completely dissolved just under 2 min for gum arabic and coffee took half of the time to become a solution. At higher concentration, only half of the solutes have dissolved during the first two minutes. The rapid dissolution in less concentrated systems is attributed by the presence of more ice crystals to sublimate that results in more pores compared to 50 and 60% formulations. It could also be affected by the needle-shaped pores that is in favour for capillary flow of water (Koh et al. 2011). Meanwhile, it is noticed that dissolution of freeze-dried 60% coffee and gum arabic was faster than that of the 50% initial concentration systems. It seems possible that the formation of large circular pores due to puffing which increased porosity of the 60% formulation led to its fast reconstitution. Similar enhanced water uptake with increasing pore size has been found during rehydration of freeze-dried carrot and dissolution of freeze-dried rice porridge (Marabi & Saguy 2004; Koh et al. 2011). Due to the small pores at

the top layer of freeze-dried 50% solution and its dense structures, dissolution process lasted longer than other freeze-dried systems.

Table 5-1 Weibull's function parameters derived from dissolution data of gum arabic using equation (7)

Concentration (%)	-20°C			-30°C			-40°C		
	k	n	R <sup>2</sup>	k	n	R <sup>2</sup>	k	n	R <sup>2</sup>
20	1.44E-02	1.367	0.998	1.63E-02	1.312	0.998	4.23E-02	1.086	0.994
30	3.15E-02	1.020	0.996	3.38E-02	0.971	0.992	1.05E-02	1.299	0.998
40	4.83E-03	1.101	0.988	5.21E-03	1.154	0.987	1.76E-03	1.220	0.994
50	1.33E-03	1.261	0.990	1.09E-03	1.260	0.989	1.29E-03	1.228	0.986
60	4.22E-03	1.275	0.993	3.66E-03	1.137	0.987	1.15E-03	1.203	0.991

Table 5-2 Weibull's function parameters derived from dissolution data of coffee using equation (7)

Concentration (%)	-20°C			-30°C			-40°C		
	k	n	R <sup>2</sup>	k	n	R <sup>2</sup>	k	n	R <sup>2</sup>
20	5.43E-02	1.107	0.979	3.28E-02	1.004	0.989	5.31E-02	1.257	0.979
30	2.20E-02	1.129	0.966	2.13E-02	1.193	0.992	3.85E-02	1.083	0.994
40	1.40E-02	1.200	0.982	3.80E-02	1.125	0.993	1.40E-02	1.212	0.976
50	5.26E-03	1.255	0.992	3.65E-03	1.380	0.997	1.38E-02	1.207	0.992
60	1.09E-02	1.537	0.989	9.43E-03	1.511	0.987	1.73E-03	1.575	0.995

In terms of trends, Weibull's equation (equation 7) was used to fit the experimental data. This equation has been suggested for modelling rehydration of porous food and that often involve different physical mechanisms of water uptake (Marabi et al. 2003; Wallach et al. 2011). The high coefficient of determination ( $0.97 < R^2 > 0.99$ ) presented in table 5-1 and 5-2 indicated that Weibull distribution is applicable in describing dissolution of the freeze-dried particles. The derived estimates of process kinetics (k) and shape parameter (n) are also listed in the table above. From the derived k values, a good correlation with the initial concentration

is shown in which smaller values were obtained on increasing concentration demonstrating the slower dissolution of high solid freeze-dried systems. Although, on certain occasions, this trend was not followed. For instance, high process kinetic was determined for reconstitution of freeze-dried 30% gum arabic as well as 40 and 50% coffee than the respective lower concentrated systems depending on the drying temperature. This inconsistency may be related to the microstructure obtained (e.g. large pores and high porosity) at such condition has enabled fast dissolution of the dried particles thereby, reducing the influence of concentration.

Meanwhile, the Weibull shape parameter  $n$  that describes the underlying principle behind transport of water during dissolution was found to be fairly constant between 0.95 to 1.5. This range of  $n$  values are indicative on the combination of several water uptake mechanisms involved during dissolution that could be the control factor on process kinetics. The mechanisms include molecular diffusion, capillary imbibition and molecular relaxation (swelling) have been described earlier in studies on drug release profiles and food rehydration (Papadopoulou et al. 2006; Marabi & Saguy 2004; Marabi et al. 2003). These studies interpreted that estimates of  $n \leq 0.75$  signifies diffusion controlled process while higher  $n$  was associated with combined mechanisms which contribute to the complexity of the wetting process. In the present work, the estimated Weibull  $n$  parameter further explains the difference in dissolution behaviour observed between gum arabic and coffee. It seems possible that the correlation between microstructure of the dried solids and properties of the materials govern the variation of mechanisms involved consequently the dissolution time.

## **5.5 Summary**

In this chapter, influence of formulation and primary drying temperature on microstructure formation as well as reconstitution time were investigated. It has been

demonstrated that high solid content formulations are susceptible to apparent structural changes even when dried at lowest temperature,  $-40^{\circ}\text{C}$  affected by the low melting temperature ( $T_m$ ). Puffed freeze-dried structures were obtained for the most concentrated system showing pore sizes as high as  $2000\mu\text{m}$  and about 50-60% porosity. The observed porous structure was explained based on the internal stress development as a result of resistance to vapour flow and high shelf temperature. Meanwhile, lower degree of puffing was displayed by the freeze-dried solids of lower initial concentration with greater portion of the dried layer that is filled with small pores. This structural difference was affected by the less resistance to vapour flow at the surface as more pores developed in the less concentrated systems due to more ice crystals development. For the 20-30% w/w solutions, freeze-drying resulted in end product having small pores with needle-like appearance and porosity around 50%.

Microstructure properties of the freeze-dried samples were fairly affected by the variation of drying temperature. Closer inspection on the porous matrix revealed the inverse relationship between pore size and the temperature applied. However, opposite effect of processing temperature on pore size development was identified for the 60% systems. Although variation in porosity between primary drying condition is very small, high porosity generally corresponds to sample with bigger pore area. For concentrations between 20-50% w/w, samples dried at  $-40^{\circ}\text{C}$  had the highest porosities but for the 60% formulations, decreasing porosity values with temperature was shown. This contradictory trend was affected by the lesser structural expansion observed for 60% systems dried at  $-40^{\circ}\text{C}$  than at higher temperatures.

Reconstitution behaviour was subsequently analysed and exponential dissolution curves were obtained for all samples. Sample's initial solid content and structural features of the freeze-dried matrix imparted more considerable effect than drying temperature on the dissolution behaviour. Coffee and less concentrated systems (20-40% w/w) took less time to

dissolve than gum arabic and freeze-dried solids from higher initial concentrations (50 and 60% w/w). The instantaneous disintegration of coffee contributed to its rapid dissolution whereas faster water uptake in 20-40% formulation was driven by the high overall porosity and capillarity. In addition, the puffed structure of 60% systems demonstrated faster reconstitution than freeze-dried solids of 50% formulation. Dissolution data had good correlation with the Weibull function and the shape parameters derived from this model indicated the complex and variable water uptake mechanisms involved during dissolution.

Understanding the microstructure formation at different process conditions helps to identify key factors contributing to the design of more efficient freeze-drying processes. Product formulation and shelf temperature each has a role in governing the porous structure of freeze-dried cake which directly influence product performance. While structural expansion obtained after freeze-drying the high solid solutions presents the potential to enhance porosity, the expansion was followed by partial melting of ice thereby inducing non-uniform freeze-dried cake appearance. A further investigation on the effect of aeration on freeze-dried microstructure of highly concentrated materials is discussed in the next chapter.

## CHAPTER 6

### Freeze-drying of aerated systems

#### 6.1 Introduction

The experimental work considered so far has been towards the designs of the two important stages in freeze drying namely freezing and sublimation steps corresponds to the process-structure-property relationship. Having studies conducted focusing on the high solid system, freeze-drying of the 50 and 60% w/w solutions that were initially incorporated with air is presented in this chapter.

In the food industry, manufacturing of products such as ice-cream, carbonated drinks, bread and coffee involved incorporation of air for the distinguish appearance and mouthfeel experience (Campbell & Mougeot 1999). Several reports have also highlighted the concept of aeration in assisting drying of the heat-sensitive, high sugar content and viscous foods known as foam-mat drying (Sangamithra et al. 2015; Ratti & Kudra 2006). Increased surface area of the materials being dried was recognized as the key factor that benefitted the dehydration process. While water can easily vaporize at high surface area, it helps to accelerate the drying duration. Thereby, making food dehydration more economical. Muthukumaran et al. (2008) and Raharitsifa & Ratti (2010) have applied foaming method before freeze-drying of egg white and apple juice. The experimental data and mathematical modelling on heat and mass transfer in these studies have shown the positive impact on improving freeze-drying efficiency as well as product quality. These previous findings gave insights on the potential of air to facilitates freeze-drying of the highly concentrated systems (e.g. 50 and 60% w/w solute).

In this chapter, work presented has focused on freeze-drying the aerated 50 and 60% solutions. Similar varied freezing conditions and primary drying shelf temperatures applied in

non-aerated systems were carried out with the aim to investigate the prospective of aeration as an additional treatment in freeze-drying the concentrated systems. Therefore, freezing profile of the aerated solutions as well as microstructure and reconstitution kinetics of the aerated freeze-dried solids are reported in relation to the different processing conditions conducted.

## 6.2 Effect of freezing conditions on microstructure and dissolution of aerated freeze-dried systems.

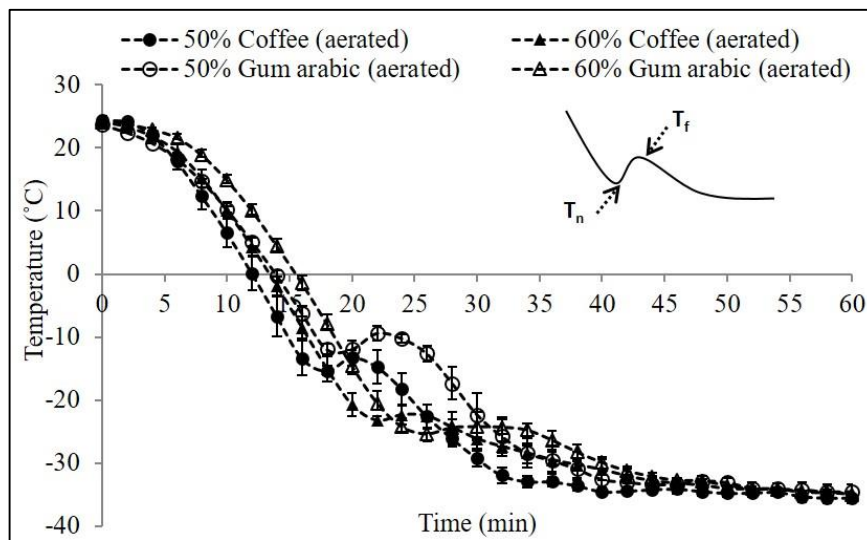


Figure 6.1 Time and temperature profiles of aerated solutions during cooling in freeze-drier at 1°C/min.

Freezing behaviour of the aerated 50 and 60% w/w gum arabic and coffee solutions were firstly evaluated. Temperature of the aerated systems during freezing to -40°C in freeze-drier operated at 1°C/min is illustrated in figure 6.1 revealing the point of ice nucleation ( $T_n$ ) and crystal growth ( $T_f$ ) for each sample (Kasper & Friess 2011). During freezing of the most concentrated systems (60% w/w),  $T_n$  and  $T_f$  were generally observed at temperatures lower than -20°C while higher values around -10 to -15°C were recorded for the 50% concentration (data in table 6-1). It can also be noted that the recorded temperature profiles are in close proximity

with the readings of non-aerated samples presented in table 4-2. Nevertheless,  $T_f$  was found to be slightly lower (by approximately  $2^\circ\text{C}$ ) in the aerated samples except for 60% coffee where  $T_f$  remained at  $-22^\circ\text{C}$ . The trend of lower  $T_n$  and  $T_f$  with increasing concentration provides further evidence that freezing the high solid systems tend to induce small supercooling ( $0.6\text{-}0.8^\circ\text{C}$ ) condition but with large freezing point depression ( $> 20^\circ\text{C}$ ) as availability of free water content is reduced for development of crystal nuclei.

Table 6-1 Effect of concentration on freezing properties of aerated coffee and gum arabic solutions

<i>Aerated system</i>	<i>50% Coffee</i>	<i>60% Coffee</i>	<i>50% Gum arabic</i>	<i>60% Gum arabic</i>
<i>Nucleation temperature, <math>T_n</math> (<math>^\circ\text{C}</math>)</i>	$-15.3 \pm 1.34$	$-23.3 \pm 1.33$	$-12.0 \pm 1.45$	$-25.4 \pm 0.23$
<i>Freezing temperature, <math>T_f</math> (<math>^\circ\text{C}</math>)</i>	$-13.2 \pm 2.17$	$-22.5 \pm 3.23$	$-10.2 \pm 1.18$	$-24.8 \pm 1.76$

The larger freezing point depression for coffee samples than gum arabic reported in section 4.3.1 were also identified in this study especially at 50% concentration. As discussed earlier, differences in molecular weight and interactions between components in coffee and gum arabic might have resulted in the temperature variation. Furthermore, molecular weight has been previously recognized as one of the characteristics that can influence freezing properties of materials (Harnkarnsujarit et al. 2012; Auleda et al. 2011). In example, presence of low molecular weight sugar in maltodextrin mixtures was reported to decrease the freezing temperature by  $2\text{-}5^\circ\text{C}$ .

In the previous experiment without aeration, these freezing properties exhibited great influence on the microstructure and quality of the final dried product in terms of pore structure, size, porosity and reconstitution behaviour. Thus, in the following sections, microstructural

characteristics of the aerated freeze-dried samples frozen with different freezing methods and its relation with reconstitution kinetics are presented.

## 6.2.1 Freezing with temperature oscillation

### 6.2.1.1 Microstructural properties

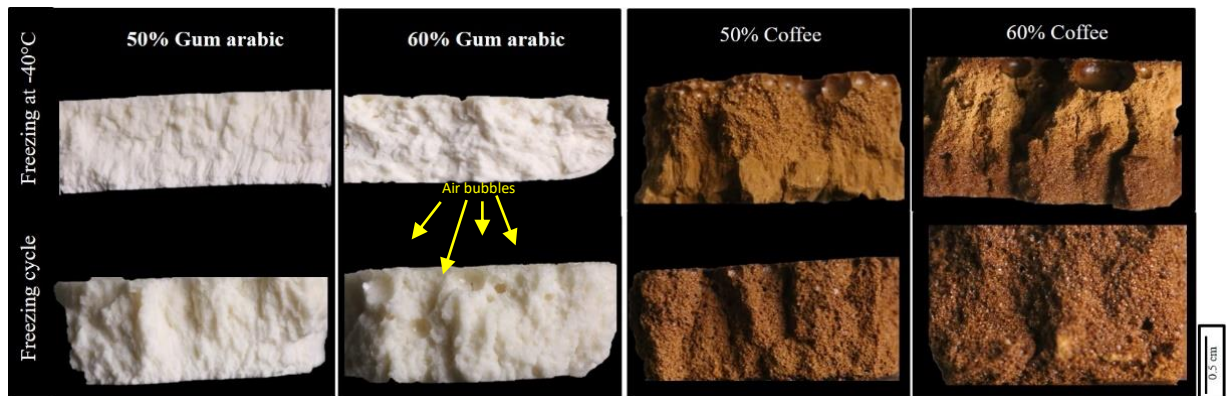


Figure 6.2 Freeze-dried cake of aerated systems after constant freezing at  $-40^{\circ}\text{C}$  and freezing with temperature oscillation.

Figure 6.2 shows the freeze-dried cake of all investigated aerated samples underwent freezing with and without temperature oscillation. Samples for the visual inspection were taken from the middle section of the freeze-dried solid to represent the typical aerated structure obtained for each system. Macroscopically, aeration appeared to impart more visible effect on the structure of freeze-dried coffee than gum arabic. Coffee samples displayed a sponge-like structure with few large air bubbles at the top of the cake which could be due to gravitational force. Meanwhile, no clear physical appearance of an aerated structure was observed for gum arabic except for the several air bubbles (indicated by yellow arrows) noticed on top of the dried solid of 60% concentration. It may be that most of the air in the gum arabic systems separated to the surface of the cake especially for the 60% formulation and caused less air left within the freeze-dried structure. This could be driven by the density difference between the air and the

system assuming the viscosity was not high enough to hold the incorporated air. This is evidence in figure 6.3 which air bubbles in gum arabic appeared to be more apparent on the surface compared to coffee before and after freeze-drying. Less air bubbles stability has also been recently found in aerated freeze-dried xanthan gum mixed with locust bean gum by Cieurzyńska & Lenart (2016) with the delicate aerated structure were discovered to be destroyed during freeze-drying.

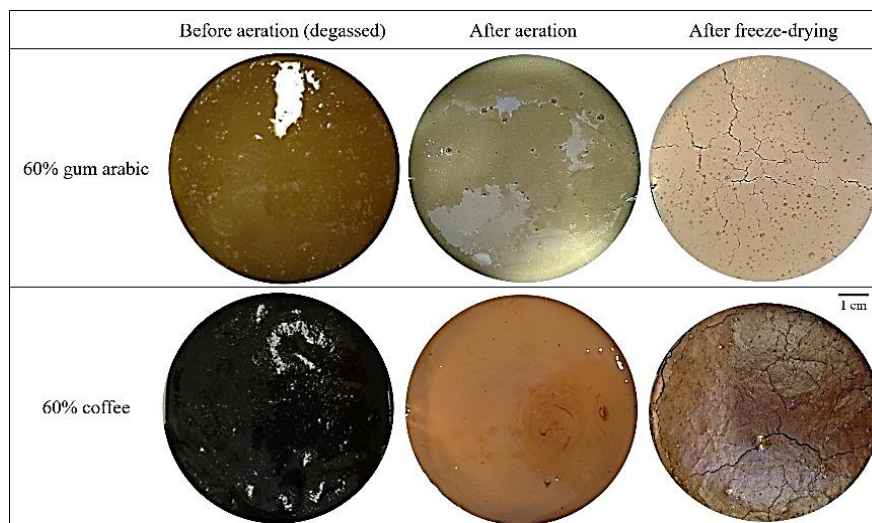


Figure 6.3 Picture of 60% solutions after being aerated and freeze-dried.

Nevertheless, homogenous dried solid of the aerated 60% systems can be seen as opposed to the puffed structure exhibited in the freeze-dried systems without aeration (see figure 4.6). This observation suggests that incorporating air into highly concentrated solution prior to freeze-drying could be advantageous in avoiding the occurrence of undesirable structural changes (e.g. melting, collapse) during drying to produce dried materials with consistent texture throughout its volume. As aforementioned, the aerated structure of liquid and semi solid foods has been associated with acceleration of the sublimation process due to the large surface area (Raharitsifa & Ratti 2010; Muthukumaran et al. 2008). It is thus possible

that the increased surface area allowed water vapour to be removed freely preventing accumulation of vapour within the drying samples. Thereby, preserving the structure established after freezing.

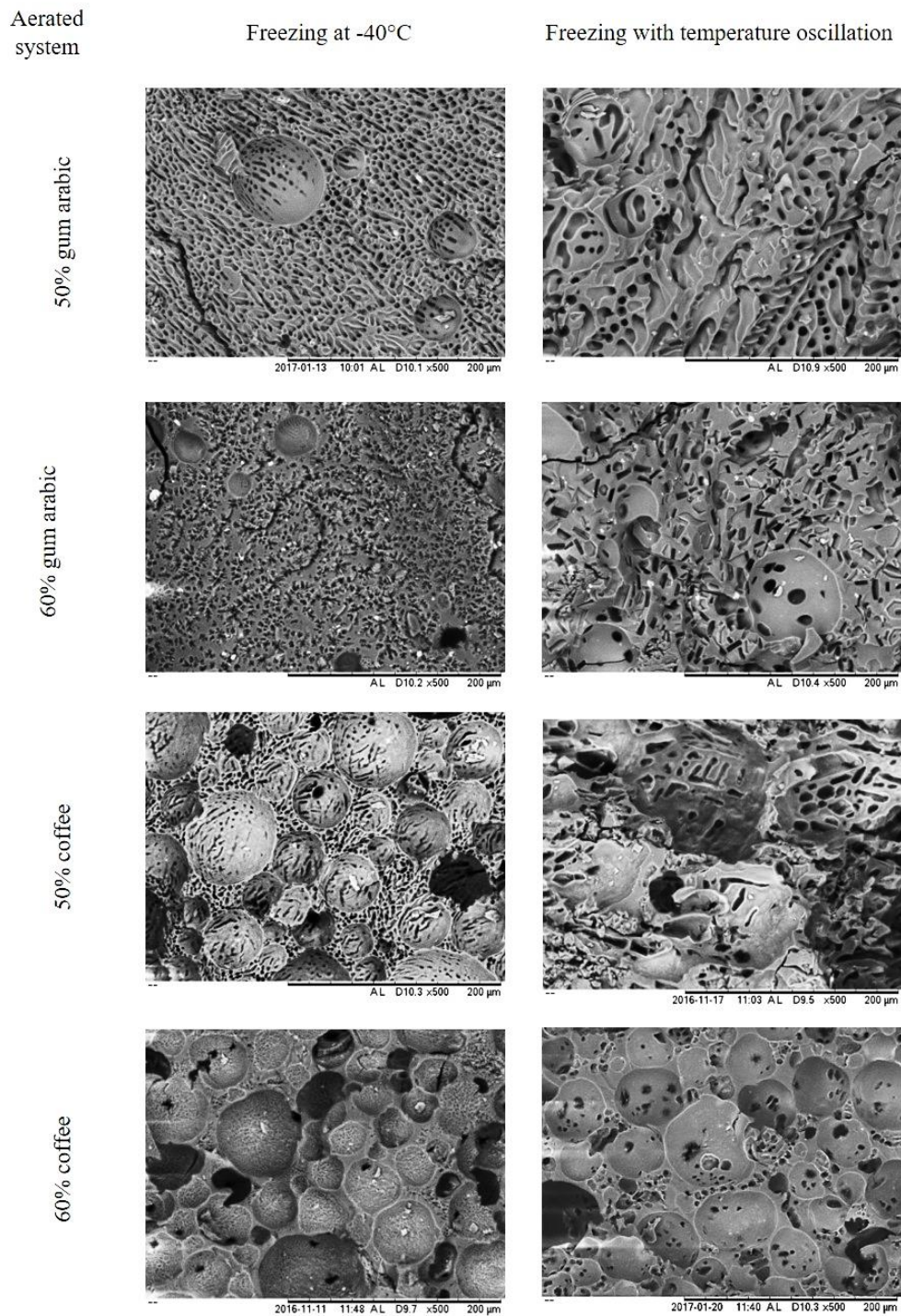


Figure 6.4 SEM images at 500x magnification of aerated freeze-dried samples affected by temperature fluctuations during freezing.

The aerated freeze-dried cakes were further analysed with SEM to examine their internal structures, and the representative images are shown in figure 6.4. Porous microstructure of

freeze-dried systems seen in chapter 4 is also evident in these SEM micrographs displaying pores of different shapes. While dendritic shaped pores formed due to sublimation of the ice crystals, aeration resulted in the development of large round entities which was not observed in the non-aerated systems (figure 4.8). The sponge-like structure of the aerated freeze-dried coffee is evident with the heterogeneous size distribution of air bubbles whereas very few air bubbles were visible within the dried gum arabic. The macro and microstructural observations indicated the better retention of air bubbles in coffee than gum arabic solutions during freeze-drying.

For the effect of fluctuating temperature during freezing, development of bigger pores is apparent in all systems studied. The freezing cycle generally increased the mean size of pores from sublimated ice crystals by a factor of 3 for each formulation (see figure 6.5) which shows consistency with the findings in section 4.3.2.2. Thus, it reinforces the fact that holding sample at temperature above  $T_g$  but below  $T_m$  induced molecular motion as viscosity is reduced above  $T_g$  enabling rearrangement of small crystals into larger crystals (Kasper & Friess 2011; Gormley et al. 2002). Bigger entrapped air bubbles were also identified upon temperature oscillation having average diameter of more than  $550\mu\text{m}$  as presented in figure 6.6. It is likely that the air bubbles coalesce during the freezing cycle due to increased mobility induced by the fluctuating shelf temperature. Moreover, oscillated samples have higher total porosity than the control systems (see figure 6.5). 50 and 60% gum arabic each had 19 and 28% porosity increment as opposed to the minimal change ( $< 10\%$ ) observed in coffee. Such small difference could be related to the fact that aerated coffee even without temperature oscillation, most of the air bubbles were well distributed within the freeze-dried structure. Also, surfaces of air bubbles in the most concentrated gum arabic from constant freezing at  $-40^\circ\text{C}$  appeared to be free of pores. Air might have shown thermal insulating effect on such condition that interfered with

the movement of growing ice crystals as effective thermal conductivity is reduced (Lopez-Quiroga et al. 2016).

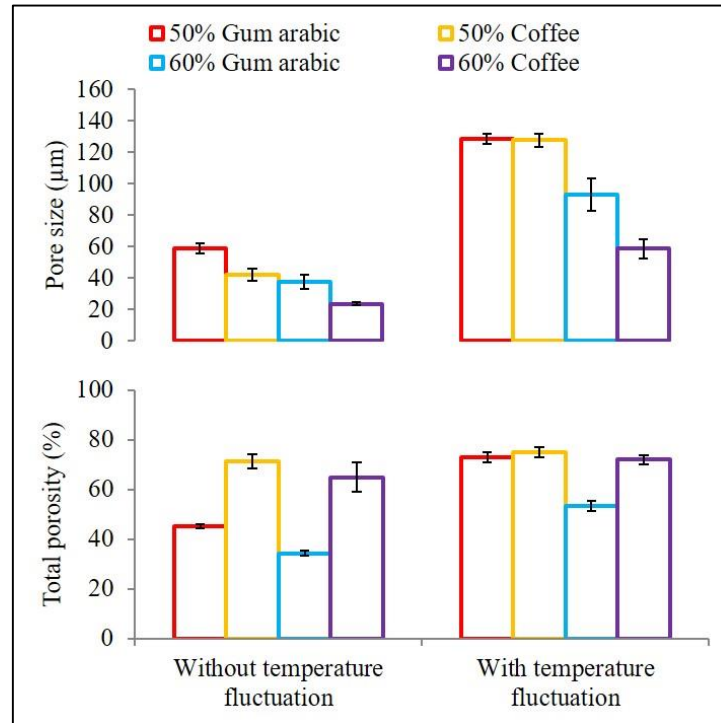


Figure 6.5 Effect of freezing cycles on mean size of ice crystals and porosity of the aerated freeze- dried systems.

Similar effect of concentration on pore size development found in experiment without aeration is shown in this aerated freeze-dried systems. At higher concentration, smaller dendrites in the range of 24 to 93µm were obtained compared to the 50% samples which have crystal pores between 42 to 148 µm. As has been discussed, this pore size variation is affected by the reduced water availability and mobility associated with high solid solutions due to increased viscosity (Homer et al., 2014; Arvanitoyannis et al., 1993). While movement of water molecule is kinetically inhibited in the 60% formulations, high driving force is required for water to crystallize resulting in low  $T_n$  and  $T_f$  in which development of small nuclei hence growth of small ice crystals is more pronounced (Kiani & Sun 2011; Searles 2001). Therefore,

small dendritic pores develop in the freeze-dried 60% systems. Contrary to the pores from sublimated ice crystals, initial solid content had little effect on the size of the incorporated air bubbles. Based on triplicate estimations from 50 air bubbles, on average, coffee have air bubbles of 540 $\mu\text{m}$  whereas in gum arabic the bubbles are around 300 to 400 $\mu\text{m}$  (see figure 6.6). The small number of bubbles quantified was due to the limited air bubbles present within the gum arabic system.

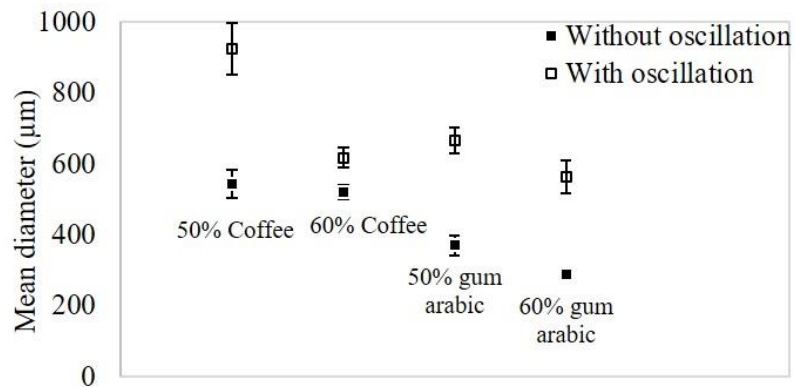


Figure 6.6 Average size of 50 air bubbles in freeze-dried structures from different freezing cycles.

### 6.2.1.2 Reconstitution

Reconstitution being a fundamental aspect in dried materials was also evaluated for these aerated freeze-dried samples. Analysis was carried out using the same method applied in section 4.3.3. Decreasing area of the dried particles during reconstitution in distilled water were quantified and plotted against time is presented in figure 6.7. As evident in previous chapters, instant disintegration of coffee caused the particles to exhibit much higher reconstitution rate than gum arabic. The maximum reconstitution time recorded for each material was 8 min and 50 min respectively. In addition, the slow reconstitution of gum arabic followed a rather linear

area reduction while coffee reduced exponentially in accordance with the reconstitution of the freeze-dried samples prepared without aeration (section 4.3.3). This finding present strong relationship between material’s characteristics and hydration mechanisms that determine the reconstitution kinetics.

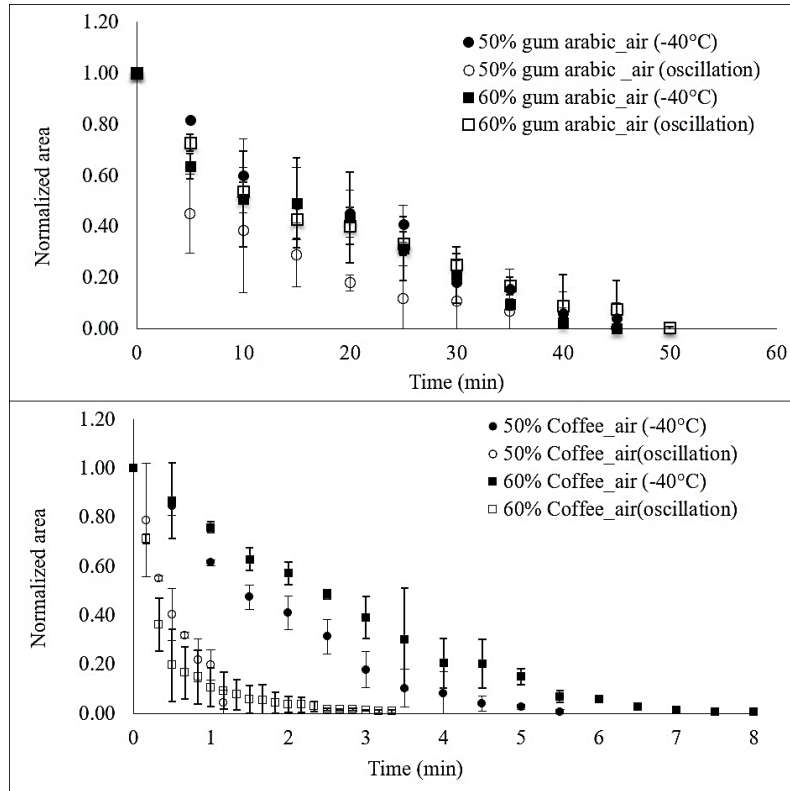


Figure 6.7 Area reduction of freeze-dried particles during reconstitution in distilled water.

It also appears that reconstitution is affected by the microstructure obtained. Systems with high overall porosity and large pores generally exhibited fast reconstitution. For instance, in aerated freeze-dried coffee, the reconstitution time reduced to about 1min and 3.5 min each for the 50% and 60% concentrations frozen with temperature oscillations. Although the reconstitution curves for freeze-dried gum arabic seemed to overlap, slightly steeper slope can be observed for the 50% gum arabic exposed to temperature fluctuation. This freezing condition has also accelerated the reconstitution of freeze-dried systems without prior aeration especially

for the 50% gum arabic and 60% coffee (see figure 4.10). This reconstitution behaviour indicates the importance of having a well-controlled freezing cycle on production of high quality freeze-dried materials (Hottot et al. 2007; Searles et al. 2001a).

### **6.2.2 Freezing with different cooling rates**

The influence of freezing with shelf-ramping (SR) and shelf pre-cooling (PC) methods on microstructure and reconstitution of the aerated freeze-dried systems is studied in this section.

Figure 6.8 shows the temperature recording during freezing in rapid freezer of both investigated freezing conditions. Based on the initial slope of each freezing method, cooling rate around  $0.64^{\circ}\text{C}/\text{min}$  and  $2.09^{\circ}\text{C}/\text{min}$  were measured for the SR and PC techniques, very close to values from non-aerated systems. During the slow cooling (SR), sample's temperature is reduced from  $20^{\circ}\text{C}$  to  $-40^{\circ}\text{C}$  within 70-80min while half of the time is required when the shelf has been pre-cooled to  $-40^{\circ}\text{C}$ . The recorded time is observed to be almost 10 min faster than in non-aerated systems (figure 4.15). The lower density of aerated samples might have speed up the freezing process.

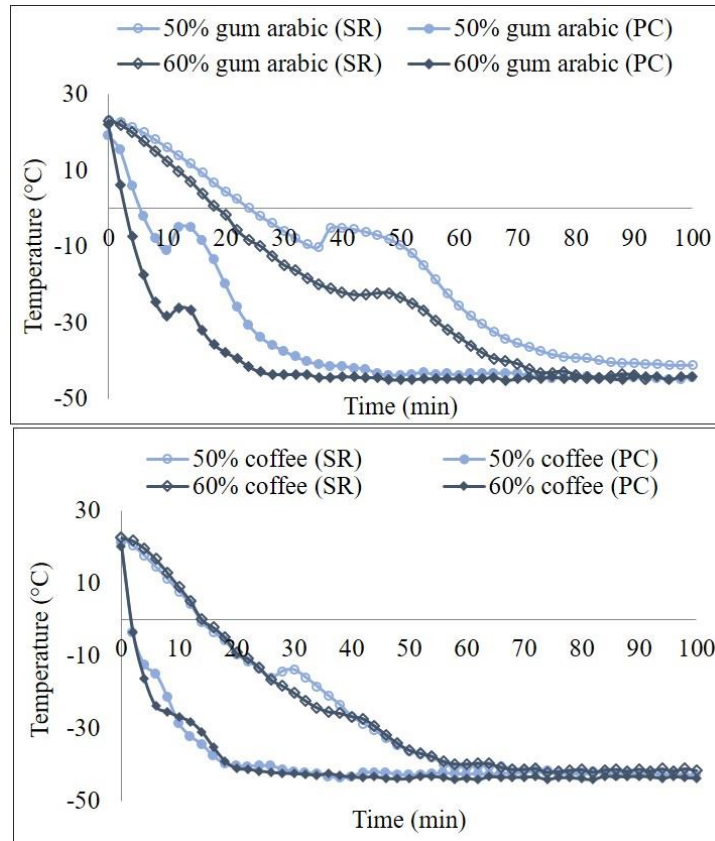


Figure 6.8 Cooling profiles of aerated solutions during shelf ramp and shelf pre-cooled freezing in rapid freezer.

Average point of nucleation and freezing were determined from the individual freezing curves as illustrated in figure 4.14. Data are presented in table 6-2 and figure 6.10 for  $T_n$  and  $T_f$  respectively. The time-temperature profiles show that supercooling which represents the activation energy for ice nucleation was only noticeable on several occasions. Curves with supercooling are followed by sharp temperature increment towards the equilibrium freezing temperature ( $T_f$ ) where latent heat of crystallization is released. Meanwhile, graphs without supercooling can be categorized into two. For instance, shelf ramp freezing of 60% gum arabic and coffee solutions displayed curves that directly goes to freezing plateau before approaching the rapid freezer's temperature set at  $-40^\circ\text{C}$  whereas product temperature ( $T_p$ ) appeared to keep decreasing towards freezing set point without apparent isothermal region to show crystal growth stage during the fast freezing (PC) of coffee solutions. For these samples, the point before sharp

temperature fall is considered as the  $T_f$  (shown in figure 6.9). Since crystallization is known to occur only when ice nuclei has been created it is rather difficult to explain this observation which was also found during the fast cooling of 50% gum arabic (see figure 4.15). In earlier section, it has been explained that crystallization could have occurred very near to the nucleation point due to rapid cooling that the peak corresponds to the latent heat of crystallization was not visible making it impossible to detect  $T_n$ . The discrepancies in freezing profile suggest that formulation characteristics (e.g. concentration, viscosity, surface tension and diffusivity) might have considerable effect on influencing the resultant heat and mass transport properties during freezing (Kiani & Sun 2011).

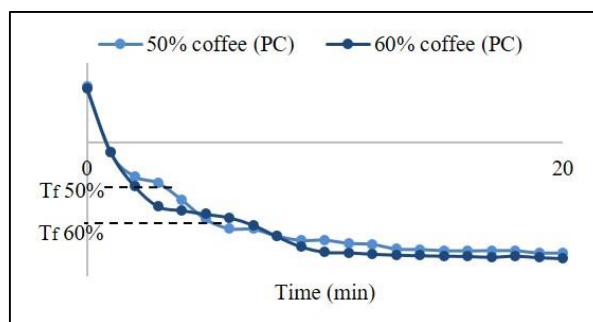


Figure 6.9 Determination of freezing temperature ( $T_f$ ) for rapidly cooled coffee solutions.

Nevertheless, lower  $T_n$  and  $T_f$  were determined for coffee and 60% w/w solutions compared to gum arabic and samples with 50% solutes. This trend has also been found in non-aerated and temperature oscillation experiments. In terms of freezing method, the effect on  $T_n$  is rather inconclusive as point of nucleation was missing for some samples due to supercooling not being observed. However, freezing on a pre-cooled shelf resulted in lower  $T_f$  values compared to SR freezing with 60% coffee had the highest temperature difference around  $5.6^\circ\text{C}$  between the two methods used (see figure 6.10).

In the meantime, strong conclusion about the effect of air on ice nucleation could not be drawn as it appeared that aeration reduced  $T_n$  for 60% gum arabic by  $4^\circ\text{C}$  but increased the

value by 3°C for 50% coffee. This inconsistency could be associated with the randomness of the nucleation process. Also, freezing of aerated solutions was generally observed at 2-4°C lower than systems without air depending on the types of material and concentration (see figure 4.16). Although, freezing of aerated 50% gum arabic showed that  $T_f$  increased by 2°C. The recorded temperatures indicated that aeration have marginal effect on the freezing properties. These freezing properties were used to relate to the freeze-dried structures.

Table 6-2 Noticeable nucleation point ( $T_n$ ) of aerated solutions from different freezing conditions.

<i>System</i>	<i>50% gum arabic</i>	<i>60% gum arabic</i>	<i>50% coffee</i>	<i>60% coffee</i>
<i>Shelf-ramping (0.6°C/min)</i>	-10.76 ± 3.15	n/o	-13.19 ± 3.98	n/o
<i>Shelf pre-cooling (2°C/min)</i>	-12.40 ± 3.65	-29.58 ± 1.99	n/o	n/o

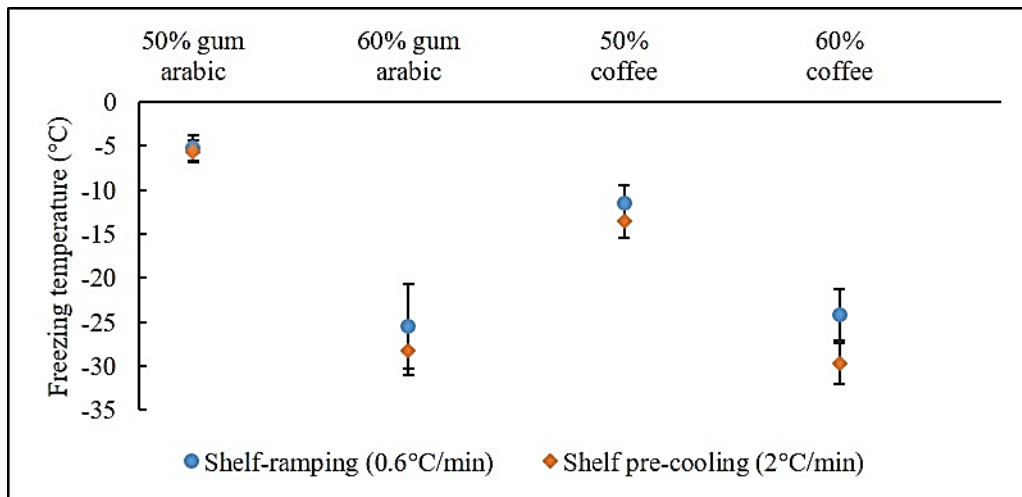


Figure 6.10 Effect of freezing conditions and concentrations on freezing temperature ( $T_f$ ) of the aerated solutions.

### 6.2.2.1 Microstructure

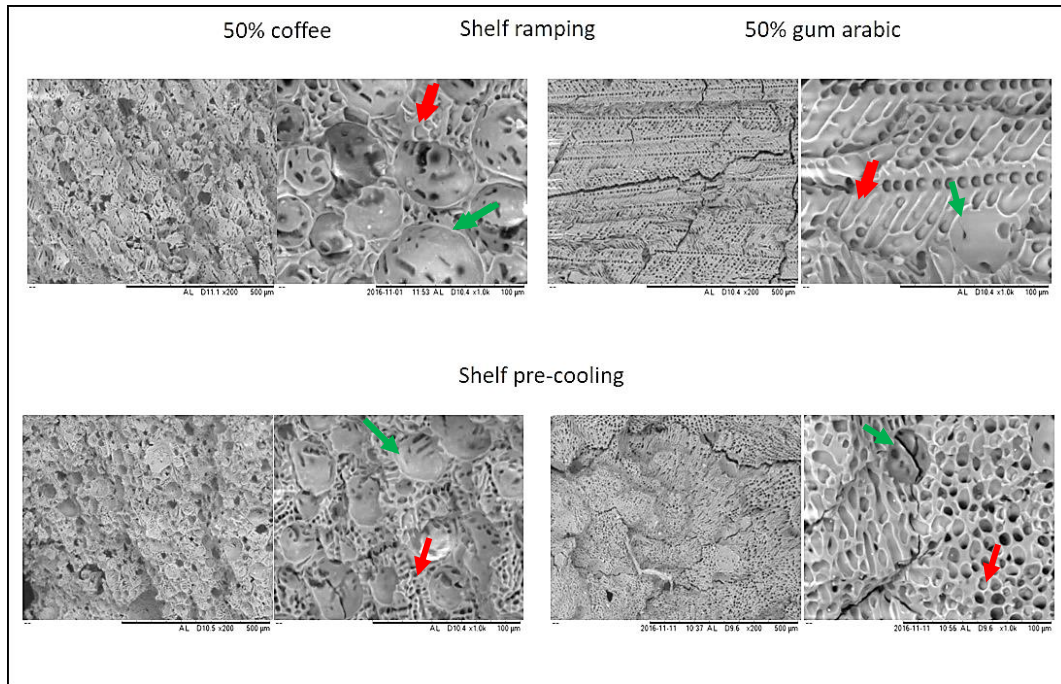


Figure 6.11 SEM images (200x, 1000x) of the aerated freeze-dried 50% coffee (left side) and 50% gum arabic (right side) after freezing with different methods. Green and red arrows each point to pores from air and ice crystals respectively.

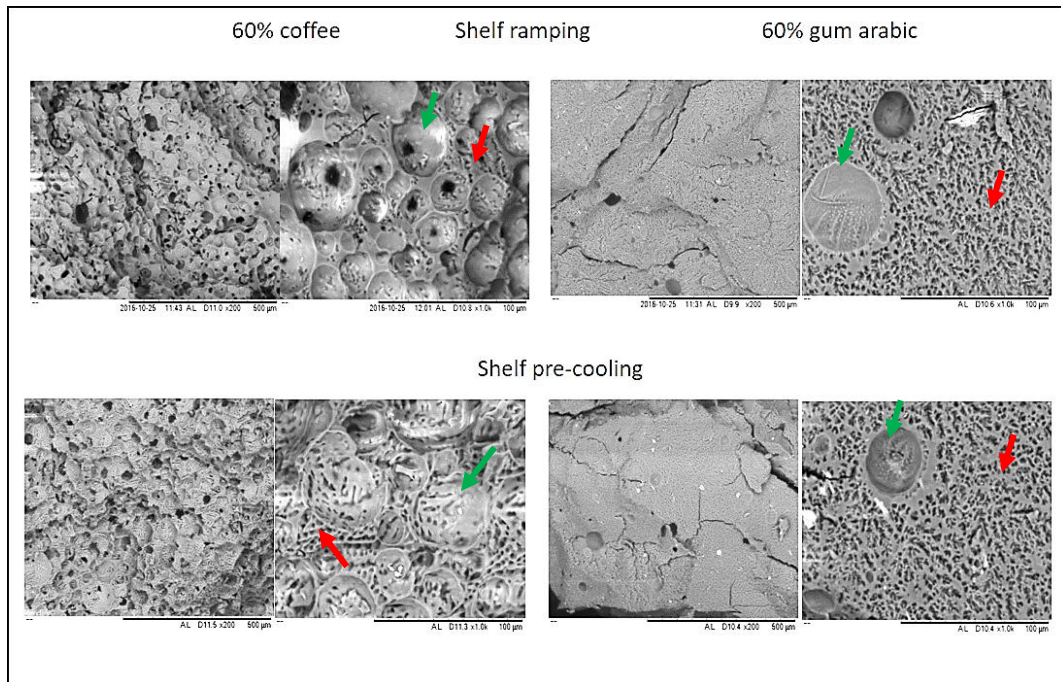


Figure 6.12 SEM images (200x, 1000x) of the aerated freeze-dried 60% coffee (left) and 60% gum arabic (right side) after freezing with different methods. Green and red arrows each point to pores from air and ice crystals respectively.

Internal microstructure of the aerated freeze-dried systems frozen at different cooling rates is shown in figure 6.11 and 6.12. Freeze-dried coffee presented a well aerated microstructure with significant distribution of air bubbles (indicated by the green arrows) apart from entities of the sublimated ice crystals (indicated by the red arrows). In contrast, freeze-dried solids of aerated gum arabic, have limited number of air bubbles within the freeze-dried cake in accordance with the microstructure observed previously in section 6.2.1.

Bigger pores were obtained after freeze-drying the 50% concentrations compared to the higher solute systems indicating large ice crystals formation. This feature is consistent with the SEM observations in chapter 4 and section 6.2.1 which is influenced by the higher water availability in less concentrated solution. On average, the 50% systems crystallized at temperature approximately 10°C higher than the 60% samples promoting growth of large ice crystals due to slower solidification front movement at high temperature (Kasper & Friess 2011;Searles 2001).

On the effect of freezing methods, SR (slow cooling) appears to have formed wider crystal dendrites in 50% systems than PC (fast cooling). The mean equivalent diameter of ice crystals measured for the slowly frozen 50% gum arabic is 30µm bigger than sample frozen with faster cooling rate (figure 6.13). It is also noted that the ice crystals displayed more of branched dendrites morphology compared to the rather circular crystals developed in the shelf pre-cooled freezing. Meanwhile for 50% coffee, the slow cooling condition only increases the equivalent diameter of ice crystals by 6µm displaying quite similar shape of ice crystals. In this sample, the entrapped air bubbles seemed to be more affected by the freezing techniques where smaller air bubbles with highest frequency between 300-400µm shown in figure 6.14 were obtained upon fast freezing. The air bubbles may have coalesced during the gradual temperature reduction (SR) that they grew in size and reduced in number.

In the case of 60% coffee, slightly smaller ice crystals and air bubbles were observed for sample frozen at slower rate (SR) than the one frozen at 2°C/min (PC). The average ice crystals size calculated for each freezing rate was 28µm and 38µm respectively. This observation contradicts the higher  $T_f$  (by 5.6°C) recorded upon SR compared to the value identified during fast freezing of 60% coffee which would normally suggest the formation of larger ice crystals. It could be that the heat and mass transfer involved during water crystallization in this sample were partly affected by the properties of materials (e.g. viscosity) compared to the freezing rates applied. Thus, affecting the actual freezing rate exerted to these samples.

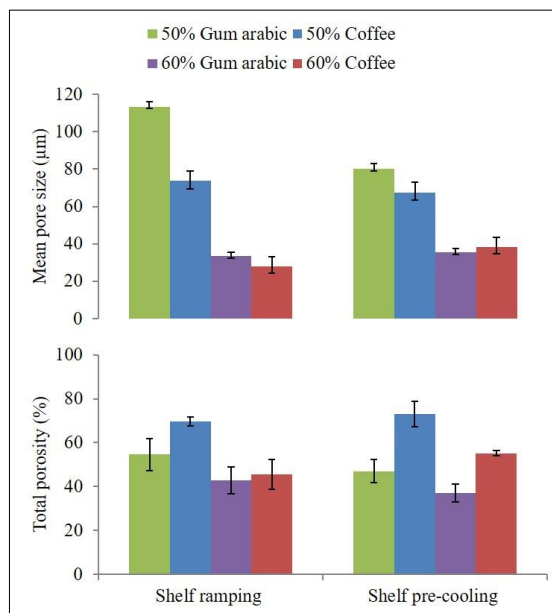


Figure 6.13 Effect of freezing conditions and concentrations on average size of ice crystals and porosity of the aerated freeze-dried systems.

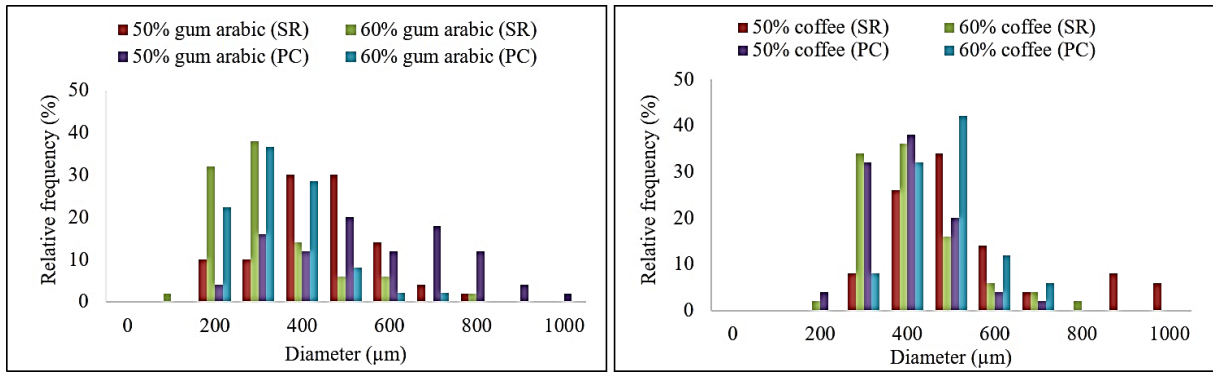


Figure 6.14 Size distribution of air bubbles in the freeze-dried matrices of aerated solutions.

The internal microstructure of 60% gum arabic appears not to be affected by the freezing methods used in which the average size of ice crystals differs only by 2 $\mu\text{m}$ . However, when comparing the porosity, slightly higher percentage (by 6%) is obtained for the shelf ramped sample. This might be contributed by the few large air bubbles of more than 600 $\mu\text{m}$  presence in the system (presented in figure 6.14). Similar to freeze-dried structure of aerated 60% gum arabic from temperature oscillation experiment (figure 6.3), there were no ice crystals formed on the surfaces of air bubbles. Ice crystals seen around the edges of the entrapped air indicates a reduction in effective thermal conductivity of the system thus, inhibited the movement of freezing front (Lopez-Quiroga et al. 2016).

Scanning electron microscopy (SEM) analysis also reveals the effect of thermal stress during dehydration on the structure of the freeze-dried samples. At lower magnification, significant cracks can be seen in the freeze-dried gum arabic which is similar to the observations made in chapter 4 and 5. The consistency of this feature demonstrates that desorption of unfrozen water from initially frozen and sublimated gum arabic tend to results in considerable increase of pressure within the system which is released by cracking (Ullrich et al. 2015). Denser microstructure (thick solid network around the pores and less entrapped air bubbles) of

gum arabic than coffee might have caused considerable development of cracks in the former system.

### 6.2.2.2 Reconstitution

Figure 6.15 shows the increasing amount of dissolving freeze-dried particles during reconstitution in 100ml distilled water. The percentage was determined based on the recorded conductivity values using equation (6) described in section 3.2.6.

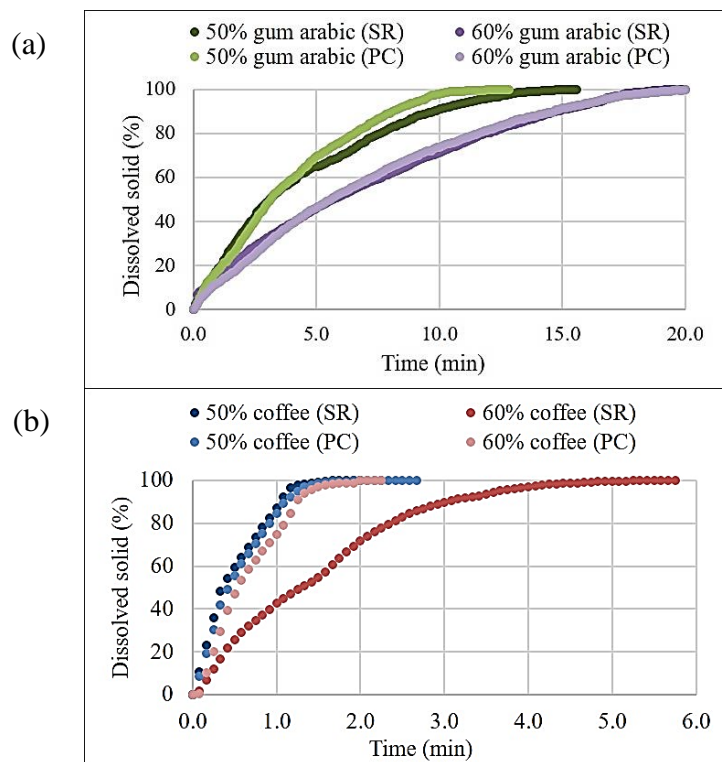


Figure 6.15 Reconstitution of the aerated freeze-dried (a) gum arabic (b) coffee particles in distilled water:

Overall, high reconstitution rate was displayed by systems that has been characterized with wide dendrite network and high porosity. As such, reconstitution was faster for the 50% systems, compared to the 60% systems with complete reconstitution achieved 7 min earlier for gum arabic and 4 min faster for coffee. Previous results on reconstitution properties has

indicated that in this study, microstructure played important roles in governing the reconstitution kinetics. Having freezing with shelf ramping and shelf pre-cooling resulted in minimal variation on the freezing properties thereby microstructure of the final dried samples, no observable differences were found during reconstitution between both freezing methods. Notably, dissolution of 60% coffee appeared to have been influenced by the freezing methods in which reconstitution time for fast frozen freeze-dried sample was 3.5min faster than the slowly frozen system comparable with the 50% coffee. The rapid dissolution is likely to be affected by the bigger mean crystal size, air bubbles and higher porosity obtained in such freezing condition. At the same time, the different reconstitution mechanisms identified previously (e.g. rapid solid disintegration and apparent water absorption) between both materials resulted in gum arabic to dissolve approximately 60-80% slower than coffee.

### 6.3 Effect of different primary drying temperatures

Similar to chapter 5, the aerated 50 and 60% w/w/ solutions were subjected to different freeze-drying cycles. Freeze-drying were conducted at three primary drying temperatures (-20°C, -30°C, -40°C). The final dried samples were characterized based on microstructure observed using X-ray Ct-scan (XRCT) and reconstitution of single particle in distilled water.

#### 6.3.1 Microstructure

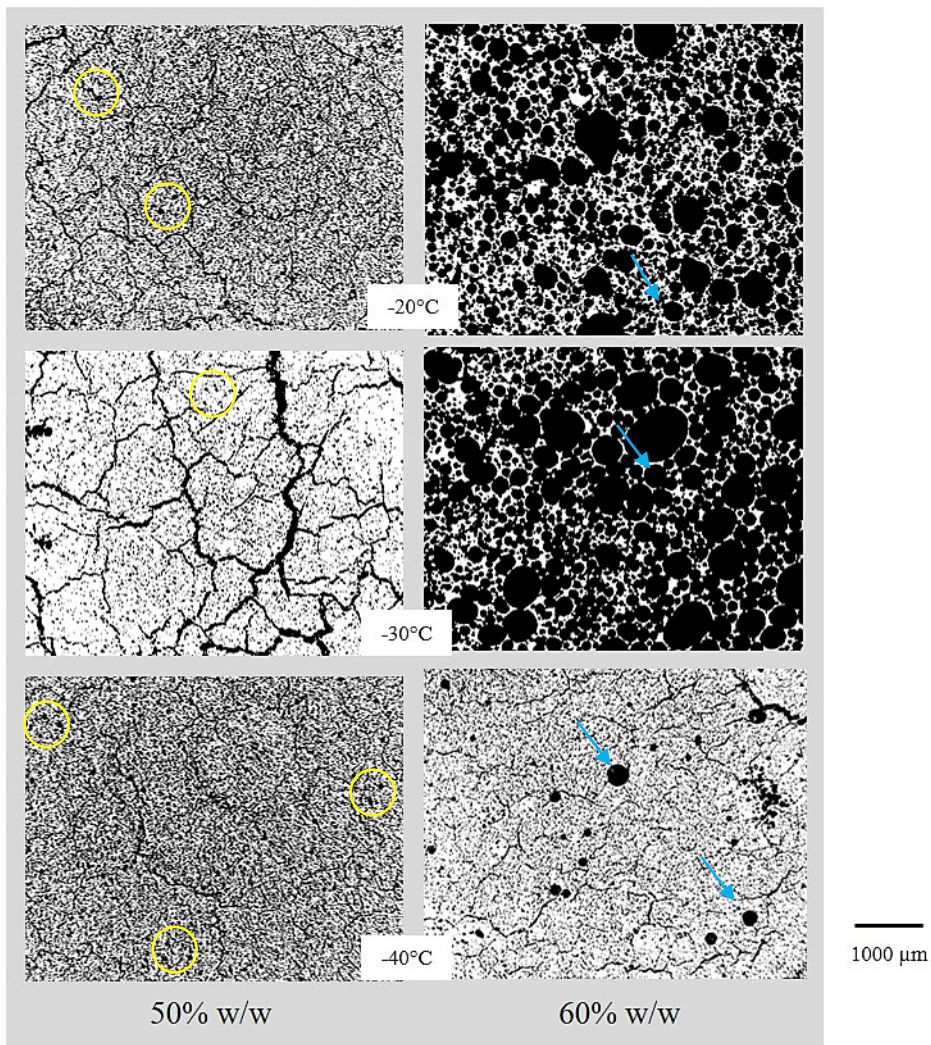


Figure 6.16 Micro CT images of aerated freeze-dried gum arabic (50 and 60% w/w) dried at -20, -30 and -40°C. Blue arrows and yellow circles represent the incorporated air.

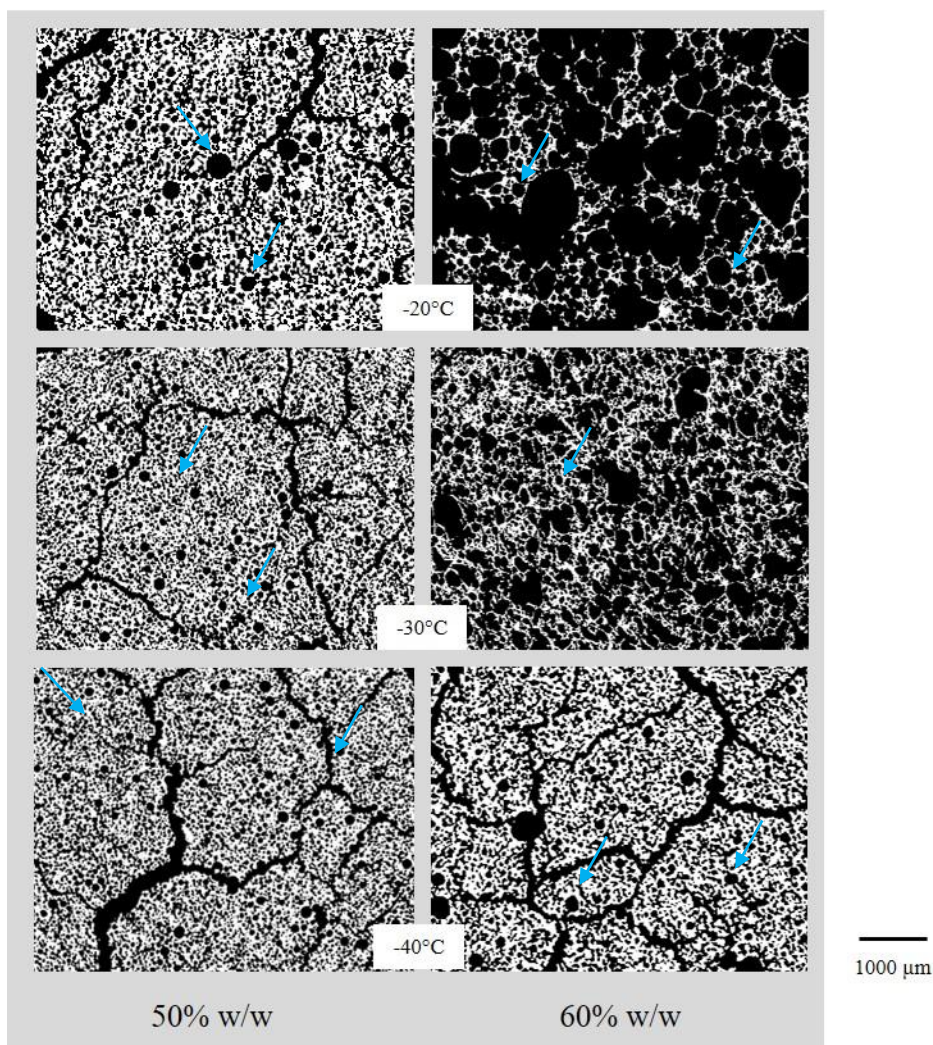


Figure 6.17 Micro CT images of aerated freeze-dried coffee (50 and 60% w/w) dried at -20, -30 and -40°C. Blue arrows represent the incorporated air.

Figure 6.16 and 6.17 compare the internal microstructure of aerated freeze-dried cakes obtained at -20, -30 and -40°C. Qualitatively, it can be discerned that 50% gum arabic had the least feature of an aerated system displaying more compact microstructure than 60% system. Mixtures of round and irregular shaped pores however, were seen in the binary images of the freeze-dried coffee and 60% gum arabic. The well-defined circular voids (indicated by blue arrows) are likely to signify the incorporated air bubbles prior to freeze-drying in which seemed to be affected by concentration and drying temperature. Although figure 6.16 suggests that gum arabic at lower initial solid content appeared not to be aerated, the incorporated air (yellow

circle) can actually be seen on a close up of the binary image as shown in figure 6.18. This observation further confirmed the instability of air bubbles within gum arabic solutions described in section 6.2.1.1. Cracking as previously discussed in chapter 4 and 5 may be associated with increased pressure during dehydration (Ullrich et al. 2015; Patel et al. 2017) were mainly developed in 50% w/w solutions and 60% systems dried at  $-40^{\circ}\text{C}$ . While cracks is in part indicative of irregular behaviour during freeze-drying (Esfandiary et al. 2016; Harnkarnsujarit et al. 2016), visual inspection of the freeze-dried cake in figure 6.2, revealed no signs of major structural deformation when the aerated solutions were freeze-dried at  $-40^{\circ}\text{C}$ . It should also be noted that cutting the sample in preparation for X-ray observation might have caused the sample to crack due to brittleness of the aerated freeze-dried solids.

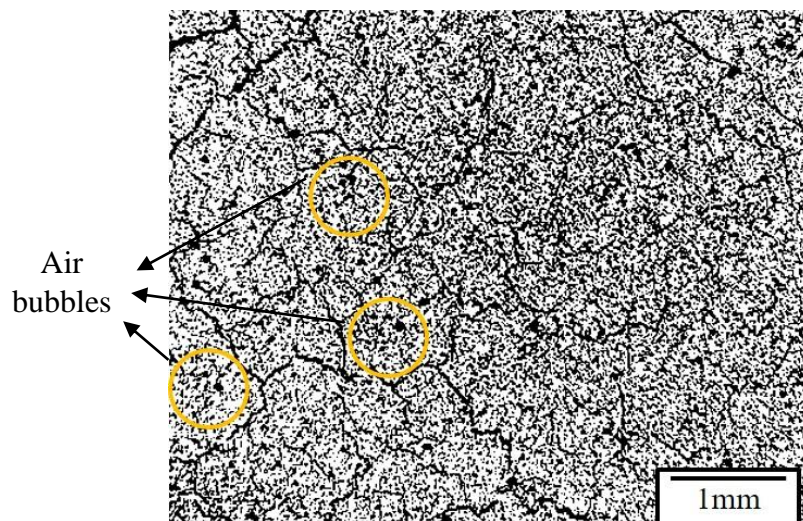


Figure 6.18 Representative of close up image of the aerated freeze-dried 50% gum arabic

From the perspective on the effect of varied primary drying temperatures, different microstructures were especially displayed by systems with higher initial solid content. The pores in the 60% systems appeared to be bigger and highly interconnected when dried at  $-20$  and  $-30^{\circ}\text{C}$  indicating significant change in volume during freeze-drying. This trend suggests that the low  $T_m$  measured for the most concentrated systems (i.e  $-15^{\circ}\text{C}$  and  $-18^{\circ}\text{C}$ ) could have

rendered material's thermodynamic stability on drying at high  $T_s$ . As described in section 5.3, melting is likely to happen under this condition and internal pressure developed as drying proceeds towards secondary drying resulting in expansion of the dried solids. While this trend match those observed earlier in the non-aerated systems, the round pores in these samples seemed smaller and more homogenous due to the entrapped air bubbles. In this case, it is believed that structure expansion in non-aerated samples formed the apparent circular pores but in aerated formulations, structural changes increased interconnectivity between the entrapped air bubbles. Meanwhile, at lowest drying temperature, the 60% formulation exhibited cracks and much smaller pores with no visible indication of structural expansion unlike the puffed structure displayed by the dried solid when aeration was not applied. Freeze-drying of the 50% initial concentration systems at different temperatures however, produced almost comparable microstructure affecting only the appearance of circular voids (air bubbles) that are observed to be bigger at high temperature. These microstructure observations while preliminary indicates aeration could be beneficial in controlling the freeze-dried structure of high solid materials.

Quantitative data of the aforementioned features are presented in terms of pore size distribution (see figure 6.19) and porosity (see figure 6.20). Cumulative size distribution also illustrates that upon primary drying at the lowest shelf temperature and initial concentration, small pores developed. In 50% gum arabic, most of the pores were measured between 25 to 75 $\mu\text{m}$  for all investigated temperatures. Slightly bigger pores, by 50 $\mu\text{m}$  developed in the 50% coffee especially from high drying temperatures (-20 and -30 $^{\circ}\text{C}$ ) indicating attribution of the incorporated air bubbles. Larger scale (by 5 times) of pore sizes was measured for the 60% solute formulation with drying at -40 $^{\circ}\text{C}$  resulted in pores of less than 200 $\mu\text{m}$ . The big pores observed in binary images of the highly concentrated systems dried at high temperatures were

measured between 200 to 1200 $\mu\text{m}$ . It can be seen that 60% gum arabic and coffee each had significant pore size increment after freeze-drying at -30 and -20 $^{\circ}\text{C}$  respectively.

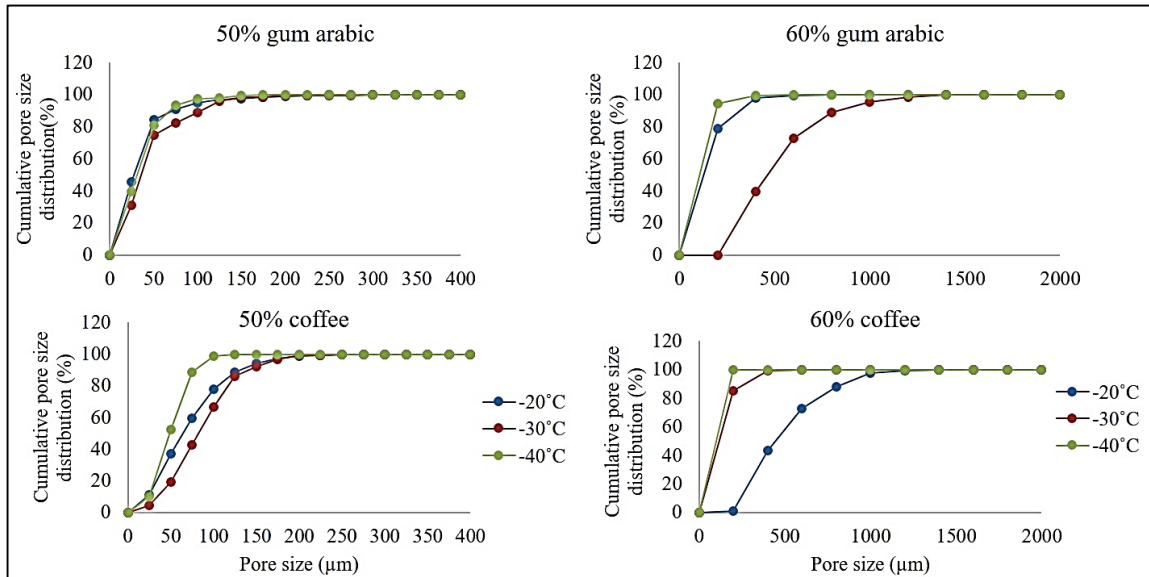


Figure 6.19 Effect of primary drying temperature and concentration on pore area equivalent diameter.

Results on porosity in figure 6.20 are in accordance with the pore sizes obtained. Overall porosity around 30% and 40% were determined for 50% gum arabic and coffee respectively showing <5% variation between temperatures studied. These values further show that the less concentrated systems were fairly affected by the range of temperature studied. Porosity of the 60% systems however, differed notably between drying temperatures in particular for coffee. Porosity for the concentrated coffee doubled when compared between the highest (-20 $^{\circ}\text{C}$ ) and coldest (-40 $^{\circ}\text{C}$ ) drying temperature applied where the higher porosity was obtained in the former condition as indicated qualitatively in figure 6.16 and 6.17. The void fractions measured in these freeze-dried systems with incorporated air bubble are slightly higher than the range found in non-aerated samples. However, at -40 $^{\circ}\text{C}$ , porosity of the aerated freeze-dried solids is lower than in non-aerated formulations due to the minor and major collapse or in this case expansion observed in 50 and 60% concentrations under this drying condition.

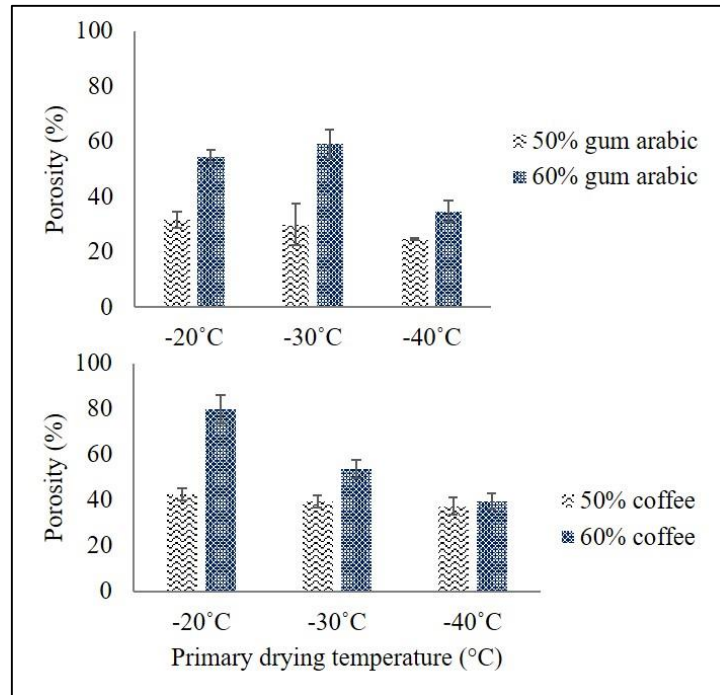


Figure 6.20 Porosity of the aerated freeze-dried solids at different drying temperatures.

### 6.3.2 Reconstitution

The freeze-dried solids of aerated solutions obtained with different formulations and primary drying shelf temperatures were dissolved in 100ml distilled water and conductivity values were recorded. Figure 6.21 illustrates the change in amount of dried particles dissolved during reconstitution derived from the conductivity measurements together with the fitted data using Weibull's equation (equation 6 in section 5.4). Parameters of this equation are presented in table 6-3 in the aspect of rate constant (k) and curve's shape parameter (n).

A good correlation with microstructure generated during freeze-drying can be noticed in the dissolution curves. It is known in this study that pore size and porosity of the freeze-dried materials increase with drying temperature. This in fact resulted in faster dissolution of the freeze-dried particles dehydrated at -20 and -30°C than the one obtained at lower temperature. However, this is not the case for 50% coffee dried at -40°C where under 30 secs half of the

solid has dissolved. This behaviour could be related to the development of more cracks that might have accelerated disintegration of this particular sample. Nevertheless, for 60% systems, dissolution of samples dried at the coldest temperature followed a gradual increment of solid dissolved suggesting no rapid initial water uptake across the small entities. Thick cell wall around the small pores makes the penetration of water into dried solid slower. Meanwhile as bigger pores appeared highly interconnected and surrounded by thin cell wall, water can easily fill up the empty space and caused rapid dissolution (Koh et al. 2011; Marabi & Saguy 2004). As expected, reconstitution was significantly slower in gum arabic (by a factor of 6) compared to coffee even though both systems were dried under the same conditions affected by the physical processes associated with water transport properties during dissolution (Marabi et al. 2003).

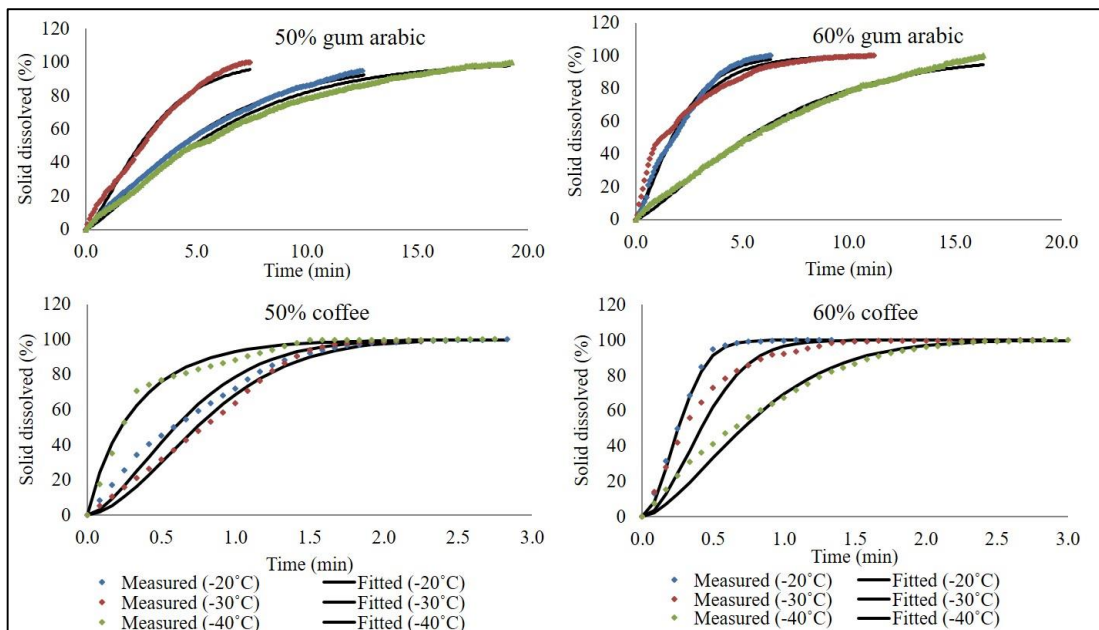


Figure 6.21 Reconstitution expressed as amount of solid dissolved against time affected by concentrations and primary drying temperatures.

The reconstitution data also exhibited good fit ( $0.97 \leq R^2 \leq 0.99$ ) with Weibull model which has been previously shown by the non-aerated freeze-dried systems (section 5.4). This

modelling allowed derivation of process kinetic constant,  $k$  and parameter  $n$  indicative on the water transport mechanism (Papadopoulou et al. 2006; Marabi et al. 2003). In this analysis,  $k$  values in the range of  $10^{-2}$  to  $10^{-4} \text{ min}^{-1}$  were obtained with higher  $k$  represents faster reconstitution. Decreasing rate of reconstitution with decreasing drying temperature can be seen in table 6.2 excluding the 50% coffee. For this particular sample, where fastest dissolution was shown by system dried at  $-40^{\circ}\text{C}$ , the  $k$  value was estimated as the highest at  $6.44 \times 10^{-2}/\text{min}$ . In terms of concentration, for freeze-dried gum arabic, the lowest  $k$  on average was obtained for 50% formulation at each temperature explaining the steeper slopes shown by 60% gum arabic. On the contrary, dried coffee with 60% initial concentration had lower  $k$  than the 50% coffee from the low drying temperature condition but sample dried at  $-20$  and  $-30^{\circ}\text{C}$  showed higher rate of dissolution. The derived rate constants confirmed the relation between microstructure and the dissolution kinetics.

Meanwhile, high  $n$  values between 0.9-1.8 were obtained reflecting the exponential dissolution curves of freeze-dried samples. This dissolution pattern with high rate at the beginning followed by gradual increment until equilibrium is reached is typically found during rehydration of dried materials showing saturation condition at the end (Cassanelli et al. 2017; Witrowa-Rajchert & Lewicki 2006; Abu-Ghannam & McKenna 1997) . Since this empirical model is generally applied to study dissolution and release profiles, the exponent  $n$  has been used to describe the water uptake mechanisms. Similar to dissolution of freeze-dried solids without prior aeration, the high  $n$  values (more than 1) suggest that combination of various mechanisms such as molecular diffusion, liquid imbibition and swelling occurred when the particles dissolved (Cascone 2017; Papadopoulou et al. 2006). The complexity of this dissolution process could be influenced by different pore sizes, structures (e.g circular, non-circular and cracks), interconnectivity of the samples and material's properties that in part may

have determined whether water movement across the porous microstructure driven by capillary flow and/or molecular diffusion. Previously, the influence of inter and intra-particle porosity on water uptake during rehydration was noted by Wallach et al. (2011) who developed dual porosity model to describe rehydration of freeze-dried wheat and carrot. In addition, behaviour of swelling and dispersion of the dissolving particles can exert influence on the mass transport properties during reconstitution (Papadopoulou et al. 2006; Saguy et al. 2005; Miller-Chou & Koenig 2003; Korsmeyer et al. 1983).

From this reconstitution analysis it is clear that structural changes imparted by drying, initial concentration and material's properties affect the ability of the freeze-dried samples to dissolve. Empirical modelling provides an adequate description on the process kinetics and give an insight on the possible water uptake mechanisms involved during reconstitution.

Table 6-3 Parameters estimated from Weibull function.

System	-20°C			-30°C			-40°C		
	k	n	R <sup>2</sup>	k	n	R <sup>2</sup>	k	n	R <sup>2</sup>
50% gum arabic	8.60E-04	1.207	0.997	8.93E-04	1.337	0.991	6.11E-04	1.241	0.996
60% gum arabic	1.80E-03	1.291	0.993	1.99E-03	1.246	0.980	5.00E-04	1.252	0.995
50% coffee	2.85E-03	1.538	0.989	1.12E-03	1.694	0.994	6.44E-02	0.910	0.986
60% coffee	4.51E-03	1.749	0.998	2.13E-03	1.800	0.977	2.00E-03	1.560	0.992

## 6.4 Summary

The potential of incorporating air into the concentrated systems before freeze-drying has been considered in this chapter. Freezing the aerated 50 and 60% w/w solutions in freeze-drier operating at 1°C/min and rapid freezer at different freezing rates (e.g 0.64°C/min and 2.09°C/min) produced freezing curves that show the marginal effect of air on the freezing

properties. In comparison with freezing profiles reported in chapter 4 (non-aerated samples), similar trends where  $T_n$  and  $T_f$  decreased at higher solute fraction and lower transition temperatures in coffee than gum arabic solutions were also demonstrated in the aerated systems.

Evaluation of the final dried materials in terms of physical appearance and microstructure attributes revealed the higher structural stability of air in coffee than gum arabic solutions during freeze-drying. Processing the aerated coffee produced freeze-dried cake with a sponge-like appearance while much less air bubbles were visible within the cake structure of aerated gum arabic solutions. For this particular sample, the separation of air bubbles and appearance of foam at the top of the dried solid was associated with the effect of gravity force due to the density difference between air and the surrounding. In addition, surfaces of air bubbles in gum arabic particularly at 60% concentration were found to be free of pores from the sublimated ice crystals that was attributed by the reduced thermal conductivity of air bubbles on movement of the freezing front. Notwithstanding these variations, homogenous freeze-dried structures were obtained when compared with the non-aerated dried solids. This improved structure uniformity reaffirmed the idea that increased in surface area provided by the air bubbles help in preventing internal pressure build-up during freeze-drying adding novelty to the present work. Microstructure analysis with SEM has also revealed the development of smaller ice crystals and lower porosity in the highly concentrated systems than the aerated 50%w/w formulation. This finding further confirm the relation between water availability and the ease of its crystallization process.

The aerated systems clearly showed enlargement of the pore network on application of temperature oscillation during freezing. Pores left by the sublimated ice crystals were measured to be tripled in size which was from 24-58 $\mu\text{m}$  to 60-130 $\mu\text{m}$  increasing the overall porosity of

the final dried solids on average by 14%. The incorporated air bubbles demonstrated similar structural response influenced by the coalescing effect during temperature fluctuation.

As observed in the non-aerated systems, the effect of varied cooling rates on microstructure of the aerated freeze-dried solutions was quite inconclusive. On certain occasions, slow cooling represented by the shelf ramp technique demonstrated larger ice crystals and incorporated air bubbles than systems frozen on a pre-cooled shelf (faster cooling). However, at higher solid content the opposite trend was reported for coffee and it seemed that gum arabic was not affected by the experimental design.

Experiment with different primary drying temperatures (-20, -30 and -40°C) revealed the development of big pores on increasing temperature and initial solid content (from 50 to 60% w/w). Microstructure of the aerated 60% freeze-dried systems were found to be affected by the variation of drying temperatures at a greater extent than the aerated dried solids of 50% concentration showing much porous structure when dried at -20 and -30°C. The increased porosity with drying temperature was linked with the low  $T_m$  of concentrated systems and internal pressure development as drying proceeds. Overall, the microstructural differences observed between the two concentrations and three drying temperatures studied (e.g. larger pores in 60% initial concentration system, and high primary drying temperatures) match those observed in experiments without aeration. However, smaller and more homogenous pores were presented by the freeze-dried structure of aerated solutions. The homogeneity indicates sign of improved freeze-dried cake appearance especially for drying at -40°C and it may be a useful alternative in controlling microstructural development of concentrated freeze-dried systems.

Freeze-dried solids from each experiment were further analysed in terms of reconstitution behaviour. Accelerated reconstitution was recorded for dehydrated solutions

having large pores and high overall porosity, the same trend reported in investigation without aeration. This result includes samples with 50% initial concentration, frozen with temperature oscillation and freeze-dried at -20 and -30°C. In the temperature oscillation experiment, the effect of freezing condition on reconstitution time was more apparent in coffee than gum arabic. Meanwhile, different freezing rates applied showed no observable influence on the dissolution kinetics due to the small difference in pore size and porosity. Reconstitution data from different freeze-drying cycles displayed good correlation with Weibull equation. Curve fitting revealed the increasing dissolution kinetics with drying temperatures that produced freeze-dried cakes with high porosity. The derived shape parameter ( $n$ ) from Weibull model extends the knowledge on physical mechanisms involved during dissolution that contribute to the complexity of dissolution process. This study also demonstrated the marked difference between dissolution of coffee and gum arabic affected by the variation in water uptake mechanisms. In addition to the correlation between microstructure and reconstitution properties shown in this analysis, water uptake mechanisms and various phenomena involved in dissolution were also recognized to play important roles on dissolution kinetics.

Summarizing this chapter, the potential to manipulate microstructure of freeze-dried highly concentrated (50 & 60% w/w) by including air to the formulation has been indicated by the increased structural uniformity and porosity.

# CHAPTER 7

## Conclusion and future work

### 7.1 Introduction

The focus of this study has centred on the concept of process-microstructure-property relationship during freeze-drying of high solid systems. This investigation was categorized into three main experimental topics including crystallization of water in concentrated solutions at different freezing conditions (chapter 4), microstructural development of varied formulations at different primary drying temperatures (chapter 5) and freeze-drying of aerated concentrated solutions (chapter 6). Analyses carried out regarding the thermal properties, sample's behaviour during processing, microstructural features and reconstitution process give insights on the phenomena involved during freezing and dehydration that influenced the property of final dried materials. Key findings drawn from each topic are presented in the next sub-sections. Main conclusion and suggestions on future research are outlined at the end of this chapter.

#### 7.1.1 Freeze-drying with different freezing conditions

The purpose of this study was to analyse ice crystal development in high solid solutions (50 and 60% w/w) affected by temperature oscillation, cooling rates and unidirectional freezing and the consequences on freeze-dried structure as well as reconstitution process.

Gum arabic and coffee solutions were first analysed for determination of onset crystallization ( $T_{f-onset}$ ), thermodynamic transition or melting ( $T_m$ ) and glass transition ( $T_g$ ) temperatures with DSC including concentrations from 20 to 60% w/w. At increasing solid content, reduction of  $T_{f-onset}$  and  $T_m$  was recorded and values were lower for coffee than gum

arabic. The decreasing trend with increasing concentration highlighted the significance of water molecule availability and mobility during phase transition process. Meanwhile,  $T_g$  despite being difficult to be identified at the highest solid content was rather constant between the concentrations analyzed. Gum arabic showed the small endothermic shift before melting peak at 10°C higher than the transition observed for coffee. In addition, at 50% solute, gum arabic demonstrated delayed ice formation with devitrification peak ( $T_d$ ) appeared after the glass transition.  $T_g$  for the most concentrated solution was expected to be higher than that of 50% systems for its limited water availability. In this case, mobility of the available water was thought to only increase when temperature is sufficiently high where glass transition can occur. The potential of processing high solid systems as an alternative to reduce energy consumption during freeze-drying was supported with the lower phase change enthalpy ( $\Delta H$ ) measured at increasing concentration.

Temperature where crystallization begins ( $T_n$ ) derived from the freezing profiles recorded at different experimental set up were generally higher than  $T_{f\text{onset}}$  measured from DSC curves. The temperature difference pointed out the relation between cooling rates and presence of impurities with nucleation of ice. The faster cooling rates exerted on the sample in freeze-drier and freezing in non-enclosed container promoted the crystallization process at higher temperatures than calorimetric analysis performed in hermetically sealed container. Both methods however, showed similar trend of lower temperatures for high solid and coffee solutions. Temperature recording has also revealed that on some occasions, supercooling peak was not apparent where sample seemed to directly reach the crystallization stage. This freezing behavior was especially observed during freezing of 60% solutions and fast cooling of 50% systems in rapid freezer. Factors of reduced supercooling at higher viscosity and immediate crystallization after nucleation were thought to contribute to such observation.

Freeze-dried structures between different freezing methods were analysed for physical appearance and microstructural attributes. Information such as structural expansion or puffing, pore structure, size and size distribution as well as porosity were shown to be affected by the initial concentration of materials and freezing conditions employed. At all investigated freezing setups, puffing was apparent in the dried solids of 60% formulation indicated by the crust layer on top of the dried cake and porous structure underneath. Structural expansion occurred to a lesser extent in 60% gum arabic and 50% concentrated freeze-dried systems displaying higher thickness of the dried layer than the melted and puffed bottom observed for 60% coffee. This non-uniformity in freeze-dried structure was the result of increased internal pressure where water vapour from sublimated ice gets trapped within the drying matrix due to high resistance at the drying interface. Obstruction of vapour flow was considered as the effect of low porosity at top crust due to less ice available for sublimation and solute accumulation at the interface during freezing which tend to increase with higher amount of solid in a solution.

In the context of internal structure, porous microstructure of the freeze-dried solids in which pore shape similar to that of dendritic ice crystals were visible under SEM imaging technique. Freeze-drying the 50% concentrated system produced freeze-dried cake with circular and large dendritic pores revealing the orientation of crystal growth parallel to the heat flow during freezing (bottom to top). Indeed, very narrow dendritic shape pores developed in the highly concentrated system due to less water content and less mobile water molecules available for crystallization.

Freezing conditions appeared to affect the microstructure in a different degree. Application of temperature oscillations which induce molecular motion during the freezing cycle, has allowed rearrangement of small ice crystals into larger dimensions. Fluctuation in temperature doubled the pore size and increased overall porosity of the final dried products.

Slow (1.3°C/min) and fast freezing (4-7°C/min) using the shelf ramping and shelf pre-cooling methods respectively, demonstrated marginal effect on the ice crystal development in the high solid solutions. According to the observed microstructure and quantification of pore size distribution as well as porosity, the general trend of decreasing ice crystal size with increasing freezing rate was only observed at a small extent. Meanwhile, puffing of the 60% coffee during freeze-drying increased its overall porosity despite the small crystal dendrites measured. The small variation found between both freezing methods indicates the insufficiency of the freezing rates established to cause considerable variation in the freezing behaviour of 50 and 60% w/w solutions due to the influence of sample's properties (e.g. viscosity). Suggestions for alternative approaches are made available in section 7.3. Experiments with unidirectional freezing while being preliminary, showed the significance of solid content on orientation of crystal growth. As water content is higher in 50% concentrated solutions compared to 60% concentrations, growth of ice crystals parallel to the heat flow was obvious under the microscopic visualization. In the meantime, splitting of the ice finger tips to the front and side of growing crystals due to concentration of solute which caused local supercooling has influenced ice crystals in 60% gum arabic to be advancing without specific orientation. Growth pattern in 60% coffee could not be identified as the sample experienced extensive puffing with no visible dried layer and pores from sublimated ice.

As aforementioned, quality of the final dried products was also evaluated in terms of interaction with water. The correlation between types of material, concentration and microstructure influenced reconstitution of the freeze-dried solids. Different phenomena involved during dissolution of dehydrated gum arabic and coffee systems exerted strong effect on the process kinetics. More apparent swelling of gum arabic particles which affects the movement of water across the dissolving particles was noticed to result in gradual increment

on amount of solid dissolved. In contrast, rapid dissolution of dried coffee particles was contributed by the tendency to disintegrate at the early stage of dissolution. Nevertheless, reconstitution analysis of both materials revealed the fast reconstitution of more porous microstructure. The observed increase in pore size and porosity with reduced initial concentration and on application of temperature oscillation has allowed faster reconstitution of the freeze-dried particles compared to the dried 60% systems frozen at  $-40^{\circ}\text{C}$  without freezing cycles. However, obviously when 60% systems exhibited structural expansion during freeze-drying, comparable reconstitution with 50% formulation was recorded due to the high porosity of the puffed layer diminishing the influence of concentration on reconstitution process. The lack of observable difference in microstructure after slow and fast freezing resulted in overlapping dissolution curves which further confirmed the sensitivity of dissolution process in this work with microstructure.

Consequently, ice crystal formation showed a significant role in governing microstructure and performance of the freeze-dried solids. Temperature oscillation and processing the 50% system have enabled large ice crystal development which increased porosity of the dried product and effectively accelerated the reconstitution process. Marginal difference on water crystallization was obtained upon freezing with shelf ramping and shelf pre-cooling methods resulted in comparable microstructure and dissolution behaviour. Sign of directional solidification with freezing from bottom towards the top of the sample was clearly visible on freezing the 50% concentrated formulation in enclosed and non-enclosed container.

### 7.1.2 Freeze-drying at different primary drying temperatures

Microstructure and reconstitution properties of freeze-dried systems from a range of initial solid content (20-60% w/w) processed at three primary drying temperatures (-20, -30, -40°C) were analysed and compared. XRCT imaging technique and conductivity measurement were utilized in the microstructural visualisation and reconstitution test respectively.

Initial solute fraction and operating primary drying temperature played essential roles in microstructure formation of the final dried products. At lower concentration (20 and 30% w/w) and drying temperature, there were no signs of structural instability during processing of both gum arabic and coffee solutions. The freeze-dried cakes of 20 and 30% formulations at all drying temperatures were characterized with distribution of small needle-like pores throughout the sample height representing the crystal dendrites. Increasing the concentration (from 40 to 60% w/w) and shelf temperature constituted a challenge in development of the freeze-dried systems as the pore structure indicated internal pressure build up. This condition has led to development of freeze-dried cakes having large circular pores underneath the dried layer and cracked structure. In addition, thickness of the dried layer was found to decrease as concentration and drying temperature increase evidence of extensive puffing.

Analysis regarding the effect of drying temperature on pore size distribution showed contradictory pattern between freeze-dried solids of 20-50% w/w concentrations and 60% w/w formulation. For most of the systems, small pores developed when dried at high temperatures ( $T_s = -20$  and  $-30^\circ\text{C}$ ) whereas under this condition, pores in the highly concentrated systems were larger than the one developed at  $-40^\circ\text{C}$  due to greater degree of structural expansion observed at high temperatures. Besides, circular pores in the high solid systems were of much

bigger magnitude (200-2000 $\mu\text{m}$ ) than the pores measured in other samples (25-400 $\mu\text{m}$ ). Porosity of the freeze-dried materials followed similar trend with the pore size distribution.

With regards to reconstitution behaviour, it appeared to correlate well with the microstructure generated. Overall, systems with needle-like and large pores as well as high porosity showed higher dissolution kinetics. As such, dissolution was three times faster for the less concentrated systems (20-40% w/w) compared to the dried solids of 50 and 60% initial concentration. Further, high drying temperatures (-20 and -30°C) associated with greater structural expansion hence larger circular pores in the 60% formulations resulted in faster reconstitution. The low porosity values measured for 50% systems contributed to its slower dissolution process. At the same time, gum arabic dissolved much slower than coffee under similar experimental conditions affected by the variation in wetting mechanisms existed between both materials. Dissolution data was further fitted with Weibull's equation and was shown to describe the dissolution profiles of all freeze-dried systems accordingly. The estimated rate constant,  $k$  generally decreased on increasing concentration correspond to the slower dissolution of concentrated freeze-dried systems excluding the puffed freeze-dried solids. The  $n$  values of more than 1 derived from the equation inferred the various mechanisms that could have involved during dissolution of the freeze-dried samples. Factors such as swelling, disintegration and capillarity or porosity were suggested could play a role simultaneously to govern the dissolution kinetics especially on the difference observed between gum arabic and coffee.

Development of freeze-dried solids with different microstructures is evidence of the relation between product formulation and operating temperature. Primary drying temperature is a critical factor as it influenced thermodynamic stability of the materials being dried. Structural expansion observed at high concentration and drying temperature although enhanced

porosity of the solid matrix and reduced the reconstitution time, it revealed the close link between processing conditions and physical appearance of the product when freeze-drying high solids content systems.

### **7.1.3 Freeze-drying of aerated systems.**

Microstructure development of high solid freeze-dried system was further investigated on aerated solutions. 50 and 60% w/w solutions were aerated accordingly with a food processor and freeze-dried at the different freezing conditions and primary drying temperatures studied in the non-aerated solutions.

Freezing profiles of the aerated solutions appeared to be in close range with the one recorded for non-aerated solutions. Inclusion of air however, had marked effect on the freeze-dried structure obtained. Visual inspection revealed the increased uniformity of the freeze-dried solids compared to the non-aerated systems, with no development of two distinct layers. As aeration increased surface area of the material being dried, it allowed water vapour to escape easily from the frozen matrix preventing the internal pressure build up reported in non-aerated system. It was also noted that air bubbles demonstrated less stability in gum arabic solution than coffee as very few bubbles were seen within the freeze-dried cake. The appearance of big bubbles on top of the cake (figure 6.2 and 6.3) suggested that the air bubbles were partially separated to the surface and that the viscosity of the solution was low enough to allow the observed separation. Unlike the air bubbles in coffee, surfaces of bubbles found in 60% gum arabic were free of pores from sublimated ice crystals attributed by the reduced thermal conductivity of air which interfered with the movement of freezing front.

Microstructure analysis with SEM images revealed that size of ice crystals and incorporated air bubbles increased when temperature oscillation was carried out during freezing and after slow freezing of the 50% concentrated formulations. Eventually, freeze-dried cake with big pores and high porosities were obtained under these process designs resulting in reduced dissolution time. At the same time, investigation with different freezing rates on 60% systems showed the opposite trend in crystal size with the observation made in the less concentrated samples. Slightly bigger ice crystals were measured in fast frozen 60% coffee than the slowly frozen sample whereas at both freezing rates, the average ice crystal size in 60% gum arabic were almost similar. As slow freezing generally associated with large crystals, this was an unexpected outcome and it was suggested that properties such as viscosity of the highly concentrated solutions significantly influence the mass and heat transfer involved in crystallization affecting the resultant freezing rate. Appearance of cracks in non-aerated systems were also seen in the aerated freeze-dried cakes especially in gum arabic. The cracked structure was thought to develop during desorption of unfrozen water from the dried matrix in the secondary drying stage. In general, the small difference obtained between different freezing rates studied, resulted in comparable dissolution behaviour.

Apart from different freezing conditions, aerated solutions were also freeze-dried at different primary drying temperatures (-20, -30 and -40°C). The investigated shelf temperatures were mainly found to affect the freeze-dried systems of aerated 60% solutions due to its lower  $T_m$  than the less concentrated systems. It was found that pore size and porosity increased with drying temperature consistent with the observation made in experiment without aeration. The highly interconnected circular pores suggested development of internal pressure during freeze-drying at -20 and -30°C. Aeration however, formed freeze-dried solids with more homogenous and smaller pores than non-aerated freeze-dried systems. Also for the 60% formulations,

primary drying conducted at  $-40^{\circ}\text{C}$  produced freeze-dried cake without indication of structural expansion exhibiting cracks and significantly smaller pores compared to the microstructure from higher operating temperatures. These microstructure features indicated that the significant structural changes during freeze-drying can be controlled with aeration. The freeze-dried structure of aerated 50% formulations did not exhibit apparent variation between the three temperatures except for the bigger air bubbles found in coffee dried at the highest temperature. Reconstitution data from this experiment demonstrated good correlation with the microstructure generated at different drying conditions. The freeze-dried solids with big pores and high overall porosity formed at high primary drying temperatures generally dissolved faster than dried particles processed at  $-40^{\circ}\text{C}$ . The high reconstitution rate was linked with the interconnectivity of large pores and thin cell wall that enabled rapid solid disintegration. At the same time, more pronounced cracks seen in 50% coffee dried at the coldest temperature accelerated its dissolution time. The use of Weibull equation was found to agree well with the dissolution data and the derived shape parameter has suggested the combination of imbibition, diffusion and swelling as the physical means of water transport during dissolution.

Overall, freeze-drying aerated solutions has produced freeze-dried solids with high structure uniformity and porosity giving an insight on the potential of aeration to control freeze-dried microstructure of highly concentrated system.

## **7.2 Conclusion**

Studying microstructure development of freeze-dried systems provide useful information on the key elements that control the performance of this dehydration technology. Concentration, aeration, freezing method and primary drying temperature all had an effect on

determining the material's characteristics. Generally, using formulation with 50% w/w solute and freezing with temperature oscillations led to growth of large ice crystals that was associated with big pores and high porosity. The porous microstructure obtained at these processing conditions contributed to the fast reconstitution of the final dried product. Also, drying at -40°C produced freeze-dried solids with reduced structural expansion. Reducing density of the materials used with aeration has demonstrated the potential to freeze-dry higher concentration (60% w/w) due to the uniform freeze-dried cake appearance especially when dried at -40°C. These findings have important application in the design of energy efficient freeze-drying technology for the reduced energy consumption potential associated with high solid formulations (> 40% w/w).

Concluding this work, investigations on microstructural development of concentrated freeze-dried solids allow a better understanding of the physical processes and further opening up opportunities for the design of reduced energy utilization in freeze-drying and manufacturing of dried product with desired characteristics.

### **7.3 Suggestions for future work**

Findings from this study provide insight on several different aspects in freeze-drying high solid solutions that would be interesting to be explored such as:

- Rheological properties of the materials could be investigated to better describe crystallization of water in concentrated system. This would provide additional avenue on explaining the heat and mass transfer involved prior to ice nucleation as supercooling in general determine how nucleation of ice and crystal growth proceeds responsible for the size, size distribution and morphology of ice crystals.

- Attempts have been carried out on freezing with fluctuating temperature to promote growth of large ice crystals. It may be possible to compare the ice crystal formation with different methods that allow control on ice nucleation temperature such as ultrasonic and microwave radiation assisted freezing. This comparison will help to extend the knowledge on how nucleation of ice can be regulated to result in ice crystals of desired sizes and shapes.
- Primary drying step is also known to be driven by the pressure difference between pressure at the sublimating ice and the drying chamber as sublimation involve of simultaneous heat and mass transfer process. While pressure at  $1 \times 10^{-4}$  bar was kept constant throughout this study, the effect of varied vacuum pressure and combination with different shelf temperature would be interesting to be explored.
- Experiment on drying conditions could also be extended by applying gradual shelf temperature increment on transition from primary to secondary drying. The result may lead to a comprehensive understanding on the physical behaviour of materials under different processing conditions.

## LIST OF REFERENCES

- Abdelwahed, W., Degobert, G., Stainmesse, S. & Fessi, H., 2006. Freeze-drying of nanoparticles: Formulation, process and storage considerations. *Advanced Drug Delivery Reviews*, 58, pp.1688–1713.
- Abu-Ghannam, N. & McKenna, B., 1997. The application of Peleg's equation to model water absorption during the soaking of red kidney beans (*Phaseolus vulgaris* L.). *Journal of Food Engineering*, 32(4), pp.391–401.
- Aguilera, J.M., 2005. Why food micro structure? *Journal of Food Engineering*, 67, pp.3–11.
- Aguilera, J.M., Stanley, D.W. & Baker, K.W., 2000. New dimensions in microstructure of food products. *Food Science & Technology*, 11, pp.3–9.
- Al-Assaf, S., Phillips, G.O., Aoki, H. & Sasaki, Y., 2007. Characterization and properties of *Acacia senegal* (L.) Willd. var. *senegal* with enhanced properties (*Acacia* (sen) SUPER GUM™): Part 1-Controlled maturation of *Acacia senegal* var. *senegal* to increase viscoelasticity, produce a hydrogel form and convert a. *Food Hydrocolloids*, 21(3), pp.319–328.
- Alizadeh, E., Chapleau, N., de Lamballerie, M. & Le-Bail, A., 2007. Effect of different freezing processes on the microstructure of Atlantic salmon (*Salmo salar*) fillets. *Innovative Food Science and Emerging Technologies*, 8(4), pp.493–499.
- Antal, T., Sikolya, L. & Kerekes, B., 2013. Assessment of Freezing Pre-Treatments for the Freeze Dried of Apple Slices. *Acta Universitatis Cibiniensis. Series E: Food Technology*, 17(2), pp.3–14.
- Araki, T. & Sagara, Y., 2006. Transport properties of cellular food materials undergoing freeze-drying. *Drying Technology: An International Journal*, (December 2012), pp.297–312.
- Arvanitoyannis, I., Blanshard, J.M.V., Ablett, S., Izzard, M.J. & Lillford, P.J., 1993. Calorimetric study of the glass transition occurring in fructose solutions. *Journal of Science Food Agriculture*, 63, pp.177–188.
- Arya, M. & Rao, L.J.M., 2007. An impression of coffee carbohydrates. *Critical Reviews in Food Science and Nutrition*, 47(1), pp.51–67.
- Asami, D.K., Hong, Y.J., Barrett, D.M. & Mitchell, A.E., 2003. Comparison of the total phenolic and ascorbic acid content of freeze-dried and air-dried marionberry, strawberry, and corn grown using conventional, organic, and sustainable agricultural practices. *Journal of Agricultural and Food Chemistry*, 51, pp.1237–1241.
- Auleda, J.M. Raventós, M., Sánchez, J. & Hernández, E., 2011. Estimation of the freezing point of concentrated fruit juices for application in freeze concentration. *Journal of Food Engineering*, 105(2), pp.289–294.
- Babin, P., Della Valle, G., Chiron, H., Cloetens, P., Hoszowska, J., Pernot, P., Réguerre, a. L.,

- Salvo, L. & Dendievel, R., 2006. Fast X-ray tomography analysis of bubble growth and foam setting during breadmaking. *Journal of Cereal Science*, 43, pp.393–397.
- Babin, P., Della Valle, G., Dendievel, R., Lourdin, D. & Salvo, L., 2007. X-ray tomography study of the cellular structure of extruded starches and its relations with expansion phenomenon and foam mechanical properties. *Carbohydrate Polymers*, 68, pp.329–340.
- Barigou, M. & Douaire, M., 2013. X-ray micro-computed tomography for resolving food microstructures. *Food Microstructures*, pp.246–272.
- Barresi, A.A., Ghio, S., Barresi, A.A., Ghio, S., Fissore, D. & Pisano, R., 2009. Freeze drying of pharmaceutical excipients close to collapse temperature: influence of the process conditions on process time and product quality. *Drying Technology*, 27(6), pp.805–816.
- Barresi, A.A., Pisano, R., Fissore, D., Rasetto, V., Velardi, S.A., Vallan, A., Parvis, M. & Galan, M., 2009. Monitoring of the primary drying of a lyophilization process in vials. *Chemical Engineering and Processing: Process Intensification*, 48(1), pp.408–423.
- Burmester, K., Fehr, H. & Eggers, R., 2011. A comprehensive study on thermophysical material properties for an innovative coffee drying process. *Drying Technology*, 29(February 2015), pp.1562–1570.
- C.S.Chang, 1988. Density and porosity with pycnometer. *Cereal Chemistry*, 65(1), pp.13–15.
- Cafarelli, B. Spada, A., Laverse, J., Lampignano, V. & Del Nobile, M.a., 2014. An insight into the bread bubble structure: An X-ray microtomography approach. *Food Research International*, 66, pp.180–185.
- Caillet, A., Cogné, C., Andrieu, J., Laurent, P. & Rivoire, A., 2003. Characterization of ice cream structure by direct optical microscopy. Influence of freezing parameters. *LWT - Food Science and Technology*, 36, pp.743–749.
- Campbell, G.M. & Mougeot, E., 1999. Creation and characterisation of aerated food products. *Trends in Food Science and Technology*, 10(9), pp.283–296.
- Cano-Chauca, M., Stringheta, P. C., Ramos, A. M. & Cal-Vidal, J., 2005. Effect of the carriers on the microstructure of mango powder obtained by spray drying and its functional characterization. *Innovative Food Science and Emerging Technologies*, 6(4), pp.420–428.
- Capek, P., Matulová, M., Navarini, L. & Suggi-Liverani, F., 2010. Structural features of an arabinogalactan-protein isolated from instant coffee powder of *Coffea arabica* beans. *Carbohydrate Polymers*, 80(1), pp.180–185.
- Cascone, S., 2017. Modeling and comparison of release profiles: Effect of the dissolution method. *European Journal of Pharmaceutical Sciences*, 106(May), pp.352–361.
- Cassanelli, M., Norton, I. & Mills, T., 2017. Role of gellan gum microstructure in freeze drying and rehydration mechanisms. *Food Hydrocolloids*, 75, pp.51–61.
- Ceballos, A.M., Giraldo, G.I. & Orrego, C.E., 2012. Effect of freezing rate on quality parameters of freeze dried soursop fruit pulp. *Journal of Food Engineering*, 111(2),

pp.360–365.

- Chang, B.S. & Patro, S.Y., 2004. Freeze-drying Process Development for Protein Pharmaceuticals. In H. R. Costantino & Pikal M.J., eds. *Lyophilization of Biopharmaceuticals*. American Association of Pharmaceutical Scientists, pp. 113–138.
- Charoenrein, S. & Preechathamwong, N., 2010. Undercooling associated with slow freezing and its influence on the microstructure and properties of rice starch gels. *Journal of Food Engineering*, 100(2), pp.310–314.
- Ciurzyńska, A. & Lenart, A., 2016. Effect of the aerated structure on selected properties of freeze-dried hydrocolloid gels. *International Agrophysics*, 30(1), pp.9–17.
- Ciurzyńska, A. & Lenart, A., 2011. Freeze-Drying - Application in Food Processing and Biotechnology - A Review. *Polish Journal of Food and Nutrition Sciences*, 61(3), pp.165–171.
- Claussen, I.C., Ustad, T. S., Strømme, I. & Walde, P. M., 2007. Atmospheric Freeze Drying—A Review. *Drying Technology*, 25(6), pp.947–957.
- Cunha, L.M., Oliveira, F.A.R. & Ilincanu, L.A., 1998. Application of the probabilistic Weibull distribution to rehydration kinetics: Relationship between the model parameters and the underlying physical mechanisms. *Proceedings of the 3rd Workshop of the Copernicus Project*, 3(September), pp.9–13.
- Dalen, G., Van Voda, A., Duijster, A., Vliet, L.V., Vergeldt, F. & Sman, R.V.D., 2013. Multi-length scale structural imaging of freeze-dried carrots and their rehydration behaviour . In *InsideFood Symposium*. Leuven, pp. 9–12.
- Datye, A.K., 2003. Electron microscopy of catalysts: Recent achievements and future prospects. *Journal of Catalysis*, 216(1–2), pp.144–154.
- Degner, B.M., Olson, K. M., Rose, D., Schlegel, V., Hutkins, R. & McClements, D. J., 2013. Influence of freezing rate variation on the microstructure and physicochemical properties of food emulsions. *Journal of Food Engineering*, 119(2), pp.244–253.
- Donald, A., He, C. & Royall, C., 2000. Applications of environmental scanning electron microscopy to colloidal aggregation and film formation. *Colloids and Surfaces A: ...*, 174(1–2), pp.37–53.
- Eddleston, M.D., Bithell, E.G. & Jones, W., 2010. Transmission electron microscopy of pharmaceutical materials. *Journal of Pharmaceutical Sciences*, 99(9), pp.4072–4083.
- Esfandiary, R., Gattu, S.K., Stewart, J.M. & Patel, S.M., 2016. Effect of freezing on lyophilization process performance and drug product cake appearance. *Journal of Pharmaceutical Sciences*, 105(4), pp.1427–1433.
- Farber, L., Tardos, G. & Michaels, J.N., 2003. Use of X-ray tomography to study the porosity and morphology of granules. *Powder Technology*, 132, pp.57–63.
- Farkas, B.E. & Singh, R.P., 1991. Physical properties of air-dried and freeze-dried chicken white meat. *Journal of Food Science*, 56(3), pp.611–615.

- Fernández, P.P., Otero, L., Guignon, B. & Sanz, P.D., 2006. High-pressure shift freezing versus high-pressure assisted freezing: Effects on the microstructure of a food model. *Food Hydrocolloids*, 20(4), pp.510–522.
- Flores, A.A & Goff, H.D., 1999. Ice crystal size distributions in dynamically frozen model solutions and ice cream as affected by stabilizers. *Journal of Dairy Science*, 82, pp.1399–1407.
- Forny, L., Marabi, A. & Palzer, S., 2011. Wetting, disintegration and dissolution of agglomerated water soluble powders. *Powder Technology*, 206(1–2), pp.72–78.
- Franks, F., 1998. Freeze-drying of bioproducts: Putting principles into practice. *European Journal of Pharmaceutics and Biopharmaceutics*, 45(3), pp.221–229.
- Frisullo, P. Laverse, J., Barnabà, M., Navarini, L. & Del Nobile, M.A., 2012. Coffee beans microstructural changes induced by cultivation processing: An X-ray microtomographic investigation. *Journal of Food Engineering*, 109(1), pp.175–181.
- Gan, K.H., Bruttini, R., Crosser, O.K. & Liapis, A.I., 2005. Freeze-drying of pharmaceuticals in vials on trays: Effects of drying chamber wall temperature and tray side on lyophilization performance. *International Journal of Heat and Mass Transfer*, 48(9), pp.1675–1687.
- Ganguly, A., Nail, S.L. & Alexeenko, A., 2013. Experimental determination of the key heat transfer mechanisms in pharmaceutical freeze-drying. *Journal of Pharmaceutical Sciences*, 102(5), pp.1610–1625.
- Garcia-Pascual, P., Sanjuan, N., Melis, R. & Mulet, A., 2006. *Morchella esculenta* (morel) rehydration process modelling. *Journal of Food Engineering*, 72(4), pp.346–353.
- Gashua, I.B., Williams, P.A. & Baldwin, T.C., 2016. Molecular characteristics, association and interfacial properties of gum Arabic harvested from both *Acacia senegal* and *Acacia seyal*. *Food Hydrocolloids*, 61, pp.514–522.
- Geidobler, R. & Winter, G., 2013. Controlled ice nucleation in the field of freeze-drying: Fundamentals and technology review. *European Journal of Pharmaceutics and Biopharmaceutics*, 85(2), pp.214–222.
- Glover, D.A., Ushida, K., Phillips, A.O. & Riley, S.G., 2009. Acacia(sen) SUPERGUM™(Gum arabic): An evaluation of potential health benefits in human subjects. *Food Hydrocolloids*, 23(8), pp.2410–2415.
- Gómez-Díaz, D., Navasa, J.M. & Quintáns-Riveiro, L.C., 2008. Intrinsic viscosity and flow behaviour of arabic gum aqueous solutions. *International Journal of Food Properties*, 11(4), pp. 773-780.
- Gormley, R., Walshe, T., Hussey, K. & Butler, F., 2002. The Effect of fluctuating vs. constant frozen storage temperature regimes on some quality parameters of selected food products. *LWT - Food Science and Technology*, 35(2), pp.190–200.
- Greco, K., Mujat, M., Galbally-kinney, K.L., Hammer, D.X., Ferguson, R.D., Ifimia, N.,

- Mulhall, P., Sharma, P., Kessler, W.J. & Pikal, M.J., 2013. Accurate prediction of collapse temperature using optical coherence tomography-based freeze-drying microscopy. *Journal of Pharmaceutical Sciences*, 102(6), pp.1773–1785.
- Hagiwara, T., Mao, J., Suzuki, T. & Takai, R., 2005. Ice Recrystallization in Sucrose Solutions Stored in a Temperature Range of -21C. to -50C. *Food Science and Technology Research*, 11(4), pp.407–411.
- Hammami, C., René, F. & Marin, M., 1999. Process-quality optimization of the vacuum freeze-drying of apple slices by the response surface method. *International Journal of Food Science & Technology*, 34(2), pp.145–160.
- Harnkarnsujarit, N., Kawai, K., Watanabe, M., & Suzuki, T., 2016. Effects of freezing on microstructure and rehydration properties of freeze-dried soybean curd. *Journal of Food Engineering*, 184, pp.10–20.
- Harnkarnsujarit, N. & Charoenrein, S., 2011. Influence of collapsed structure on stability of Beta-carotene in freeze-dried mangoes. *Food Research International*, 44(10), pp.3188–3194.
- Harnkarnsujarit, N., Charoenrein, S. & Roos, Y.H., 2012. Microstructure formation of maltodextrin and sugar matrices in freeze-dried systems. *Carbohydrate Polymers*, 88(2), pp.734–742.
- Harnkarnsujarit, N., Kawai, K. & Suzuki, T., 2016. Impacts of freezing and molecular size on structure, mechanical properties and recrystallization of freeze-thawed polysaccharide gels. *LWT - Food Science and Technology*, 68, pp.190–201.
- Heertje, I., 1993. Structure and Function of Food Products: A Review. *Food Structure*, 12(3), pp.343–364.
- Herremans, E., Bongaers, E., Estrade, P., Gondek, E., Hertog, M., Jakubczyk, E., Nguyen Do Trong, N. & Rizzolo, A., 2013. Microstructure-texture relationships of aerated sugar gels: Novel measurement techniques for analysis and control. *Innovative Food Science and Emerging Technologies*, 18(April), pp.202–211.
- Hillbrick, G.C., McMahon, D.J. & Mcmanus, W.R., 1999. Microstructure of indirectly and directly heated ultra-high-temperature (UHT) processed milk examined using transmission electron microscopy and immunogold labelling. *LWT- Food Science and Technology*, 494, pp.486–494.
- Hogekamp, S. & Schubert, H., 2003. Rehydration of food powders. *Food Science and Technology International*, 9(3), pp.223–235.
- Homer, S., Kelly, M. & Day, L., 2014. Determination of the thermo-mechanical properties in starch and starch/gluten systems at low moisture content - A comparison of DSC and TMA. *Carbohydrate Polymers*, 108(1), pp.1–9.
- Hottot, A., Vessot, S. & Andrieu, J., 2004. A direct characterization method of the ice morphology. relationship between mean crystals size and primary drying times of freeze-drying processes. *Drying Technology*, 22(8), pp.2009–2021.

- Hottot, A., Vessot, S. & Andrieu, J., 2007. Freeze drying of pharmaceuticals in vials: Influence of freezing protocol and sample configuration on ice morphology and freeze-dried cake texture. *Chemical Engineering and Processing: Process Intensification*, 46(7), pp.666–674.
- Huang, L., Zhang, M., Mujumdar, A.S., Sun, D., Tan, G. & Tang, S., 2009. Studies on decreasing energy consumption for a freeze-drying process of apple slices. *Drying Technology*, 27(9), pp.938–946.
- James, B., 2009. Advances in “wet” electron microscopy techniques and their application to the study of food structure. *Trends in Food Science & Technology*, 20(3–4), pp.114–124.
- Jin, J., Yurkow, E.J., Adler, D. & Lee, T.C., 2018. Improved freeze-drying efficiency by ice nucleation proteins with ice morphology modification. *Food Research International*, 106, pp.90–97.
- Kaale, L.D. & Eikevik, T.M., 2014. The development of ice crystals in food products during the superchilling process and following storage, a review. *Trends in Food Science & Technology*, 39(2), pp.91–103.
- Kabláb, M., 1993. Practical aspects of electron microscopy in dairy research. *Food Structure*, 12(1), pp.95–114.
- Karathanos, V.T., Anglea, S. & Karel, M., 1996. Structural collapse of plant materials during freeze-drying. *Journal of Thermal Analysis*, 47, pp.1451–1461.
- Kasper, J.C. & Friess, W., 2011. The freezing step in lyophilization: Physico-chemical fundamentals, freezing methods and consequences on process performance and quality attributes of biopharmaceuticals. *European Journal of Pharmaceutics and Biopharmaceutics*, 78(2), pp.248–263.
- Kaufmann, S.F.M. & Palzer, S., 2011. Food structure engineering for nutrition, health and wellness. *Procedia Food Science*, 1, pp.1479–1486.
- Khalid, S.A., Musa, A.M., Saeed, A.M., Abugroun, E.A., Sid Ahmed, E.O., Ghalib, M.B., Elnima, E., Alkarib, S.Y., Abdelsalam, T.M. & Abdelgader, A., 2014. Manipulating dietary fibre: Gum Arabic making friends of the colon and the kidney. *Bioactive Carbohydrates and Dietary Fibre*, 3(2), pp.71–76.
- Khalloufi, S. & Ratti, C., 2003. Quality Deterioration of Freeze-dried Foods as Explained by their Glass Transition Temperature and Internal Structure. *Journal of Food Science*, 68(3), pp.892–903.
- Khan, M.I.H., Wellard, R. M., Nagy, S.A., Joardder, M.U.H. & Karim, M.A., 2017. Experimental investigation of bound and free water transport process during drying of hygroscopic food material. *International Journal of Thermal Sciences*, 117, pp.266–273.
- Kiani, H., Sun, D.W., Zhang, Z., Al-Rubeai, M., Naciri, M., 2013. Ultrasound-assisted freezing of *Lactobacillus plantarum subsp. plantarum*: The freezing process and cell viability. *Innovative Food Science and Emerging Technologies*, 18, pp.138–144.
- Kiani, H., Zhang, Z., Delgado, A. & Sun, D.W., 2011. Ultrasound assisted nucleation of some

- liquid and solid model foods during freezing. *Food Research International*, 44(9), pp.2915–2921.
- Kiani, H. & Sun, D.W., 2011. Water crystallization and its importance to freezing of foods: A review. *Trends in Food Science and Technology*, 22(8), pp.407–426.
- Klang, V., Valenta, C. & Matsko, N.B., 2013. Electron microscopy of pharmaceutical systems. *Micron*, 44(1), pp.45–74.
- Kochs, M., Körber, C.H., Heschel, I. & Nunner, B., 1993. The influence of the freezing process on vapour transport during sublimation in vacuum-freeze-drying of macroscopic samples. *International Journal of Heat and Mass Transfer*, 36(7), pp.1727–1738.
- Kodama, T., Sawada, H., Hosomi, H., Takeuchi, M., Wakiyama, N., Yonemochi, E. & Terada, K., 2013. Determination for dry layer resistance of sucrose under various primary drying conditions using a novel simulation program for designing pharmaceutical lyophilization cycle. *International Journal of Pharmaceutics*, 452(1–2), pp.180–187.
- Koh, S., Rhim, J.W. & Kim, J.M., 2011. Effect of freezing temperature on the rehydration properties of freeze-dried rice porridge. *Korean Journal of Food Science and Technology*, 43(4), pp.509–512.
- Korsmeyer, R.W., Gurny, R., Doelker, E., Buri, P. & Peppas, N.A., 1983. Mechanisms of solute release from porous hydrophilic polymers. *International Journal of Pharmaceutics*, 15(1), pp.25–35.
- Kosmidis, K. & Macheras, P., 2007. Monte Carlo simulations for the study of drug release from matrices with high and low diffusivity areas. *International Journal of Pharmaceutics*, 343(1–2), pp.166–172.
- Kravtchenko, T.P. et al., 1999. A novel method for determining the dissolution kinetics of hydrocolloid powders. *Food Hydrocolloids*, 13(3), pp.219–225.
- Krokida, M.K., Karathanos, V.T. & Maroulis, Z.B., 1998. Effect of freeze-drying conditions on shrinkage and porosity of dehydrated agricultural products. *Journal of Food Engineering*, 35(4), pp.369–380.
- Krokida, M.K. & Philippopoulos, C., 2005. Rehydration of dehydrated foods. *Drying Technology*, 23(4), pp.799–830.
- Kumar, C., Karim, M. a. & Joardder, M.U.H., 2014. Intermittent drying of food products: A critical review. *Journal of Food Engineering*, 121, pp.48–57.
- Landis, E.N. & Keane, D.T., 2010. X-ray microtomography. *Materials Characterization*, 61, pp.1305–1316.
- Langton, M. & Hermansson, A.-M., 1996. Image analysis of particulate whey protein gels. *Food Hydrocolloids*, 10(2), pp.179–191.
- Leiter, F., 2015. Food Freezing : Crystal structure and size. *Reference Module Food Science*, pp.1–8.

- Leloux, M.S., 1999. The influence of macromolecules on the freezing of water. *Journal of Macromolecular Science, Part C: Polymer Reviews*, 39(1), pp.1–16.
- Levi, G. & Karel, M., 1995. Volumetric shrinkage (collapse) in freeze-dried carbohydrates above their glass transition temperature. *Food Research International*, 28(2), pp.145–151.
- Lewicki, P.P., 1998. Effect of pre-drying treatment, drying and rehydration on plant tissue properties: A review. *International Journal of Food Properties*, 1(December 2012), pp.1–22.
- Lewis, L.M., Johnson, R.E., Oldroyd, M.E., Ahmed, S.S., Joseph, L., Saracovan, I. & Sinha, S., 2010. Characterizing the Freeze-drying behavior of model protein formulations. *AAPS PharmSciTech*, 11(4), pp.1580–1590.
- Li, B. & Sun, D.-W., 2002. Novel methods for rapid freezing and thawing of foods – A review. *Journal of Food Engineering*, 54(3), pp.175–182.
- Liapis, A.I. & Bruttini, R., 2008. Exergy analysis of freeze drying of pharmaceuticals in vials on trays. *International Journal of Heat and Mass Transfer*, 51(15–16), pp.3854–3868.
- Liliana, S.-C., Diana, P.V.-M. & Alfredo, A.A., 2015. Structural, physical, functional and nutraceutical changes of freeze-dried fruit. *African Journal of Biotechnology*, 14(6), pp.442–450.
- Lim, K.S. & Barigou, M., 2004. X-ray micro-computed tomography of cellular food products. *Food Research International*, 37, pp.1001–1012.
- Liu, J., 2006. Physical characterization of pharmaceutical formulations in frozen and freeze-dried solid states: techniques and applications in freeze-drying development. *Pharmaceutical Development and Technology*, 11(1), pp.3–28.
- Liu, Y., Zhao, Y. & Feng, X., 2008. Exergy analysis for a freeze-drying process. *Applied Thermal Engineering*, 28(7), pp.675–690.
- Lopez-Quiroga, E., Wang, R., Gouseti, O., Fryer, P. J. & Bakalis, S., 2016. Crystallisation in concentrated systems: A modelling approach. *Food and Bioproducts Processing*, 100, pp.525–534.
- Lopez-Quiroga, E., Wang, R., Gouseti, O., Fryer, P. J. & Bakalis, S., 2015. Modelling freezing processes of high concentrated systems. *IFAC-PapersOnLine*, 28(1), pp.749–754.
- Lopez-Quiroga, E., Antelo, L.T. & Alonso, A.A., 2012. Time-scale modeling and optimal control of freeze-drying. *Journal of Food Engineering*, 111(4), pp.655–666.
- Luo, R. & Zhou, G., 2008. Mathematical optimization for energy consumption during freeze-drying of cooked beef slice. *Journal of Food Process Engineering*, 31(5), pp.583–601.
- M., N. T., K., Sakata, M., S, A.-A. & Phillips, G.O., 2011. Effect of AGP on emulsifying stability of Gum arabic. *Gum Arabic*, pp. 269–274.
- Machado, M.D.F. Oliveira, F. a R., Gekas, V. & Singh, R.P., 1998. Kinetics of moisture uptake and soluble-solids loss by puffed breakfast cereals immersed in water. *International*

- Journal of Food Science and Technology*, 33(1993), pp.225–237.
- Marabi, A. Livings, S., Jacobson, M. & Saguy, I.S., 2003. Normalized Weibull distribution for modeling rehydration of food particulates. *European Food Research and Technology*, 217(4), pp.311–318.
- Marabi, A. & Saguy, I.S., 2004. Effect of porosity on rehydration of dry food particulates. *Journal of the Science of Food and Agriculture*, 84(10), pp.1105–1110.
- Martínez, L. Villalobos, R., Sánchez, M., Cruz, J., Ganem, A. & Melgoza, L.M., 2009. Monte Carlo simulations for the study of drug release from cylindrical matrix systems with an inert nucleus. *International Journal of Pharmaceutics*, 369(1–2), pp.38–46.
- Meda, L. & Ratti, C., 2005. Rehydration of freeze-dried strawberries at varying temperatures. *Journal of Food Process Engineering*, 28(3), pp.233–246.
- Meste, M.L., Champion, D., Roudaut, G., Blond, G. & Simatos, D., 2002. Glass transition and food technology: A critical appraisal. *Journal of Food Science*, 67(7), pp.2444–2458.
- Miller-Chou, B.A. & Koenig, J.L., 2003. A review of polymer dissolution. *Progress in Polymer Science (Oxford)*, 28(8), pp.1223–1270.
- Moreno, F.L. Raventós, M., Hernández, E., Santamaría, N., Acosta, J., Pirachican, O., Torres, L. & Ruiz, Y., 2015. Rheological Behaviour, Freezing Curve, and Density of Coffee Solutions at Temperatures Close to Freezing. *International Journal of Food Properties*, 18(March), pp.426–438.
- Mortazavi, a & Tabatabaie, F., 2008. Study of ice cream freezing process after treatment with ultrasound. *World Applied Sciences Journal*, 4(2), pp.188–190.
- Moses, J.A. Norton, T., Alagusundaram, K. & Tiwari, B.K., 2014. Novel Drying Techniques for the Food Industry. *Food Engineering Reviews*, 6(3), pp.43–55.
- Mousavi, R. Miri, T., Cox, P.W. & Fryer, P.J., 2007. Imaging food freezing using X-ray microtomography. *International Journal of Food Science and Technology*, 42, pp.714–727.
- Muse, M.R. & Hartel, R.W., 2004. Ice cream structural elements that affect melting rate and hardness. *Journal of dairy science*, 87(1), pp.1–10..
- Mussatto, S.I. Machado, E.M.S., Martins, S. & Teixeira, J.A., 2011. Production, composition, and application of coffee and its industrial residues. *Food and Bioprocess Technology*, 4, pp.661–672.
- Muthukumaran, A., Ratti, C. & Raghavan, V., 2008. Foam-mat freeze drying of egg white-mathematical modeling Part II: Freeze drying and modeling. *Drying Technology*, 26(4), pp.513–518.
- Nakagawa, K. & Ochiai, T., 2006. Influence of controlled nucleation by ultrasounds on ice morphology of frozen formulations for pharmaceutical proteins freeze-drying. *Chemical Engineering and Processing: Process Intensification*, 45, pp.783–791.

- Nireesha, G.R. Divya, L., Sowmya, C., Venkateshan, N., Niranjana Babu, M. & Lavakumar, V., 2013. Lyophilization / Freeze Drying - An Review. *International Journal Of novel Trends in pharmaceutical sciences*, 3(4), pp.87–98.
- Noronha, N. Duggan, E., Ziegler, G.R., Stapleton, J.J., O’Riordan, E.D. & O’Sullivan, M., 2008. Comparison of microscopy techniques for the examination of the microstructure of starch-containing imitation cheeses. *Food Research International*, 41(5), pp.472–479.
- Nunes, F.M. & Coimbra, M.A., 2002. Chemical characterization of the high-molecular-weight material extracted with hot water from green and roasted robusta coffees as affected by the degree of roast. *Journal of Agricultural and Food Chemistry*, 50(24), pp.7046–7052.
- Oddone, I., Barresi, A.A. & Pisano, R., 2017. Influence of controlled ice nucleation on the freeze-drying of pharmaceutical products: the secondary drying step. *International Journal of Pharmaceutics*, 524(1–2), pp.134–140.
- Osman, M.E., Williams, P.A., Menzies, A.R. & Phillips, G.O., 1993. Characterization of commercial samples of gum arabic. *Journal of Agricultural and Food Chemistry*, 41(1), pp.71–77.
- Otero, L., Martino, M., Zaritzky, N., Solas, M., & Sanz, P. D. 2000. Preservation of microstructure in peach and mango during high-pressure-shift freezing. *Journal of Food Science*, 65(3), pp.466–470.
- Overcashier, D.E., Patapoff, T.W. & Hsu, C.C., 1999. Lyophilization of protein formulations in vials: Investigation of the relationship between resistance to vapor flow during primary drying and small-scale product collapse. *Journal of Pharmaceutical Sciences*, 88(7), pp.688–695.
- Papadopoulou, V., Kosmidis, K., Vlachou, M. & Macheras, P., 2006. On the use of the Weibull function for the discernment of drug release mechanisms. *International Journal of Pharmaceutics*, 309(1–2), pp.44–50.
- Pardo, J.M., Suess, E. & Niranjana, K., 2002. An investigation into the relationship between freezing rate and mean ice crystal size for coffee extracts. *Food and Bioprocess Processing*, 80(September), pp.176–182.
- Parker, A., Rigby-Singleton, S., Perkins, M., Bates, D., Le Roux, D., Roberts, C.J., Madden-Smith, C., Lewis, L., Teagarden, D.L., Johnson, R.E. & Ahmed, S.S., 2010. Determination of the influence of primary drying rates on the microscale structural attributes and physicochemical properties of protein containing lyophilized products. *Journal of Pharmaceutical Science*, 99(11), pp.4617–4629.
- Pasquale M.F., Baiano, A., Zanini, F., Mancini, L., Tromba, G., Dreossi, D., Montanari, F., Scuur, N. & Nobile, M.A.D., 2005. Three-dimensional quantitative analysis of bread crumb by X-ray microtomography. *Food Science*, 70(3), pp.223–229.
- Passos, C.P., Cepeda, M. R., Ferreira, S. S., Nunes, F. M., Evtuguin, D. V., Madureira, P., & Coimbra, M. A., 2014. Influence of molecular weight on in vitro immunostimulatory properties of instant coffee. *Food Chemistry*, 161, pp.60–66.

- Patel, S.M., Nail, S.L., Pikal, M.J., Geidobler, R., Winter, G., Hawe, A., Davagnino, J., Rambhatla Gupta, S., 2017. Lyophilized drug product cake appearance: What is acceptable? *Journal of Pharmaceutical Sciences*, 106(7), pp.1706–1721.
- Patel, S.M., Bhugra, C. & Pikal, M.J., 2009. Reduced pressure ice fog technique for controlled ice nucleation during freeze-drying. *AAPS PharmSciTech*, 10(4), pp.1406–1411.
- Patel, S.M., Doen, T. & Pikal, M.J., 2010. Determination of end point of primary drying in freeze-drying process control. *AAPS PharmSciTech*, 11(1), pp.73–84.
- Patel, S.M. & Pikal, M.J., 2011. Emerging freeze-drying process development and scale-up issues. *AAPS PharmSciTech*, 12(1), pp.372–378.
- Paulus, M.J. Gleason, S S., Kennel, S.J., Hunsicker, P R., Johnson, D K., 2000. High resolution X-ray computed tomography: An emerging tool for small animal cancer research. *Neoplasia*, 2(1–2), pp.62–70.
- Peppas, N.A. & Brannon-Peppas, L., 1994. Water diffusion and sorption in amorphous macromolecular systems and foods. *Journal of Food Engineering*, 22(1), pp.189–210.
- Peters, B.H., Molnár, F. & Ketolainen, J., 2014. Structural attributes of model protein formulations prepared by rapid freeze-drying cycles in a microscale heating stage. *European Journal of Pharmaceutics and Biopharmaceutics*, 87(2), pp.347–356.
- Petzold, G. & Aguilera, J.M., 2009. Ice morphology: Fundamentals and technological applications in foods. *Food Biophysics*, 4(4), pp.378–396.
- Phillips, A.O. & Phillips, G.O., 2011. Biofunctional behaviour and health benefits of a specific gum arabic. *Food Hydrocolloids*, 25(2), pp.165–169.
- Pikal, M.J., Shah, S.R., 1990. The secondary drying stage of freeze-drying: Drying kinetics as a function of temperature and chamber. *Int. J. Pharmaceut.*, 60, pp.203–217.
- Pikal, M.J., Roy, M.L. & Shah, S., 1984. Mass and heat transfer in vial freeze-drying of pharmaceuticals: role of the vial. *Journal of pharmaceutical sciences*, 73, pp.1224–1237.
- Pikal, M.J. & Shah, S.R., 1990. The collapse temperature in freeze-drying: dependence on measurement methodology and rate of water removal from the glassy phase, *Int. J. Pharm.*, 62, pp.165–186.
- Prosapio, V. & Norton, I., 2017. Influence of osmotic dehydration pre-treatment on oven drying and freeze drying performance. *LWT - Food Science and Technology*, 80, pp.401–408.
- Raharitsifa, N. & Ratti, C., 2010. Foam-mat freeze-drying of apple juice part 1: Experimental data and ann simulations. *Journal of Food Process Engineering*, 33, pp.268–283.
- Rahman, M.S., Guizani, N., Al-Khaseibi, M., Ali Al-Hinai, S., Al-Maskri, S. S. & Al-Hamhami, K., 2002. Analysis of cooling curve to determine the end point of freezing. *Food Hydrocolloids*, 16(6), pp.653–659.
- Rahman, M.S., 2006. State diagram of foods: Its potential use in food processing and product stability. *Trends in Food Science and Technology*, 17(3), pp.129–141.

- Rahman, M.S., 2001. Toward prediction of porosity in foods during drying: A brief review. *Drying Technology*, 19(1), pp.1–13.
- Rambhatla, S., Ramot, R., Bhugra, C. & Pikal, M. J., 2004. Heat and mass transfer scale-up issues during freeze drying: II. Control and characterization of the degree of supercooling. *AAPS PharmSciTech*, 5(4), p.E58.
- Rambhatla, S., Tchessalov, S. & Pikal, M.J., 2006. Heat and mass transfer scale-up issues during freeze-drying, III: control and characterization of dryer differences via operational qualification tests. *AAPS PharmSciTech*, 7(2), p.E39.
- Randall, R.C., Phillips, G.O. & Williams, P.A., 1989. Fractionation and characterization of gum from Acacia senegal. *Food Hydrocolloids*, 3(1), pp.65–75.
- Ratti, C., 2001. Hot air and freeze-drying of high-value foods: A review. *Journal of Food Engineering*, 49, pp.311–319.
- Ratti, C. & Kudra, T., 2006. Drying of foamed biological materials: Opportunities and challenges. *Drying Technology*, 24(9), pp.1101–1108.
- Renard, D., Lavenant-Gourgeon, L., Ralet, M. C. & Sanchez, C., 2006. Acacia senegal gum: Continuum of molecular species differing by their protein to sugar ratio, molecular weight, and charges. *Biomacromolecules*, 7(9), pp.2637–2649.
- Reyes, A., Vega, R., Bustos, R. & Araneda, C., 2008. Effect of processing conditions on drying kinetics and particle microstructure of carrot. *Drying Technology*, 26(10), pp.1272–1285.
- Robles, C.M., Quintanilla-Carvajal, M. X., Moreno, F. L., Hernández, E. R., M. & Ruiz, Y., 2016. Ice morphology modification and solute recovery improvement by heating and annealing during block freeze-concentration of coffee extracts. *Journal of Food Engineering*, 189, pp.72–81.
- Roos, Y. & Karel, M., 1991. Amorphous State and Delayed Ice Formation in Sucrose Solutions. *Int. J. Food. Sci. Tech.*, 26, pp.553–566.
- Roos, Y. & Karel, M., 1991. Applying state diagrams to food processing and development. *Food Technology*, 45(12).
- Roos, Y. & Karel, M., 1990. Differential scanning calorimetry study of phase transitions affecting the quality of dehydrated materials. *Biotechnology Progress*, pp.159–163.
- Roos, Y.H., 1997. Frozen State Transitions in Relation To Freze Drying. *Journal of thermal analysis*, 48, pp.535–544.
- Roos, Y.H., Karel, M., Labuza, T.P., Levine, H., Mathlouthi, M., Reid, D., Shalaev, E. & Slade, L., 2013. Melting and crystallization of sugars in high-solids systems. *Journal of Agricultural and Food Chemistry*, 61(13), pp.3167–3178.
- Roos, Y.H. & Karel, M., 1993. Melting and glass transitions of low molecular weight carbohydrates. *Carbohydrate Research*, 238(C), pp.39–48.
- Rovira, S., López, M.B., Ferrandini, E. & Laencina, J., 2011. Hot topic: microstructure

quantification by scanning electron microscopy and image analysis of goat cheese curd. *Journal of dairy science*, 94(3), pp.1091–1097.

- Ruiz-Cabrera, M.A., Rivera-Bautista, C., Grajales-Lagunes, A., González-García, R. & Schmidt, S.J., 2016. State diagrams for mixtures of low molecular weight carbohydrates. *Journal of Food Engineering*, 171, pp.185–193.
- Sablani, S.S., Rahman, M. S., Al-Kuseibi, M. K., Al-Habsi, N. A., Al-Belushi, R. H., Al-Marhubi, I., Al-Amri, I. S.I., 2007. Influence of shelf temperature on pore formation in garlic during freeze-drying. *Journal of Food Engineering*, 80(1), pp.68–79.
- Sablani, S.S. & Rahman, M.S., 2002. Pore formation in selected foods as a function of shelf temperature during freeze drying. *Drying Technology*, 20(7), pp.1379–1391.
- Sacha, G.A. & Nail, S.L., 2009. Thermal analysis of frozen solutions: Multiple glass transitions in amorphous systems. *Journal of Pharmaceutical Sciences*, 98(9), pp.3397–3405.
- Sadikoglu, H., Liapis, A.I. & Crosser, O.K., 1998. Optimal Control of the Primary and Secondary Drying Stages of Bulk Solution Freeze Drying in Trays. *Drying Technology*, 16(3–5), pp.399–431.
- Sagara, Y., 2001. Advances in transport phenomena during freeze-drying of food materials: Fundamentals and applications. *Food Science and Technology Research*, 7(3), pp.183–190.
- Sagara, Y. & Ichiba, J., 1994. Measurement of transport properties for the dried layer of coffee solution undergoing freeze drying. *Drying Technology*, 12(5), pp.1081–1103..
- Saguy, I.S., Marabi, A. & Wallach, R., 2005. Liquid imbibition during rehydration of dry porous foods. *Innovative Food Science and Emerging Technologies*, 6(1), pp.37–43.
- Sahni, E.K. & Pikal, M.J., 2017. Modeling the secondary drying stage of freeze drying: development and validation of an excel-based model. *Journal of Pharmaceutical Sciences*, 106(3), pp.779–791.
- Saifullah, M. Yusof, Y. A., Chin, N. L., Aziz, M. G., 2016. Physicochemical and flow properties of fruit powder and their effect on the dissolution of fast dissolving fruit powder tablets. *Powder Technology*, 301, pp.396–404..
- Sakiyama, T. & Yano, T., 1990. Effects of air and water contents on the effective thermal-conductivity of air-impregnated gels. *Agr. Biol. Chem. Tokyo.*, 54(6), pp.1375–1380.
- Sanchez, C., Nigen, M., Mejia Tamayo, V., Doco, T., Williams, P., Amine, C. & Renard, D., 2017. Acacia gum: History of the future. *Food Hydrocolloids*.
- Sanchez, C., Schmitt, C., Kolodziejczyk, E., Lapp, A., Gaillard, C. & Renard, D., 2008. The Acacia gum arabinogalactan fraction is a thin oblate ellipsoid: a new model based on small-angle neutron scattering and ab initio calculation. *Biophysical Journal*, 94(2), pp.629–639.
- Sánchez, J. Hernández, E., Auleda, J. M. & Raventós, M., 2011. Freeze concentration of whey

- in a falling-film based pilot plant: Process and characterization. *Journal of Food Engineering*, 103(2), pp.147–155.
- Sandy V.B., Messagie, I., Loey, A.V. & Hendrickx, M., 2005. S : Sensory and nutritive qualities of food influence of low-temperature blanching combined with high-pressure shift. *Sensory and Nutritive Qualities of Food*, 70(4), pp.304–308.
- Sangamithra, A.V., Sivakumar, J., Swamy, G. & Kuppuswamy, K., 2015. Foam-mat drying of food materials: A Review. *Journal of Food Processing and Preservation*, 39(6), pp.3165–3174.
- Sanz, P.D. de Elvira, C., Martino, M., Zaritzky, N., Otero, L. & Carrasco, J.a., 1999a. Freezing rate simulation as an aid to reducing crystallization damage in foods. *Meat Science*, 52, pp.275–278.
- Scutellà, B., Plana-Fattori, A., Passot, S., Bourlès, E., Fonseca, F., Flick, D. & Trélea, I. C., 2017. 3D mathematical modelling to understand atypical heat transfer observed in vial freeze-drying. *Applied Thermal Engineering*, 126, pp.226–236.
- Searles, J.A., 2010. Freeze Drying / Lyophilization of Pharmaceutical and Biological Products. In L. Rey & J. C. May, eds. *Freeze Drying / Lyophilization of Pharmaceutical and Biological Products*. New York: Informa Healthcare, pp. 1–28.
- Searles, J.A., Carpenter, J.F. & Randolph, T.W., 2001a. Annealing to optimize the primary drying rate, reduce freezing-induced drying rate heterogeneity, and determine T'g pharmaceutical lyophilization. *Journal of Pharmaceutical Sciences*, 90(7), pp.872–887.
- Searles, J.A., Carpenter, J.F. & Randolph, T.W., 2001b. The ice nucleation temperature determines the primary drying rate of lyophilization for samples frozen on a temperature-controlled shelf. *Journal of Pharmaceutical Sciences*, 90(7), pp.860–871.
- Seetapan, N., Gamonpilas, C., Methacanon, P. & Fuongfuchat, A., 2015. Effect of cryogenic freezing on textural properties and microstructure of rice flour/tapioca starch blend gel. *Journal of Food Engineering*, 151, pp.51–59.
- Seo, J.A. Kim, S. J., Kwon, H.J., Yang, Y. S., Kim, H.K. & Hwang, Y.H., 2006. The glass transition temperatures of sugar mixtures. *Carbohydrate Research*, 341(15), pp.2516–2520.
- Shafiur Rahman, M., 2001. Toward prediction of porosity in foods during drying: A brief review. *Drying Technology, An International Journal*, 19(1), pp.1–13.
- Sharma, A., Jana, A.H. & Chavan, R.S., 2012. Functionality of milk powders and milk-based powders for end use applications-A review. *Comprehensive Reviews in Food Science and Food Safety*, 11(5), pp.518–528.
- Silva, J.V.C., Legland, D., Cauty, C., Kolotuev, I. & Floury, J., 2015. Characterization of the microstructure of dairy systems using automated image analysis. *Food Hydrocolloids*, 44, pp.360–371.
- Skrdla, P.J., 2007. A simple model for complex dissolution kinetics: A case study of norfloxacin. *Journal of Pharmaceutical and Biomedical Analysis*, 45(2), pp.251–256.

- Souza, D.S., Pimentel, J.D.R., Prado, M.M., Marques, L G., & Narain, N, 2011. Rehydration characteristics of freeze-dried avocado ( *Persea americana* ). *Chemical Engineering*, p.6.
- Stokes, D., 2013. *Environmental scanning electron microscopy (ESEM): principles and applications to food microstructures*, Woodhead Publishing Limited.
- Tang, X. & Pikal, M.J., 2004. Design of freeze-drying processes for pharmaceuticals: practical advice. *Pharmaceutical Research*, 21(2), pp.191–200.
- Teraoka, Y., Saito, A. & Okawa, S., 2002. Ice crystal growth in supercooled solution. *International Journal of Refrigeration*, 25(2), pp.218–225.
- To, E.C. & Flink, J.M., 1978. “Collapse”, a structural transition in freeze dried carbohydrates: II. Effect of solute composition. *International Journal of Food Science & Technology*, 13(6), pp.567–581.
- Trelea, I.C., Passot, S., Fonseca, F. & Marin, M., 2007. An Interactive Tool for the Optimization of Freeze-Drying Cycles Based on Quality Criteria. *Drying Technology*, 25(5), pp.741–751.
- Tsinontides, S.C., Rajniak, P., Pham, D., Hunke, W.A., Placek, J. & Reynolds, S.D, 2004. Freeze drying - Principles and practice for successful scale-up to manufacturing. *International Journal of Pharmaceutics* 280 (1-2), pp. 1-16.
- Tsourouflis, S., Flink, J.M. & Karel, M., 1976. Loss of structure in freeze-dried carbohydrates solutions: Effect of temperature, moisture content and composition. *Journal of the Science of Food and Agriculture*, 27(6), pp.509–519.
- Ullrich, S., Seyferth, S. & Lee, G., 2015. Measurement of shrinkage and cracking in lyophilized amorphous cakes. Part II: Kinetics. *Pharmaceutical Research*, 32(8), pp.2503–2515.
- Vaclavik, V.A & Christian, E.W., 2008. Baked Products: Batters and Dough. *Essentials of Food Science* 565.
- Velardi, S.A. & Barresi, A.A., 2008. Development of simplified models for the freeze-drying process and investigation of the optimal operating conditions. *Chemical Engineering Research and Design*, 86(1 A), pp.9–22.
- Voda, A., Homan, N., Witek, M., Duijster, A., van Dalen, G., van der Sman, R., Nijssse, J., van Vliet, L., Van As, H. & van Duynhoven, J., 2012. The impact of freeze-drying on microstructure and rehydration properties of carrot. *Food Research International*, 49(2), pp.687–693.
- Wallach, R., Troygot, O. & Saguy, I.S., 2011. Modeling rehydration of porous food materials: II. the dual porosity approach. *Journal of Food Engineering*, 105(3), pp.416–421.
- Wang, D. & Martynenko, A., 2016. Estimation of total, open-, and closed-pore porosity of apple slices during drying. *Drying Technology*, 34(8), pp.892–899.
- Wang, J., Li, Y.Z., Chen, R.R., Bao, J.Y. & Yang, G. M., 2007. Comparison of volatiles of banana powder dehydrated by vacuum belt drying, freeze-drying and air-drying. *Food Chemistry*, 104(483), pp.1516–1521.

- Wang, R., Zhang, M. & Mujumdar, A.S., 2010. Effects of vacuum and microwave freeze drying on microstructure and quality of potato slices. *Journal of Food Engineering*, 101(2), pp.131–139.
- White, K.L. & Bell, L.N., 1999. Glucose loss and maillard browning in solids as affected by porosity and collapse. *Journal of Food Science*, 64(6), pp.1010–1014.
- Witrowa-Rajchert, D. & Lewicki, P.P., 2006. Rehydration properties of dried plant tissues. *International Journal of Food Science and Technology*, 41(9), pp.1040–1046.
- Xanthakis, E., Le-Bail, A. & Ramaswamy, H., 2014. Development of an innovative microwave assisted food freezing process. *Innovative Food Science and Emerging Technologies*, 26, pp.176–181.
- Xu, Y., Zhang, M., Mujumdar, A.S., Duan, X. & Jin-cai, S., 2006. A two-stage vacuum freeze and convective air drying method for strawberries. *Drying Technology*, 24(February 2015), pp.1019–1023.
- Yu, K.C., Chen, C.C. & Wu, P.C., 2011. Research on application and rehydration rate of vacuum freeze drying of rice. *Journal of Applied Sciences*, 11(3), pp.535–541.
- Zea, L.P., Yusof, Y. A., Aziz, M.G., Ling, C.N. & Amin, N.A.M., 2013. Compressibility and dissolution characteristics of mixed fruit tablets made from guava and pitaya fruit powders. *Powder Technology*, 247, pp.112–119.
- Zhai, S., Taylor, R., Sanches, R. & Slater, N.K.H., 2003. Measurement of lyophilisation primary drying rates by freeze-drying microscopy. *Chemical Engineering Science*, 58(11), pp.2313–2323.
- Zhao, J.H., Liu, F., Wen, X., Xiao, H.W. & Ni, Y.Y., 2015. State diagram for freeze-dried mango: Freezing curve, glass transition line and maximal-freeze-concentration condition. *Journal of Food Engineering*, 157, pp.49–56.
- Zheng, L. & Sun, D.W., 2006. Innovative applications of power ultrasound during food freezing processes - A review. *Trends in Food Science and Technology*, 17, pp.16–23.